Uncovering Reproductive Roles Of Cell Wall Glycoproteins In Flowering Plants

by

Cecilia M. Lara Mondragón

A dissertation submitted in partial fulfillment
of the requirements for the degree of
Doctor of Philosophy
(Molecular, Cellular and Developmental Biology)
in the University of Michigan
2022

Doctoral Committee:

Assistant Professor Cora A. MacAlister, Chair
Professor, Steven Clark
Professor John Schiefelbein
Professor Kristen Verhey

Cecilia M. Lara-Mondragón

laracm@umich.edu

ORCID iD: 0000-0001-7313-805X

© Cecilia M. Lara-Mondragón 2022

Dedication

A mi familia.

Acknowledgements

To all who directly or indirectly contributed to the completion of this work.

Table of Contents

List of Tables

List of Figures

Abstract

Plant cells are surrounded by a polysaccharide-rich extracellular matrix, the cell wall. The cell wall constitutes the interphase of interaction between the cell and its surrounding environment, as well as a medium for cell-cell communication within plant tissues. In addition to polysaccharides, the wall hosts a vast array of proteins with putative roles in these processes, although characterization of such functions remains to be determined. Comparative studies indicate that evolutionary milestones in the land plant clade (e.g., transition to land, flowering plant radiation) correlate with the expansion in the number of cell wall genes; trend also observed in the most abundant group of wall proteins, the Hydroxyproline-rich glycoprotein family (HRGP). While most of the currently known functions of canonical HRGPs are related to cell wall architecture, the existence of a plethora of noncanonical HRGPs (chimeras and hybrids) indicate potential functional diversification within the family. The expansion of the HRGP family, particularly during the radiation of the flowering plants (angiosperms), suggests the emergence of novel functions related to processes exclusive to angiosperms. Angiosperms are the most abundant and diverse group in the plant kingdom and their current ecological success has been, in part, associated to their unique sexual reproduction mechanism: immobile sperm cells are transported by a remarkably fast-growing structure, the pollen tube, to receptive ovules deeply embedded in the maternal tissues of the pistil. Since angiosperm sexual reproduction involve, on one hand, rapid cell growth by the pollen tube to deliver male gametes and, on the other hand, the establishment of cell-cell communication as the pollen tube traverses the female

tissues, we investigated the participation of noncanonical HRGPs during both these processes. On the male side, our research sheds light on the function of two HRGP chimeras, the Arabidopsis class I formins AtFH3 and AtFH5, acting as molecular linkers between actin cytoskeleton and the cell wall during pollen tube elongation. Our results revealed that the extracellular domain of AtFH3 and AtFH5, which contain distinct HRGP-like *O*-glycans, plays an important role in spatially constraining these proteins to specific plasma membrane domains and consequently, contributing to the regulation of their respective actin nucleation activities. On the female side, our results indicate that HRGP accumulation are correlated with the establishment of receptivity in tomato pistils. Through a combination of immunological methods and high throughput mRNA sequencing, we identified novel noncanonical HRGPs with potential functions supporting pollen tube growth through the pistil and/or as guidance cues for ovular targeting. Together, our findings constitute a step forward to understanding the functional specialization of noncanonical HRGPs during reproductive processes in flowering plants.

Chapter 1. Insights Into the Function Of Plant Cell Wall Glycoproteins

The extracellular matrix of plant cells, the cell wall, was observed for the first time under a microscope by Robert Hooke and reported in his work *Micrographia* (Hooke, 1665). This seminal discovery, from which the biological sense of the term *'cell'* derived, marked the beginning of new era in the study of the natural world. Apart from aiding our understanding of fundamental questions in biology, the cell wall constitutes the primary interface of interaction between a plant cell and its environment and, therefore not surprisingly, an increasing amount of evidence suggests a pivotal role in multiple biological processes including morphogenesis, cell-cell communication, and response to biotic and abiotic stresses (Gorelova et al., 2021; Houston et al., 2016; Tameshige et al., 2015).

The prevailing notion of the primary cell wall is that of a complex, highly dynamic network composed of distinct polysaccharides and less than 10% of proteins (Anderson & Kieber, 2020). Traditionally considered as structural components, the Hydroxyproline (Hyp) Rich glycoprotein (HRGP) family is the most abundant group of proteins in the wall (Johnson et al., 2017). Emerging evidence suggests that some members of the HRGP family, particularly the non-canonical HRGPs (e.g., Proline-rich Extensin Receptor Kinase –PERKs, Leucine-rich Repeat Extensin proteins –LRXs, class I Formins, Fasciclin-like Arabinogalactan proteins –FLAs, Hybrid Arabinogalactan Extensins –HAEs), may be involved in additional roles such as cellular communication and/or cell wall integrity sensing in a variety of biological contexts (e.g.,

development, stress responses, reproduction), although further studies are necessary to better understand the underlying mechanisms. A handful of reports exemplify the complex interactions between HRGPs and other biomolecules. In the wall, ARABINOXYLAN PECTIN ARABINOGALACTAN PROTEIN1 (APAP1) covalently binds to pectins (Tan et al., 2003). Similarly, once secreted to the extracellular space, Extensins (EXT) self-assemble and form a network that serve as scaffold for pectin assembly (Cannon et al., 2008). On the cytoplasmic side, it has been reported that chimeric HRGPs establish interaction with intracellular components as well as the cell wall (cytoskeleton and class I Formins –Cvrčková, 2013). These studies suggest that intracellular and extracellular components exist as a continuum, and HRGPs possibly act as molecular linkers, having important implications for wall architecture, function and possibly signal transduction (Chebli et al., 2021; Jaillais & Ott, 2020).

Adding another layer of complexity to the study of molecular processes *in muro*, the polysaccharide composition of the wall is known to vary across species and, even within the same organism, to change throughout development, cell type and/or upon stimulus (Anderson & Kieber, 2020; Houston et al., 2016; Levesque-Tremblay et al., 2015), making the molecular dissection of wall-related processes a challenging endeavor. In this chapter, we review the current state of knowledge of the cell wall as a dynamic structure, with particular emphasis on non-canonical members of the HRGP family and their emerging roles beyond architectural components of the cell wall.

1.1. Biology of the Cell Wall

1.1.1. Cell Wall Polysaccharides

The cell wall is primarily composed of polysaccharides. Cellulose is among the most abundant type of polysaccharide in the primary wall, usually found in the form of microfibrils of approximately 3 nm in diameter (Anderson & Kieber, 2020). Cellulose β-(1,4)-linked glucan chains are polymerized in the plasma membrane by Cellulose Synthase Complexes (CSC), which travel along the microtubules secreting glucan chains to the apoplastic space (Bringmann et al., 2012). Among the non-cellulosic polysaccharides, hemicelluloses refer to a group of structurally and physiochemically distinct polysaccharides that typically facilitate crosslinking of other polysaccharides in the wall; this group include xyloglucans, xylans, mannans, glucomannans and β-(1→3, 1→4)-glucans. Hemicelluloses are primarily synthesized in the Golgi apparatus, although in some cases, further modification occurs after secretion into the apoplastic space (Anderson & Kieber, 2020; Scheller & Ulvskov, 2010). Pectins are another highly abundant group of non-cellulosic polysaccharides present in the primary wall, comprising three major types: homogalacturonan (HG), rhamnogalacturonan-I (RG-I) and rhamnogalacturonan-II (RG-II). Pectins, together with hemicelluloses form a covalently linked matrix in which cellulose microfibrils are embedded. Like hemicelluloses, pectins are synthesized in the Golgi apparatus and secreted to the apoplast. HGs are secreted in a highly methylesterified form and can subsequently undergo de-methylesterification *in muro*. De-methylesterified HGs can form intramolecular Ca^{2+} bridges, forming a gel (Levesque-Tremblay et al., 2015). Similarly, RG-II molecules can undergo boron-mediated crosslinking (O'Neill et al., 2004). As a gel, the pectin matrix exhibits interesting physical properties: small environmental changes (e.g., matrix composition, temperature, ionic strength, or pH) can cause drastic changes in volume (swelling or shrinkage), a phenomenon known as volume phase transition. In gels, volume phase transition occurs abruptly, and phases with differing degrees of swelling simultaneously coexist (Dušek &

Dušková-Smrčková, 2020). It has been proposed that, as phase transition has profound effects on the properties of gels including porosity, adhesion, hydration, and rigidity; this phenomenon may similarly modulate the properties of the pectin matrix, thus, having important implications in different biological processes in plants (Haas et al., 2021; Höfte et al., 2012; Willats et al., 2001). This idea is supported by recent evidence that phase transition occurs during the deposition of the exine layer in pollen grain development (Radja et al., 2019). Other biological processes that involve phase transition in the wall remain to be described; however, the idea that the gel-like properties of the pectin matrix might modulate cell wall extensibility during cell growth is an interesting scenario (Haas et al., 2021; Willats et al., 2001). Furthermore, it has been suggested that phase transition in the pectin matrix may contribute to the nanoscale organization of the wall by compartmentalizing polysaccharide modifying enzymes to specific domains, although the driving forces behind this remain to be determined (Haas et al., 2021).

1.1.2. Proteins in the Cell Wall

The advent of high throughput technologies, combined with genetic and biochemical studies, allowed the identification of a plethora of proteins in the cell wall. Cell wall proteins (CWP) are a heterogeneous group with variable abundance between cell types, species, and environmental conditions (Albenne et al., 2014). Based on proteomics studies, CWPs can be broadly classified into several different functional groups: 1) proteins that modify polysaccharides; this category includes enzymes that directly modify polysaccharides (e.g., polygalacturonases, lyases, hydrolases, etc.) and non-enzymatic remodelers (e.g., expansins) (Albenne et al., 2014; Rose et al., 2004); 2) proteases (e.g., Asp-, Cys-, Ser-proteases and Ser-carboxypeptidases); 3) proteins that bind to carbohydrates (plant lectins) (Lannoo & Van Damme, 2014; Wang et al., 2020); 4) CWP with putative signaling roles (e.g., Arabinogalactan glycoproteins); 5) structural proteins

(e.g. Extensins and Gly-rich proteins (Cannon et al., 2008), and 6) proteins with unknown functions (Albenne et al., 2014; Jamet et al., 2006, 2008).

A significant fraction of CWPs undergo extensive posttranslational modifications. *N*-glycosylation, the addition of glycophosphatidylinositol (GPI)-anchors, Pro hydroxylation and *O*-glycosylation are among the most commonly reported CWP posttranslational modifications (Duruflé et al., 2017). *N*-glycosylation of Asn residues within Asn-X-Ser/Thr motifs (where X can be any aminoacid except Pro) occurs in the endoplasmic reticulum (ER) and it is believed to be important for proper folding of secreted or membrane proteins as they are trafficked to their respective destinations (Strasser, 2014, 2016). The addition of GPI-anchors or glypiation also occurs in the ER; this modification tethers proteins to the ER lumen and later, after secretion, to the outer leaflet of the plasma membrane (Borner et al., 2003). GPI-anchors are thought to confer several properties to their bearers including a high degree of lateral mobility in the plasma membrane, targeting to specific plasma membrane microdomains, conditional cleavage –thus, selective secretion to the apoplast–, and potential for spontaneous re-anchoring to the membrane through the GPI-anchor's lipid moiety (Desnoyer & Palanivelu, 2020). Pro hydroxylation and *O*-glycosylation are posttranslational modifications present in the HRGP family, which will be discussed in detail in the next section.

1.2. Hydroxyproline-rich Glycoproteins: Classification, Biosynthesis, and Function

HRGPs are a large, multigenic family of proteins characterized by biased aminoacid composition. As their name indicate, these proteins possess a high content of Pro in their sequences. Pro residues in HRGPs are enzymatically converted to Hyp in a context-dependent manner by membrane-anchored Prolyl-hydroxylases, P4Hs (Duruflé et al., 2017; Kieliszewski &

Lamport, 1994). Pro hydroxylation of HRGPs is thought to initiate in the ER and continue on the Golgi (Nguema-Ona et al., 2014). The P4H family in *Arabidopsis* consists of 13 members expressed across different tissues and experimental evidence indicates that they may exhibit substrate specificity (Petersen et al., 2021; Velasquez et al., 2015). After Pro hydroxylation, HRGPs undergo *O*-glycosylation in the Golgi apparatus. *O*-glycosylation of Hyp residues occurs in a sequence dependent manner. Based on their glycosylation motifs, HRGPs can be classified into Extensins (EXTs), Arabinogalactan glycoproteins (AGPs), Proline-Rich Proteins (PRPs), hybrid and chimeric HRGPs. In the next section, the machinery involved in *O*-glycosylation of each category, as well as described functions for some members of the HRGP family will be reviewed.

1.2.1. Extensins

Classical EXTs are highly repetitive, secreted proteins defined by the presence of Ser-Hyp$_{(3-5)}$ glycosylation motifs that are modified by the addition of short linear arabinose chains (Kieliszewski & Lamport, 1994). *O*-arabinosylation of EXTs is performed by the consecutive activity of several phylogenetically unrelated arabinosyltransferases: Hydroxyproline-*O*-arabinosyltransferases (HPAT1-3), Reduced Residual Arabinose (RRA1-3), Xyloglucanase113 (XEG113) and Extensin Arabinose Deficient (ExAD) (Egelund et al., 2007; Gille et al., 2009; Møller et al., 2017; Ogawa-Ohnishi et al., 2013; Velasquez et al., 2011). In the EXT glycosylation motifs, the Ser residues can also be monogalactosylated by the Serine-*O*-galactosyltransferase SGT1 (Deepak et al., 2007; Xie et al., 2011). In addition to glycosylation motifs, classical EXTs also possess interspersed Tyr-containing motifs (Tyr-X-Tyr, where X is a variable aminoacid), which are important for inter and intramolecular crosslinking. Glycosylated EXTs are amphiphilic molecules, a property thought to be an important driver of self-assembly

post secretion (Cannon et al., 2008). Molecular, non-covalent assembly of EXT networks is later reinforced by crosslinking of Tyr residues by the action of Extensin Peroxidases (EPs) (Mishler-Elmore et al., 2021). EXTs, in the acidic pH of the cell wall, carry a positive net charge, thus allowing ionic interactions with negatively charged polysaccharides of the wall, like pectins (Cannon et al., 2008; Chen et al., 2015). The EXT networks are thought to serve as a scaffold for pectin assembly (Lamport et al., 2011). Among the members of the EXT family, AtEXT3 is the best characterized genetically and biochemically. Loss of function of *AtEXT3*, initially named *ROOT-SHOOT-HYPOCOTYL-DEFECTIVE* (*RSH*), exhibited embryo lethality, specifically, a severe disruption in cell plate formation during embryo cytokinesis (Hall & Cannon, 2002). Consistent with the predicted self-assembly properties of EXTs, AtEXT3 isolated from *Arabidopsis* cell cultures formed staggered dendritic patterns when visualized by Atomic Force Microscopy (AFM). Based on these results and the *rsh* phenotype, it was suggested that AtEXT3 forms a network that serves as a scaffold for supramolecular assembly of pectins in the forming cell plate during embryo development (Cannon et al., 2008). Among other potential functions for EXTs beyond cell plate formation during embryo development, EXTs had been implicated in defense responses upon pathogen infection or wounding. Immunolocalization studies detected accumulation of EXT epitopes upon infection by distinct pathogens (Deepak et al., 2007; Xie et al., 2011) and upregulation of EXT crosslinking (Plancot et al., 2013; Velasquez et al., 2011), suggesting a mechanism of cell wall reinforcement to prevent further infection.

1.2.2. Arabinogalactan Glycoproteins

AGPs are highly glycosylated proteins with up to 90% of their total composition consisting of carbohydrates. In AGPs, clustered, non-contiguous Hyp residues (Hyp-X-Hyp-X, where X is Gly, Ala, Ser or Thr) are modified by the addition of β-1,3-galactan backbones decorated with β-

1,6-galactose side chains. AG-glycans can be further decorated with α-arabinose, β-(methyl)glucuronic acid, α-rhamnose, and α-fucose (Ma et al., 2017). Since AGPs are glycosylated by the addition of complex glycans, it is predicted that around 15 different glycosyltransferases are involved in their synthesis including galactosyltransferases (GALTs), arabinosyltransferases, fucosyltransferases (FUTs), rhamnosyltransferases, glucuronosyltransferases (GLCATs), xylosyltransferases and glucuronic acid methyltransferases (Nguema-Ona et al., 2014; Silva et al., 2020). Glycosylation initiation requires the activity of hydroxyproline-*O*-GALTs from the Carbohydrate Active Enzyme (CAZy) GT31 family. In Arabidopsis, eight members of this family have been implicated in this reaction, GALT2-6, and Hydroxyproline Galactosyltransferases (HPGT1-3) (Zhang et al., 2021). Precise characterization of the enzymes responsible for the elongation of the β–1,3-galactan backbone requires further study, although this enzymatic activity was observed *in vitro* for two members of the GT31 family (At1g77810 and GALT31A) and GALT29A from the GT29 family (Dilokpimol et al., 2014; Geshi et al., 2013). The β–1,3-galactan backbone of AGPs is decorated with glucuronic acid (GlcA), added in a reaction presumably catalyzed by three reported enzymes: GlcAT14A, GlcAT14B and GlcAT14C (Zhang et al., 2020).

AGPs are ubiquitous in the plant kingdom and they are reported to exhibit developmental and stress-induced changes in gene expression and glycan patterning across taxa (Knox et al., 1991; Knox, 1992; Lamport et al., 2006). Due to their dynamic changes, it is believed that these glycoproteins participate in cell signaling, although the molecular mechanisms remain elusive. Recent structural evidence suggests that the GlcA moieties associated to AGPs might have important biological implications: β–linked GlcA moieties in AGPs had been shown to interact

with calcium ions, a finding that led to the AGP-Ca^{2+} capacitor hypothesis. This model postulates that AGPs and Ca^{2+} reversibly associate in a pH dependent manner, therefore, regulating the availability of calcium in the cell surface. Local acidification in the plasma membrane, presumably mediated by the action of H^{+}-ATPases, causes dissociation of the AGP-Ca^{2+} complex, allowing internalization of Ca^{2+} against its concentration gradient (Lamport & Várnai, 2013). Extracellularly, it is known that Ca^{2+} and de-methylesterified HGs can form intramolecular bridges, altering the mechanical properties of the cell wall (Levesque-Tremblay et al., 2015). Together, the AGP-Ca^{2+} capacitor model suggests that AGPs play a regulatory role in calcium homeostasis during intra and extracellular processes. Recently, it was reported that the *glcat14a/b/d* and *glcat14a/b/e* mutants exhibited a drastic reduction in glucuronidation and lower calcium binding capacity (~80% reduction compared to the wild type), as well as pleiotropic defects including reduced trichome branching, shorter stems, altered calcium waves in roots and sterility. Suppression of several developmental defects was achieved by increasing calcium concentration in the medium, supporting the AGP-Ca^{2+} capacitor model (Lopez-Hernandez et al., 2020).

To date, the best characterized member of the family, at a genetic and biochemical level, is LeAGP-1 from tomato (Gao & Showalter, 2000; Sun, Kieliszewski, et al., 2004; Sun, Zhao, et al., 2004). LeAGP-1 is a canonical member of the AGP family, attached to the plasma membrane by a GPI anchor. Additionally, when expressed in tobacco cell cultures, GFP:LeAGP-1 localized to plasma membrane extensions known as Hechtian strands upon plasmolysis. These results suggest a potential role for AGPs in Hechtian adhesion, establishing a molecular linkage between the plasma membrane and the cell wall. Tomato plants overexpressing LeAGP-1 exhibited a

variety of vegetative defects, such as enhanced lateral branching and reduced stem elongation and compromised fertility (seed size and seed set reduction) (Sun, Kieliszewski, et al., 2004). The pleiotropic effects observed in plants overexpressing LeAGP-1 illustrates the plethora of biological processes AGPs have been associated with, including embryo development, cell differentiation, xylem development, programmed cell death, and several aspects of reproductive biology (Chaves et al., 2002; Cheung et al., 1995; Gao & Showalter, 2000; Knox, 1997; Nothnagel, 1997). How AGPs regulate these biological processes at the molecular level is yet to be described. While the AGP-Ca^{2+} capacitor model offers some potential mechanistic insights into their function, this model implies a single mode of action for a highly diverse, multigenic family that exhibits tightly regulated patterning during development/stress responses. To date, the extent of structural diversity among AGP glycans is unknown, however, considering that they constitute a significant fraction of AGP composition, the likelihood of functional significance other than Ca^{2+} chelation remains an open possibility for future studies.

1.2.3. Proline-rich Glycoproteins

PRPs display the lowest degree of glycosylation (~1% total weight) within the HRGP family. PRPs typically contain repetitive Pro-Pro-Val-Tyr-Lys motifs, although, this group tend to be less well defined compared to EXT and AGPs as the number of repeats vary across taxa and among PRP members of the same species (Josè-Estanyol & Puigdomènech, 2000; Xu et al., 2013). In Arabidopsis, *AtPRP3* was implicated in root hair development (Bernhardt & Tierney, 2000), while the gain of function of its paralog in rice *OsPRP3* displays an increase in tolerance to cold temperatures (Gothandam et al., 2009). In cotton, *GhPRP5* acts as a negative regulator of fiber development (Xu et al., 2013). At the transcriptional level, several studies had reported an increase in mRNA levels in response to various stresses, such as drought, temperature and

salinity (Creelman & Mullet, 1991; Zhan et al., 2012). In rice, downregulation of two repetitive PRPs, RePRP1 and RePRP2 is correlated to a decrease in sensitivity to abscisic acid, a plant phytohormone induced during stress responses (Tseng et al., 2013). Compared to other members of the HRGP family, our understanding of this group, is in its infancy. Further studies are necessary to fully understand the mechanistic basis for PRP involvement during these processes.

1.2.4. Non Canonical HRGPs: Hybrids and Chimeras

For simplicity, HRGP glycoproteins had been historically classified into the three main groups described in the previous sections; however, bioinformatic studies of different plant genomes revealed the existence of a plethora of protein sequences with HRGP-like motifs in their sequences or proteins with putative glycosylation motifs that fit more than one HRGP category. Therefore, it has been proposed that the HRGP family comprises a spectrum with varying degrees of glycosylation; this classification includes non-canonical family members: hybrid HRGPs — which exhibit glycosylation motifs present in AGPs, EXTs and/or PRPs in their sequences, and chimeric HRGPs — proteins with HRGP-like glycosylation motifs and domains of unrelated function (Johnson et al., 2017; Showalter et al., 2010; Showalter & Basu, 2016). Since non-canonical HRGPs often exhibit a low degree of sequence similarity among species, cataloging these proteins commonly require a combination of approaches in addition to homology searches, including the search of secretion signals, biased aminoacid composition (high content of Pro), the presence of HRGP-like glycosylation motifs (EXT, AGP or PRP -like) and/or the presence of GPI anchor sequences (Johnson et al., 2017; Liu et al., 2020). While the selection criteria between studies are different, the presence of hybrids and chimeric HRGPs has been generally described across taxa. Among the proteins identified are Hybrid AGP-EXT proteins (HAEs), PRP-AGP hybrids, EXT-PRP hybrids and a variety of chimeric proteins,

including Fasciclin-like Arabinogalactan glycoproteins (FLAs), plastocyanin-like AGPs, Early Nodulin-Like (ENODLs), Xylogen-like AGPs, class I Formin Homology proteins (FHs), Leucine-rich Repeat Extensins (LRXs), Lipid Transfer-like Proteins (LTPs), Proline-rich Extensin Like proteins (PERKs) and chimeric HRGPs with domains of unknown function (DUF) (Johnson et al., 2017; Liu et al., 2016; Showalter et al., 2010). Our understanding of the mechanistic basis for the function of chimeric and hybrid HRGPs is limited and, in the case of chimeric proteins, the significance of HRGP-like motifs for protein function is poorly understood and the presence of *O*-glycans in these motifs is speculative (Borassi et al., 2016; Martinière et al., 2011; Showalter & Basu, 2016). Interestingly, chimeric and hybrid HRGPs had been implicated in diverse processes such as sensing of cell wall integrity (Fabrice et al., 2018; Herger et al., 2019), vascular tissue differentiation (Motose et al., 2004) and reproductive processes such as pollen tube guidance in flowering plants (Hou et al., 2016).

1.3. Why are there so many HRGPs? — Functional Diversification of the HRGP Family.

Multicellularity evolved independently in multiple lineages across the tree of life (Grosberg & Strathmann, 2007). Although the mechanisms that gave rise to multicellularity in plants are unknown, it is thought that its retainment in the lineage may have been advantageous for survival as their aquatic ancestors transitioned to a terrestrial environment (Pires & Dolan, 2012). Evolution of multicellularity and adaptation to the terrestrial environment was accompanied by the emergence of complex networks for cell-cell communication, recognition, and novel mechanisms of cell adhesion. Land plants or Embryophytes often exhibit an expansion in the number of cell wall related genes compared to algae (Popper et al., 2011), a trend also observed in the HRGP family, where an approximate 4-fold increase in HRGP gene number is observed

between green algae and mosses (Johnson et al., 2017). In addition to terrestrialization, the emergence of specific HRGPs is also correlated to major events in Embryophyte evolution such as the early radiation of flowering plants (Johnson et al., 2017; Ma et al., 2017). The association between evolutionary milestones in land plant evolution and the expansion of the HRGP family indicates a possible role for these proteins in novel cellular communication networks and/or novel structural roles as cell walls became specialized across lineages.

Genome-wide studies in *Pyrus bretschneideri*, the Chinese white pear, suggests that whole genome duplication is a major driving force in the expansion of the HRGP family. In this study, the authors also observed highly divergent expression patterns among HRGPs, further contributing to the emergence of novel functions for those genes retained after whole genome duplication (Jiao et al., 2018). Supporting this hypothesis, transcriptomic analyses in different species revealed highly dynamic expression patterns across tissues, developmental stages, and induction upon biotic and abiotic stresses (Abedi et al., 2020; Lara-Mondragón & MacAlister, 2021; Pereira et al., 2014; Sujeeth et al., 2012).

Repetitive sequences are prone to insertions/deletions caused by rearrangements during replication (i.e., endoreplication) or through recombination (Smith, 1976). These rearrangements are thought to be a pervasive driving force for the emergence novel HRGPs, especially events that maintain the protein structure and reading frame of the repeats in the protein backbone. Additionally, the presence of long Pro-rich motifs in a sequence is thought to enable chromosomal exchange, giving rise to chimeric sequences by domain swapping and further increasing functional diversity if maintained throughout evolution (Jiao et al., 2018; Lee et al.,

2007). A comparative study between two closely related species of the green alga genus *Chlamydomonas* showed that the repetitive regions (glycosylation motifs) of two chimeric HRGP genes involved in specifying mating type (*SAG1* and *SAD1*) have diverged significantly by selective endoduplication, suggesting that this process might be implicated in reproductive isolation and speciation within this group (Lee et al., 2007). Non-canonical HRGPs are also highly expressed in reproductive tissues in angiosperms (Cheung et al., 1995; Fabrice et al., 2018; Hou et al., 2016; Li et al., 2010; Sede et al., 2018), thus, it is possible that similar mechanisms of speciation may also operate in this clade.

1.4. Non-canonical HRGPs in Angiosperm Sexual Reproduction

Flowering plants or angiosperms dominate the current landscape, constituting up to 90% of the extant flora (Condamine et al., 2020). Theories aiming to explain their fast rise and diversification suggest that part of their evolutionary success is due to key reproductive adaptations (Crepet & Niklas, 2009). Unlike other plant groups, in angiosperms, the ovules are enclosed by maternal tissues, in a structure collectively called the pistil. The pistil confers protection to ovules from the environment, while also forming a barrier to fertilization.

Successful fertilization requires proper delivery of sperm cells to a receptive ovule. This process inherently involves the establishment of intimate interactions and cellular communication between the elongating pollen tube and pistil tissues: it is estimated that pollen tubes interact with at least seven different cell types along their journey through the pistil (Palanivelu & Tsukamoto, 2012). On the female side, the pistil must recognize compatible pollen grains and provide cues to trigger pollen hydration, support pollen tube growth within the transmitting tract in the style and once in the ovary, provide positional cues for the pollen tube to target receptive

ovules. On the male side, fast polarized growth, responsiveness to female-produced cues and the ability to burst upon ovule contact to release sperm cells is crucial for fertilization (Dresselhaus & Franklin-Tong, 2013; Palanivelu & Tsukamoto, 2012). Interestingly, studies of several non-canonical HRGPs had identified roles in virtually every single step of sexual reproduction. In this section, we will further review reported roles in both, female and male related processes during pollen-pistil interaction, highlighting their functional diversity as well discuss the potential mechanisms by which these proteins function.

1.4.1. Pollen Recognition

The first checkpoint in angiosperm sexual reproduction occurs when dehydrated pollen grains land on the receptive surface of the pistil, the stigma. If compatible, pollen grains hydrate, germinate and elongate through the highly secretory tissues of the style (transmitting tract). AGP and EXT-like moieties had been detected through immunofluorescence in both the stigma and the transmitting tract in a number of species with remarkably distinct floral morphology; these include apple, Arabidopsis, tomato and tobacco (Cheung et al., 1995; Coimbra et al., 2007; Lara-Mondragón & MacAlister, 2021; Losada & Herrero, 2012). In *Nicotiana tobaccum*, the AGP-EXT hybrid Pistil Extensin-Like Protein class III (PELPIII) accumulates in the extracellular matrix of the transmitting tract cells as the pistil becomes mature and after pollination, PELPIII translocates to the callose plugs and cell wall of elongating pollen tubes (Bosch et al., 2001; de Graaf et al., 2003). While it is currently unknown whether PELPIII promotes growth of pollen tubes, genetic evidence indicates that PELPIII mediates incompatibility responses during interspecific pollination. PELPIII accumulation correlated with the inhibition of pollen tube growth when *N. tobaccum* pistils were pollinated with pollen from *N. obtusifolia* or *N. repanda.* Inhibition of pollen tube growth in incompatible pollinations was significantly reduced when the

expression of PELPIII was downregulated in *N. tobaccum* pistils, further supporting the role of PELPIII in prezygotic interspecific incompatibility (Eberle et al., 2013). Further studies indicated that the pollen tube growth inhibitory function of PELPIII possibly lies in its N-terminus, as introduction of an N-terminus altered PELPIII into *N. tobaccum* PELPIII RNAi lines was unable to rescue interspecific pollination arrest (Alves et al., 2019). This study suggests that divergence of the N-terminus domain in PELPIII may be a mechanism for reproductive isolation in the *Nicotiana* genus.

1.4.2. Pollen Tube Growth

Pollen tube elongation occurs in a polarized manner: continuous secretion of new cell wall materials and plasma membrane to a focused point allows tube elongation. Pollen tubes are the fastest tip-growing cells in nature, reaching up to ~12 mm per hour in species like maize (House & Nelson, 1958). Such fast growth requires the coordination of intracellular dynamics (i.e., targeted secretion, cytoskeleton organization) and cell wall assembly. Proper assembly of the wall is crucial to maintain cell shape and resist turgor pressure while simultaneously allowing extensibility at the elongating tip. In Arabidopsis, several chimeric HRGPs had been implicated in different pathways that regulate pollen tube integrity and establishment/maintenance of polarity. The functions of these proteins will be reviewed next.

1.4.2.1. Leucine-rich Repeat Extensins (LRXs)

The protein structure of LRXs consists in a Leu-rich C-terminus domain and a variable EXT-like N-terminus domain joined by a Cys-rich region. In Arabidopsis, the LRX family is composed of 11 members, where 4 of them are expressed in pollen (LRX8-11) (Baumberger et al., 2003). Loss of function of LRX8-11 causes a severe reduction of seed set due to defective pollen

germination (Fabrice et al., 2018). *lrx* mutant pollen tubes also exhibit abnormal deposition of cell wall polymers (Sede et al., 2018). LRXs do not possess a membrane anchoring signal but they localize to the plasma membrane and cell wall (Fabrice et al., 2018). Genetic, biochemical, and structural studies has shown that LRXs interact with secreted peptides Rapid Alkalinization Factors (RALFs) to regulate pollen tube integrity (Mecchia et al., 2017; Moussu et al., 2020). RALF peptides are known to bind a family of Receptor-like Kinases (CrRLK1L, *Cr* for *Catharanthus roseus*, where they were first characterized – Schulze-Muth et al., 1996). ANXUR1/2 and Buddha's Paper Seal 1/2 (BUPS1/2) are members of CrRLK1L family and their binding to RALF4/19 peptides regulates the maintenance of pollen tube integrity and, once in contact with a receptive ovule, mediate pollen tube disintegration to allow discharge of the sperm cells for fertilization (Ge et al., 2019). RALF4/19 also bind to pollen LRXs, and structural studies indicate that binding affinity to LRXs or ANX-BUPS receptors depends on redox state induced conformational changes in the structure of RALFs (Moussu et al., 2020). LRX-RALF4 interaction was shown to have a negative effect in pollen germination and elongation (Covey et al., 2010). How the same ligand RALF4/19 regulate BUPS-ANX and LRX function and whether these pathways converge in the regulation of pollen tube growth and integrity remains to be determined. Structural studies of LRXs indicate that the LRR domain mediates binding to RALF peptides, and this binding potentially induces conformational changes in its EXT domain. Additionally, when RALF4 is bound to LRX, it adopts a conformational change that exposes basic residues, which the authors speculated, could serve as an interaction surface for acidic cell wall components (i.e., pectins) and/or other cell surface proteins (Moussu et al., 2020). The functional significance of the EXT domain in LRX remains to be determined, however, it has been speculated that it might act as an anchor to the cell wall (Ge et al., 2019).

1.4.2.2. Proline-rich Extensin-like Receptor Kinases (PERKs)

PERKs are transmembrane proteins with an intracellular kinase domain and extracellular EXT-like glycosylation motifs. The PERK family in Arabidopsis is composed of 15 members (PERK1-15). Seven members of the PERK family (PERK3-7,11-12) are expressed in pollen tubes (Nakhamchik et al., 2004). Genetic studies showed that PERK5 and PERK12 are necessary for proper pollen tube growth. Loss of function alleles *perk5-1* and *perk12-1* and the double mutant *perk5-1 perk12-1* exhibit reduced seed set due to pollen tube growth defects, specifically, reduced growth rate due to altered distribution of cell wall polysaccharides as well as altered ROS homeostasis (Borassi et al., 2021). How PERKs regulate cell wall assembly and ROS homeostasis is unknown and potential downstream players of PERKs are yet to be identified. The EXT motifs present in the extracellular domain of PERKs are thought to act as sensors of the EXT-pectin network in the cell wall, although experimental evidence is still lacking (Borassi et al., 2016; Marzol et al., 2018).

1.4.2.3. Class I Formin Homology Proteins (FHs)

The class I Formin Homology (FH) family in Arabidopsis is composed of 11 members. Class I FH proteins are characterized by the presence of FH1 and FH2 domains, a transmembrane domain and a Pro-rich extracellular domain (ECD) akin to HRGPs (Borassi et al., 2016; Cvrčková, 2013; Cvrčková et al., 2004). The FH2 domain dimer participate in the nucleation of actin filaments, while the FH1 domain binds to profilin-actin complexes, enhancing the rate of actin nucleation/elongation (Paul et al., 2008). The activity of several members of the FH family in Arabidopsis has been characterized *in vitro*, however, little is known about the mechanisms that regulate their activity (Gisbergen & Bezanilla, 2013). FH proteins are widely expressed

across tissues, during development and induced upon biotic stress (Cvrčková et al., 2004). Most studies of FH proteins in Arabidopsis have focused on actin related functions, among the best characterized members of the family are AtFH1, AtFH3 and AtFH5. AtFH1 is ubiquitously expressed and exhibits i*n vitro* actin nucleating and bundling activity (Banno & Chua, 2000; Michelot et al., 2005). Under normal conditions, AtFH1 loss of function alleles displayed no apparent phenotype; however, plants exhibited increased sensitivity to Latrunculin B, an inhibitor of actin polymerization as well as treatment with Oryzalin, an herbicide that disrupts microtubule polymerization. These results suggested that, in addition to its activity as an actin nucleator, AtFH1 also regulates microtubule dynamics (Rosero et al., 2013), although this mechanism might be indirect since AtFH1 does not co-localize with microtubules (Martinière et al., 2011) . Moderate expression of AtFH1 in *N. tobaccum* pollen tubes stimulated pollen tube growth, while its overexpression induced supernumerary actin cable formation, arresting polarized growth supporting its actin-nucleation activity *in vivo* (Cheung & Wu, 2004). The ECD of AtFH1 was reported to establish direct interaction with the cell wall, confining the protein to specific plasma membrane domains (Martinière et al., 2011).

AtFH5 is expressed in vegetative tissues as well as in pollen grains and pollen tubes. GFP fused AtFH5 localized to the forming cell plate during cytokinesis and, consistent with its localization pattern, the loss of function allele exhibited defects in cell division in the endosperm (Ingouff et al., 2005). Later studies demonstrated that AtFH5 exhibits a polar localization in elongating pollen tubes (restricted to the elongating tip) and genetic studies demonstrated its function regulating actin dynamics during tip growth (Cheung et al., 2010; Lan et al., 2018).

In pollen tubes, actin is organized into three functionally distinct subarrays: 1) thick actin bundles disposed along the axis of growth, important for the cyclic motion of large organelles and cytoplasmic streaming, 2) the subapical actin collar, made of finer actin filaments and thought to be important to maintain cytoplasmic zonation and the apical area enriched in secretory vesicles, and 3) fine, highly dynamic apical actin that is presumed to serve as a pool for the formation of the subapical actin collar (Qu et al., 2015). RNAi mediated knockdown of the *N. tobaccum* AtFH5 homolog in pollen tubes, NtFH5, caused a significant decrease in apical actin, as well as wavy pollen tubes (meandering) and disruption of the typical cytoplasmic organization (Cheung et al., 2010). Analysis of T-DNA insertion mutants in Arabidopsis showed a milder phenotype compared to the study by Cheung et. al (2010); the authors reported a significant reduction in germination, growth rate and decreased accumulation of apical actin (Lan et al., 2018). AtFH5 also functions during pollen germination, propelling vesicles in the cytoplasm and eventually translocating to the plasma membrane to form an actin collar-like structure where the pollen tube will emerge (Liu et al., 2018). More recently, the same group showed that AtFH5 acts in conjunction with pollen-expressed profilins PRF4 and PRF5 during the formation of the actin collar-like structure in pollen grains (Liu et al., 2021).

AtFH3 is specifically expressed in pollen. Overexpression of AtFH3 induced thickening of axial actin cables in elongating pollen tubes, while AtFH3 downregulation induced pollen tube widening, shortening, tip swelling and disruption of the cytoplasmic streaming (Ye et al., 2009). Like the T-DNA insertion line disrupting AtFH5, the phenotype of AtFH3's loss of function allele was mild, showing a reduction in germination, growth rate and accumulation of apical actin as well as altered cytoplasmic streaming (Lan et al., 2018). In the same study, phenotypic

analysis of the double mutant *fh3-1 fh5-2* showed more drastic defects compared to the single mutants; however, pollen fertility was not completely abolished, suggesting possible genetic redundancy among the members of the family or other possible mechanisms regulating actin nucleation yet to be described.

Beyond the study by Martinière et al., (2011), our functional understanding of the ECD of class I formins is limited. The HRGP motifs in the ECD of AtFH1 were implicated in its association to the wall, although the mechanism is yet unclear. Since the ECD of AtFH1 contains EXT-like motifs, it has been speculated that, like PERKs, it may interact with the EXT-pectin network, possibly establishing a cell wall sensing mechanism (Borassi et al., 2016; Marzol et al., 2018).

1.4.3. Ovular Targeting

Once pollen tubes have traversed the transmitting tract, they must abruptly redirect their growth to target receptive ovules, specifically the embryo sac. To date, a number of molecules, including nitric oxide (Prado et al., 2008), Defensin-like secreted peptides (LUREs —Okuda et al., 2009), γ-aminobutyric acid (GABA) (Palanivelu et al., 2003), have been implicated in pollen tube guidance. Similarly, members of the HRGP family, primarily AGP and AGP-like proteins had been reported to participate in this process. In the embryo sac, specialized cells known as synergids secrete LURE peptides, which serve as pollen tube attractants (Okuda et al., 2009). An ovular-produced arabinogalactan polysaccharide, 4-*O*-methyl-glucuronosyl arabinogalactan (AMOR) is necessary to render pollen tubes competent to respond to LURE attractants (Mizukami et al., 2016). AMOR is presumably derived from the side chains of AGPs, which pave the path of pollen tubes through the pistil (Dresselhaus & Coimbra, 2016). Accumulation of AGP glycans has been reported in distinct tissues in the ovary, including the micropyle, an

orifice in the ovule through which the pollen tube penetrates for fertilization; the synergid cells in the embryo sac; the funiculus, a connective tissue between the embryo sac and the placenta in the ovary and the ovule integuments (Coimbra et al., 2008; Lara-Mondragón & MacAlister, 2021; Losada & Herrero, 2012). A group of AGP chimeric proteins has been implicated in this stage of pollen-pistil interaction, the Early Nodulin-like Proteins (ENODLs).

ENODLs or ENs are predicted GPI-anchored proteins characterized by the presence of plastocyanin-like domains and AGP-like glycosylation motifs. The EN family is composed of 22 members in Arabidopsis (Mashiguchi et al., 2009), from which five are highly expressed in female tissues (funiculus and ovules; *EN11-15*). Phylogenetic analyses revealed that EN11-15 are exclusive to the angiosperm clade, suggesting their involvement in angiosperm specific processes such as pollen-pistil interaction. ENs accumulate in the surface of synergid cells. Disruption of the expression of all female-expressed ENs (*EN11-15*) lead to ovule abortion and partial defects in ovule targeting (i.e., pollen tube overgrowth and rupture failure). EN14 was reported to interact with FERONIA (FER), a plasma membrane localized receptor kinase previously implicated in controlling pollen tube reception (Escobar-Restrepo et al., 2007), thus possibly participating in FER-mediated signaling pathways during pollen-pistil interaction (Hou et al., 2016).

Due to the presence of plastocyanin-like domains, ENs are classified as a subclass of phytocyanins. Phytocyanins are small-secreted proteins known to mediate electron transfer during redox reactions (Nersissian et al., 1998). Overexpression of a member of the phytocyanin family in Arabidopsis displayed defects in pollen behavior such as pollen tube meandering and

growth arrest (Dong et al., 2005); suggesting a role for this family in pollen guidance. The AGP motifs in ENs had not been studied; however, since both ENs and canonical AGPs are GPI-anchored, it has been hypothesized that they may also act as diffusible signals (Hou et al., 2016). How the phytocyanin domains and AGP glycosylation motifs function in this family is currently unknown.

1.4.4. Gametophyte Development

In addition to the processes discussed above, several reports indicate that non-canonical HRGPs also participate in reproductive development. In particular, the Fasciclin-like AGP (FLA) family has been associated to male gametophyte development. RNAseq analysis in Arabidopsis and tomato, indicate that members of the FLA family exhibit enriched expression in mature pistil tissues (in Arabidopsis, *AtFLA8* and *AtFLA10* — Costa et al., 2019; in tomato, *SlyFLA9* — (Lara-Mondragón & MacAlister, 2021); however, further dissection of the function of these genes is necessary.

FLAs are characterized by the presence of at least one Fasciclin domain (FAS1) and AGP-like glycomotifs, as well as a GPI-anchor in some cases. FAS1 proteins were initially identified as cell surface proteins with presumed roles in the formation of axon bundles or fascicles in grasshopper (Bastiani et al., 1987). Targeted thermal denaturation of Fas1 in the same model led to disruption in axon adhesion during neural development (Jay & Keshishian, 1990). FAS1 proteins in mammals have been confirmed to participate in cell-cell and cell-extracellular matrix adhesion (Seifert, 2018). In mammals, FAS1 proteins are known to bind Integrins, a family of cell surface receptors that mediate crosstalk between the cytoskeleton and extracellular matrix (Takada et al., 2007). No true homologs of the Integrin family had been identified in plants

(Whittaker & Hynes, 2002), thus crosstalk between these structures is mediated by different proteins, possibly class I formins. Based on the reports regarding the function of FAS1 proteins in animals, FLAs in plants might share a role for cell-adhesion, however no functional studies had been reported to date.

Genetic studies in Arabidopsis and rice demonstrated distinct functions for FLA genes during pollen development. Broadly, pollen development can be divided in three stages: 1) differentiation of the microspore (pollen) mother cells and meiosis, 2) post-meiotic development of the microspore and 3) microspore mitosis. In the first stage, the microspore mother cell undergoes meiosis to form haploid microspore tetrads. The microspore mother cell synthesizes a callose layer prior to tetrad formation to separate and protect the developing microspores. The callose wall is a transient structure that is degraded later in development; however, it serves as a scaffold for the assembly of additional polymer layers in the pollen grain (intine and exine). Free microspores go through one or two rounds of cell division (depending on the species) while the pollen grain wall continues to form. The tapetum, a cell layer lining the anther cavity plays an essential during this process by coordinating developmental transitions as well as secreting material for pollen wall formation (Gómez et al., 2015; Wilson & Zhang, 2009). In Arabidopsis, AtFLA3 is a GPI-anchored protein enriched in pollen grains and tubes. RNAi induced silencing of *AtFLA3* resulted in partial pollen abortion, defect occurring during the transition from uninucleate microspores to bicellular pollen. Closer examination of pollen morphology revealed defects in the intine layer, possibly due to abnormal cellulose accumulation. In this study, overexpression of *AtFLA3* also led to reduced seed set and anther abnormalities (Li et al., 2010). More recently, another member of the FLA family in Arabidopsis, *AtFLA14* was reported to

function during pollen development. The knockout mutant *fla14* did not show any apparent phenotype under normal conditions; however, high humidity conditions induced premature pollen germination inside the anthers. Overexpression of *AtFLA14*, on the other hand, led to shrunken pollen grains, defect also associated to the uninucleate microspore stage. Deposition of intine was abolished in abnormal pollen grains while apparently 'normal' pollen grains exhibited thickened intine layers (Miao et al., 2021). Transcriptomic analysis of members of the FLA family in Arabidopsis in male tissues suggests a temporal control of expression, where six different FLA genes (*AtFLA21*, *AtFLA20*, *At5g16920*, *AtFLA5*, *AtFLA14*, *AtFLA3*; sorted from early to late stages of development) act sequentially during male gametophyte development (Seifert, 2018).

In rice, a loss of function allele derived from EMS mutagenesis, *osfla1*, like Arabidopsis, exhibited abnormalities during pollen development. *osfla1* mutants were vegetatively normal but displayed reduced seed set due to pollen abortion. In rice, free microspores undergo two rounds of mitosis prior to anther dehiscence (mature pollen is tricellular when released). By the second cell division, the tapetal layer is degenerated. Inspection of *osfla1* mutants revealed that that tapetal layer thickening and degeneration failure correlated with microspore collapse (Deng et al., 2022).

1.5. Thesis Overview

Although a considerable amount of work has been directed at deciphering the function of the HRGP family, the mechanisms by which most members of the family operate, especially non-canonical HRGPs, remain elusive. As evidenced throughout this first chapter, the study of

HRGPs represents several challenges. First, it is common to observe no phenotypic effects when studying loss of function of members of this family. This phenomenon is often related to genetic redundancy, thus, requiring the generation of higher order mutants. Currently, the use of CRISPR-Cas9 has been proven useful to shorten the generation time of higher order mutants, as shown by Zhang et al., (2021) where knockout of five members of the GALT family (*GALT2-6*) were generated to disrupt AGP glycosylation. Secondly, HRGP *O*-glycosylation is a plant specific modification, consequently limiting the number of biochemical tools for their study. While available, the use of plant expression systems requires specific considerations compared to bacterial protein expression systems. In the second chapter, the development of a protocol for protein expression in a plant system, partial purification through metal affinity chromatography and detection of *O*-glycosylation is described. The protocol in chapter two was developed to address a currently unanswered, fundamental question regarding the function of the HRGP family: are non-canonical HRGPs post translationally modified?

The third chapter of this thesis explores the later question while focusing on a family of HRGP chimeric proteins, AtFH3 and AtFH5, thought to participate in polarized growth in pollen tubes as actin nucleation factors. This work investigated the functional significance of the extracellular domain (ECD) of these proteins, which contain HRGP-like motifs of two different subgroups, AGPs and EXTs, respectively. We provide genetic and biochemical evidence for *O*-glycosylation in AtFH3 and AtFH5 as well as evidence the effects of such posttranslational modifications in their respective subcellular localization. This study not only provide evidence for the first time that chimeric HRGPs are modified like canonical members of the family, but also sheds light on the diversity of functions across the family: class I formins AtFH3 and AtFH5

act as molecular linkers between the actin cytoskeleton and the cell wall during pollen tube growth, a crucial process for successful fertilization in angiosperms.

Lastly, in the fourth chapter, we explore another key aspect of reproductive biology: pistil mediated pollen guidance. The pistil plays an active role in recognizing compatible pollen and providing a rich environment for its growth as well as guidance cues to ensure fertilization. HRGPs, particularly AGPs, had been implicated throughout this process in different species. Although tomato is an agronomically relevant species, our understanding of fertilization, a process crucial for fruit production, is poorly understood. Combining immunological techniques with high throughput mRNA sequencing, we identified a subpopulation of AGPs, that localize specifically to the micropyle of unfertilized ovules as well as members of the AGP family with enriched expression in these tissues, setting the basis for future functional studies.

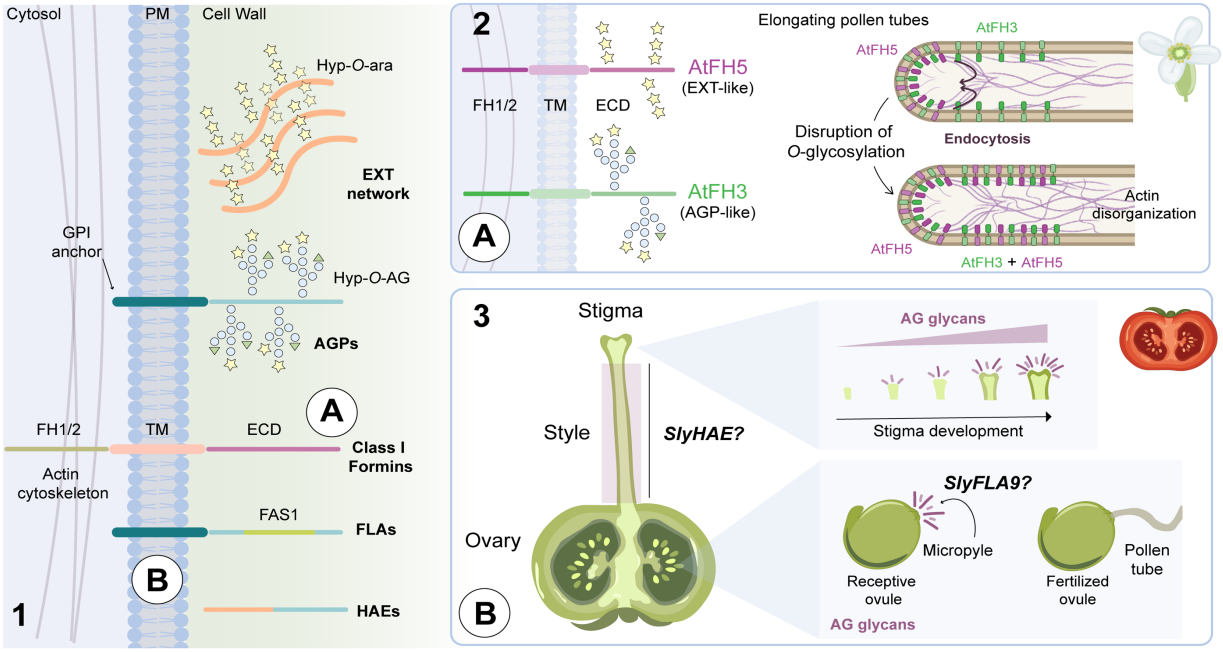

Figure 1-1 Thesis overview.

1) *Classification of the HRGP family*. Canonical members of the HRGP family are Extensins (EXTs) and Arabinogalactan glycoproteins (AGPs). EXTs are *O*-arabinosylated (Hyp-*O*-ara) and once secreted to the apoplast, self-assemble forming a network that serve as scaffold for pectin assembly. Canonical AGPs bear *O*-arabinogalactan glycans (Hyp-*O*-AG) and are often associated to the plasma membrane (PM) by GPI anchors. Non canonical members of the HRGP family investigated in this thesis are shown in the bottom: Class I formins, Fasciclin-like Arabinogalactan glycoproteins (FLAs) and Hybrid AGP-EXTs (HAEs). Class I formins (AtFHs) are transmembrane proteins (TM) with intracellular Formin Homology 1 and 2 domains (FH1/2) and extracellular domains (ECD) with HRGP-like motifs. Two members of this family AtFH3 and AtFH5 were studied in the context of pollen tube growth in *Arabidopsis thaliana* (A). FLAs, have Fasciclin 1-like domains (FAS1). The role of both FLAs and HAEs during pistil development and pollen-pistil interaction were investigated in tomato (B). **2)** *Summary of findings of Chapter 3*. Pollen expressed class I formins (AtFH5 and AtFH3) exhibit different localization patterns in elongating pollen tubes. The ECD of both AtFH3 and AtFH5 is necessary for proper PM localization. The ECDs of AtFH3 and AtFH5 contain distinct HRGP-like motifs. These motifs are *O*-glycosylated and disruption of the HRGP glycosylation pathway causes abnormalities in plasma membrane localization and actin disorganization in pollen tubes. **3)** *Summary of findings in Chapter 4*. Tomato pistils accumulate AGPs upon reaching a mature, receptive stage. Progressive accumulation of AGPs in the stigma surface occur as the pistil becomes mature (anthesis). In unfertilized ovules, accumulation of AGP glycans in the micropyle. Micropylar AGP accumulation dissipated after pollen contact. Analysis of AGP gene expression identified two members of the family with enriched expression in the style: *SlyHAE*, an AGP-EXT hybrid highly expressed in the style and *SlyFLA9*, a Fasciclin-like AGP with enriched expression in the ovary.

1.6. References

Abedi, T., Castilleux, R., Nibbering, P., & Niittylä, T. (2020). The Spatio-Temporal Distribution of Cell Wall-Associated Glycoproteins During Wood Formation in Populus. *Frontiers in Plant Science*, *11*. https://www.frontiersin.org/article/10.3389/fpls.2020.611607

Albenne, C., Canut, H., Hoffmann, L., & Jamet, E. (2014). Plant Cell Wall Proteins: A Large Body of Data, but What about Runaways? *Proteomes*, *2*(2), 224–242. https://doi.org/10.3390/proteomes2020224

Alves, C. M. L., Noyszewski, A. K., & Smith, A. G. (2019). Structure and function of class III pistil-specific extensin-like protein in interspecific reproductive barriers. *BMC Plant Biology*, *19*(1), 118. https://doi.org/10.1186/s12870-019-1728-8

Anderson, C. T., & Kieber, J. J. (2020). Dynamic Construction, Perception, and Remodeling of Plant Cell Walls. *Annual Review of Plant Biology*, *71*(1), 39–69. https://doi.org/10.1146/annurev-arplant-081519-035846

Bastiani, M. J., Harrelson, A. L., Snow, P. M., & Goodman, C. S. (1987). Expression of fasciclin I and II glycoproteins on subsets of axon pathways during neuronal development in the grasshopper. *Cell*, *48*(5), 745–755. https://doi.org/10.1016/0092-8674(87)90072-9

Baumberger, N., Doesseger, B., Guyot, R., Diet, A., Parsons, R. L., Clark, M. A., Simmons, M. P., Bedinger, P., Goff, S. A., Ringli, C., & Keller, B. (2003). Whole-Genome Comparison of Leucine-Rich Repeat Extensins in Arabidopsis and Rice. A Conserved Family of Cell Wall Proteins Form a Vegetative and a Reproductive Clade,. *Plant Physiology*, *131*(3), 1313–1326. https://doi.org/10.1104/pp.102.014928

Bernhardt, C., & Tierney, M. L. (2000). Expression of AtPRP3, a Proline-Rich Structural Cell Wall Protein from Arabidopsis, Is Regulated by Cell-Type-Specific Developmental Pathways Involved in Root Hair Formation1. *Plant Physiology*, *122*(3), 705–714. https://doi.org/10.1104/pp.122.3.705

Borassi, C., Sede, A. R., Mecchia, M. A., Mangano, S., Marzol, E., Denita-Juarez, S. P., Salgado Salter, J. D., Velasquez, S. M., Muschietti, J. P., & Estevez, J. M. (2021). Proline-rich extensin-like receptor kinases PERK5 and PERK12 are involved in pollen tube growth. *FEBS Letters*, *595*(20), 2593–2607. https://doi.org/10.1002/1873-3468.14185

Bosch, M., Knudsen, J. S., Derksen, J., & Mariani, C. (2001). Class III Pistil-Specific Extensin-Like Proteins from Tobacco Have Characteristics of Arabinogalactan Proteins. *Plant Physiology*, *125*(4), 2180–2188. https://doi.org/10.1104/pp.125.4.2180

Bringmann, M., Landrein, B., Schudoma, C., Hamant, O., Hauser, M.-T., & Persson, S. (2012). Cracking the elusive alignment hypothesis: The microtubule–cellulose synthase nexus unraveled. *Trends in Plant Science*, *17*(11), 666–674. https://doi.org/10.1016/j.tplants.2012.06.003

Cannon, M. C., Terneus, K., Hall, Q., Tan, L., Wang, Y., Wegenhart, B. L., Chen, L., Lamport, D. T. A., Chen, Y., & Kieliszewski, M. J. (2008). Self-assembly of the plant cell wall requires an extensin scaffold. *Proceedings of the National Academy of Sciences*, *105*(6), 2226–2231. https://doi.org/10.1073/pnas.0711980105

Chaves, I., Regalado, A. P., Chen, M., Ricardo, C. P., & Showalter, A. M. (2002). Programmed cell death induced by (β-d-galactosyl)3 Yariv reagent in Nicotiana tabacum BY-2 suspension-cultured cells. *Physiologia Plantarum*, *116*(4), 548–553. https://doi.org/10.1034/j.1399-3054.2002.1160414.x

Cheung, A. Y., & Wu, H. (2004). Overexpression of an Arabidopsis Formin Stimulates Supernumerary Actin Cable Formation from Pollen Tube Cell Membrane. *The Plant Cell*, *16*(1), 257–269. https://doi.org/10.1105/tpc.016550
Coimbra, S., Jones, B., & Pereira, L. G. (2008). Arabinogalactan proteins (AGPs) related to pollen tube guidance into the embryo sac in Arabidopsis. *Plant Signaling & Behavior*, *3*(7), 455–456. https://doi.org/10.4161/psb.3.7.5601
Condamine, F. L., Silvestro, D., Koppelhus, E. B., & Antonelli, A. (2020). The rise of angiosperms pushed conifers to decline during global cooling. *Proceedings of the National Academy of Sciences*, *117*(46), 28867–28875. https://doi.org/10.1073/pnas.2005571117
Costa, M., Pereira, A. M., Pinto, S. C., Silva, J., Pereira, L. G., & Coimbra, S. (2019). In silico and expression analyses of fasciclin-like arabinogalactan proteins reveal functional conservation during embryo and seed development. *Plant Reproduction*, *32*(4), 353–370. https://doi.org/10.1007/s00497-019-00376-7
Covey, P. A., Subbaiah, C. C., Parsons, R. L., Pearce, G., Lay, F. T., Anderson, M. A., Ryan, C. A., & Bedinger, P. A. (2010). A Pollen-Specific RALF from Tomato That Regulates Pollen Tube Elongation. *Plant Physiology*, *153*(2), 703–715. https://doi.org/10.1104/pp.110.155457
Creelman, R. A., & Mullet, J. E. (1991). Water deficit modulates gene expression in growing zones of soybean seedlings. Analysis of differentially expressed cDNAs, a new β-tubulin gene, and expression of genes encoding cell wall proteins. *Plant Molecular Biology*, *17*(4), 591–608. https://doi.org/10.1007/BF00037046
Crepet, W. L., & Niklas, K. J. (2009). Darwin's second "abominable mystery": Why are there so many angiosperm species? *American Journal of Botany*, *96*(1), 366–381. https://doi.org/10.3732/ajb.0800126
Cvrčková, F. (2013). Formins and membranes: Anchoring cortical actin to the cell wall and beyond. *Frontiers in Plant Science*, *4*. https://www.frontiersin.org/article/10.3389/fpls.2013.00436
Cvrčková, F., Novotný, M., Pícková, D., & Žárský, V. (2004). Formin homology 2 domains occur in multiple contexts in angiosperms. *BMC Genomics*, *5*(1), 44. https://doi.org/10.1186/1471-2164-5-44
Deng, Y., Wan, Y., Liu, W., Zhang, L., Zhou, K., Feng, P., He, G., & Wang, N. (2022). OsFLA1 encodes a fasciclin-like arabinogalactan protein and affects pollen exine development in rice. *Theoretical and Applied Genetics*. https://doi.org/10.1007/s00122-021-04028-1
Dilokpimol, A., Poulsen, C. P., Vereb, G., Kaneko, S., Schulz, A., & Geshi, N. (2014). Galactosyltransferases from Arabidopsis thaliana in the biosynthesis of type II arabinogalactan: Molecular interaction enhances enzyme activity. *BMC Plant Biology*, *14*(1), 90. https://doi.org/10.1186/1471-2229-14-90
Dong, J., Kim, S. T., & Lord, E. M. (2005). Plantacyanin Plays a Role in Reproduction in Arabidopsis. *Plant Physiology*, *138*(2), 778–789. https://doi.org/10.1104/pp.105.063388
Dresselhaus, T., & Coimbra, S. (2016). Plant Reproduction: AMOR Enables Males to Respond to Female Signals. *Current Biology*, *26*(8), R321–R323. https://doi.org/10.1016/j.cub.2016.03.019
Duruflé, H., Hervé, V., Balliau, T., Zivy, M., Dunand, C., & Jamet, E. (2017). Proline Hydroxylation in Cell Wall Proteins: Is It Yet Possible to Define Rules? *Frontiers in Plant Science*, *8*. https://www.frontiersin.org/article/10.3389/fpls.2017.01802
Escobar-Restrepo, J.-M., Huck, N., Kessler, S., Gagliardini, V., Gheyselinck, J., Yang, W.-C., & Grossniklaus, U. (2007). The FERONIA Receptor-like Kinase Mediates Male-Female

Interactions During Pollen Tube Reception. *Science*, *317*(5838), 656–660. https://doi.org/10.1126/science.1143562
Fabrice, T. N., Vogler, H., Draeger, C., Munglani, G., Gupta, S., Herger, A. G., Knox, P., Grossniklaus, U., & Ringli, C. (2018). LRX Proteins Play a Crucial Role in Pollen Grain and Pollen Tube Cell Wall Development. *Plant Physiology*, *176*(3), 1981–1992. https://doi.org/10.1104/pp.17.01374
Gao, M., & Showalter, A. M. (2000). Immunolocalization of LeAGP-1, a modular arabinogalactan-protein, reveals its developmentally regulated expression in tomato. *Planta*, *210*(6), 865–874. https://doi.org/10.1007/s004250050691
Ge, Z., Cheung, A. Y., & Qu, L.-J. (2019). Pollen tube integrity regulation in flowering plants: Insights from molecular assemblies on the pollen tube surface. *New Phytologist*, *222*(2), 687–693. https://doi.org/10.1111/nph.15645
Geshi, N., Johansen, J. N., Dilokpimol, A., Rolland, A., Belcram, K., Verger, S., Kotake, T., Tsumuraya, Y., Kaneko, S., Tryfona, T., Dupree, P., Scheller, H. V., Höfte, H., & Mouille, G. (2013). A galactosyltransferase acting on arabinogalactan protein glycans is essential for embryo development in Arabidopsis. *The Plant Journal*, *76*(1), 128–137. https://doi.org/10.1111/tpj.12281
Gómez, J. F., Talle, B., & Wilson, Z. A. (2015). Anther and pollen development: A conserved developmental pathway. *Journal of Integrative Plant Biology*, *57*(11), 876–891. https://doi.org/10.1111/jipb.12425
Gorelova, V., Sprakel, J., & Weijers, D. (2021). Plant cell polarity as the nexus of tissue mechanics and morphogenesis. *Nature Plants*, *7*(12), 1548–1559. https://doi.org/10.1038/s41477-021-01021-w
Gothandam, K. M., Nalini, E., Karthikeyan, S., & Shin, J. S. (2009). OsPRP3, a flower specific proline-rich protein of rice, determines extracellular matrix structure of floral organs and its overexpression confers cold-tolerance. *Plant Molecular Biology*, *72*(1), 125. https://doi.org/10.1007/s11103-009-9557-z
Grosberg, R. K., & Strathmann, R. R. (2007). The Evolution of Multicellularity: A Minor Major Transition? *Annual Review of Ecology, Evolution, and Systematics*, *38*(1), 621–654. https://doi.org/10.1146/annurev.ecolsys.36.102403.114735
Haas, K. T., Wightman, R., Peaucelle, A., & Höfte, H. (2021). The role of pectin phase separation in plant cell wall assembly and growth. *The Cell Surface*, *7*, 100054. https://doi.org/10.1016/j.tcsw.2021.100054
Hall, Q., & Cannon, M. C. (2002). The Cell Wall Hydroxyproline-Rich Glycoprotein RSH Is Essential for Normal Embryo Development in Arabidopsis. *The Plant Cell*, *14*(5), 1161–1172. https://doi.org/10.1105/tpc.010477
Harholt, J., Suttangkakul, A., & Vibe Scheller, H. (2010). Biosynthesis of Pectin1. *Plant Physiology*, *153*(2), 384–395. https://doi.org/10.1104/pp.110.156588
Herger, A., Dünser, K., Kleine-Vehn, J., & Ringli, C. (2019). Leucine-Rich Repeat Extensin Proteins and Their Role in Cell Wall Sensing. *Current Biology*, *29*(17), R851–R858. https://doi.org/10.1016/j.cub.2019.07.039
Höfte, H., Peaucelle, A., & Braybrook, S. (2012). Cell wall mechanics and growth control in plants: The role of pectins revisited. *Frontiers in Plant Science*, *3*, 121. https://doi.org/10.3389/fpls.2012.00121
House, L. R., & Nelson, O. E., JR. (1958). Tracer study of pollen tube growth cross-sterile maize. *Journal of Heredity*, *49*(1), 18–21. https://doi.org/10.1093/oxfordjournals.jhered.a106755

Houston, K., Tucker, M. R., Chowdhury, J., Shirley, N., & Little, A. (2016). The Plant Cell Wall: A Complex and Dynamic Structure As Revealed by the Responses of Genes under Stress Conditions. *Frontiers in Plant Science*, *7*, 984. https://doi.org/10.3389/fpls.2016.00984
Ingouff, M., Gerald, J. N. F., Guérin, C., Robert, H., Sørensen, M. B., Damme, D. V., Geelen, D., Blanchoin, L., & Berger, F. (2005). Plant formin AtFH5 is an evolutionarily conserved actin nucleator involved in cytokinesis. *Nature Cell Biology*, *7*(4), 374–380. https://doi.org/10.1038/ncb1238
Jamet, E., Albenne, C., Boudart, G., Irshad, M., Canut, H., & Pont-Lezica, R. (2008). Recent advances in plant cell wall proteomics. *PROTEOMICS*, *8*(4), 893–908. https://doi.org/10.1002/pmic.200700938
Jay, D. G., & Keshishian, H. (1990). Laser inactivation of fasciclin I disrupts axon adhesion of grasshopper pioneer neurons. *Nature*, *348*(6301), 548–550. https://doi.org/10.1038/348548a0
Jiao, H., Liu, X., Sun, S., Wang, P., Qiao, X., Li, J., Tang, C., Wu, J., Zhang, S., & Tao, S. (2018). The unique evolutionary pattern of the Hydroxyproline-rich glycoproteins superfamily in Chinese white pear (Pyrus bretschneideri). *BMC Plant Biology*, *18*(1), 36. https://doi.org/10.1186/s12870-018-1252-2
Josè-Estanyol, M., & Puigdomènech, P. (2000). Plant cell wall glycoproteins and their genes. *Plant Physiology and Biochemistry*, *38*(1), 97–108. https://doi.org/10.1016/S0981-9428(00)00165-0
Knox, J. P. (1997). The use of Antibodies to Study the Architecture and Developmental Regulation of Plant Cell Walls. In K. W. Jeon (Ed.), *International Review of Cytology* (Vol. 171, pp. 79–120). Academic Press. https://doi.org/10.1016/S0074-7696(08)62586-3
Lamport, D. T. A., Kieliszewski, M. J., & Showalter, A. M. (2006). Salt stress upregulates periplasmic arabinogalactan proteins: Using salt stress to analyse AGP function*. *New Phytologist*, *169*(3), 479–492. https://doi.org/10.1111/j.1469-8137.2005.01591.x
Lannoo, N., & Van Damme, E. J. M. (2014). Lectin domains at the frontiers of plant defense. *Frontiers in Plant Science*, *5*, 397. https://doi.org/10.3389/fpls.2014.00397
Lara-Mondragón, C. M., & MacAlister, C. A. (2021). Arabinogalactan glycoprotein dynamics during the progamic phase in the tomato pistil. *Plant Reproduction*. https://doi.org/10.1007/s00497-021-00408-1
Lee, J.-H., Waffenschmidt, S., Small, L., & Goodenough, U. (2007). Between-Species Analysis of Short-Repeat Modules in Cell Wall and Sex-Related Hydroxyproline-Rich Glycoproteins of *Chlamydomonas*. *Plant Physiology*, *144*(4), 1813–1826. https://doi.org/10.1104/pp.107.100891
Levesque-Tremblay, G., Pelloux, J., Braybrook, S. A., & Müller, K. (2015). Tuning of pectin methylesterification: Consequences for cell wall biomechanics and development. *Planta*, *242*(4), 791–811. https://doi.org/10.1007/s00425-015-2358-5
Li, J., Yu, M., Geng, L.-L., & Zhao, J. (2010). The fasciclin-like arabinogalactan protein gene, FLA3, is involved in microspore development of Arabidopsis. *The Plant Journal*, *64*(3), 482–497. https://doi.org/10.1111/j.1365-313X.2010.04344.x
Liu, X., McKenna, S., Welch, L. R., & Showalter, A. M. (2020). Bioinformatic Identification of Plant Hydroxyproline-Rich Glycoproteins. In Z. A. Popper (Ed.), *The Plant Cell Wall: Methods and Protocols* (pp. 463–481). Springer. https://doi.org/10.1007/978-1-0716-0621-6_26
Lopez-Hernandez, F., Tryfona, T., Rizza, A., Yu, X. L., Harris, M. O. B., Webb, A. A. R., Kotake, T., & Dupree, P. (2020). Calcium Binding by Arabinogalactan Polysaccharides Is Important for Normal Plant Development. *The Plant Cell*, *32*(10), 3346–3369. https://doi.org/10.1105/tpc.20.00027

Marzol, E., Borassi, C., Bringas, M., Sede, A., Rodríguez Garcia, D. R., Capece, L., & Estevez, J. M. (2018). Filling the Gaps to Solve the Extensin Puzzle. *Molecular Plant*, *11*(5), 645–658. https://doi.org/10.1016/j.molp.2018.03.003
Mashiguchi, K., Asami, T., & Suzuki, Y. (2009). Genome-Wide Identification, Structure and Expression Studies, and Mutant Collection of 22 Early Nodulin-Like Protein Genes in Arabidopsis. *Bioscience, Biotechnology, and Biochemistry*, *73*(11), 2452–2459. https://doi.org/10.1271/bbb.90407
Mecchia, M. A., Santos-Fernandez, G., Duss, N. N., Somoza, S. C., Boisson-Dernier, A., Gagliardini, V., Martínez-Bernardini, A., Fabrice, T. N., Ringli, C., Muschietti, J. P., & Grossniklaus, U. (2017). RALF4/19 peptides interact with LRX proteins to control pollen tube growth in Arabidopsis. *Science*, *358*(6370), 1600–1603. https://doi.org/10.1126/science.aao5467
Miao, Y., Cao, J., Huang, L., Yu, Y., & Lin, S. (2021). FLA14 is required for pollen development and preventing premature pollen germination under high humidity in Arabidopsis. *BMC Plant Biology*, *21*(1), 254. https://doi.org/10.1186/s12870-021-03038-x
Michelot, A., Guérin, C., Huang, S., Ingouff, M., Richard, S., Rodiuc, N., Staiger, C. J., & Blanchoin, L. (2005). The Formin Homology 1 Domain Modulates the Actin Nucleation and Bundling Activity of Arabidopsis FORMIN1. *The Plant Cell*, *17*(8), 2296–2313. https://doi.org/10.1105/tpc.105.030908
Motose, H., Sugiyama, M., & Fukuda, H. (2004). A proteoglycan mediates inductive interaction during plant vascular development. *Nature*, *429*(6994), 873–878. https://doi.org/10.1038/nature02613
Moussu, S., Broyart, C., Santos-Fernandez, G., Augustin, S., Wehrle, S., Grossniklaus, U., & Santiago, J. (2020). Structural basis for recognition of RALF peptides by LRX proteins during pollen tube growth. *Proceedings of the National Academy of Sciences*, *117*(13), 7494–7503. https://doi.org/10.1073/pnas.2000100117
Nakhamchik, A., Zhao, Z., Provart, N. J., Shiu, S.-H., Keatley, S. K., Cameron, R. K., & Goring, D. R. (2004). A Comprehensive Expression Analysis of the Arabidopsis Proline-rich Extensin-like Receptor Kinase Gene Family using Bioinformatic and Experimental Approaches. *Plant and Cell Physiology*, *45*(12), 1875–1881. https://doi.org/10.1093/pcp/pch206
Nersissian, A. M., Immoos, C., Hill, M. G., Hart, P. J., Williams, G., Herrmann, R. G., & Valentine, J. S. (1998). Uclacyanins, stellacyanins, and plantacyanins are distinct subfamilies of phytocyanins: Plant-specific mononuclear blue copper proteins. *Protein Science: A Publication of the Protein Society*, *7*(9), 1915–1929. https://doi.org/10.1002/pro.5560070907
Nothnagel, E. A. (1997). Proteoglycans and Related Components in Plant Cells. In K. W. Jeon (Ed.), *International Review of Cytology* (Vol. 174, pp. 195–291). Academic Press. https://doi.org/10.1016/S0074-7696(08)62118-X
O'Neill, M. A., Ishii, T., Albersheim, P., & Darvill, A. G. (2004). RHAMNOGALACTURONAN II: Structure and Function of a Borate Cross-Linked Cell Wall Pectic Polysaccharide. *Annual Review of Plant Biology*, *55*(1), 109–139. https://doi.org/10.1146/annurev.arplant.55.031903.141750
Palanivelu, R., Brass, L., Edlund, A. F., & Preuss, D. (2003). Pollen Tube Growth and Guidance Is Regulated by POP2, an Arabidopsis Gene that Controls GABA Levels. *Cell*, *114*(1), 47–59. https://doi.org/10.1016/S0092-8674(03)00479-3
Paul, A. S., Paul, A., Pollard, T. D., & Pollard, T. (2008). The role of the FH1 domain and profilin in formin-mediated actin-filament elongation and nucleation. *Current Biology: CB*, *18*(1), 9–19. https://doi.org/10.1016/j.cub.2007.11.062

Pires, N. D., & Dolan, L. (2012). Morphological evolution in land plants: New designs with old genes. *Philosophical Transactions of the Royal Society B: Biological Sciences*, *367*(1588), 508–518. https://doi.org/10.1098/rstb.2011.0252
Popper, Z. A., Michel, G., Hervé, C., Domozych, D. S., Willats, W. G. T., Tuohy, M. G., Kloareg, B., & Stengel, D. B. (2011). Evolution and Diversity of Plant Cell Walls: From Algae to Flowering Plants. *Annual Review of Plant Biology*, *62*(1), 567–590. https://doi.org/10.1146/annurev-arplant-042110-103809
Prado, A. M., Colaço, R., Moreno, N., Silva, A. C., & Feijó, J. A. (2008). Targeting of Pollen Tubes to Ovules Is Dependent on Nitric Oxide (NO) Signaling. *Molecular Plant*, *1*(4), 703–714. https://doi.org/10.1093/mp/ssn034
Pu, J., Putnis, C. V., & Wang, L. (2021). AFM imaging and single-molecule recognition of plant cell walls. *Trends in Plant Science*. https://doi.org/10.1016/j.tplants.2021.11.010
Qin, L., Liu, L., Tu, J., Yang, G., Wang, S., Quilichini, T. D., Gao, P., Wang, H., Peng, G., Blancaflor, E. B., Datla, R., Xiang, D., Wilson, K. E., & Wei, Y. (2021). The ARP2/3 complex, acting cooperatively with Class I formins, modulates penetration resistance in Arabidopsis against powdery mildew invasion. *The Plant Cell*, *33*(9), 3151–3175. https://doi.org/10.1093/plcell/koab170
Robert Hooke. (1665). *Micrographia, or some physiological descriptions of minute bodies made by magnifying glasses, with observations and inquiries thereupon. By R. Hooke.* Printed by JoMartyn, and JaAllestry, printers to the Royal Society.
Rose, J. K., Saladié, M., & Catalá, C. (2004). The plot thickens: New perspectives of primary cell wall modification. *Current Opinion in Plant Biology*, *7*(3), 296–301. https://doi.org/10.1016/j.pbi.2004.03.013
Rosero, A., Žárský, V., & Cvrčková, F. (2013). AtFH1 formin mutation affects actin filament and microtubule dynamics in Arabidopsis thaliana. *Journal of Experimental Botany*, *64*(2), 585–597. https://doi.org/10.1093/jxb/ers351
Scheller, H. V., & Ulvskov, P. (2010). Hemicelluloses. *Annual Review of Plant Biology*, *61*(1), 263–289. https://doi.org/10.1146/annurev-arplant-042809-112315
Schulze-Muth, P., Irmler, S., Schröder, G., & Schröder, J. (1996). Novel Type of Receptor-like Protein Kinase from a Higher Plant (Catharanthus roseus): cDNA, gene, intramolecular autophosphorylation and identification of a threonine important for auto- and substrate phosphorylation. *Journal of Biological Chemistry*, *271*(43), 26684–26689. https://doi.org/10.1074/jbc.271.43.26684
Sede, A. R., Borassi, C., Wengier, D. L., Mecchia, M. A., Estevez, J. M., & Muschietti, J. P. (2018). Arabidopsis pollen extensins LRX are required for cell wall integrity during pollen tube growth. *FEBS Letters*, *592*(2), 233–243. https://doi.org/10.1002/1873-3468.12947
Seifert, G. J. (2018). Fascinating Fasciclins: A Surprisingly Widespread Family of Proteins that Mediate Interactions between the Cell Exterior and the Cell Surface. *International Journal of Molecular Sciences*, *19*(6), 1628. https://doi.org/10.3390/ijms19061628
Sexauer, M., Shen, D., Schön, M., Andersen, T. G., & Markmann, K. (2021). Visualizing polymeric components that define distinct root barriers across plant lineages. *Development*, *148*(23), dev199820. https://doi.org/10.1242/dev.199820
Sherrier, D. J., Taylor, G. S., Silverstein, K. A. T., Gonzales, M. B., & VandenBosch, K. A. (2005). Accumulation of extracellular proteins bearing unique proline-rich motifs in intercellular spaces of the legume nodule parenchyma. *Protoplasma*, *225*(1), 43–55. https://doi.org/10.1007/s00709-005-0090-x

Smith, G. P. (1976). Evolution of repeated DNA sequences by unequal crossover. *Science (New York, N.Y.)*, *191*(4227), 528–535. https://doi.org/10.1126/science.1251186
Sujeeth, N., Kini, R. K., Shailasree, S., Wallaart, E., Shetty, S. H., & Hille, J. (2012). Characterization of a hydroxyproline-rich glycoprotein in pearl millet and its differential expression in response to the downy mildew pathogen Sclerospora graminicola. *Acta Physiologiae Plantarum*, *34*(2), 779–791. https://doi.org/10.1007/s11738-011-0879-5
Sun, W., Zhao, Z. D., Hare, M. C., Kieliszewski, M. J., & Showalter, A. M. (2004). Tomato LeAGP-1 is a plasma membrane-bound, glycosylphosphatidylinositol-anchored arabinogalactan-protein. *Physiologia Plantarum*, *120*(2), 319–327. https://doi.org/10.1111/j.0031-9317.2004.0236.x
Takada, Y., Ye, X., & Simon, S. (2007). The integrins. *Genome Biology*, *8*(5), 215. https://doi.org/10.1186/gb-2007-8-5-215
Tameshige, T., Hirakawa, Y., Torii, K. U., & Uchida, N. (2015). Cell walls as a stage for intercellular communication regulating shoot meristem development. *Frontiers in Plant Science*, *6*, 324. https://doi.org/10.3389/fpls.2015.00324
Tan, L., Eberhard, S., Pattathil, S., Warder, C., Glushka, J., Yuan, C., Hao, Z., Zhu, X., Avci, U., Miller, J. S., Baldwin, D., Pham, C., Orlando, R., Darvill, A., Hahn, M. G., Kieliszewski, M. J., & Mohnen, D. (2013). An Arabidopsis Cell Wall Proteoglycan Consists of Pectin and Arabinoxylan Covalently Linked to an Arabinogalactan Protein. *The Plant Cell*, *25*(1), 270–287. https://doi.org/10.1105/tpc.112.107334
Tseng, I.-C., Hong, C.-Y., Yu, S.-M., & Ho, T.-H. D. (2013). Abscisic Acid- and Stress-Induced Highly Proline-Rich Glycoproteins Regulate Root Growth in Rice. *Plant Physiology*, *163*(1), 118–134. https://doi.org/10.1104/pp.113.217547
Wang, Y., Wang, Y., & Wang, Y. (2020). Apoplastic Proteases: Powerful Weapons against Pathogen Infection in Plants. *Plant Communications*, *1*(4), 100085. https://doi.org/10.1016/j.xplc.2020.100085
Whittaker, C. A., & Hynes, R. O. (2002). Distribution and Evolution of von Willebrand/Integrin A Domains: Widely Dispersed Domains with Roles in Cell Adhesion and Elsewhere. *Molecular Biology of the Cell*, *13*(10), 3369–3387. https://doi.org/10.1091/mbc.e02-05-0259
Willats, W. G. T., McCartney, L., Mackie, W., & Knox, J. P. (2001). Pectin: Cell biology and prospects for functional analysis. *Plant Molecular Biology*, *47*(1), 9–27. https://doi.org/10.1023/A:1010662911148
Wilson, Z. A., & Zhang, D.-B. (2009). From Arabidopsis to rice: Pathways in pollen development. *Journal of Experimental Botany*, *60*(5), 1479–1492. https://doi.org/10.1093/jxb/erp095
Xu, W.-L., Zhang, D.-J., Wu, Y.-F., Qin, L.-X., Huang, G.-Q., Li, J., Li, L., & Li, X.-B. (2013). Cotton PRP5 gene encoding a proline-rich protein is involved in fiber development. *Plant Molecular Biology*, *82*(4), 353–365. https://doi.org/10.1007/s11103-013-0066-8
Zhan, X., Wang, B., Li, H., Liu, R., Kalia, R., Zhu, J.-K., & Chinnusamy, V. (2012). *Arabidopsis proline-rich protein important for development and abiotic stress tolerance is involved in microRNA biogenesis*. PNAS. https://www.pnas.org/doi/abs/10.1073/pnas.1216199109
Zhang, Y., Held, M. A., Kaur, D., & Showalter, A. M. (2021a). CRISPR-Cas9 multiplex genome editing of the hydroxyproline-O-galactosyltransferase gene family alters arabinogalactan-protein glycosylation and function in Arabidopsis. *BMC Plant Biology*, *21*, 16. https://doi.org/10.1186/s12870-020-02791-9

Zhang, Y., Held, M. A., Kaur, D., & Showalter, A. M. (2021b). CRISPR-Cas9 multiplex genome editing of the hydroxyproline-O-galactosyltransferase gene family alters arabinogalactan-protein glycosylation and function in Arabidopsis. *BMC Plant Biology*, *21*(1), 16. https://doi.org/10.1186/s12870-020-02791-9
Zhang, Y., Held, M. A., & Showalter, A. M. (2020). Elucidating the roles of three β-glucuronosyltransferases (GLCATs) acting on arabinogalactan-proteins using a CRISPR-Cas9 multiplexing approach in Arabidopsis. *BMC Plant Biology*, *20*(1), 221. https://doi.org/10.1186/s12870-020-02420-5
Zhao, Y., Man, Y., Wen, J., Guo, Y., & Lin, J. (2019). Advances in Imaging Plant Cell Walls. *Trends in Plant Science*, *24*(9), 867–878. https://doi.org/10.1016/j.tplants.2019.05.009

Chapter 2. Partial Purification And Immunodetection f Cell Surface Glycoproteins From Plants [1]

Cecilia M. Lara-Mondragón and Cora A. MacAlister*

University of Michigan, Department of Molecular, Cellular and Developmental Biology

*Corresponding author, macalist@umich.edu

2.1. Abstract

Cell surface glycoproteins in plants were first described more than 50 years ago, and yet, the precise mechanisms by which they operate remain elusive to this day. Studying glycoproteins is often challenging due to their subcellular localization (many secreted or membrane associated) and the extent of glycosylation present on the protein backbone, which can have profound effects on protein structure and behavior. In plants, additional layers of complexity exist as cell surface glycoproteins are in close contact, and in some cases, establish direct linkages with the polysaccharide networks present in the cell wall. In this chapter, we guide the reader through a protocol aimed to address the glycosylation status of a presumed cell surface glycoprotein. First, we discuss the advantages and disadvantages of using plants as homologous expression systems for recombinant glycoprotein production. Next, we describe a protocol for microsomal enrichment, followed by partial purification by affinity chromatography and finally glycodetection by immunoblotting using monoclonal antibodies targeting cell wall glycans. We

[1] Published chapter: Lara-Mondragón, C. M., & MacAlister, C. A. (2020). Chapter 12—Partial purification and immunodetection of cell surface glycoproteins from plants. In C. T. Anderson, E. S. Haswell, & R. Dixit (Eds.), Methods in Cell Biology (Vol. 160, pp. 215–234). Academic Press. DOI: 10.1016/bs.mcb.2020.05.003

particularly focus on the hydroxyproline-rich glycoprotein (HRGP) family, the most abundant family of glycoproteins in the plant cell wall. We provide examples of two putative HRGP chimeric proteins, one akin to extensins and the second an arabinogalactan protein (AGP)-like protein. For the latter, we provide an AGP-specific protocol to ensure enrichment of members of this group, which can be used independently or in conjunction with the described protocol. Throughout the chapter, we provide recommendations for the handling of plant glycoproteins and highlight special considerations for experimental design, along with troubleshooting suggestions.

2.2. Key words

Arabinogalactan proteins; Glycoprotein; Hydroxyproline-rich glycoproteins; Immunodetection; Plant cell wall; Protein purification.

2.3. Introduction

Plant cells are spatially restricted by a polysaccharide-rich extracellular matrix, the cell wall. Due to high turgor pressure within the cell, the plasma membrane and cell wall are in close contact, forming a continuum presumed to have important roles in signal transduction during development and adaptive responses (Jaillais & Ott, 2020; Vaahtera et al., 2019). The plasma membrane-cell wall interface hosts a vast array of proteins (hereafter called cell surface proteins, CSPs), the functions of which are mostly unknown. CSPs comprise a broad spectrum, from plasma membrane-associated proteins (with transmembrane regions or glycosylphosphatidylinositol (GPI) anchors) to apoplast-secreted proteins (Liu et al., 2015). The biochemical, structural and functional characterization of CSPs is particularly challenging due to their intrinsic nature: they are in close contact with the highly insoluble polysaccharide network

of the cell wall, some can form very strong bonds to components of the wall and most of them are (or are predicted to be) heavily post-translationally modified (Jamet et al., 2006). Glycosylation is one of the major post-translational modifications of CSPs and, in general, is considered crucial for their structures and functions (Varki et al., 2009). The known biological functions of glycans can be grouped into three main categories: structural, modulatory and cell-cell/cell-extracellular matrix recognition. Described structural roles of glycans include maintenance of protein solubility and structure, prevention of proteasomal degradation, and contribution to proper folding of newly synthesized polypeptides in the ER (Breitling & Aebi, 2013; Nagashima et al., 2018). Among their modulatory roles, glycans influence how and when the underlying protein can establish interactions with other (glyco)proteins; the addition of specific glycans can prevent precocious interactions of proteins while they are on their way through the secretory pathway (Varki & Gagneux, 2017; Zhang & Wang, 2016). Finally, glycans on CSPs are thought to be crucial for intrinsic (intra-species) and extrinsic (inter-species) cell-cell recognition (Varki, 2017).

Many of the abovementioned glycan functions have been well documented for metazoan models. In plant models, glycans are presumed to have similar roles; however, these roles remain to be described in detail, and due to the close relationship between the plasma membrane and cell wall, new, plant-specific functions are likely to exist for glycans on CSPs (Strasser, 2016).

A significant number of CSPs belong to the hydroxyproline-rich glycoprotein (HRGP) family. HRGPs are broadly distributed across the plant kingdom and have been identified in all species studied from green algae to angiosperms (Johnson, Cassin, Lonsdale, Bacic, et al., 2017; Lamport, 1974; X. Liu et al., 2016). The total content of HRGPs in the primary cell wall varies

by species; for example, HRGPs account for ~ 2% of cell wall dry weight in tomato cell cultures and 10% in sycamore (*Acer pseudoplatanus*) cell suspension. Similarly, HRGP content varies between tissues within the same plant: in *Pisum sativum*, HRGPs account for 1.1% of cell wall dry weight in roots, but only 0.5% in cotyledons (Keegstra et al., 1973; Lamport, 1966). Due to the ubiquity of HRGPs in cell walls, they were initially thought to play mostly architectural roles; however, during the last decade, they have been found to play important roles as signaling molecules during development, stress responses and reproduction through unknown mechanism(s) (Cheung et al., 1995; Lamport et al., 2011; Nguema-Ona et al., 2014; Ohyama et al., 2009). HRGPs tend to be expressed by large multigenic families, broadly classified in three subgroups, including the heavily glycosylated arabinogalactan proteins (AGPs), the moderately glycosylated extensins (EXTs), and the weakly glycosylated proline-rich proteins (PRPs). In addition, a great number of hybrids (with multiple HRGP domains), chimeras (with non-HRGP related domains) and small peptides exist, adding a layer of complexity to their study (Hijazi et al., 2014). HRGPs are highly repetitive, intrinsically disordered proteins as a result of the high content of proline in their polypeptide backbones. Due to this bias in protein sequence, models to predict protein structure or identify related genes by homology searches are often impractical and require more refined approaches (Johnson et al., 2017; Liu et al., 2016). Many of the enzymes required for HRGP glycosylation have been identified only recently, and little is known about the effects of the different types of glycans on protein structure and function (Basu et al., 2013; Ogawa-Ohnishi et al., 2013; Showalter & Basu, 2016).

Understanding the function of CSPs requires knowledge of their post-translational modifications. While several sequence motifs have been identified as glycosylation signals, the glycosylation

status of the vast majority of CSPs has not been directly demonstrated. For example, the EXT family is characterized by the presence of multiple $SerPro_{(3–5)}$ motifs. In this sequence context, the prolines are hydroxylated and receive a short linear chain of arabinose sugars (Kieliszewski & Lamport, 1994; Shpak et al., 2001). AGPs on the other hand are characterized by dipeptide motifs like Ala-Pro, Ser-Pro or Thr-Pro. In these sequence contexts, the prolines are hydroxylated and then receive an arabinogalactan chain (Showalter, 2001; Showalter & Basu, 2016). While these sequences are modified in the EXT or AGP protein context, how they might be modified in another protein context, like a chimeric or hybrid HRGP, and whether this modification status changes based on cell identity or environmental conditions, are unknown. Therefore, sequence similarity is not sufficient evidence to predict the post-translational modification status of a CSP of interest and direct chemical evidence is required. Here, we describe a general protocol for the homologous expression of a genetically tagged membrane associated CSP, its partial purification by metal affinity chromatography and finally, the detection of its putative glycosylation using specific antibodies (Figure 2-1). We have used the protocol below to purify integral plasma membrane CSPs; however, this protocol could be equally well applied for proteins associated with different membranous compartments (for example, GPI-anchored or ER/Golgi-associated proteins). In addition, we describe an alternative (or complementary) approach for the enrichment of CSPs with arabinogalactan glycomodules (AGP or AGP-like proteins). Finally, given that the CSP is purified in its native state, it could be used for different downstream applications in addition to glycoprofiling by immunodetection (for example, interaction assays or mass spectrometry). Throughout the protocol, we highlight specific circumstances when handling CS glycoproteins might present challenges and provide several potential alternatives to consider.

2.4. Materials, reagents, and equipment

2.4.1. Plant expression system

– Stably transformed *Arabidopsis* lines or transiently expressing plants

2.4.2. Microsome isolation

– Porcelain mortar (145 mL capacity) and pestle (Fisher Scientific, 12-961A and 12-961-5A)
– Liquid nitrogen
– PVPP (polyvinylpolypyrrolidone) suspension: 10% w/v PVPP in distilled sterile water (dH_2O)
– PVPP equilibration buffer: 200 mM Tris pH 7.4, 40% (w/v) sucrose, 20 mM EDTA (ethylenediaminetetraacetic acid), 20 mM EGTA (ethylene glycol-bis(β-aminoethyl ether)-N,N,N′,N′-tetraacetic acid), 10 mM KCl, 0.4% (w/v) casein
– Extraction buffer: 100 mM Tris pH 7.4, 8% (w/v) sucrose, 5% (v/v) glycerol, 10 mM EDTA pH 8, 10 mM EGTA pH 8, 5 mM KCl, 1 mM DTT, 1 mM PMSF (phenylmethylsulfonyl fluoride), 0.2–0.5% (w/v) casein, protease inhibitor cocktail (Pierce, A32963). PMSF and protease inhibitor cocktails should be added immediately prior use
– Sterile nylon filter/cell strainer, 70 μm pore size (Thermo Scientific, 22363548)
– Falcon conical centrifuge tubes, 15 and 50 mL volumes (Fisher Scientific, 12-565-268 and 14-432-22)
– Ultracentrifuge, fixed angle rotor and suitable ultracentrifuge tubes
– Solubilization buffer: 10 mM Tris pH 7.5, 150 mM NaCl, 5 mM EDTA, 1% Triton x-100

– BCA assay kit for protein quantification (Thermo Scientific, 23225)

2.4.3. Enrichment of arabinogalactan glycoproteins

– β-d-Glucosyl-Yariv reagent (BioSupplies Australia, 100-2)
– 1% (w/v) NaCl in water
– 2% (w/v) NaCl in water
– Anhydrous dimethyl sulfoxide (DMSO) (Sigma, 67-68-5)
– Acetone (Sigma, 67-64-1)

2.4.4. Immobilized Metal Affinity Chromatography

– 1 mL resin bed HisPur Ni-NTA spin columns (Thermo Scientific, 88225)
– Dilution buffer: 10 mM Tris pH 7.5, 150 mM NaCl
– Equilibration buffer: 10 mM Tris pH 7.5, 150 mM NaCl, 0.5 mM EDTA, 0.1% Triton, 10 mM Imidazole
– Wash buffer: 10 mM Tris pH 7.5, 150 mM NaCl, 0.1% Triton x-100, 25 mM Imidazole
– Elution buffer: 10 mM Tris pH 7.5, 150 mM NaCl, 0.1% Triton x-100, 1 M Imidazole
– Regeneration buffer: 20 mM MES, 100 mM NaCl pH 5 (optional)

2.4.5. Glycosylation immunodetection

– SDS-PAGE supplies
– Western blot supplies
– Anti-glycan monoclonal antibodies—Several are available through PlantProbes, CarboSource, Kerafast or Megazyme.

2.5. Methods

2.5.1. Choosing a plant expression system

Membrane proteins are usually expressed at low levels in the cell, and obtaining sufficient amounts for biochemical, structural or functional studies is usually one of the first challenges to overcome. Careful consideration must be taken when selecting a suitable expression system. In some cases, the use of a non-plant, heterologous expression system has proven to be useful to elucidate CSP functions. For example, the extracellular domain of the FERONIA (FER) Receptor Kinase (FERecd) was expressed and purified from bacteria. Later, the authors demonstrated that the FERecd, which possess a Malectin domain, is capable of binding to pectin, an abundant polysaccharide *in muro* (Feng et al., 2018). However, significant limitations exist with non-plant expression systems, particularly when studying glycosylated CSPs whose modifications are plant-specific, as is true for the HRGPs and is likely to be true for many other CSPs. Therefore, to determine the native glycosylation status of CSPs, *in planta* expression is essential. A powerful strategy to facilitate purification and detection of the protein of interest is the use of protein tags (6–10xHis, FLAG, GFP, etc.), especially when antibodies against the protein of interest are not available. Similarly, the use of genetically tagged protein allows for additional downstream applications such as *in vivo* visualization of its subcellular localization if a fluorescent tag is used, or immunological detection *in situ*, using antibodies against the protein tag. After selecting the appropriate tag for the protein of interest, transgenic plants will need to be generated. Expressing the recombinant protein in the same species as the native protein increases the likelihood of proper protein folding and processing. Additionally, in the case of the plant model *Arabidopsis thaliana*, a collection of available mutant backgrounds could be used to increase the production of recombinant proteins by disrupting the machinery

involved in overexpression-induced transcriptional or post-transcriptional gene silencing (Butaye et al., 2004) or to investigate the effect of the loss of function of a particular post-translational modification (von Schaewen et al., 2018).

The two most commonly used plant expression systems are stable *Arabidopsis* transformants and transiently transformed *Nicotiana benthamiana* leaves. Expression in *Arabidopsis* offers a number of advantages, as stable *Agrobacterium*-mediated transformation protocols are well characterized and highly reproducible (Bent, 2000; Clough & Bent, 1998). In addition, unlike heterologous systems, recombinant proteins will likely undergo proper post-translational modifications and/or associate with their native partners, which might be required for proper protein stability. Generating stable lines is, however, a time-consuming labor and transformants can display unpredictable expression due to random gene insertion/positional effects, transgenerational silencing (especially when using strong promoters to drive expression, i.e., CaMV 35S; Matsunaga et al., 2019) and/or detrimental physiological effects due to recombinant protein overaccumulation. Alternatively, transient expression through tobacco mesophyll agroinfiltration could be used as a faster expression system, accelerating recombinant protein production significantly and producing sufficient yields for biochemical studies (Li, 2011). Transient expression in *Arabidopsis* mesophyll protoplasts by PEG (polyethylene glycol)-mediated transfection could be considered as another alternative for homologous expression (Yoo et al., 2007), although the recombinant protein yield could be limited due to limited volumes of starting tissue. Regardless of the selected expression platform, it must be noted that overexpression can cause artifacts such as improper folding, protein mis-localization, aggregation or degradation; in such scenarios, an inducible expression system or the use of the

native promoter should be considered as an alternative (Borghi, 2010). Due to deep evolutionary conservation of the machinery involved in glycoprotein biosynthesis (Fangel et al., 2012), glycoproteins expressed in either of the abovementioned plant systems will likely be processed in a similar manner. Furthermore, certain protein glycosylation pathways share a common origin between metazoans and land plants (Wang et al., 2017), which through genetic engineering, has allowed for expression and proper modification of mammalian proteoglycans in plant systems (Schoberer & Strasser, 2018; Yang et al., 2012).

Regarding the expression construct, it is important to note that since most CSPs are targeted for secretion or are (plasma) membrane associated, an N-terminal affinity tag could interfere with this process. For downstream Nickel affinity chromatography, we have successfully used a C-terminal His-tag. The hexahistidine tag (6x-His) is commonly used for IMAC (immobilized metal affinity chromatography); however, when working with integral membrane proteins, the use of a longer tag (8x or 10x-His) generally improves IMAC affinity. In addition, the use of a linker fluorescent protein between the tag and protein of interest has proven to be particularly useful in our hands (e.g., GFP6xHis, using the pMDC83 binary vector; Curtis & Grossniklaus, 2003) as it (1) improves protein solubility, (2) allows for *in vivo* visualization of the fusion protein and (3) is useful to check that the recombinant protein displays proper subcellular localization (Figure 2-2).

2.6. Microsome isolation

A great number of CSPs are targeted for secretion or membrane associated and detection from a crude plant lysate could be hindered due to their low abundance; therefore, enriching the

protein input by membrane isolation greatly improves CSP immunodetection. In this section, we describe a general protocol to isolate membrane fractions through ultracentrifugation.

2.6.1. Protocol

Before processing the tissue

Plant tissues contain abundant polyphenolic secondary metabolites. After cell lysis, the presence of polyphenols in the plant homogenate can interfere with downstream applications such as protein quantification or mass spectrometry. Polyvinylpolypyrrolidone (PVPP) is a water insoluble polymer capable of absorbing polyphenolic compounds and removing them when used during protein extraction (Wang et al., 2008). The following two steps describe the preparation of a PVPP pellet that will be later used to remove polyphenols from the tissue homogenate.

1. Aliquot 4 mL of PVPP suspension per sample into 15 mL conical tubes. Spin down at 600 × g (swinging bucket rotor) for 3 min at 4 °C.
2. Remove supernatant and resuspend pellet in 4 mL of PVPP equilibration buffer by vortexing. Incubate on ice (~ 15–30 min).

Tissue processing

3. While PVPP pellet is equilibrating, snap-freeze tissue with liquid nitrogen and grind finely using mortar and pestle. Place ~ 5 mL of ground material into a 15 mL conical tube and add 8–10 mL of ice-cold extraction buffer. Vortex thoroughly.
4. Spin down equilibrated PVPP at 600 × g for 3 min at 4 °C. Discard supernatant and replace with tissue homogenate (~ 8 mL). Vortex and incubate on ice for 10 min.
5. Spin down 600 × g for 3 min at 4 °C and transfer supernatant to a fresh tube.
6. Filter the homogenate through a sterile, 70 μm pore size nylon filter to remove tissue debris.

7. Aliquot equivalent volumes of filtered homogenate into suitable ultracentrifuge tubes and verify they are properly balanced for ultracentrifugation. Collect microsomal fractions by ultracentrifugation at 100,000 × g for 1 h at 4 °C. Discard supernatant and reconstitute pellet in membrane protein solubilization buffer. We routinely resuspend the pellet in a total volume of 3 mL of solubilization buffer; alternatively, pellets can be stored at − 70 or − 80 °C and resuspended later.
8. Measure total protein concentration of the solubilized microsomes using the BCA assay. The expected yield varies depending on the tissue source; using mature *Arabidopsis* leaves we have obtained up to 5 mg/mL of total protein. The presence of the protein of interest in the microsomal fraction can be assessed at this stage by Western blot (Figure 2-2).

2.6.2. Special considerations and optimization

After high-speed centrifugation (100,000 × g) the microsomal fraction should contain membranes from the plasma membrane, Golgi apparatus, endoplasmic reticulum (ER), vacuolar membranes and various endosomal vesicles. Conventional microsomal isolation protocols include a “pre-clearance step” in which the tissue homogenate is centrifuged at a lower speed to remove unwanted organelles (nuclei, mitochondria and chloroplasts). As described by Abas and Luschnig (2010), the pre-clearance step during the isolation of plant microsomal fractions is dispensable and, when working with limited plant material, results in unnecessary loss of membranes. Therefore, taking into account the findings of Abas & Luschnig (2010), our protocol excludes pre-clearance and the final microsomal fractions also includes mitochondria and lysed chloroplasts, which in our experience do not interfere with immunodetection or protein purification.

The solubilization of the membrane pellet is a critical step during the preparation of membrane proteins. During this step, membrane proteins are extracted from the lipid bilayer to an aqueous environment by the use of detergents. Different types of detergents are available (nonionic, ionic and zwitterionic) and should be selected based on downstream applications (Duquesne & Sturgis, 2010). For example, when the purified protein is required for downstream applications that do not require its native structure (i.e., SDS-PAGE and Western blot), ionic detergents such as sodium dodecyl sulfate (SDS) could be used. SDS is extremely efficient in solubilizing membrane proteins but often leads to protein denaturation, rendering proteins inactive. Some protein purification protocols are compatible with either denaturing or native conditions (i.e., His-tagged protein purification). It is recommended to test different detergents and conditions (detergent concentration, pH, ionic strength, etc.) in order to identify the optimal solubilization buffer for each membrane protein. Although identifying the optimal buffer is a trial and error task, prediction tools could be useful to determine, for example, a starting point for buffer pH using the theoretical isoelectric point based on the amino acid sequence of the protein of interest (pI calculator, Expasy). Additionally, when handling membrane proteins, it is recommended to use a relatively low concentration of NaCl (150 mM or less in some cases) in the solubilization buffer as membrane protein solubility often suffers at higher ionic strengths.

2.7. Enrichment of arabinogalactan glycoproteins

Among HRGPs, AGPs are the most heavily glycosylated, with carbohydrate side chains accounting for ~ 90% of the total molecular weight (Knoch et al., 2014). This particular feature makes their isolation and characterization cumbersome. Fortunately, the discovery of the synthetic glycoside dye β-glucosyl-Yariv has been extremely useful because this reagent is

capable of selectively binding to AGP glycans, precipitating them (Kitazawa et al., 2013). The β-Yariv reagent has been widely used for in situ detection, quantification, chemical disruption in vivo and AGP purification. The AGP-unreactive α-galactosyl-Yariv reagent is commonly used as a negative control for these experiments. If the protein of interest belongs to the AGP family or is predicted to be modified by the addition of AG side chains, β-Yariv precipitation can be performed to enrich for total AGP proteins. If the protein of interest is detected post-precipitation, this would serve as evidence of AG modification (Figure 2-4B). On the other hand, β-Yariv precipitation could be used as a pre-enrichment step before His-purification to reduce the complexity of the total protein input.

2.7.1. Protocol

1. Starting from 1 to 2 mg of total microsomal protein, add an equal volume of 1 mg/mL β-Yariv dissolved in 1% (w/v) NaCl. Incubate, rotating gently, at 4 °C overnight.
2. Centrifuge at 21,000 × g for 10 min.
3. Wash pellet twice with 1% (w/v) NaCl.
4. Resuspend pellet in 250 µL of DMSO, 750 µL cold acetone and 10 µL of 2% (w/v) NaCl. Spin at 21,000 × g for 10 min. After centrifugation, the upper, pink-colored phase corresponds to dissociated β-Yariv reagent while the pellet contains AGPs. Repeat step 3 three times.
5. Resuspend pellet in sample buffer for SDS-PAGE or buffer of choice (Figure 2-4B).

2.8. Partial purification by immobilized metal affinity chromatography (IMAC)

The microsomal fraction isolation in the previous steps helps to reduce the complexity of the input during affinity chromatography. Once the presence of the protein of interest has been

confirmed in the microsomal fraction (Figure 2-2), partial purification can be performed. In this section, we describe a general protocol for partial purification using Nickel columns.

2.8.1. Protocol

1. Starting from 1 to 2 mg of total microsome protein (or AGP-enriched fraction), add dilution buffer to the sample to reduce EDTA and Triton x-100 concentrations to 0.5 mM and 0.1% (v/v), respectively (for example, to an aliquot of 500 µL of total microsomal protein, add 5 mL of dilution buffer). Imidazole can prevent non-specific binding to the IMAC column if used at low concentrations in the binding buffer. Once diluted, rotate sample end-to-end in the cold room for 1 h to aid complete solubilization.
2. Place a HisPur Ni-NTA column in a 15 mL conical tube and spin at 700 × g for 2 min at 4 °C. Plug column and equilibrate with 3 mL of equilibration buffer. Incubate for 5 min on ice. Unplug the column and place it in a 15 mL conical tube, spin at 700 × g for 2 min and discard the flow through.
3. Plug the column and add diluted sample to column and incubate for 1 h in cold room, rotating gently. Spin column at 700 × g for 2 min and collect flow through. Save an aliquot to analyze later.
4. Wash the resin with 3 mL of washing buffer. Spin at 700 × g for 2 min. Repeat wash two additional times (three washes total). Collect and save aliquot of first wash to analyze later.
5. Elute by adding 1 mL of elution buffer. Spin at 700 × g for 2 min and save flow through. Repeat elution step 2 additional times, collecting eluates separately.
6. Regenerate column by adding 10 mL of regeneration buffer. Discard flow through.
7. Wash the column with 10 mL of dH2O. Discard flow through.

8. Finally, add 1 mL of 20% ethanol. Store the resin at 4 °C.
9. Assess the yield and purity of protein purification by Western blot or silver stain. Make sure to load equivalent amounts of each fraction to provide an accurate comparison (Figure 2-3).

2.8.2. Special considerations and optimization

High concentrations of detergents and EDTA can interfere with the affinity of His-tagged proteins to nickel ions; thus, dilution is required to reduce their concentration to minimal levels. In this protocol, the nonionic detergent Triton x-100 is used to maintain membrane protein solubility and therefore, it must be present at all times. We have successfully His-purified membrane proteins using a concentration of 0.5 mM EDTA and 0.1% Triton x-100. On the other hand, membrane proteins can be isolated in detergent-free environments. Native, functional membrane protein extraction by using lipid bilayer nanodiscs (Denisov & Sligar, 2016) or nanodisc-like particles stabilized by styrene maleic acid (SMA) co-polymers (forming SMA co-polymer-protein-lipid complexes, SMALPs) (Postis et al., 2015) aim at maintaining proteins in their native—or as close as possible—to their native lipid environment.

Adding low concentrations of imidazole to the binding and washing buffer can reduce non-specific binding (5–10 and 10–25 mM, respectively, is recommended by manufacturer). The imidazole concentration must be determined experimentally for each protein. In some cases, when the affinity of the tagged protein to the IMAC column is low, the presence of imidazole in the binding buffer can disrupt its binding entirely. The addition of imidazole will likely

modify the pH of the buffer; thus, it is important to verify the solution pH and re-adjust before use.

Elution can be achieved by increasing the concentration of imidazole in the buffer (250 mM up to 1 M). It is recommended to test a gradient with increasing concentrations of imidazole in order to determine the optimal elution condition. The presence of imidazole in the eluate should not interfere with downstream applications such as SDS-PAGE and immunodetection, but it can be removed by dialysis if desired. Other elution procedures include “stripping” of the Nickel ions from the column using EDTA (the eluate will contain the protein of interest and metal ions as a complex). Aliquot the eluate and store at − 70 or − 80 °C to prevent degradation. Finally, after elution using imidazole buffer, the column can be regenerated and reused. After regeneration, it is recommended to reuse the column to purify only the same recombinant protein as cross-contamination could occur. If EDTA stripping is the elution method of choice, column reuse would not be possible unless the column is recharged with nickel sulfate.

2.9. Immunodetection of glycosylation

A battery of commercially available monoclonal antibodies (mAbs) have been widely used as tools to detect cell surface molecules (Knox, 1992; Paul Knox et al., 1995). The online catalog for these mAbs can be found at CarboSource (US-based) or PlantProbes (for the UK) among other distributors. These antibodies, available as hybridoma supernatant, were generally raised against purified plasma membranes or cell wall fractions, including fractions enriched in non-cellulosic polysaccharides like xyloglucans and pectins. The

epitope characterization of many of these antibodies was done by ELISA-competitive binding assays. To test whether the antigen was a carbohydrate or protein, the antigen was treated with protease and/or chemically deglycosylated with anhydrous hydrogen fluoride before antibody binding (Knox et al., 1995). Several of these mAbs were raised against known HRGPs and possess carbohydrate epitopes, binding to AGP glycan side chains or EXT linear arabinose moieties. In this section, we describe an example of immunodetection with JIM19, a putative anti-EXT mAb and JIM13, putative anti-AGP mAb (Figure 2-4A). To produce JIM19, rats were immunized with guard cell protoplasts from pea. Currently, the epitope is unknown; however, it displays high reactivity to a purified EXT from carrot and its binding is periodate-sensitive and thus carbohydrate-based (Knox et al., 1991; Woodward et al., 1985). The antigen of JIM13 is better characterized. In general, anti-AGP mAbs were determined by their reactivity toward exudate gums, such as gum Arabic, gum tragacanth and other glycoprotein members of the AGP family. Based on competitive inhibition binding assays to gum arabic, JIM13's most efficient inhibitor is the oligosaccharide d-GlcpA-β(1-3)-d-GalpA-α(1-2)-l-Rha (Knox et al., 1991; Yates et al., 1996).

2.9.1. Protocol

1. Run eluted protein on a 10% SDS-PAGE gel, transfer to a nitrocellulose membrane and block for 1 h with 5% (w/v) non-fat dry milk in 1 × Tris-buffered saline, 0.1% Tween 20 buffer (TBST), gently shaking at room temperature.
2. Incubate the membrane overnight with an appropriate primary antibody (e.g., JIM19 or JIM13 diluted 1:10 in blocking buffer) at 4 °C.
3. Wash the membrane three times with 10–15 mL of 1 × TBST, 10 min each.

4. Incubate the membrane with secondary antibody (anti-rat-HRP diluted 1:2000 in blocking buffer) for 1 h at room temperature, gently shaking.
5. Wash membrane twice with 1 × TBST and once with 1 × Tris-buffered saline (TBS), for 10 min each.
6. Incubate membrane with chemiluminescent substrate for detection (Figure 2-4A).

2.9.2. Special considerations and optimization

During SDS-PAGE, migration of glycoproteins is typically affected by the presence of glycan side chains attached to the peptide chain. The presence of SDS during electrophoresis helps linearize proteins, and confers an overall negative charge, allowing for protein separation by size. Glycans do not interact with SDS in the same manner as polypeptides and, in some cases, terminal sugars in the side chain have their own charges, which typically affects electrophoretic mobility. Depending on the extent and heterogeneity of glycosylation, glycoproteins tend to display apparent higher molecular weights than predicted; they can run as bands of multiple sizes or even display smeared patterns (Packer et al., 2009). Additionally, the degree of glycosylation of a given protein can greatly affect its solubility, thermal stability and resistance to proteases (Lamport, 1980). In our own experience, we have observed temperature-induced cleavage of the tag from our glycoprotein of interest. This observed heat-sensitivity for recombinant HRGPs expressed in planta has been reported elsewhere, though the reason behind it remains elusive (Estévez et al., 2006; W. Sun, Kieliszewski, et al., 2004).

After partial purification, we recommend determining the recovery of the protein of interest by measuring the protein concentration in each of the eluted fractions by colorimetric assays (e.g., Bradford or BCA) or absorbance at 280 nm, and comparing the concentration of the eluate(s)

versus the total protein input. To determine the purity of the protein of interest, the proteins present in the eluate of each fraction can be separated by SDS-PAGE and visualized by gel staining. If complete purification was achieved, the eluate(s) should display a single band, corresponding to the protein of interest. It is worth noting that routinely used gel-stain techniques like Coomassie Blue staining are far less sensitive for glycoproteins, leading to weak or no detection (H. J. Møller & Poulsen, 2009). Among the recommended techniques for glycoprotein gel detection are the Periodic Acid/Schiff method, which produces a purple color after oxidation of diol groups near glycosidic linkages (Kapitany & Zebrowski, 1973), silver staining or a combination of both (Moller & Poulsen, 1995). We have successfully used silver staining for detection after purification; however, due to the aforementioned issues regarding glycoprotein electrophoretic mobility, we recommend performing immunodetection using a specific antibody raised against the protein of interest or an antibody raised against a tag to determine apparent molecular mass directly.

When performing immunodetection using the abovementioned plant anti-glycan mAbs, results must be interpreted with caution. Although the initial antigen used to produce these antibodies is known, the specific identity/structure of the epitopes they recognize has generally not been well defined. Recent attempts to characterize the antigens of different collections of cell wall glycan-directed mAbs (JIM, CCRC and LM mAb series) demonstrated that their reactivity toward the same putative glycan epitope varies, presumably reflecting the complexity and structural diversity of glycans present in the cell wall (Pattathil et al., 2010).We recommend testing more than one mAb when addressing the glycosylation status of the protein of interest, and similarly, it

is recommended to validate the results experimentally by an additional, independent approach (e.g., mass spectrometry).

2.10. Conclusions

The plant cell wall is a highly dynamic compartment, constantly modified throughout development and in response to environmental cues. The plasticity of the cell wall is likely regulated by proteins embedded within, or cell surface proteins associated with, this compartment. High throughput studies have identified a large number of plant cell wall-associated proteins from different species under different conditions or developmental stages (WallProtDB; San Clemente & Jamet, 2015). A significant number of cell surface proteins are predicted to be glycosylated and, how glycosylation affects the structure and function of its protein backbone remains to be elucidated. In this chapter, we described a general pipeline to purify and address the glycosylation of two putative HRGP-like integral plasma membrane proteins. This method is suitable for cell surface proteins other than members of the HRGP family and could serve as a starting point for the study of the many cell surface (glyco)proteins identified that still require validation and further biochemical or structural characterization, to identify their potential post-translational modifications and finding novel interactions with other protein or cell wall polymers.

2.11. Acknowledgments

This research is supported by the National Science Foundation under Grant No. IOS-1755482. Would like to thank Alexandria Dorchak for her excellent technical support and contributions during the development of this protocol.

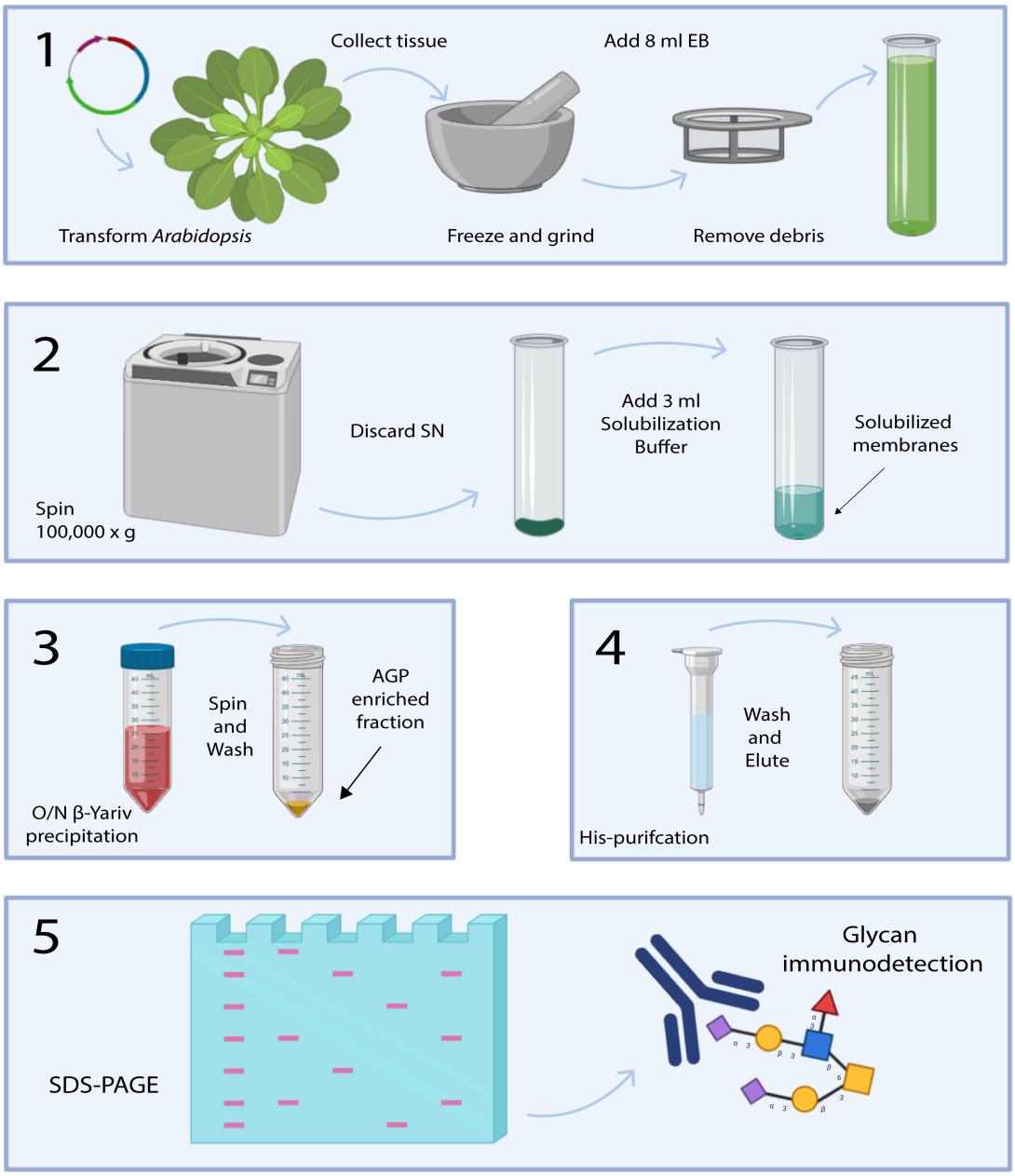

Figure 2-1 Protocol overview.

From the processing of plant material **(1)**, microsomal isolation **(2)** to the immunodetection of partially purified glycoproteins **(5)**. Step **(3)** is an optional approach specifically for AGP or AGP-like protein enrichment, the AGP-enriched fraction could be used directly for the immunodetection of the protein of interest **(5)** or to decrease the complexity of the input prior to metal affinity chromatography **(4)**. EB: elution buffer; SN: supernatant. Illustration created with BioRender.com.

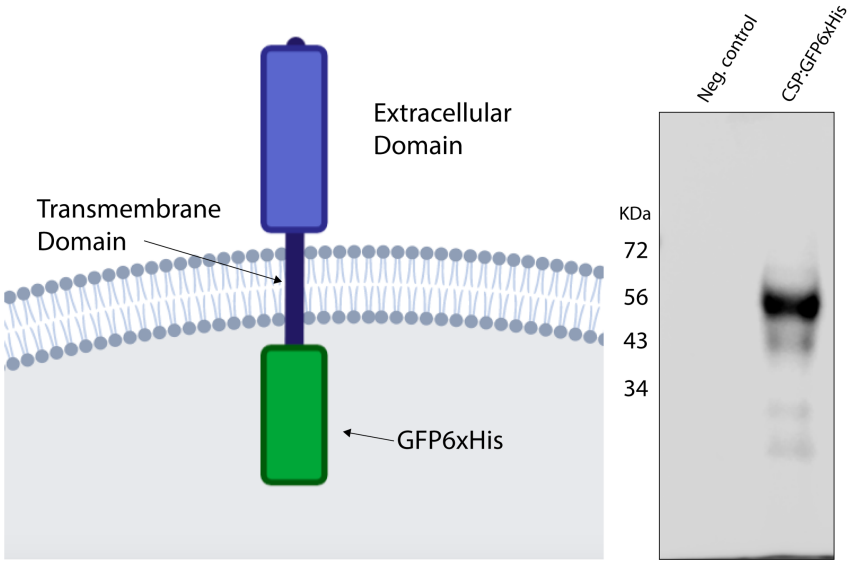

Figure 2-2 Immunodetection of a cell surface glycoprotein.

CSP translational fusion to a C-terminus GFP6xHis tag. The schematic on the left shows the tagged CSP architecture. The gel was equally loaded with 15 µg of the total microsomal fraction isolated from mature leaves. The negative control corresponds to total microsomes from untransformed wild type Columbia plants. Primary antibody for detection is a polyclonal anti-rabbit-GFP (Invitrogen, # A-11122). The predicted size for the protein backbone is 52 kDa. Protein schematic created with BioRender.com.

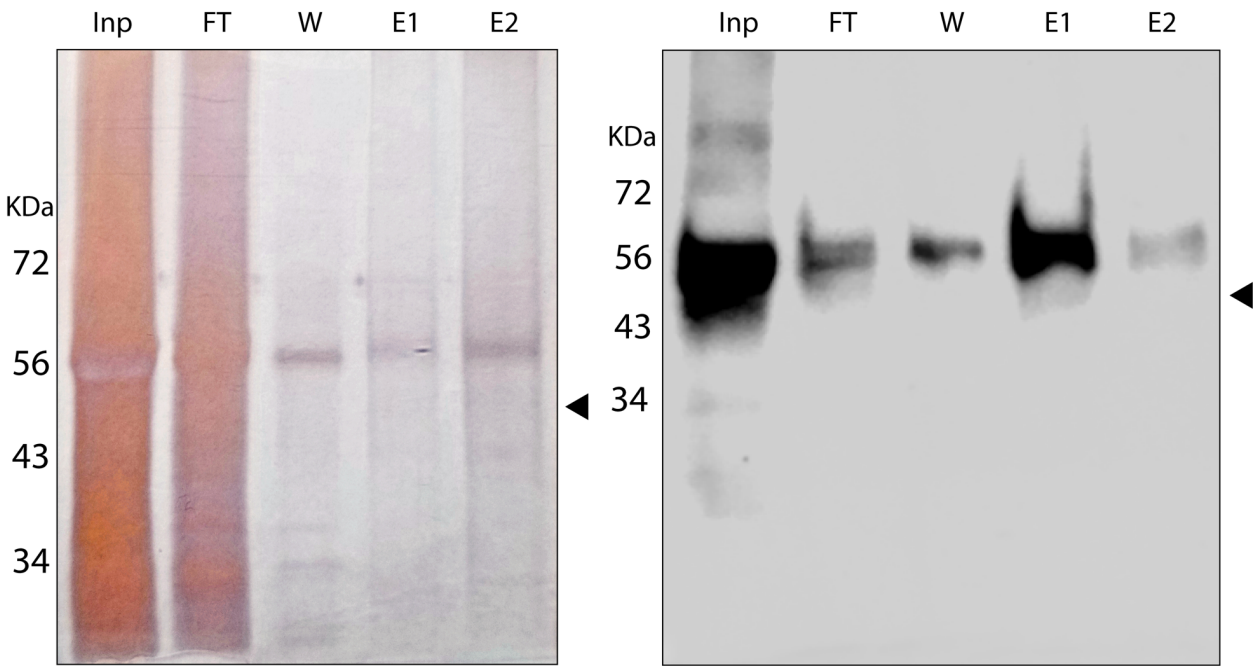

Figure 2-3 Assessment of CSP:GFP6xHis purification efficiency.

Equivalent concentrations of each fraction were loaded onto a 10% SDS-PAGE gel and silver stained (left) or used for immunodetection (right) with anti-GFP polyclonal antibody. Inp: input, total microsomes; FT: flow through; W: first wash; E1: elution 1 and E2: elution 2. Arrowheads indicate the predicted size of CSP:GFP6xHis (52 kDa).

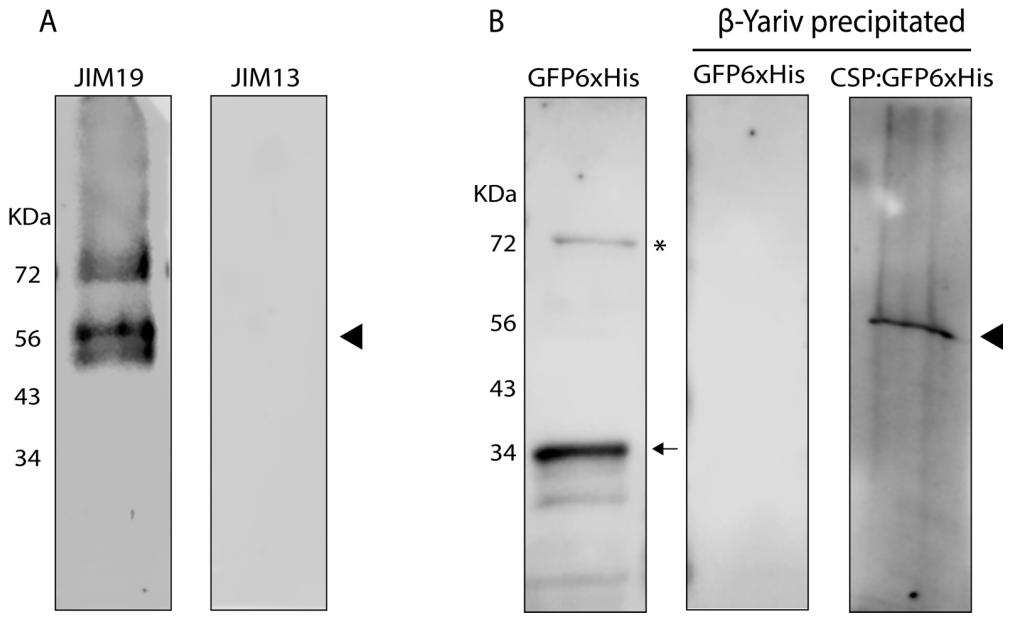

Figure 2-4 Glycoprofiling by immunodetection.

(A) After His-partial purification, CSP:GFP6xHis was loaded onto a 10% SDS-PAGE gel for immunoblotting with anti-glycan antibodies. The amino acid sequence of the CSP contains predicted hydroxyproline-*O*-arabinosylation motifs. JIM19, a monoclonal antibody that recognizes this modification, bound to the eluate enriched in CSP:GFP6xHis. The JIM13 antibody binds to AGP glycan moieties and does not display reactivity toward the partially purified protein. Black arrowhead: observed size of CSP:GFP6xHis with anti-GFP antibody. **(B)** Example of β-Yariv precipitation from total microsomes. A different CSP fusion, predicted to be modified by the addition of AG-glycans, was precipitated overnight with β-Yariv, and the AGP-enriched fraction was analyzed by immunodetection (primary polyclonal antibody anti-rabbit-GFP, Invitrogen, # A-11122). To show the specificity of β-Yariv purification, total soluble protein from plants expressing cytosolic GFP6xHis was treated similarly. GFP6xHs is no longer detectable in the AGP-enriched fraction. Arrow: Free GFP (~ 34 kDa), Star: non-specific binding, black arrowhead: AGP-like CSP:GFP6xHis (predicted size of the protein backbone = 47 kDa).

2.12. References

Abas, L., & Luschnig, C. (2010). Maximum yields of microsomal-type membranes from small amounts of plant material without requiring ultracentrifugation. *Analytical Biochemistry*, 401, 217–227.

Basu, D., Liang, Y., Liu, X., Himmeldirk, K., Faik, A., Kieliszewski M., et al. (2013) Functional identification of a hydroxyproline-O-galactosyltransferase specific for arabinogalactan protein biosynthesis in *Arabidopsis. Journal of Biological Chemistry*, 288, 10132–10143.

Bent, A. (2000) Arabidopsis in Planta Transformation. Uses, Mechanisms, and Prospects for Transformation of Other Species. *Plant Physiology*, 124, 1540-1547; DOI: doi.org/10.1104/pp.124.4.1540.

Breitling, J., & Aebi, M. (2013). N-linked protein glycosylation in the endoplasmic reticulum. *Cold Spring Harbor perspectives in biology*, 5(8), a013359. DOI: doi.org/10.1101/cshperspect.a013359.

Borghi L. (2010) Inducible Gene Expression Systems for Plants. In: Hennig L., & Köhler C. (Eds.) Plant Developmental Biology. Methods in Molecular Biology (Methods and Protocols), 655. *Humana Press*, Totowa, NJ.

Butaye, K. M. J., Goderis, I., Wouters, P. E., Pues, J. M., Delaure, S. L., Broekaert, et al. (2004) Stable high-level transgene expression in Arabidopsis thaliana using gene silencing mutants and matrix attachment regions. The Plant Journal, 39(3):440-449.

Cheung, A., Wang, H. & Wu, H. M. (1995) A floral transmitting tissue-specific glycoprotein attracts pollen tubes and stimulates their growth. *Cell*, 82(3):383-393.

Clough S. J. & Bent, A. F. (1998) Floral dip: A simplified method for Agrobacterium-mediated transformation of Arabidopsis thaliana. *The Plant Journal*, 16:735-43.

Curtis, M. & Grossniklaus, U. (2003) A Gateway Cloning Vector Set for High-Throughput Functional Analysis of Genes in Planta. *Plant Physiology*, 133(2):462-469, DOI: doi.org/10.1104/pp.103.027979.

Denisov, I.G. & Sligar, S.G. (2016) Nanodiscs for structural and functional studies of membrane proteins. *Nature Structural and Molecular Biology*. 23:481-486.

Duquesne, K. & Sturgis, J. N. (2010) Membrane Protein Solubilization. *Methods in Molecular Biology*, 601:205-17.

Estévez, J. M., Kieliszewski, M. J., Khitrov, N., & Somerville, C. (2006). Characterization of synthetic hydroxyproline-rich proteoglycans with arabinogalactan protein and extensin motifs in Arabidopsis. *Plant Physiology*, 142(2), 458–470. DOI:10.1104/pp.106.084244.

Fangel, J.U., Ulvskov, P., Knox, J.P., Middelsen, M. D., Harholt, J., Popper, Z. A., Willats, W. G. T. (2012) Cell wall evolution and diversity. *Frontiers in Plant Science*, 3, 152 DOI: doi.org/10.3389/fpls.2012.00152.

Feng, W., Kita, D., Peaucelle, A., Cartwright, H. N., Doan, V., Duan, Q., Liu, M. C., et al. (2018) The FERONIA Receptor Kinase Maintains Cell-Wall Integrity during Salt Stress through Ca2+ Signaling. *Current Biology*, 28(5):666-675. DOI: doi.org/10.1016/j.cub.2018.01.023.

Hijazi, M., Velasquez, S. M., Jamet, E., Estevez, J. M., & Albenne, C. (2014). An update on post-translational modifications of hydroxyproline-rich glycoproteins: toward a model highlighting their contribution to plant cell wall architecture. *Frontiers in Plant Science*, 5, 395. DOI: doi.org/10.3389/fpls.2014.00395.

Jaillais, Y. & Ott, T. (2019) The nanoscale organization of the plasma membrane and its importance in signaling - a proteolipid perspective. *Plant Physiology*, DOI: doi.org/10.1104/pp.19.01349.
Jamet, E., Canut, H., Boudart, G., Pont-Lezica, R. (2006) Cell wall proteins: a new insight through proteomics. *Trends in Plant Science*, 11(1):33-39.
Johnson K. L., Cassin, A. M., Lonsdale, A., Wong, G. K., Soltis, D. E., Miles, N. W., Melkonian, M., Melkonian, B., Deyholos, M. K., Leebens-Mack, J., Rothfels, C. J., Stevenson, D. W., Graham, S. W., Wang, X., Wu, S., Pires, J. C., Edger, P. P., Carpenter, E. J., Bacic, A., Doblin, M. S., Schultz, C. J. (2017a) Insights into the Evolution of Hydroxyproline-Rich Glycoproteins from 1000 Plant Transcriptomes. *Plant Physiology*, 174, 904-921.
Johnson, K. L., Cassin, A. M., Lonsdale, A., Bacic, A., Doblin, M., Schultz, C. J. (2017b) Pipeline to identify Hydroxyproline-rich Glycoproteins. *Plant Physiology*, 174, 886-903. DOI: doi.org/10.1104/pp.17.00294.
Kapitany, R. A. & Zebrowski, E. J. (1973) A High Resolution PAS Stain for Polyacrylamide Gel Electrophoresis. *Analytical Biochemistry*, 56:361-369.
Kieliszewski, M. J. & Lamport, D. T. A. (1993) Extensin: repetitive motifs, functional sites, post-translational codes, and phylogeny. *The Plant Journal*, 5(2), 157-172.
Kitazawa,K., Tryfona, T.,Yoshimi, Y., Hayashi,Y., Kawauchi, S., et al. (2013) β-Galactosyl Yariv Reagent Binds to the β-1,3-Galactan of Arabinogalactan Proteins, *Plant Physiology*, 161, 1117-1126.
Knoch, E., Dilokpimol, A. & Geshi, N. (2014). Arabinogalactan proteins: focus on carbohydrate active enzymes. *Frontiers in Plant Science*, 5, 198, DOI: doi.org/10.3389/fpls.2014.00198.
Knox, J. P., Linstead, P. J., Peart, J., Cooper, C. & Roberts, K. (1991) Developmentally regulated epitopes of cell surface arabinogalactan-proteins and their relation to root tissue pattern formation. *The Plant Journal*, 1, 317-326.
Knox, J. P. (1992) Molecular probes for the plant cell surface. *Protoplasma*, 167, 1-9.
Knox, J. P., Peart, J. & Neill, S. (1995) Identification of novel cell surface epitopes using a leaf epidermal-strip assay system. *Planta*, 196, 266-270.
Lamport, D. (1966) The Protein Component of Primary Cell Walls. *Advances in Botanical Research*, 2:151-218.
Lamport, D. (1974) The Role of Hydroxyproline-Rich Proteins in the Extracellular Matrix of Plants. In Hay, E., King, T., Papaconstatinou, J. (Eds.) Macromolecules Regulating Growth and Development. The Thirtieth Symposium The Society for Developmental Biology (pp. 113-130). Academic Press.
Lamport, D. (1980) Structure and Function of Plant Glycoproteins. In Preiss, J. (Ed), The Biochemistry of Plants: A Comprehensive Treatise, Volume 3: Carbohydrates: Structure and Function (pp. 501-536). Academic Press.
Lamport, D. T., Kieliszewski, M. J., Chen, Y., & Cannon, M. C. (2011). Role of the extensin superfamily in primary cell wall architecture. *Plant Physiology*, 156(1), 11–19.
Li, X. (2011). Infiltration of Nicotiana benthamiana Protocol for Transient Expression via Agrobacterium. Bio-101: e95. DOI: doi.org/10.21769/BioProtoc.95.
Liu, Z., Persson, S., Sánchez-Rodríguez, C. (2015) At the border: the plasma membrane–cell wall continuum, *Journal of Experimental Botany*, 66, 1553-1563.
Liu, X., Wolfe, R., Welch, L. R., Domozych, D. S., Popper, Z. A., & Showalter, A. (2016) Bioinformatic identification and analysis of extensins in the plant kingdom. *PLoS ONE*, 11: e0150177.

Matsunaga, W., Shimura, H., Shirakawa, S., Isoda, R., Inukai, T., Matsumura, T., & Masuta, C. (2019). Transcriptional silencing of 35S driven-transgene is differentially determined depending on promoter methylation heterogeneity at specific cytosines in both plus- and minus-sense strands. *BMC Plant Biology*, 19, 24. DOI:10.1186/s12870-019-1628-y.
Møller, H. J. & Poulsen, J. H. (1995) Improved methods of silver staining of glycoproteins in thin sodium dodecyl sulfate polyacrylamide gels. *Analytical Biochemistry*, 226(7), 371-374.
Møller, H. J. & Poulsen, J. (2002) Staining of Glycoproteins/Proteoglycans in SDS-Gels. In Walker, J.M. (Ed.) The Protein Protocols Handbook: Second edition (pp. 773-778). Humana Press.
Nagashima, Y., von Schaewen, A., & Koiwa, H. (2018) Function of N-glycosylation in plants. *Plant Science*; 274, 70-79.
Nguema-Ona, E., Vicré-Gibouin, M., Gotté, M., Plancot, B., Lerouge, P., Bardor, M., & Driouich, A. (2014). Cell wall O-glycoproteins and N-glycoproteins: aspects of biosynthesis and function. *Frontiers in Plant Science*, 5, 499. DOI: doi.org/10.3389/fpls.2014.00499.
Ogawa-Ohnishi, M., Matsushita, W. & Matsubayashi, Y. (2013) Identification of three hydroxyproline O-arabinosyltransferases in Arabidopsis thaliana. *Nature Chemical Biology* 9, 726–730. DOI: doi.org/10.1038/nchembio.1351.
Ohyama K, Shinohara H, Ogawa-Ohnishi M, & Matsubayashi Y. (2009) A glycopeptide regulating stem cell fate in Arabidopsis thaliana. *Nature Chemical Biology*, 5:578–580.
Packer, N., Ball, M., Devine, P., & Patton, W. Detection of glycoproteins in gels and blots. In Walker, J.M. (Ed.) The Protein Protocols Handbook: Second edition (pp. 761-772). Humana Press.
Pattathil, S., Avci, U., Baldwin, D., Swennes, A. G., Mc Gill, J., et al., (2010) A Comprehensive Toolkit of Plant Cell Wall Glycan-Directed Monoclonal Antibodies. *Plant Physiology*, 153, 514-525.
Postis, V., Rawson, S., Mitchell, J.K., Lee, S.L., Parslow, R.A. et al. (2015) The use of SMALPs as a novel membrane protein scaffold for structure study by negative stain electron microscopy. *Biochimica et Biophysica Acta- Biomembranes*. 1848(2):496-501.
San Clemente, H., Jamet, E. (2015) WallProtDB, a database resource for plant cell wall proteomics. *Plant Methods*. 11(1):2.
Schoberer, J. and Strasser, R. (2018) Plant glyco-biotechnology. *Seminars in Cell & Developmental Biology*, 80:133-141.
Showalter A. M. (2001). Arabinogalactan-proteins: structure, expression and function. *Cellular and Molecular Life Sciences*, 58, 1399–1417.
Showalter, A. M., & Basu, D. (2016). Extensin and Arabinogalactan-Protein Biosynthesis: Glycosyltransferases, Research Challenges, and Biosensors. *Frontiers in Plant Science*, 7, 814.
Shpak, E. L., Barbar, E., Leykman, J. F., & Kieliszewski, M. (2001) Contiguous Hydroxyproline residues direct Hydroxyproline Arabinosylation in Nicotiana tabacum. *Journal of Biological Chemistry*; 276, 11272-11278.
Strasser R. (2016). Plant protein glycosylation. *Glycobiology*, 26(9), 926–939. DOI: doi.or/10.1093/glycob/cww023.
Sun, W., Zhao, D., Hare, M., Kieliszewski, M. J., & Showalter, A. M. (2004) Tomato Le-AGP-1 is a plasma membrane-bound, glycosylphosphatidylinositol-anchored arabinogalactan-protein. *Physologia Plantarum*, 120, 319-327.
Talmadge, K., Keegstra, K., Bauer, W., Albersheim, P. (1972) The structure of Plant Cell Walls. *Plant Physiology*, 51:158-173.

Vaahtera, L., Schulz, J. & Hamann, T. (2019) Cell wall integrity maintenance during plant development and interaction with the environment. *Nature Plants* 5, 924–932. DOI: doi.org/10.1038/s41477-019-0502-0.
Varki A., Freeze H. H., & Gagneux, P. (2009) Evolution of glycan diversity. In Varki A., Cummings R.D., Esko J.D., Freeze H.H., Stanley H.H., Bertozzi C.R., Hart G.W., and Etzler M.E., (Eds), *Essentials of Glycobiology* (pp. 281–292). Cold Spring Harbor, NY: Cold Spring Harbor Laboratory Press.
Varki, A. (2017) Biological roles of glycans. *Glycobiology*, 27, 3-49.
Varki A. & Gagneux P. (2017). Biological Functions of Glycans. In Varki A., Cummings R.D., Esko J.D., Freeze H.H., Stanley H.H., Bertozzi C.R., Hart G.W., & Etzler M.E., (Eds.), Essentials of Glycobiology. Cold Spring Harbor, NY: Cold Spring Harbor Laboratory Press.
von Schaewen, A., Jeong, I. S., Rips, S., Fukudome, A., Tolley, J., Nagashima, Y., Fischer, K., Kaulfuerst-Soboll, H., & Koiwa, H. (2018). Improved recombinant protein production in Arabidopsis thaliana. *Plant Signaling & Behavior*, 13(6), e1486149. DOI: doi.org/10.1080/15592324.2018.1486149.
Wang, W., Tai, F., & Chen, S. (2012) Optimizing protein extraction from plant tissues for enhanced proteomics analysis. *Journal of Separation Science*, 31, 2032-2039.
Wang, P., Wang, H., Gai, J., TIan, X., Zhang, X., Lv, Y., & Jian, Y. (2017) Evolution of protein N-glycosylation process in Golgi apparatus which shapes diversity of protein N-glycan structures in plants, animals and fungi. *Scientific Reports* 7, 40301. DOI: doi.org/10.1038/srep40301.
Woodward, M. P., Young, W. W. Jr., & Bloodgood, R. A. (1985) Detection of monoclonal antibodies specific for carbohydrate epitopes using periodate oxidation. *Journal of Immunology Methods*, 78, 143-153.
Yang, Z., Drew, D., Jørgensen, B., Mandel U., Bach, S.S., Ulvskov, P., Levery, S.B., Bennett, E., Clausen, H., & Petersen, B. (2012) Engineering Mammalian Mucin-type O-glycosylation in Plants. *Journal of Biological Chemistry*, 287, 11911-11923.
Yoo, S.D., Cho, Y.H., & Sheen, J. (2007) Arabidopsis mesophyll protoplasts: a versatile cell system for transient gene expression analysis. *Nature protocols*, 2, 1565-1572.
Zhang, X., & Wang, Y. (2016). Glycosylation Quality Control by the Golgi Structure. *Journal of Molecular Biology,* 428, 3183–3193.z

Chapter 3. *O*-Glycosylation Of The Extracellular Domain Of Pollen Class I Formins Modulates Their Plasma Membrane Mobility [2]

Cecilia M. Lara-Mondragón, Alexandria Dorchak and Cora A. MacAlister*

University of Michigan, Department of Molecular, Cellular and Developmental Biology

*Corresponding author, macalist@umich.edu

Running title: Glycosylation and mobility of pollen class I formins

Highlight: The extracellular domains of class I formins are O-glycosylated similar to hydroxyproline-rich cell wall glycoproteins. Protein localization and lateral mobility are altered depending on the type of *O*-glycan attached.

3.1. Abstract

In plant cells, linkage between the cytoskeleton, plasma membrane and cell wall is crucial to maintain cell shape. In highly polarized pollen tubes, this coordination is especially important to allow rapid tip-growth and successful fertilization. Class I formins contain cytoplasmic actin-nucleating formin homology domains as well as a Pro-rich extracellular domain (ECD) and are candidate coordination factors. Here, we investigated the functional significance of the extracellular domain of two pollen-expressed class I formins: AtFH3, which does not have a

[2] Chapter published: Lara-Mondragón, C. M., Dorchak, A., & MacAlister, C. A. (2022). *O*-Glycosylation of the extracellular domain of pollen class I formins modulates their plasma membrane mobility. *Journal of Experimental Botany*, erac131. DOI: doi.org/10.1093/jxb/erac131.

polar localization and AtFH5, which is limited to the growing tip region. We show that the ECD of both is necessary for their function and identify distinct *O*-glycans attached to these sequences, AtFH5 being Hyp-arabinosylated and AtFH3 carrying arabinogalactan chains. Loss of Hyp-arabinosylation altered the plasma membrane localization of AtFH5 and disrupted actin cytoskeleton organization. Moreover, we show that *O*-glycans differentially affect lateral mobility in the plasma membrane. Together, our results support a model of protein sub-functionalization where AtFH5 and AtFH3, restricted to specific plasma membrane domains by their ECDs and the glycans attached to them, organize distinct subarrays of actin during pollen tube elongation.

Keywords: Cell wall, glycosylation, actin, cytoskeleton, pollen tube, tip growth, formin

Abbreviations: formin homology (FH), extracellular domain (ECD), plasma membrane (PM), hydroxyproline-rich cell wall glycoprotein (HRGP)

3.2. Introduction

Plant cells are enclosed in a polysaccharide-rich extracellular matrix, the cell wall. Interconnection between the cytoskeleton, plasma membrane (PM), and cell wall is crucial in shaping plant cells, during cell growth, and in response to stimuli (Baluška et al., 2003; Chebli et al., 2021; Jaillais & Ott, 2020). In highly polarized plant cells, such as pollen tubes, the coordination of the F-actin cytoskeleton, secretion machinery and cell wall assembly is pivotal to allow fast growth (Bascom et al., 2018). Furthermore, cytoskeleton and cell wall coordination permit timely delivery and proper positioning of PM or PM-associated proteins, allowing the pollen tube to respond to mechanical and chemical cues along its journey through the pistil

(Chebli et al., 2012; Dresselhaus & Franklin-Tong, 2013; Hafidh & Honys, 2021). In pollen tubes, as in other plant cells, the precise mechanism by which cell wall, PM and cytoskeleton establish a linkage is not fully understood, although it is believed that interactions between these structures vary depending on the tissue and cell type (Chebli et al., 2021). Evidence of interaction between a GPI-anchored proteoglycan ARABINOXYLAN PECTIN ARABINOGALACTAN PROTEIN1 (APAP1) and pectic polysaccharides in the wall was reported previously (Tan et al., 2013), further suggesting that covalent interactions between distinct biomolecules in the cell wall exist.

Class I formins are transmembrane proteins with a Pro-rich extracellular domain (ECD) and intracellular actin-nucleating Formin Homology (FH1 and FH2) domains (Gisbergen & Bezanilla, 2013), making them suitable candidates to mediate cell wall-PM-cytoskeleton linkage. While the actin nucleating/bundling activity of members of this family of proteins in Arabidopsis has been thoroughly studied (Blanchoin & Staiger, 2010; J. Wang et al., 2012), our understanding of the functional significance of the ECD is limited to a handful of reports. The ECD of class I formins generally possess a high content of Pro residues, resembling the glycosylation motifs of hydroxyproline-rich cell wall glycoproteins (HRGPs). HRGP-like motifs present in the ECDs of class I formins belong to two subgroups: Extensins (EXT) and arabinogalactan glycoproteins (AGP) (Borassi et al., 2016; Liu et al., 2016). EXT are highly repetitive proteins defined by the presence of Ser-$Pro_{(3-5)}$ motifs (Kieliszewski & Lamport, 1994), where (hydroxy)proline (hyp) residues are modified by the addition of short linear chains of arabinosides (Petersen et al., 2021; Shpak et al., 2001). AGPs, on the other hand, are glycosylated by the addition of branched arabinogalactan (AG) glycans in their clustered

dipeptide Ser-Pro, Thr-Pro, Ala-Pro, Gly-Pro repeats (Tan et al., 2003). In Arabidopsis, the vegetative formin AtFH1 is immobilized in the PM by the interaction of its ECD EXT-like motifs and the cell wall (Martinière et al., 2011). Similarly, it was reported that the interaction between the ECD of the SYMBIOTIC FORMIN 1 (SYFO1) and the cell wall is necessary to induce root hair curling during nodule development in *Medicago truncatula* (Liang et al., 2021). Both reports highlight the importance and versatility of the ECD in formin cell wall anchoring; however, further studies are necessary to elucidate the nature of this interaction. Despite the evidence of the importance of the EXT-like motifs present in the ECD of class I formins and their putative role in protein immobilization, experimental evidence of *O*-glycosylation of such motifs is lacking.

Two members of the class I formin family, AtFH3 and AtFH5, regulate cortical actin polymerization during pollen germination and tube elongation (Cheung et al., 2010; Liu et al., 2018; Liu et al., 2021; Ye et al., 2009). Genetically tagged versions of AtFH3 and AtFH5 showed distinct localization patterns in pollen tubes: AtFH3 localizes throughout the pollen tube's PM, while AtFH5 is restricted to the apical PM. Based on their localization patterns and genetic studies (Cheung et al., 2010; Lan et al., 2018), it is hypothesized that AtFH3 and AtFH5 participate in the organization of distinct subarrays of actin microfilaments. AtFH3 stimulates the polymerization and bundling of actin filaments in the pollen tube shank (Ye et al., 2009), whereas AtFH5 mediates the assembly of a fine network of apical and subapical actin (Cheung et al., 2010). The mechanistic basis class I formin sub functionalization during pollen tube elongation remains to be described; however, the observation that the replacement of the ECD of AtFH5 with the intracellular FH1/2 domains of AtFH3 mimics the localization of wild-type

AtFH5 (Lan et al., 2018), suggests that the ECD might be responsible for their spatial patterning and important for their functional diversification.

Here, we further explored the functional significance of the ECD of pollen class I formins AtFH3 and AtFH5. We demonstrate that the ECD of both AtFH3 and AtFH5 are necessary for their PM localization. Furthermore, we provide evidence that the HRGP-like motifs in their ECDs are post-translationally modified by the addition of distinct *O*-glycans, consistent with predictions based on the hyp-contiguity hypothesis. Additionally, our results suggest that these post-translational modifications likely modulate their interaction with the extracellular matrix and lateral mobility in the plasma membrane.

3.3. Materials and Methods

3.3.1. Plant material and growth conditions

Arabidopsis plants were grown under long day photoperiods (16 h light and 8 h dark) in a temperature-controlled growth room at 23°C. The *hpat1-2* (SALK_120066), *hpat2-2* (SM_3_38225) and *hpat3-1* (SALK_047668) triple mutant's recovery was described previously (MacAlister et al., 2016). *fh3-1* (SALK_150350) and *fh5-2* (SALK_044464) T-DNA insertion alleles in the Columbia-0 background (Lan et al., 2018) were obtained from the Arabidopsis Biological Resource Center (ABRC). *fh3-1* and fh5-2 lines were genotyped with the primers published by (Lan et al., 2018). *fh3-1* or *fh5-2* were crossed with the *hpat1,2,3* mutant to generate higher order mutants *hpat1,2,3/fh3-1* and *hpat1,2,3/fh5-2*. The primers used for genotyping of the *hpat1,2,3* triple mutant are listed in Table 3-1.

3.3.2. Molecular cloning and plant transformation

The coding region of AtFH1(AT3G25500.1), AtFH3 (AT4G15200.1) and AtFH5 (AT5G54650.1) were amplified from cDNA derived from leaves (AtFH1) or pollen (AtFH3/5) using the Phusion® High-Fidelity DNA Polymerase (M0530S, NEB) and the primers listed in Table 3-1. ECD and modified versions were generated by overlap extension PCR. PCR fragments were cloned into Gateway entry vectors using BP Clonase II™ (11789-020; Invitrogen). Then full length and ECD modified versions were recombined using LR Clonase II™ into a modified pFAST-R01 binary vector (Shimada et al., 2010). Cloning of mNeonGreen into the pFAST-R01 was performed as in Beuder et al., 2020 for protein localization. For photoconversion assays, mEosFP was cloned into the same vector, pFAST-R01. For protein purification and FRAP assays, the signal peptide, ECD and transmembrane domain of AtFH1, AtFH3 and AtFH5 were amplified from entry clones using the primers listed in Table 3-1, adding attB recombination sites for Gateway cloning. The PCR products were recombined using LR Clonase II into the pMDC83 binary vector for CaMV 35S promoter expression (Curtis & Grossniklaus, 2003). Arabidopsis plants were transformed by the floral dipping method (Clough & Bent, 1998).

3.3.3. Pollen assays

Pollen germination medium (PGM) modified from (Rodriguez-Enriquez et al., 2013) (10% [w/v] sucrose, 0.01% [w/v] boric acid, 1 mM $CaCl_2$, 1 mM $Ca(NO_3)_2$, 1 mM KCl, 0.03% [w/v] casein enzymatic hydrolysate, 0.01% [w/v] myo-inositol, 0.1 mM spermidine, 10 mM γ-aminobutyric acid, 500 µM methyl jasmonate, pH adjusted to 8.0, and for solid PGM, solidified with 1% [w/v] low melting temperature agarose) was used for all *in vitro* growth assays and live-cell imaging.

For pollen live-cell imaging, CoverWell™ (Grace Bio-Labs, GBL635051) silicone chambers were placed on top of a glass slide, filled with molten PGM and solidified on a flat surface for ~1 min. Once solidified, pollen grains were dusted on top of the medium and carefully covered with a coverslip. The samples were incubated for 50 min at room temperature in a humid chamber consisting of a plastic box with damp paper towels prior to imaging.

3.3.4. Live-cell imaging

Pollen tubes expressing the full length and altered ECD versions of AtFH3 and AtFH5 fused to mNG from three independent transgenic lines were imaged using a Leica SP5 laser scanning confocal microscope, with a 488 nm excitation laser, an RSP500 dichroic beam splitter and HyD detectors capturing signal in the 588 - 670 nm wavelength range. Z-stacks were captured throughout the width of each pollen tube, with automatically optimized Z-slice steps. At least 15 pollen tubes were imaged for each construct in both Columbia and *hpat1,2,3* backgrounds. Image analysis was performed using ImageJ. To measure fluorescence intensity, a segmented line along the pollen tube periphery, starting from the tip pole towards the shank was drawn in the medial Z-section. Using the *plot profile* tool in ImageJ, the pixel gray value along the line distance was measured, with distance 0 representing the tip pole. The values of fluorescence intensity over distance for each of the genotype-construct combinations was fitted using a linear mixed-effect model with a random slope accounting for within-group variability in cell fluorescence (table 3-2) using the *lme4* package in R (Bates et al., 2015). A maximum likelihood ratio test was used to determine the best fit model, results of this test and *lme4* diagnostics are shown in Table 3-2. Coefficient estimates were extracted and compared for statistical significance using the sJPlot R package.

For FM4-64 staining and Brefeldin A treatment (BFA), pollen tubes expressing AtFH3:mNG or AtFH5:mNG in the Columbia and *hpat1,2,3* background, were grown as described in the '*Pollen assays*' section, but incubated without coverslips. After 45 min of incubation, 12 µM of FM4-64 in liquid PGM was added on top of the pollen tubes and incubated for 15 additional min (total incubation 60 min). Pollen tubes were then incubated for 60 minutes with the mock treatment (PGM + methanol) or BFA treatment (25 µM BFA in PGM). For plasmolysis experiments, pollen tubes expressing AtFH3:mNG or AtFH5:mNG in the Columbia background were grown as mentioned above, after 45 min of incubation on regular solid PGM, they were transferred to imaging chambers with solid PGM with 25% of sucrose to induce plasmolysis. 12 µM of FM4-64 in liquid PGM with 25% sucrose was added on top and pollen tubes were then incubated for 10 min. A coverslip was placed gently on top of the silicone chamber, and samples imaged using a Leica SP5 laser scanning confocal microscope with the same settings as above for mNG and for FM4-64, laser excitation was set up at 514 nm wavelength, a DD458/514 dichroic beam splitter, and a HyD detector capturing light in a 620-783 nm wavelength range was used.

Fluorescence Recovery After Photobleaching (FRAP) assays were performed in epidermal cells of Arabidopsis stable lines expressing AtFH1ecd:GFP, AtFH3ecd:GFP or AtFH5ecd:GFP, using the FRAP LAS application wizard of the Leica TCS SP8 confocal microscope. For excitation, the white light laser was set up for excitation at 488 nm, notch filter set NF488 and PMT detector capturing light in the 496-558 nm wavelength range, maintaining minimum laser intensity to prevent unwanted photobleaching during time-lapse imaging. Photobleaching of a circular ROI (1 μm^2 area) in a single Z-plane was performed using the white light laser set up at 488 nm and

100% intensity for 10 seconds. Recovery of GFP fluorescence was documented by capturing images every 2 seconds for 1 minute post photobleaching. For mEosFP photoconversion assays in pollen tubes expressing AtFH3:mEosFP, AtFH5:mEosFP or deletion versions of their respective Pro-rich regions (AtFH3Δ[P]:mEosFP or AtFH5Δ[P]:mEosFP), excitation of the green from of mEosFP (mEosFP-G), white light laser was setup at 505, while for the red from of mEosFP (mEosFP-R) set up at 569 nm; notch filter set NF488/561/633, PMT detectors captured light at 490-516 nm for mEosFP-G and 570-635 nm wavelength range for mEosFP-R. Photoconversion of an ROI (for AtFH3 a rectangular ROI of 8 μm^2 area in the pollen tube's subapical region or shank, for AtFH5 a circular ROI of 5 μm^2 area near the subapical region of the pollen tube) was achieved with a 405 laser diode, 80% intensity for 8-14 seconds in the pollen tube medial plane. After photoconversion, recovery of mEosFP-G was recorded for 1-2 minutes. Recovery curves for GFP were calculated according to Zheng et al. (2011). Kymographic analyses of the mEosFP photoconversion data were performed by measuring the fluorescence intensity along the pollen tube periphery over time, then the mean fluorescence values then were normalized to their maximum value and kymographs were built in RStudio.

3.3.5. Pollen tube F-actin immunolabeling

F-actin staining of pollen tubes was performed following the protocol by (Qu et al., 2020). with some modifications. Briefly, Columbia wild-type and *hpat1,2,3* pollen tubes were grown on a pad of solid PGM pH 7 for 50 min in a humid chamber at room temperature (three biological replicates, *n*=20 pollen tubes per replicate). To disrupt HRGP *O*-glycosylation or perturb AGP function, wild-type pollen tubes were treated with 30 μM β-Yariv or increasing concentrations of 3-4-Dehydro-DL-proline (3-4-DHP, 10, 20 or 30 μM) dissolved in liquid PGM and incubated for

45 min prior to the fixation step (*n*=10 pollen tubes per treatment, two biological replicates). Additionally, to determine the effect of the deletion of FH1/FH2 domains on actin organization, wild-type pollen tubes, fh3-1, fh5-2 and *fh3-1* AtFH3ΔECD:mNG or *fh5-2* AtFH5ΔECD:mNG lines were grown in the same system (imaging chambers with sold PGM pH 7 for 50 min, *n*>15 pollen tubes per genotype, two biological replicates). After incubation, pollen tubes were incubated for 1 h at 28°C with fixative (300 µM m-maleimidobenzoyl-N-hydroxysulfosuccinimide ester, MBS, in liquid PGM pH 7). The fixative was removed by capillarity using Kimwipes (Kimtech, AA120) and the tubes were washed for 10 min with wash buffer 1 (150 µM MBS in liquid PGM pH 7, 0.05% v/v Nonidet P-40), followed by three washes for 10 min each with wash buffer 2 (50 mM Tris-HCl pH7.4, 200 mM NaCl, 10% [w/v] sucrose, 0.05% [v/v] Nonidet P-40). Pollen tubes were then incubated with CytoPainter Phalloidin-iFluor 488 Reagent (1:1000 in wash buffer 2; Abcam, ab176753) or CytoPainter Phalloidin-iFluor 594 (1:1000 in wash buffer 2; Abcam, ab176757) overnight at 4°C in the dark. The following day, pollen tubes were washed twice with wash buffer 2 for 10 min, protecting samples from light. A coverslip was placed carefully on top of the PGM pad and the samples were imaged with the Leica SP5 laser scanning confocal microscope, using a 488 nm excitation laser, an RSP500 dichroic beam splitter and HyD detectors capturing signal in the 495 – 600 nm wavelength range for samples incubated with CytoPainter Phalloidin-iFluor 488, while samples incubated with CytoPainter Phalloidin-iFluor 594 were imaged using a 561 nm excitation laser, and DD458/514 dichroic beam splitter and HyD detectors capturing light 590 – 670 nm wavelength range . All genotypes were imaged using identical settings (laser intensity, gain and line averaging). Z-stacks were taken throughout the width of each pollen tube, with a Z-slice step of 0.5 µm. Image analysis was performed using ImageJ. Signal intensity was measured in maximum intensity

projections as the mean gray value in a 5 µm x 10 µm rectangular region in the pollen tube tip. To measure filament angles, semi-projections of two to three adjacent z-slices were generated and filament angle degree with respect to the axis of growth was measured. From 20 pollen tubes of each genotype, n ≥ 700 filament angles were measured, and their respective distributions plotted. 3D surface plots were built using the orthogonal view and 3D interactive surface plot tools in ImageJ.

3.3.6. Genetic complementation

Single insertion, Columbia wild-type lines expressing AtFH3:mNG or AtFH5:mNG and their ΔECD:mNG versions were introgressed to the *fh3-1* or the *fh5-2* background, respectively. Germination percent was measured after 3 hours of incubation for the wild-type, *fh3-1*, *fh5-2* mutant backgrounds and complemented lines *fh3-1C* or *fh3-1* AtFH3ΔECD:mNG and *fh5-2C* or *fh5-2* AtFH5ΔECD:mNG in three independent assays (n > 1000).

3.3.7. Microsome isolation, B-Yariv precipitation, and protein purification

Adult leaves from *Arabidopsis* stable lines expressing AtFH1ecd:GFP6xHis, AtFH3ecd:GFP6xHis and AtFH5ecd:GFP6xhis or free GFP6xHis under the CaMV 35S promoter were used as source for all protein assays. Protein methods are described in detail in Lara-Mondragón & MacAlister (2020). Briefly, ground frozen leaves were homogenized in extraction buffer (100 mM Tris-HCl pH 7.5, 8% sucrose, 5% glycerol, 10 mM EDTA, 10 mM EGTA, 5 mM KCl, 1 mM DTT, 1 mM PMSF, 0.4% casein and Pierce protease inhibitor cocktail (Thermo Scientific, A32953). The homogenate was incubated for 10 min with 4 mg of polyvinylpolypyrrolidone (PVPP) on ice, spun down for 3 min at 600 x g and 4°C to remove

insoluble particles. The homogenate was filtered through a 70 μm pore size nylon strainer to remove tissue debris (Thermo Scientific, 22363548). Microsomal fractions were collected by ultracentrifugation at 100,000 x g for 1 hour at 4°C. The microsomal fractions were emulsified in a buffer containing 10 mM Tris pH 7.5, 150 mM NaCl, 5 mM EDTA and 1% triton. Protein concentration of emulsified microsomes was determined using the Pierce BCA assay kit (Thermo Scientific, 23225).

Precipitation of arabinogalactan glycoproteins (AGPs) was performed by incubating 1-2 mg of microsomal fractions with 1 mg/mL β-Yariv dissolved in 1% (w/v) NaCl overnight. The following day, samples were spun down at 21,000 x g for 10 min and the pellet washed with 1% NaCl twice. Finally, the β-Yariv/AGP complex was dissociated by serially adding with 250 μl of DMSO, 750 μl cold acetone and 10 μl of 2% NaCl and spun down at 21,000 x g for 10 min. This last step was repeated 2 more times and finally, the pellet containing AGP glycoproteins was resuspended in sample buffer and separated in a 10% SDS-PAGE gel. The resolved fractions were then analyzed by Western blot with anti-GFP antibody (Invitrogen, # A-11122).

3.3.8. Phylogenetic analysis

Protein sequences of all 11 members of the class I formin family were aligned using ClustalX. Then, a maximum parsimony tree with 1000 bootstrap replicates was constructed using Phylip 3.698 (Fenselstein, 1989).

3.4. Results

3.4.1. The ECD of pollen-expressed formins is necessary for PM localization

To evaluate the contribution of the ECD to the localization patterns of AtFH3 and AtFH5, we generated a series of C-terminus translational fusions of AtFH3 and AtFH5 to the fluorescent protein mNeonGreen (mNG) (Figure 3-1A-B). Consistent with previous reports (Cheung et al., 2010; Lan et al., 2018), when expressed in the wild-type background, the localization of AtFH3 and AtFH5 displayed two distinct patterns: AtFH3 localized throughout the pollen tube periphery (Figure 3-1D), whereas AtFH5 was restricted to the apical PM (Figure 3-1J). Loss of function alleles of AtFH3 (*fh3-1*) or AtFH5 (*fh5-2*) display reduced pollen germination and pollen tube growth *in vitro* (Lan et al., 2018). In our growth conditions, however, only pollen germination had a statistically significant reduction (Figure 3-1C, Figure 3-7A). We therefore only used pollen germination for further phenotypic analysis. To test whether our translational fusions were functional, we introgressed AtFH3:mNG into the *fh3-1* background and AtFH5:mNG into the *fh5-2* background, which resulted in full rescue of the germination defect, indicating that the fusion proteins were functional (Figure 3-1C).

Interestingly, deletion of the ECD in both AtFH3 (Figure 3-1E) and AtFH5 (Figure 3-1K), resulted in a drastic reduction of the PM localization of the fusion proteins and intracellular accumulation, despite possessing intact secretion signals and transmembrane domains (Figure 3-1A). Introgression of AtFH3ΔECD:mNG and AtFH5ΔECD:mNG into the corresponding mutant backgrounds failed to rescue the germination defect, suggesting that the ECD of both AtFH3 and AtFH5 is necessary for their function (Figure 3-7B). Actin organization in the *fh3-1* and *fh5-2* mutant backgrounds was reported to be altered (Lan et al., 2018), particularly, reduced actin accumulation and filament disorganization in the apical area. Since the deletion of the ECDs of AtFH3 and AtFH5 were unable to rescue the germination defect in their respective mutant

backgrounds, we investigated whether actin organization remained defective in these lines. Consistent with prior observations by Lan et al. (2018), both *fh3-1* and *fh5-2* pollen tubes exhibited reduced actin labeling intensity in the apex compared to wild-type pollen tubes (Figure 3-8A-C) and, similarly, reduced accumulation of apical actin filaments was observed in the lines expressing the ΔECD:mNG versions of AtFH3 and AtFH5 (Figure 3-8D-E). Together, these results complement our genetic studies (Figure 3-7B) and suggest that the FH1/FH2 domains of AtFH3/5 are unable to function properly in the absence of their respective ECDs.

3.4.2. The lack of Hyp-O-Arabinosylation alters AtFH5 patterning

Our results indicate that the ECD of class I formins is necessary for their proper PM localization (Figure 3-1, Figure 3-7). The ECDs of both AtFH3 and AtFH5 are Pro-rich; AtFH3 possess clustered AGP-like glycosylation motifs, while AtFH5 contains EXT-like motifs (Figure 3-1B). We hypothesized that the Pro-rich region of the ECD of these proteins, containing glycosylation motifs, might contribute to their distinct localization patterns. To explore this hypothesis, we investigated the effect of smaller deletions of the Pro-rich regions of AtFH3 (AtFH3Δ[P]:mNG) and AtFH5 (AtFH5Δ[P]:mNG) on their respective subcellular localization, and additionally, for AtFH5, a smaller deletion including its EXT-like motifs (AtFH5Δ{SPPP}:mNG) (Figure 3-1A,B). The PM localization of AtFH3Δ[P]:mNG was unaffected compared to AtFH3:mNG (Figure 1D,F). AtFH5:mNG exhibited a polar localization, restricted to the elongating tip (Figure 3-1J). Interestingly, a moderate but significant expansion in the localization of the version where the Pro-rich region of AtFH5 compared to the full-length version was observed (Figure 3-1J, L). To assess whether such differences in polarized patterning were statistically significant, we applied a linear mixed-effect model (LMEM) to the data, comprising measurements of the mean

fluorescence intensity over distance, with 0 μm being the pollen tube tip (Figure 3-1R, see supplemental table 3-2 for model parameters). The model shows a negative relationship between fluorescence intensity and distance (Figure 3-1R, Table 3-2): the mean fluorescence intensity (mFI) estimate for AtFH5:mNG in the wild type background was 116.36 (95% CI =[100.92, 131.79]) and decreased over distance reaching an estimate of 48.01 (95% CI =[32.61, 63.41]) at 15 μm from the tip. AtFH5Δ[P]:mNG and AtFH5Δ{SPPP}:mNG were localized in the apical PM (Figure 3-1L-M), although, the localization of the Pro-rich region deletion exhibited a significant increase in the MFI estimate at 10 μm (MFI = 93.77, 95% CI =[71.42, 116.13], p-value < 0.05) and at 15 μm from the tip in the AtFH5Δ[P]:mNG (MFI = 72.94, 95% CI=[50.56, 95.31], p-value < 0.05, Figure 3-1V) version compared to AtFH5:mNG, suggesting that its plasma membrane localization extended beyond the subapical region. No significant differences in the intercept estimates of AtFH5Δ{SPPP}:mNG compared to the full-length AtFH5:mNG were observed.

Based on the localization analyses and altered localization observed in AtFH5Δ[P]:mNG, which contains HRGP-like motifs (Figure 3-1B,R-V), we hypothesized that potential glycosylation of these residues is necessary for the apical localization of AtFH5. Hydroxyproline-*O*-arabinosyltransferases (HPATs) initiate the addition of arabinosides to hydroxyproline residues within Ser-$Pro_{(3-5)}$ motifs (Ogawa-Ohnishi et al., 2013). The loss of function of HPAT1 and HPAT3 displays a severe male reproductive defect; pollen tubes lacking hyp-*O*-arabinosylation display a range of phenotypes including reduced rates of elongation, initiation of secondary tips, and pollen tube rupture (Beuder et al., 2020; MacAlister et al., 2016). To further explore the effect of hyp-*O*-arabinosylation in the localization of AtFH5, we expressed all previous

constructs in the *hpat1,2,3* background and investigated changes in their subcellular localization. Interestingly, AtFH5:mNG greatly expanded its localization beyond the apical PM (Figure 3-1J, N), supporting our hypothesis. LMEM intercept estimates for the full length AtFH5:mNG the *hpat1,2,3* background exhibited significant differences throughout the measured distances (Figure 3-1S-V), starting at the tip with an estimated MFI of 182.64 (95% CI=[156.73,208.56], p-value <0.001) and reaching at 15 µm an MFI estimate of 126.44 (95% CI:[100.61, 152.26], p-value < 0.001). When expressed in the *hpat1,2,3* background, the localization AtFH5Δ[P]:mNG exhibited no difference in its MFI estimate at the tip or subapical area but a significant increase compared to wild-type farther from the tip (Figure 3-1P,U-V); AtFH5Δ{SPPP}:mNG displayed a similar behavior, however, a higher MFI estimate was only observed at 15 µm from the tip (Figure 3-1Q, V). The deletion of the ECD for both AtFH3 and AtFH5, as in the WT background, caused intracellular accumulation in *hpat1,2,3* pollen tubes (Figure 3-1H, O).

3.4.3. Pollen tubes lacking O-glycosylation exhibit altered F-actin organization

The extent of cytoskeleton, PM and cell wall interconnection is often evidenced by reciprocal defects in cytoskeleton organization or cell wall structure when one is disrupted (Chebli et al., 2021). Our group recently showed that *hpat* mutant pollen tubes exhibit an altered distribution of cell wall polymers (Beuder et al., 2020). Based on our findings on the localization of AtFH5 in the *hpat1,2,3* background, we predicted that mutant pollen tubes will exhibit actin disorganization, potentially as a result of AtFH5 mislocalization (Figure 3-1). We analyzed the organization of the actin cytoskeleton in pollen tubes grown *in vitro* by fluorescent labeling of actin filaments with phalloidin (Figure 3-2). Compared to wild-type tubes, mutant pollen tubes

displayed a significant decrease in fluorescence intensity (Figure 3-2A-B). In addition, *hpat1,2,3* pollen tubes showed distinct organization of F-actin compared to wild-type pollen tubes (Figure 3-2A). To quantitatively assess the extent of actin disorganization in mutant pollen tubes, we measured the angles formed by individual filaments in semi-projections (2 to 3 adjacent *z*-slices) relative to the axis of growth throughout the pollen tube width. In wild-type pollen tubes, most filaments formed acute angles (≤ 30°), oriented almost parallel to the growth axis. Actin filaments in *hpat1,2,3* pollen tubes, on the other hand, formed angles in a wider degree range, including 90° angles, which were absent in the wild type (Figure 3-2C). In wild-type pollen tubes, large organelles (lipid droplets, amyloplasts, Golgi) remain restricted to the shank, while the tip is enriched in small endo/exocytic vesicles (Figure 3-2D), forming a region known as the 'clear zone' (Cheung & Wu, 2007). Proper organization of the actin cytoskeleton in pollen tubes is important to maintain said cytoplasmic zonation; disruption of actin disorganization often leads to invasion of the clear zone (G. Li et al., 2018). In *hpat1,2,3* pollen tubes, we observed occasional invasion of the clear zone by large particles displaying erratic movement over time (~23% of tubes, N=17, Figure 3-2E). Clear zone invasion was not observed in any of the analyzed wild-type pollen tubes (N=14).

The F-actin organization defects observed in *hpat1,2,3* pollen tubes are consistent with potential ectopic AtFH5 activity due to mislocalization and/or potential interference with AtFH3 activity. Alternatively, although not mutually exclusive, F-actin disorganization could be a consequence of the altered cell wall organization in mutant pollen tubes (Beuder et al., 2020), ultimately altering the linkage between cell wall-actin cytoskeleton and disrupting cell polarity. To better understand the potential genetic interactions between pollen class I formins, particularly AtFH5,

and HPATs, we generated quadruple mutants *hpat1,2,3/fh3-1* and *hpat1,2,3/fh5-2* and evaluated the effects in pollen tube morphology compared to the *hpat1,2,3* mutant. Interestingly, phenotypic analyses of the quadruple mutants showed a significant increase in pollen tube branching compared to the *hpat1,2,3* background while the percentage of pollen tube bursting in the triple mutants remained unchanged (Figure 3-2F-G), suggesting that pollen tube branching is potentially a consequence of altered F-actin dynamics rather than compromised cell wall integrity.

As determined earlier, the mNG fusions of AtFH3 and ECD modified versions did not exhibit an altered PM localization in the *hpat1,2,3* mutant background (Figure 3-1D-I). Considering that the ECD of AtFH3 contains AGP-like motifs, we investigated whether interfering with AGP glycosylation and potentially, the posttranslational modification of the ECD of AtFH3, could also have an effect in F-actin organization. The β-Yariv reagent binds selectively to the β-1,3-galactan main chains of AGPs, precipitating them (Kitazawa et al., 2013). β-Yariv is not only used to precipitate AGPs *in vitro,* but also to perturb AGP function *in vivo* (Přerovská et al., 2021). Thus, we incubated *in vitro* grown pollen tubes with 30 µM β-Yariv and stained the actin cytoskeleton with fluorescent phalloidin. Altered pollen tube morphology and growth arrest was observed after treatment, while F-actin organization, particularly in the apical and subapical region was altered (Figure 3-9A-B). Furthermore, to simultaneously disturb *O*-glycosylation of AGP and EXT, and potentially, the ECDs of AtFH3/5, we evaluated the effect in actin organization upon treatment with 3,4-Dehydro-DL-proline (3,4-DHP). 3,4-DHP is a selective inhibitor of prolyl hydroxylases, thus, effectively disrupting *O*-glycosylation of HRGPs (X. Zhang et al., 2014). The three tested concentrations of 3,4-DHP tested (10, 20 and 30 µM)

induced changes in pollen tube morphology (i.e. branching and bulging), as well as an altered distribution of actin filaments (Figure 3-9C-F). Taken together, these results suggest that F-actin organization in elongating pollen tubes is sensitive to perturbations in HRGP *O*-glycosylation pathways, possibly affecting the function of pollen class I formins.

3.4.4. AtFH5's apical PM localization is maintained by endocytosis

Our results indicate that the apically restricted localization of AtFH5 in elongating pollen tubes is dependent on the ECD and its potential post-translational modification by HPATs (Figure 3-1). However, other mechanisms such as endocytosis are known to limit the distribution of other secreted, tip-localized proteins in pollen tubes (Grebnev et al., 2017; Röckel et al., 2008). To investigate whether endocytosis is involved in the observed patterning of AtFH3 and AtFH5, we evaluated the effects of Brefeldin A (BFA) treatment on their localization in *in vitro* grown pollen tubes. The fungal metabolite BFA is known to disrupt plant cell membrane trafficking by blocking exocytosis while allowing endocytosis to occur (Baluška et al., 2002). Pollen tube growth is arrested when treated with BFA, inducing the accumulation of FM4-64 positive membrane aggregates in the subapical region (Brefeldin-induced aggregates, BIA) (Parton et al., 2003). Reports suggest that treatment also enhances endocytosis in pollen tubes (Wang et al., 2005). Therefore, we hypothesized that if endocytosis played a role in AtFH5 localization, BFA treatment would cause its intracellular accumulation, co-localizing with BIAs. Pollen tubes expressing either AtFH3:mNG or AtFH5:mNG were stained with FM4-64 and then treated with BFA for 60 min. After treatment, we observed that AtFH5:mNG was completely depleted from the PM, accumulating in the subapical region and co-localizing with FM4-64 stain (Figure 3-3C,D). The localization of AtFH3, on the other hand, remained unchanged compared to the mock

treatment (Figure 3-3A, B). These results suggest endocytic internalization of AtFH5 in the pollen tube's shank participates in restricting its accumulation beyond the apical PM.

3.4.5. The ECDs of class I formins bear distinct types of O-glycans

O-glycosylation of the ECD of class I formins has long been speculated (Banno & Chua, 2000; Borassi et al., 2016); however, direct evidence is still lacking. To address this question, we generated genetically tagged versions of the ECD of pollen formins AtFH3 (AtFH3ecd:GFP6xHis) and AtFH5 (AtFH5ecd:GFP6xHis), also including the vegetative formin, AtFH1 (AtFH1ecd:GFP6xHis) (Figure 3-4B). These constructs contained their respective signal peptides and transmembrane domains, and as expected, localized to the plasma membrane when expressed transiently in tobacco leaves (Figure 3-4A). Immunodetection of the tagged ECDs in the microsomal fraction isolated from stable Arabidopsis lines showed higher sizes than predicted based on the aminoacid sequences (Figure 3-4D), potentially indicating the presence of post-translational modifications on the protein backbones.

According to the hydroxyproline contiguity hypothesis (Shpak et al., 2001) and based on the aminoacid sequences of the ECDs of the selected formins (Figure 3-2B), we hypothesized that the ECD of AtFH3 will bear AGP-like glycans, while the ECDs of AtFH1 and AtFH5, will be primarily *O*-arabinosylated. To address their glycosylation status, we followed two strategies: first, we investigated the presence of AG glycans in the ECDs by utilizing the synthetic reagent β-Yariv (Figure 3-4B). Microsomal fractions derived from transiently transformed tobacco leaves expressing the GFP-tagged ECDs of AtFH1, AtFH3 or AtFH5 were incubated with β-Yariv and, the resulting AGP-enriched fractions were analyzed by immunodetection. Our results

showed that among all the analyzed ECDs, AtFH3ecd:GFP6xHis was greatly enriched in the fraction precipitated by β-Yariv . Free GFP did not display reactivity towards the β-Yariv reagent, demonstrating the specificity of this assay (Figure 3-4B,C).

The second approach consisted in protein purification by metal affinity chromatography followed by immunodetection with anti-glycan antibodies. While we attempted to purify all three ECDs from Arabidopsis stable lines (Figure 3-4D), an acceptable level of purity to allow glycoprofiling was only achieved for AtFH1ecd:GFP6xHis (figure 3-10C). After protein purification, AtFH1ecd:GFP6xHis was probed with two anti-glycan antibodies: anti-hyp-ara (JIM19) and anti-hyp-AG (JIM13) (Knox, 1995; Knox et al., 1991; Yates & Knox, 1994). Hyp-*O*-arabinosylation was detected in the input of both, microsomes derived from plants expressing AtFH1ecd:GFP6xHis and non-transformed plants (Input, Figure 3-4E); however, after His-purification, glycosylation was only detected in the eluate of AtH1ecd:GFP6xHis (Elution, Figure 3-4E). Supporting our hypothesis, the observed band in the AtFH1ecd:GFP6xHis corresponds to the size observed when probing with anti-GFP (Figure 3-4D). Consistent with the β-Yariv precipitation assay, purified AtFH1ecd:GFP6xHis did not show reactivity to anti-hyp-AG antibodies (figure 3-10C,D), supporting our hypothesis.

HRGP-like motifs are present in the ECDs across most members of the class I formin family (Figure 3-11, Borassi et al., 2016). In addition to AtFH1 and AtFH5, AtFH9 and AtFH10 possess EXT-like motifs; AtFH11, like AtFH3, contains exclusively AGP-like motifs. The remaining members of the family (AtFH2, AtFH4, AtFH6 and AtFH8) possess short AGP-like, clustered dipeptides (2-3 repeats) and Ser-Pro-Pro repeats that, like the Ser-$Pro_{(3-5)}$ EXT motifs, can be

modified by the addition of arabinosides (Estévez et al., 2006; Shpak et al., 2001). Taken together, our results provide the first direct biochemical evidence suggesting that the chimeric HRGP motifs present in the ECDs of members of the class I formin family are *O*-glycosylated and that these post-translational modifications might be widespread across the clade.

3.4.6. The ECDs of pollen class I formins display distinct lateral plasma membrane mobility

Integral membrane (or PM associated) proteins facing the cell wall display restricted lateral mobility (Martinière et al., 2012), AtFH1, a class I formin expressed in vegetative tissues is immobilized in the PM by its interaction with the cell wall (Martinière et al., 2011). Based on these observations, class I formins had been regarded as candidates to mediate physical membrane anchoring to the wall or Hechtian adhesion (Lamport et al., 2018; Pont-Lezica et al., 1993). In addition, AGPs were reported to co-localize with membranous thread-like structures (Hechtian strands) upon plasmolysis, thus having potential role in Hechtian adhesion (Sardar et al., 2006). Similarly, canonical EXTs had been shown to serve as a scaffold for pectin supramolecular assembly and to covalently crosslink with pectin polysaccharides (Cannon et al., 2008), also having the potential to establish interactions with the wall through a distinct mechanism. Given that our biochemical studies provided evidence for the presence of AGP-like glycans in the ECD of AtFH3 and putative EXT-like glycans in the ECD of AtFH5 (Figure 3-4), we investigated whether Hechtian adhesion in pollen tubes was reduced in the loss of function alleles *fh3-1* and *fh5-2*. Plasmolyzed wild-type, *fh3-1* and *fh5-2* pollen tubes were stained with the lipophilic dye FM4-64 and imaged through confocal microscopy. Although FM4-64 positive structures were observed to localize in the apoplastic space upon plasmolysis in all three genotypes, a quantitative assessment of the extent of adhesion among genotypes was limited due

to the size of the Hechtian strands, which were below the resolution achieved by confocal microscopy (Figure 3-12A). Neither AtFH3 nor AtFH5 had been reported to localize to Hechtian strands in pollen tubes, thus, we induced plasmolysis in our complemented lines (*fh3-1 C* and *fh5-2 C*) and stained them with FM4-64. We found that AtFH3:mNG colocalized with FM4-64 positive membranous extensions that remained in contact with the wall upon plasmolysis. AtFH5:mNG signal was also observed in the apoplastic space, however, only partial colocalization was observed (Figure 3-12B). These results indicate that the ECDs of AtFH3 and AtFH5 establish distinct types of interactions with the wall, with AtFH3 and AG glycans in their ECD possibly involved in Hechtian adhesion in elongating pollen tubes.

Having determined that both AtFH3 and AtFH5 establish interaction with the wall (figure 3-12B) and based on our localization studies, particularly the expansion of AtFH5 PM localization in the *hpat1,2,3* mutant background (Figure 3-2J, N), we asked whether the presence of distinct types of glycans in their ECDs (Figure 3-4), has implications in their lateral mobility.

First, we investigated the lateral mobility of the ECDs of AtFH1, AtFH3 and AtFH5 eliminating the influence of their respective intracellular domains. We performed Fluorescence Recovery After Photobleaching (FRAP) assays in epidermal cells of Arabidopsis leaves expressing the ECD GFP-tagged versions in Figure 3-4A-B. As expected for cell wall-interacting PM proteins and consistent with Martinière et al. (2011, 2012), all three constructs exhibited limited lateral diffusion; however, significant differences in the degree of recovery were observed among ECDs: AtFH3 exhibited almost no recovery of fluorescence post photobleaching (mobile fraction 12 ± 3.6%, n=9), while AtFH5 and AtFH1 displayed comparatively higher recovery

(mobile fraction 46.5 ± 8.1%, n=11 and 60.9 ± 11.6%, n=8, respectively) (Figure 3-5). AtFH1 and AtFH5, both containing EXT-like motifs in their ECDs, displayed similar recovery curves and lateral mobility. In contrast, AtFH3, which contains AGP-like glycomodules was highly restricted, suggesting that the different glycans attached to these proteins (Figure 3-4C, E) greatly influence their mobility.

Next, we investigated the effect of the F-actin cytoskeleton in protein anchoring *in situ*. Considering that AtFH3 interacts with a much more stable subarray of actin bundles in the pollen tube's shank, while AtFH5 participates in the nucleation of highly dynamic, finer actin filaments in the apical and subapical region (Cheung et al., 2010; Qu et al., 2015); we sought to determine whether this interaction has an effect in the protein lateral diffusion or if, as reported for AtFH1 in epidermal cells (Martinière et al., 2012), the ECD is primarily responsible of protein anchoring (Figure 3-5). Due to the high photostability of the mNG protein observed when attempting FRAP experiments, we generated translational fusions of the full length AtFH3/5 and the Pro-rich region deletions (Δ[P], Figure 3-1A-B) with the photoconvertible protein mEosFP (Mathur et al., 2010). Upon exposure to blue light, mEosFP irreversibly switches its emission spectrum from green to red. Lateral diffusion of the green mEosFP (mEosFP-G) is tracked over time akin to FRAP experiments but without potential cell photodamage (Wozny et al., 2012). We predicted that if protein anchorage is dependent on the ECD, Δ[P]:mEosFP fusions might display an increase in their lateral diffusion compared to their full length counterparts. Kymographic analyses revealed no difference in lateral diffusion pattern between AtFH3:mEosFP and AtFH3Δ[P]:mEosFP (Figure 3-6), suggesting that both the ECD and the intracellular domains participate in anchoring AtFH3 to the plasma membrane. In the case of AtFH5, we observed an

overall higher lateral mobility compared to AtFH3; however, the patterning observed in the kymographic analysis and high mEosFP-G recovery (Figure 3-10) might be partially due to rapid pollen tube elongation and continuous secretion of non-photoconverted protein. Thus, the contribution of the actin cytoskeleton in AtFH5, remains to be determined. The observed influence of the actin cytoskeleton on protein mobility in AtFH3 is consistent with its involvement in nucleation/bundling of actin filaments in the pollen tube shank (Qu et al., 2015; Thomas, 2012).

3.5. Discussion

Here, we provide functional insights on the ECD of class I formins and their role as molecular linkers mediating the crosstalk between the cell wall, PM and actin cytoskeleton. The study of AtFH3 and AtFH5 in elongating pollen tubes offered a unique system to evaluate the functional significance of the ECD of class I formins, as both AtFH3 and AtFH5 are expressed in the same cell structure and yet, display a unique spatial patterning (Figure 3-1D, J). While differences in their intracellular actin nucleation activities, differential affinity to profilin or other unknown interactors might modulate their respective patterning (Cheung et al., 2010; Lan et al., 2018; C. Liu et al., 2021; Thomas, 2012), our results suggest a pivotal role for the ECD in their localization; as evidenced by the failure of the ΔECD:mNG versions to localize to the PM and/or the inability to rescue the germination defect or actin organization in their respective transcriptional null backgrounds (Figure 3-1E, K; Figures 3-7 to 3-8). Interestingly, reports on other members of the family indicate that the ECD is required for their localization in different cellular structures: the ECD of AtFH8 is necessary for translocation from the nucleus to the newly formed cell wall after cell division (Xue et al., 2011), while the ECD of AtFH2 is

necessary for plasmodesmata localization in epidermal cells (Diao et al., 2018), suggesting that the ECD plays a role in protein localization not only in pollen-expressed formins but might be required for the proper plasma membrane localization across the class I family. Furthermore, our study provides evidence for the presence of post-translational modifications of the HRGP-like glycomotifs present in the ECDs of two members of the family (Figure 3-4), following the predictions of the hydroxyproline contiguity hypothesis (Shpak et al., 2001) and setting the precedent of *O*-glycosylation for other members of the class I formin family and possibly other HRGP chimeras (Leucin-Rich Repeat Extensins– LRXs, Proline-rich Extensin-like Receptor Kinases– PERKs, etc.). Naturally, the next question relates to the significance of these post-translational modifications in the protein's function. Our data indicate that the ECDs containing EXT-like motifs (AtFH1, AtFH5) exhibit increased lateral mobility relative to the ECD of AtFH3, which contains AGP-like motifs (Figure 3-5). Although the underlying mechanism requires further investigation, these results raise intriguing scenarios. HRGPs exhibit virtually all properties that define Intrinsically Disordered Proteins (IDPs): high content of Pro residues in their sequences, repetitive motifs, and the presence of PTMs in such motifs (Johnson, Cassin, Lonsdale, Bacic, et al., 2017); these features confer flexibility to the protein's conformation and structure plasticity, permitting transient molecular interactions (Uversky, 2019). Increasing evidence indicates that IDPs and disordered regions have important roles in cellular signaling (Hsiao et al., 2020; X. Sun et al., 2012). In particular, classical EXT and AGPs are believed to play antagonistic roles in cell wall polysaccharide remodeling (Lamport et al., 2011). EXTs form supramolecular networks that serve as scaffold for the assembly and crosslinking of pectin in the primary cell wall (Showalter & Basu, 2016), whereas AGPs putatively act as pectin plasticizers by regulating availability of Ca^{2+} in the periplasm (Lamport et al., 2018; Lopez-Hernandez et al.,

2020; Silva et al., 2020). Therefore, if the ECD of class I formins shares dynamic structural features of IDPs and known biochemical properties of EXT and/or AGPs, they might interact with cell wall polysaccharides or other extracellular (glyco)proteins, potentially establishing a cell wall sensing module. Supporting this hypothesis, we provide evidence that both AtFH3 and AtFH5 interact with the wall and that, upon plasmolysis, both exhibit apoplastic localization, with AtFH3 primarily colocalizing with plasma membrane extensions that remain anchored to the wall (supplemental figure 3-12B), suggesting a potential role for Hechtian adhesion, a mechanism proposed to act as an important mechanotransduction mechanism during tip growth (Lamport et al., 2018).

Finally, polarized growth in pollen tubes requires coordination between cell wall assembly and F-actin dynamics. Decoupling of these processes leads to disruption of growth, as observed in *hpat* mutant pollen tubes (MacAlister et al., 2016, Figure 3-2). Although *hpat1,2,3* pollen tubes exhibit compromised cell wall integrity most likely due to the lack of arabinosylation of their canonical targets, EXTs (Beuder et al., 2020), we provide genetic and biochemical evidence of novel chimeric targets that establish a linkage between cell wall, plasma membrane and actin cytoskeleton. Our data indicates that AtFH5 is maintained to the apical membrane by endocytosis (Figure 3-3) and the lack of hyp-*O*-arabinosylation alters its patterning (Figure 3-1). Whether the EXT-like motifs in AtFH5 are directly modified remains to be determined; however, we were able to detect hyp-*O*-arabinosylation in AtFH1, another class I formin with EXT-like motifs (Figure 3-4E), suggesting that these motifs might be modified by HPATs. In the case of the ECD of AtFH3, we were able to show reactivity to the β-Yariv reagent, indicating the presence of arabinogalactan glycans (Figure 3-4B,C). While the ECD alone restricts protein

mobility in epidermal cells (Figure 3-5), we also found that in highly polarized and fast-growing cells like pollen tubes, the actin cytoskeleton also plays an important role in immobilizing AtFH3, to the plasma membrane, possibly through Hechtian adhesion (Figure 3-6, Figure 3-12B). Although both pollen formins had been demonstrated to have *in vitro* actin nucleation activity (Ingouff et al., 2005; Ye et al., 2009), a recent genetic study showed that AtFH5's activity is enhanced by pollen-expressed reproductive profilins 4 and 5 (PRF4 and PRF5) during the formation of collar-like structure in germinating pollen grains (Liu et al., 2021). *In vitro* studies show that profilin has an enhancing effect on formin activity, acting as pools for fast nucleation and polymerization of actin filaments (Romero et al., 2004). While the effect of PRF4/5 on AtFH3's activity remains to be investigated, these observations open the scenario where AtFH5 participates in rapid nucleation/polymerization of cortical actin of highly dynamic apical and subapical actin arrays in pollen tubes and its ECD accounts for the protein's anchoring, while AtFH3 is anchored to the shank of the pollen tube by its ECD and association with more stable axial actin filaments.

3.6. Acknowledgements

This work was supported by the National Science Foundation under Grant No. IOS-1755482 to CAM. CMLM receives fellowship funding from the Mexican Council of Science and Technology (CONACYT - 773973).

3.7. Author Contributions

CAM conceptualized the study and acquired funding. CLM performed the research, analyzed the data and wrote the manuscript. CAM and CLM edited the manuscript. AD produced resources necessary to the completion of the project.

3.8. Data availability

The data supporting the findings of this study are available from the corresponding author, Cora A. MacAlister, upon request.

3.9. Conflict of Interest Statement

The authors have no conflicts to declare.

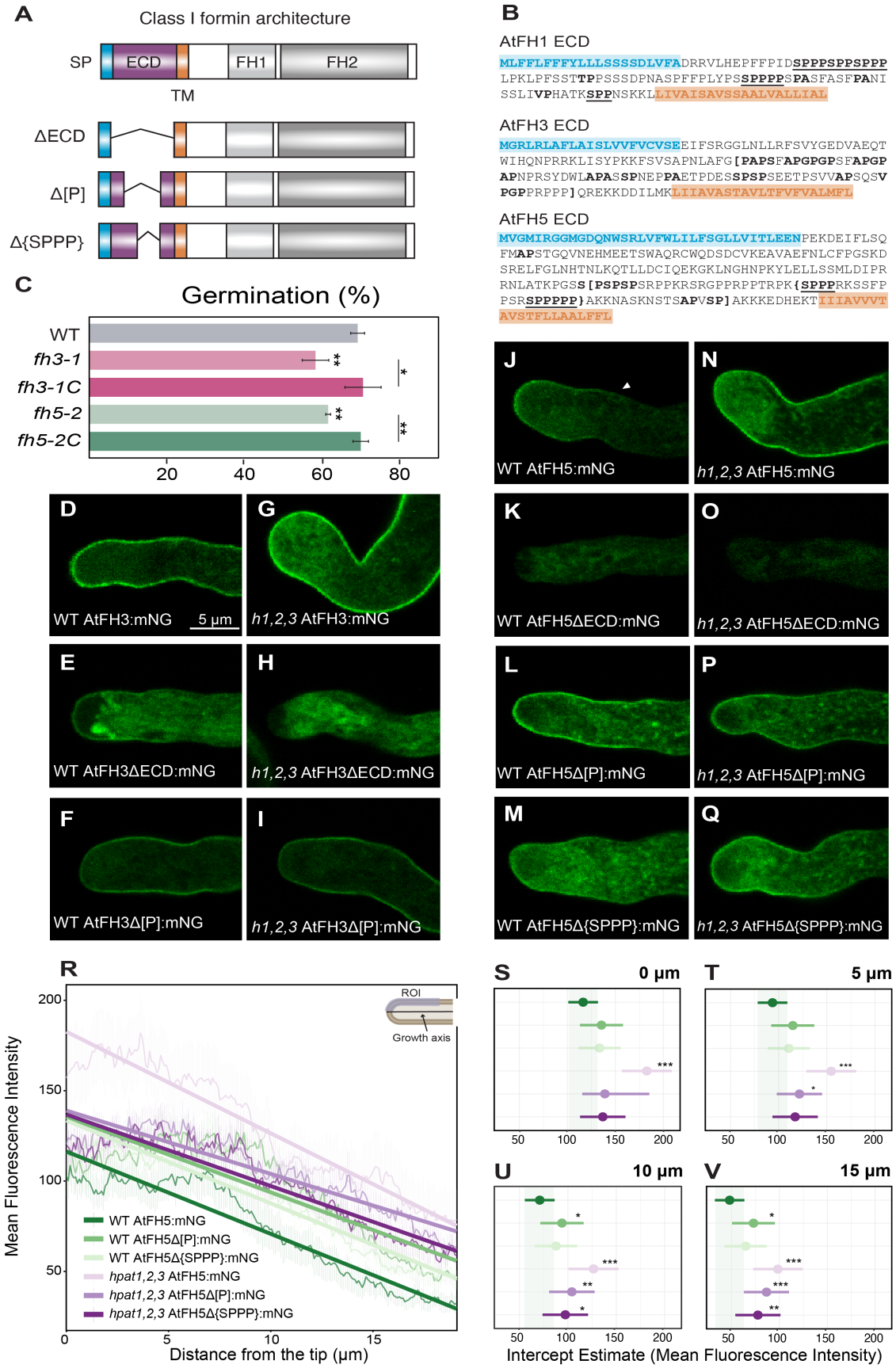
A
Class I formin architecture
SP
ECD
FH1
FH2
TM
ΔECD
Δ[P]
Δ{SPPP}
B
AtFH1 ECD
MLFFLFFFYLLLSSSSDLVFADRRVLHEPFFPIDSPPPSPPSPPP
LPKLPFSSTTPPSSSDPNASPFFPLYPSSPPPPSPASFASFPANI
SSLIVPHATKSPPNSKKLLIVAISAVSSAALVALLIAL
AtFH3 ECD
MGRLRLAFLAISLVVFVCVSEEIFSRGGLNLLRFSVYGEDVAEQT
WIHQNPRRKLISYPKKFSVSAPNLAFG[PAPSFAPGPGPSFAPGP
APNPRSYDWLAPASSPNEPPAETPDESSPSPSEETPSVVAPSQSV
PGPPRPPP]QREKKDDILMKLIIAVASTAVLTFVFVALMFL
AtFH5 ECD
MVGMIRGGMGDQNWSRLVFWLILFSGLLVITLEENPEKDEIFLSQ
FMAPSTGQVNEHMEETSWAQRCWQDSDCVKEAVAEFNLCFPGSKD
SRELFGLNHTNLKQTLLDCIQEKGKLNGHNPKYLELLSSMLDIPR
RNLATKPGSS[PSPSPSRPPKRSRGPPRPPTRPK{SPPPRKSSFP
PSRSPPPPP}AKKNASKNSTSAPVSP]AKKKEDHEKTIIAVVVT
AVSTFLLAALFFL
C
Germination (%)
WT
fh3-1
fh3-1C
fh5-2
fh5-2C
20
40
60
80
D
WT AtFH3:mNG
5 μm
G
h1,2,3 AtFH3:mNG
E
WT AtFH3ΔECD:mNG
H
h1,2,3 AtFH3ΔECD:mNG
F
WT AtFH3Δ[P]:mNG
I
h1,2,3 AtFH3Δ[P]:mNG
J
WT AtFH5:mNG
N
h1,2,3 AtFH5:mNG
K
WT AtFH5ΔECD:mNG
O
h1,2,3 AtFH5ΔECD:mNG
L
WT AtFH5Δ[P]:mNG
P
h1,2,3 AtFH5Δ[P]:mNG
M
WT AtFH5Δ{SPPP}:mNG
Q
h1,2,3 AtFH5Δ{SPPP}:mNG
R
ROI
Growth axis
Mean Fluorescence Intensity
200
150
100
50
0
5
10
15
Distance from the tip (μm)
WT AtFH5:mNG
WT AtFH5Δ[P]:mNG
WT AtFH5Δ{SPPP}:mNG
hpat1,2,3 AtFH5:mNG
hpat1,2,3 AtFH5Δ[P]:mNG
hpat1,2,3 AtFH5Δ{SPPP}:mNG
S
0 μm
T
5 μm
U
10 μm
V
15 μm
50
100
150
200
Intercept Estimate (Mean Fluorescence Intensity)

Figure 3-1 The loss of O-arabinosylation disrupts the localization of AtFH5.

A) General protein architecture of class I formins. SP: signal peptide, ECD: extracellular domain, TM: transmembrane domain, FH1: Formin Homology 1 domain, FH2: Formin Homology 2 domain. The altered versions of the ECD of AtFH3/5 are shown below: ΔECD, the entire extracellular domain was removed (purple region). In the Δ[P] versions, the Pro-rich region within square brackets (shown in B) was removed. Only for AtFH5, the Δ{SPPP} version lacked the EXT-like motifs within the brackets (AtFH5 ECD sequence, shown in B). **B)** ECD sequences of AtFH1 (vegetative) and pollen expressed AtFH3 and AtFH5. Amino acids in blue correspond to the signal sequence (SP in A); residues in orange correspond to the transmembrane domain (TM in A); amino acids in bold correspond to predicted AG glycomodules, while boldened underlined residues correspond to EXT-like glycosylation motifs. In AtFH3 and AtFH5 ECDs, regions within [] or {} correspond to deletions. **C)** Germination defects of the *fh3-1* and *fh5-2* transcriptional null alleles are rescued by expression of the full length AtFH3 or AtFH5 fused to mNeonGreen (mNG). Pollen germination *in vitro* was measured after 3 h. Three biological replicates per genotype ($n > 1000$), '*' and '**' mark statistically significant differences (Student's T-test adjusted p-value < 0.05 and adjusted p-value < 0.005, respectively). **D to F)** Full length AtFH3, ΔECD and Δ[P] versions expressed in WT or *hpat1,2,3* (*h1,2,3*) *in vitro* grown pollen tubes **(G to I)**. **J to M)** Full length AtFH5, ΔECD, Δ[P] and Δ{SPPP} mNG fusions expressed in the WT background or the *hpat1,2,3* background **(N to Q).** Arrowhead in **(J)** indicates the boundary of AtFH5 plasma membrane localization. **R)** Linear mixed-effect model with random slope fitted onto the data (fluorescence intensity over distance) measured for each construct-genotype combination. Mean fluorescence is shown in the plot as solid lines and shaded area represents standard error. Trendlines predicted by the model are shown in the same color scheme. Y-intercepts (mean fluorescence intensity) predicted by the model (dots) and their 95% confidence intervals (bars) at the tip (0 µm, **S**), subapical region (5 µm, **T**), 10 µm **(U)** or 15 µm **(V)** from the tip. Stars indicate a statistically significant difference using the WT AtFH5:mNG as reference. '*' indicates p-value < 0.05, '**' p-value < 0.005 and '***' p-value <0.001. Over 15 pollen tubes from three independent transgenic lines were measured per genotype and construct.

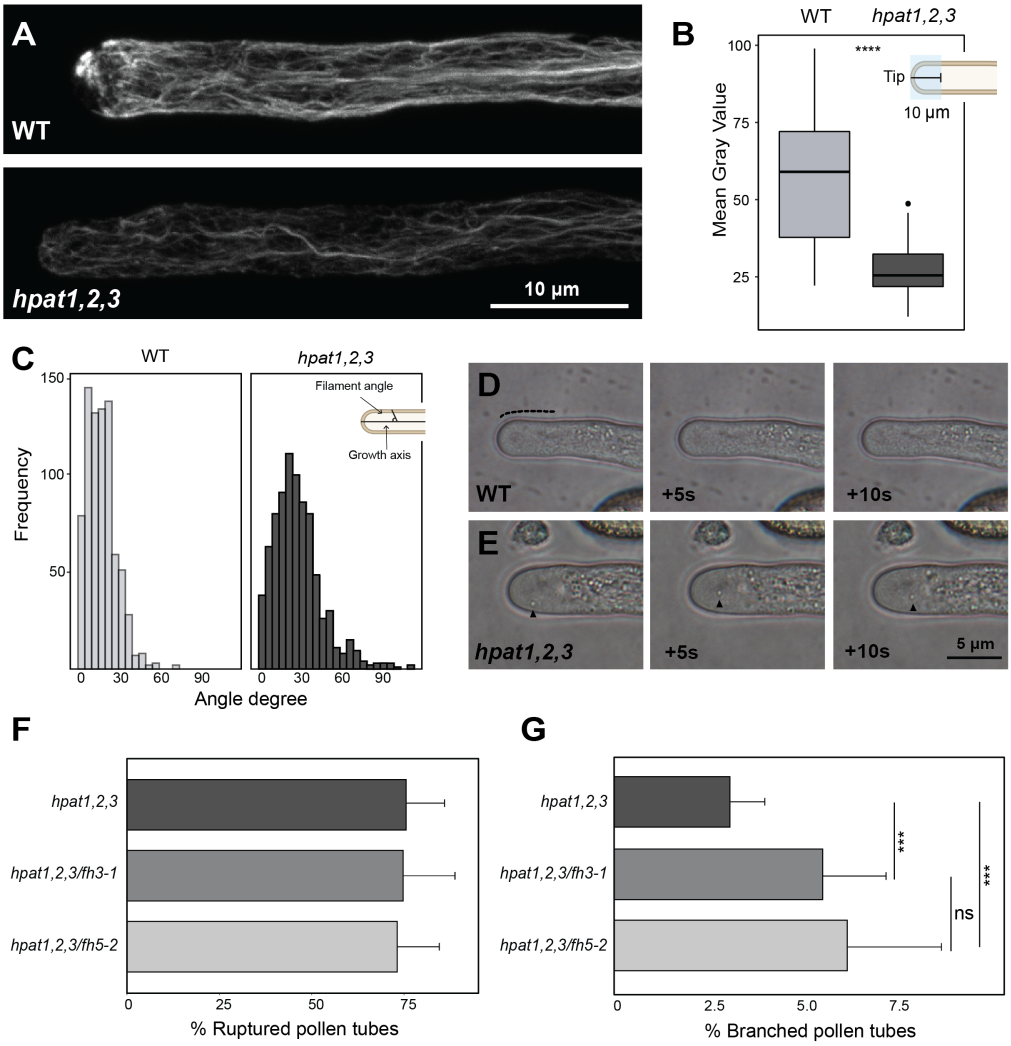

Figure 3-2 Pollen tubes lacking O-arabinosylation display F-actin cytoskeleton disorganization.

A) Representative images of *in vitro* germinated pollen tubes stained with phalloidin-iFluor 488, top: wild-type, bottom: *hpat1,2,3*. **B)** Quantification of fluorescence intensity in the apical-subapical region (10 µm from tip dome toward the shank, blue shaded square in top right schematic). *n*=20 for each genotype, '****' statistically significant difference (Student's T-test, p-value < 0.0005). **C)** Actin filament angle distribution in wild-type (left) and mutant pollen tubes (right). Angles were measured with respect to the growth axis (top right schematic), over 700 filaments from 20 tubes were measured for each genotype. **D)** Wild type pollen tubes grown in vitro (*n*=14). The apical 'clear zone' is indicated with a dashed line. **E)** Invasion of the apical clear zone in *hpat1,2,3* pollen tubes grown *in vitro*. Micrographs represent time series from the same pollen tube, arrowhead indicates invasive particle (*n*=17). **F to G)** Phenotyping of triple *hpat1,2,3/fh3-1* and *hpat1,2,3/fh5-2* mutants. Compared to *hpat1,2,3* pollen tubes, *hpat1,2,3/fh3-1* and *hpat1,2,3/fh5-2* mutants showed increased pollen tube branching **(F)** but not increased pollen tube rupture **(G).** Mean and SD of pollen branching/rupture measured after 3 h of germination *in vitro*, > 5 biological replicates per genotype (*n* > 2500), '***' statistically significant difference (Student's T-test adjusted p-value < 0.005), 'ns' indicates no statistically significant difference.

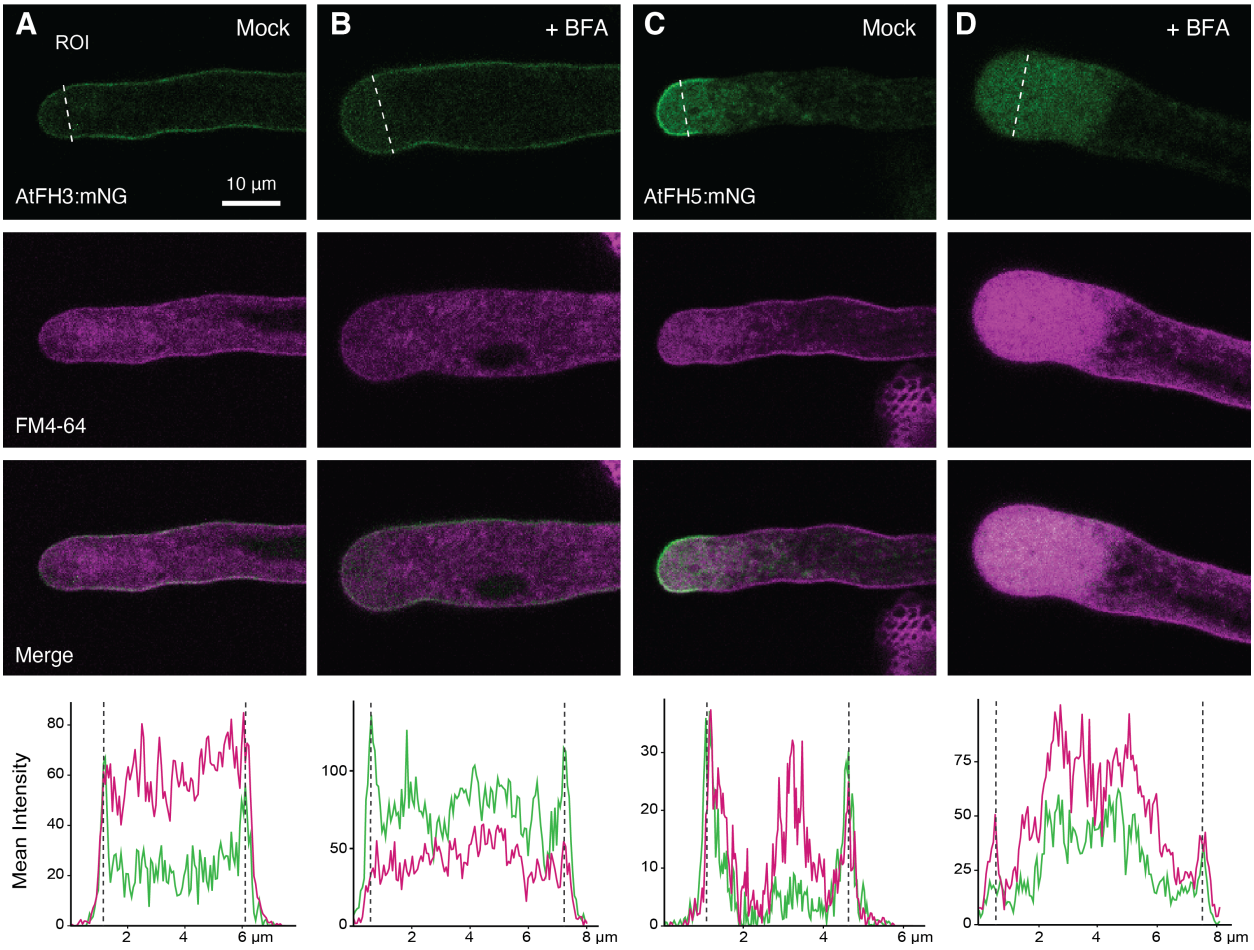

Figure 3-3 AtFH5 is subapically internalized by endocytosis.

Representative images of pollen tubes expressing AtFH3:mNG **(A, B)** or AtFH5:mNG **(C, D)** treated with Brefeldin-A (BFA). Pollen tubes were grown *in vitro* and stained with the lipophilic dye FM4-64 (12 µM). Pollen tubes were then incubated with BFA (25 µM in liquid germination medium) **(B, D)** or a mock treatment (methanol in liquid germination medium) **(A, C)** for 60 min ($n > 20$ per construct and treatment). The plots in the bottom represent mean intensity quantification for mNG signal (green) or FMF-64 (magenta) in an ROI traced with white dashed line across the pollen tube width in the subapical region of the pollen tube for each treatment. In charts, dotted lines represent the edges of the pollen tube.

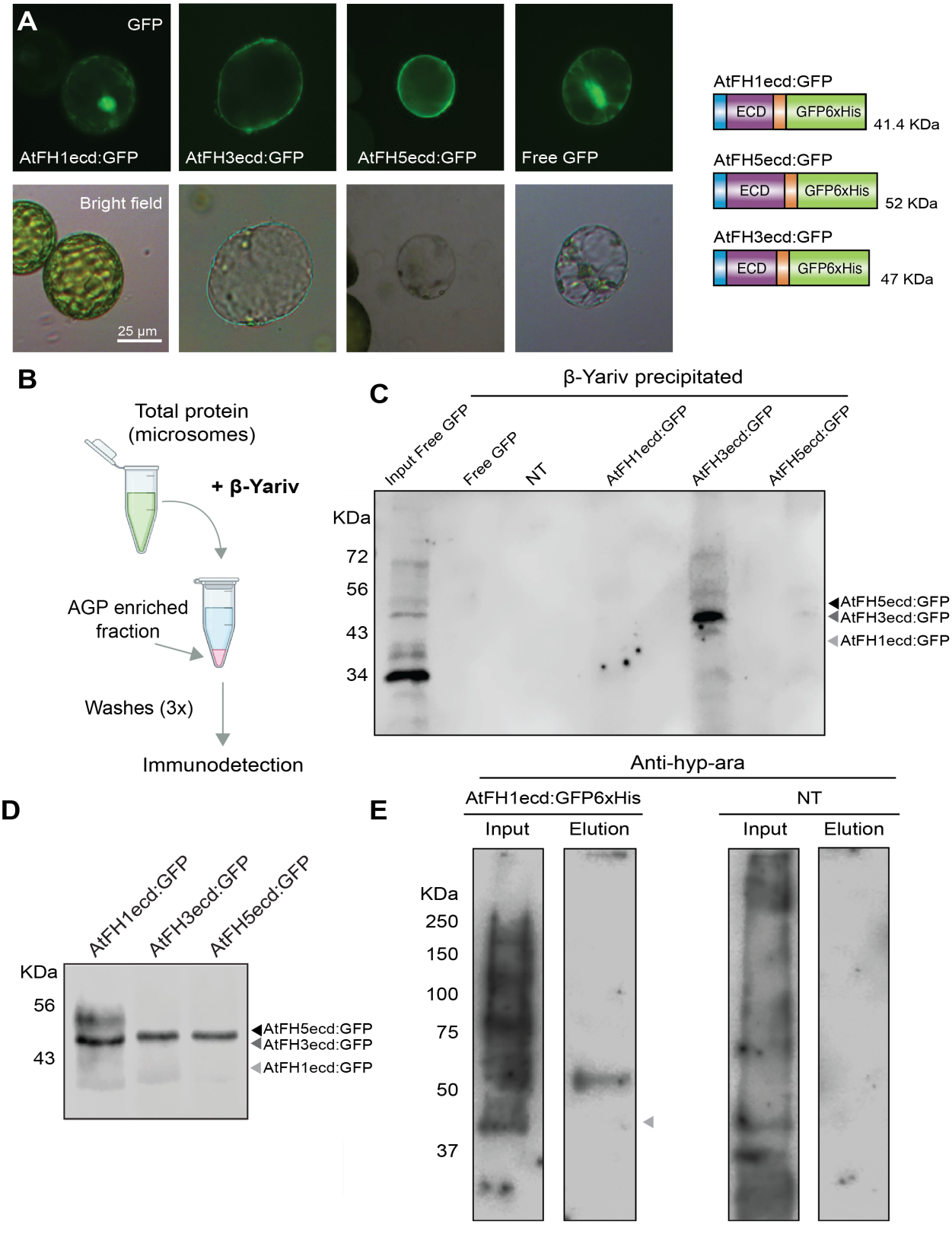
A
GFP
AtFH1ecd:GFP
AtFH3ecd:GFP
AtFH5ecd:GFP
Free GFP
Bright field
25 µm
AtFH1ecd:GFP
ECD
GFP6xHis
41.4 KDa
AtFH5ecd:GFP
ECD
GFP6xHis
52 KDa
AtFH3ecd:GFP
ECD
GFP6xHis
47 KDa
B
Total protein
(microsomes)
+ β-Yariv
AGP enriched
fraction
Washes (3x)
Immunodetection
C
β-Yariv precipitated
Input Free GFP
Free GFP
NT
AtFH1ecd:GFP
AtFH3ecd:GFP
AtFH5ecd:GFP
KDa
72
56
43
34
AtFH5ecd:GFP
AtFH3ecd:GFP
AtFH1ecd:GFP
D
AtFH1ecd:GFP
AtFH3ecd:GFP
AtFH5ecd:GFP
KDa
56
43
AtFH5ecd:GFP
AtFH3ecd:GFP
AtFH1ecd:GFP
E
Anti-hyp-ara
AtFH1ecd:GFP6xHis
Input
Elution
NT
Input
Elution
KDa
250
150
100
75
50
37

Figure 3-4 The HRGP-like motifs in the ECDs of class I formins are O-glycosylated.
A) GFP-tagged ECDs of AtFH1 (AtFH1ecd:GFP), AtFH3 (AtFH3ecd:GFP) and AtFH5 (AtFH5ecd:GFP) are localized to the plasma membrane of protoplasts isolated from transiently transformed tobacco leaves. On the right, protein schematic of GFP tagged ECDs and their predicted sizes. **B)** Schematic of precipitation of AGP and AGP-like proteins from total protein fractions with the β-Yariv reagent. **C)** Immunodetection of β-Yariv precipitated proteins with anti-GFP antibody. Microsomes used as input for all samples were isolated from agroinfiltrated tobacco leaves. NT: Non-Transformed control. **D)** Immunodetection with anti-GFP antibody of GFP-tagged ECDs from total microsomal fractions derived from Arabidopsis stable lines. **E)** Left: Immunodetection of hyp-arabinosylation of total microsomal fractions derived from plants expressing AtFH1ecd:GFP6xHis (Input, 20 µg) or His-purified FH1ecd:GFP6xHis (2.25% of total eluate). A band corresponding to the band observed for FH1ecd:GFP6xHis in **D)** was detected when probing with anti-hyp-ara antibody. Right: As a negative control, microsomes derived from non-transformed plants (NT) were probed with anti-hyp-ara. No visible bands are detected in the eluate after His-purification of NT samples. Predicted sizes of the protein backbone are marked with arrowheads.

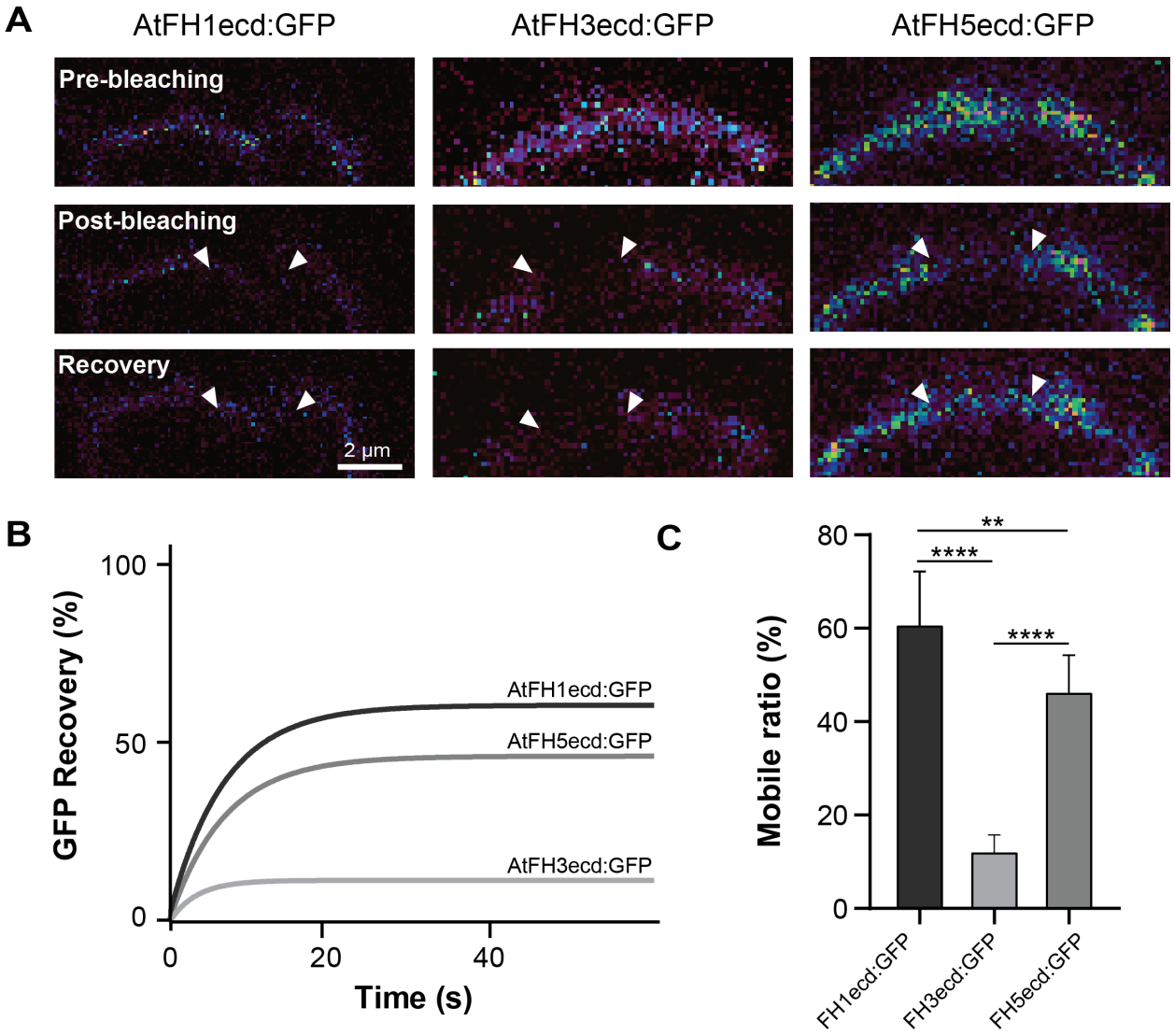

Figure 3-5 The ECDs of class I formins exhibit different degrees of lateral mobility.

A) Representative images of Fluorescence Recovery After Photobleaching (FRAP) assays in Arabidopsis epidermal cells expressing AtFH1ecd:GFP, AtFH3ecd:GFP or AtFH5ecd:GFP. These constructs correspond to those depicted in Figure 4B. White arrowheads represent the boundaries of the photobleached area and recovery images represent the last time-point captured after photobleaching (60 s). **B)** FRAP curves revealed very low mobility for AtFH3ecd:GFP compared to AtFH1ecd:GFP and AtFH5ecd:GFP. **C)** Quantification of the mobile fraction of AtFH1ecd:GFP (*n*= 8), AtFH3ecd:GFP (*n*= 9) and AtFH5ecd:GFP (*n*= 11). Stars represent statistical significance (Student's T-test, '****' adjusted p-value < 0.0005, '**' adjusted p-value < 0.005).

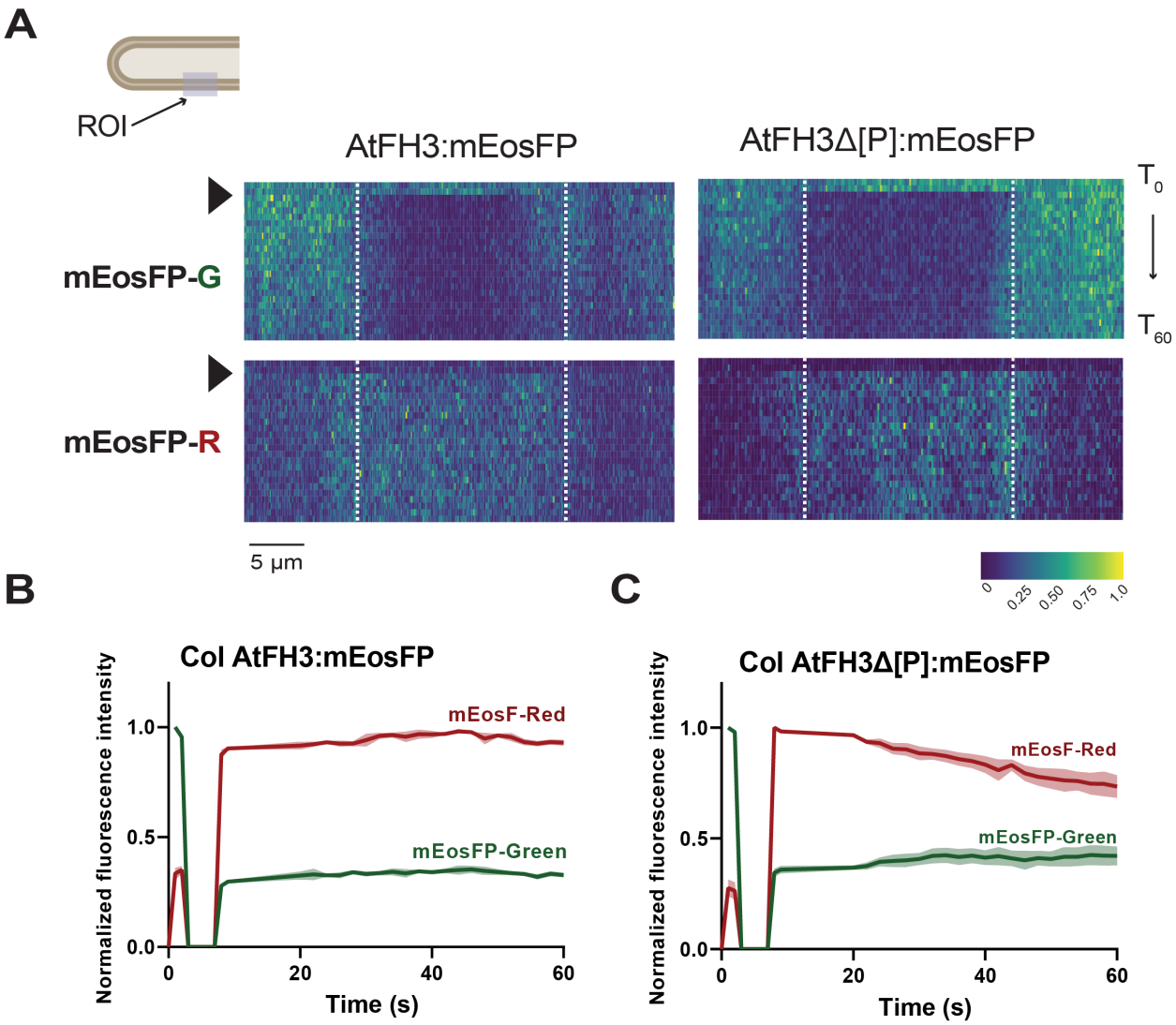

Figure 3-6 Interaction of AtFH3 with the actin cytoskeleton limits its lateral diffusion.

A) Lateral diffusion dynamics of AtFH3:mEosFP (left) or AtFH3Δ[P]:mEosFP (right) after photoconversion in the wild-type background. Kymographs represent the normalized fluorescence intensity in the photoconverted region (ROI indicated in pollen tube schematic corresponds to the region delineated with dashed white lines within kymographs) and surrounding area for the green form of mEosFP (mEosFP-G, top panels) or photoconverted red form of mEosFP (mEosFP-R, bottom panels) over time (T). Black arrowhead indicates the time of photoconversion. The color scale indicates the normalized fluorescence intensity from 0 to the highest intensity value possible, 1. **B)** Quantification of AtFH3 mean normalized fluorescence intensity (colored lines) of mEosFP-G or mEosFP-R in the ROI, pre and post photoconversion and standard error (shading), *n*=8. **C)** Quantification of AtFH3Δ[P]:mEosFP-G or AtFH3Δ[P]:mEosFP-R pre and post-photoconversion, *n*=7.

3.10. Supplemental material

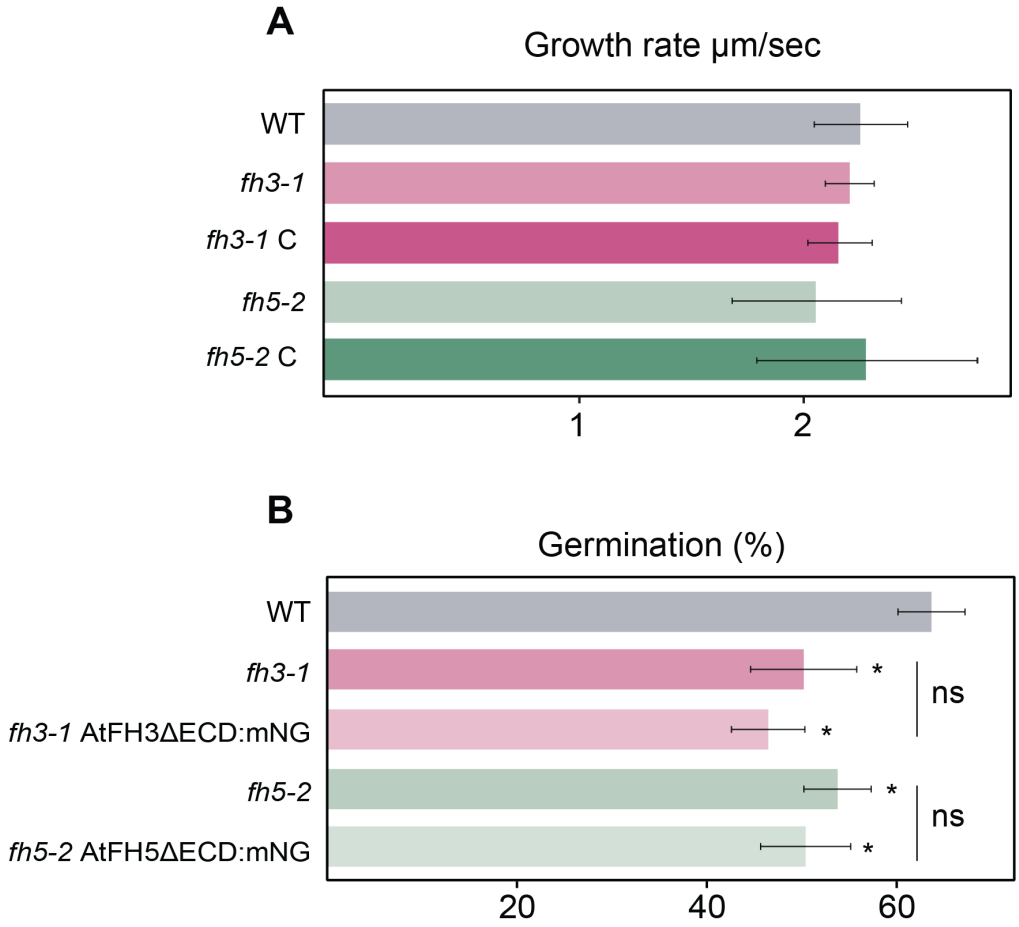

Figure 3-7 Phenotyping of pollen tubes of fh3-2 and fh5-2 loss of function alleles.

A) Quantification of pollen tube growth rate in *fh3-1*, *fh5-2* and complemented lines with AtFH3 or AtFH5 translational fusions with mNG, no statistically significant differences in growth rate compared to wild-type pollen tubes were detected. Growth rate was measured over a period of 15 min. **B)** Introgression of AtFH3ΔECD:mNG or AtFH5ΔECD:mNG into *fh3-1* or *fh5-2*, respectively, does not rescue their germination defect. Pollen germination *in vitro* was measured after 3 h. Three biological replicates per genotype, '*' statistically significant difference (Student's T-test adjusted p-value < 0.05, $n > 1000$). 'ns' indicates no statistically significant difference.

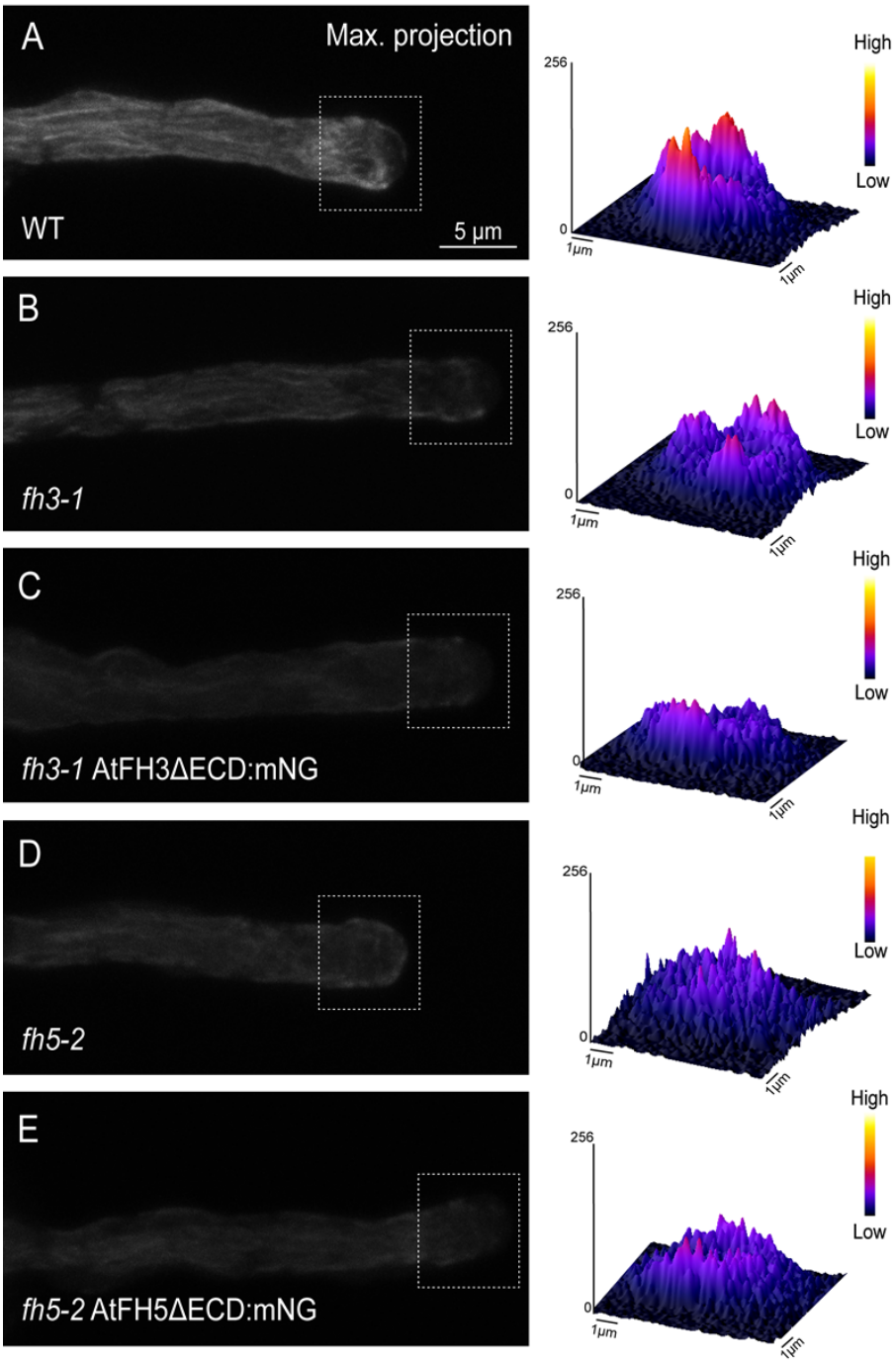

Figure 3-8 The ECD of pollen formins is necessary for proper F-actin organization.

AtFH3 **(A)** and AtFH5 **(B)** loss of function alleles and ECD deleted versions **(D, E)** exhibit reduced pollen tube actin labeling. *In vitro* grown pollen tubes (N≥10 per genotype) were labeled with Phalloidin-iFluor 594. On the left, surface 3D plots of the distribution of fluorescence intensity values within the apical region (white dashed box). Color scale represents pixel intensity gray value (Low=0, High=256).

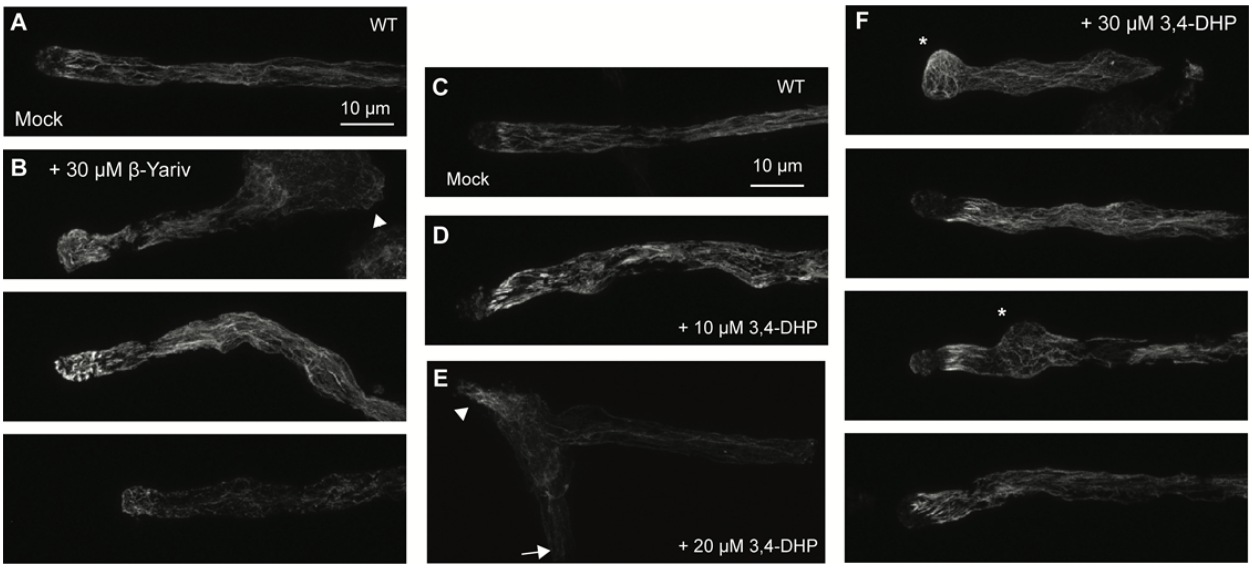

Figure 3-9 Chemical disruption of O-glycosylation induces F-actin disorganization.

Disruption of *O*-glycosylation alters F-actin organization in pollen tubes. *In vitro* grown wild-type pollen tubes (WT) were incubated with a mock treatment **(A,C),** 30 µM β-Yariv **(B)**, 10 µM 3,4 DHP **(D),** 20 µM 3,4-DHP (**E**) or 30 µM 3,4-DHP **(F)** and then the actin cytoskeleton was stained with Phalloidin-iFluor 488 (*n*=10 per treatment). Secondary tips are indicated with white arrowheads, '*' indicates bulging, and in D, white arrow indicates primary tip.

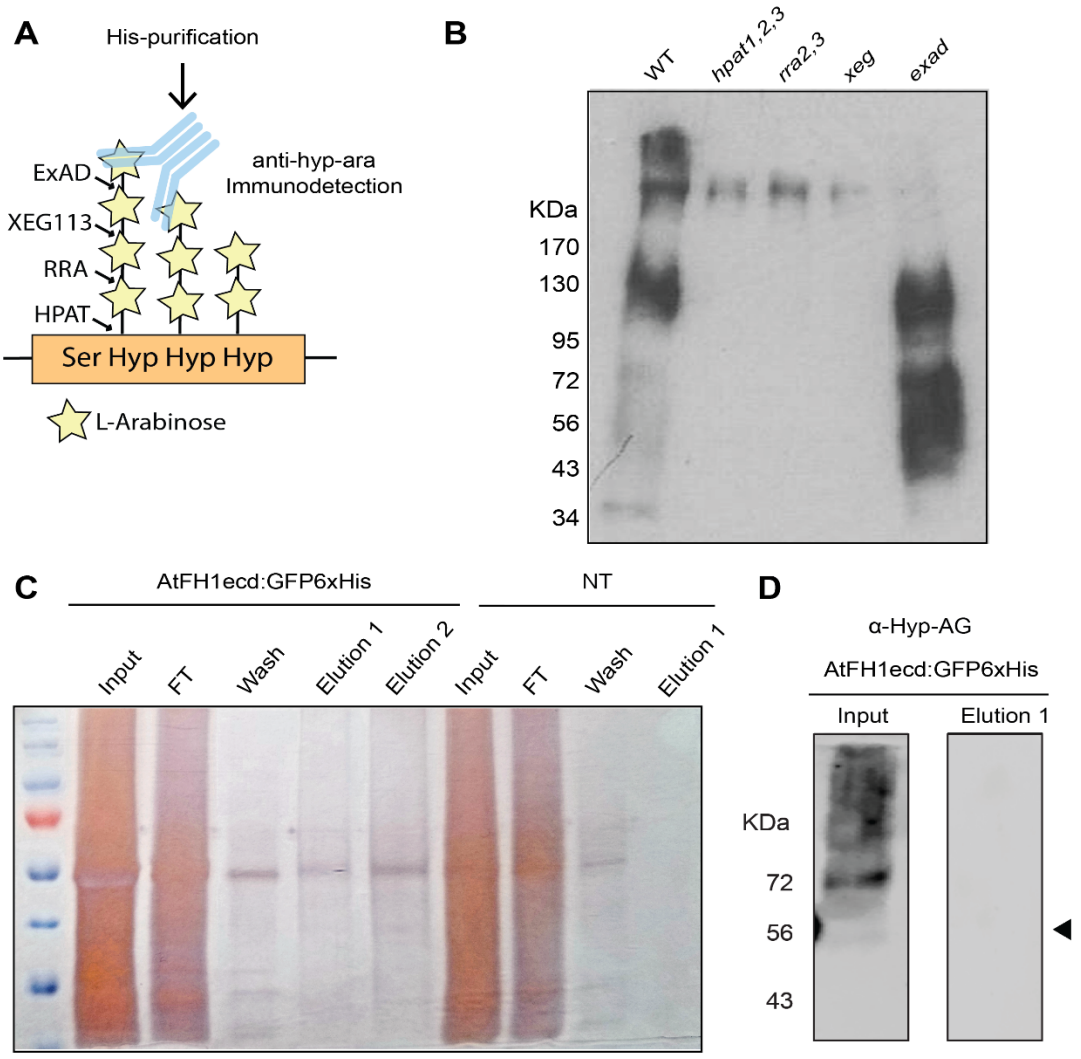

Figure 3-10 Anti-glycosylation antibody validation

A) Strategy for glycoprofiling purified ECD domains. **B)** Hyp-*O*-ara antibody validation. Total protein extracts from Columbia wild type, *hpat1,2,3*, *rra2,3*, *xeg* or *exad* seedlings were probed with the anti-hyp-O-ara antibody JIM19. After HPATs add the first arabinose sugar, the linear chain is serially extended by the glycosyltransferases indicated in A. Loss of signal is observed in protein extracts derived from *hpat1,2,3*, *rra2,3* or *xeg* seedlings, suggesting that the epitope of this antibody is a linear arabinose chain of at least three sugars. **C)** Silver staining of fractions collected during His purification of AtFH1ecd:GFP6xHis or a non-transformed (NT) negative control. **D)** Input and Elution 1 from AtFH1ecd:GFP6xHis was probed with an anti-hyp-AG antibody (JIM13).

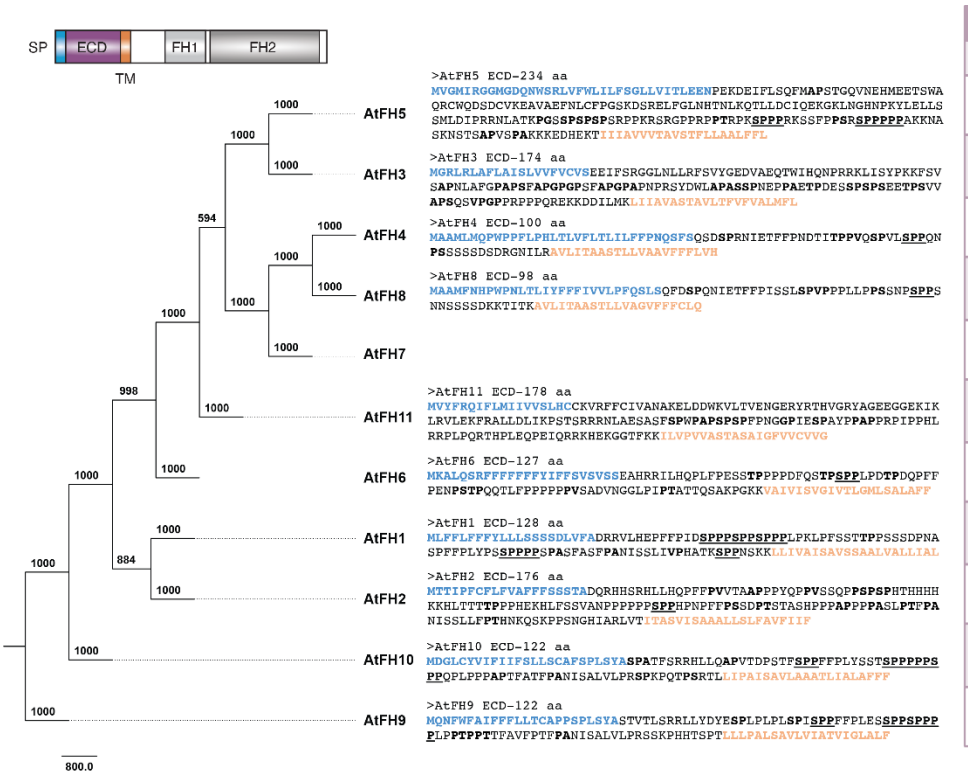

EXT-like		AGP-like
$SP_{(2)}$	$SP_{(3-5)}$	$(XP)_n$
0	2	1
0	0	6
1	0	1
1	0	1
n/a	n/a	n/a
0	0	1
1	0	1
1	3	0
1	0	1
0	2	0
2	1	1

Figure 3-11 Putative O-glycosylation sites in the ECDs of the formin class I family

Maximum parsimony phylogeny of class I formins with 100 bootstrap replicates (bootstrap value indicated in nodes). On the left, the sequences of their respective ECDs and presumed glycomotifs. Amino acid residues in bold letters correspond to XP dipeptides where the letter X represents A,S,T or G. AGP-like motifs were annotated in the table only when at least two repeats were contiguous within the sequence. Bold, underlined amino acid residues correspond to EXT-like motifs. AtFH7 lacks a transmembrane domain. n/a: not applicable.

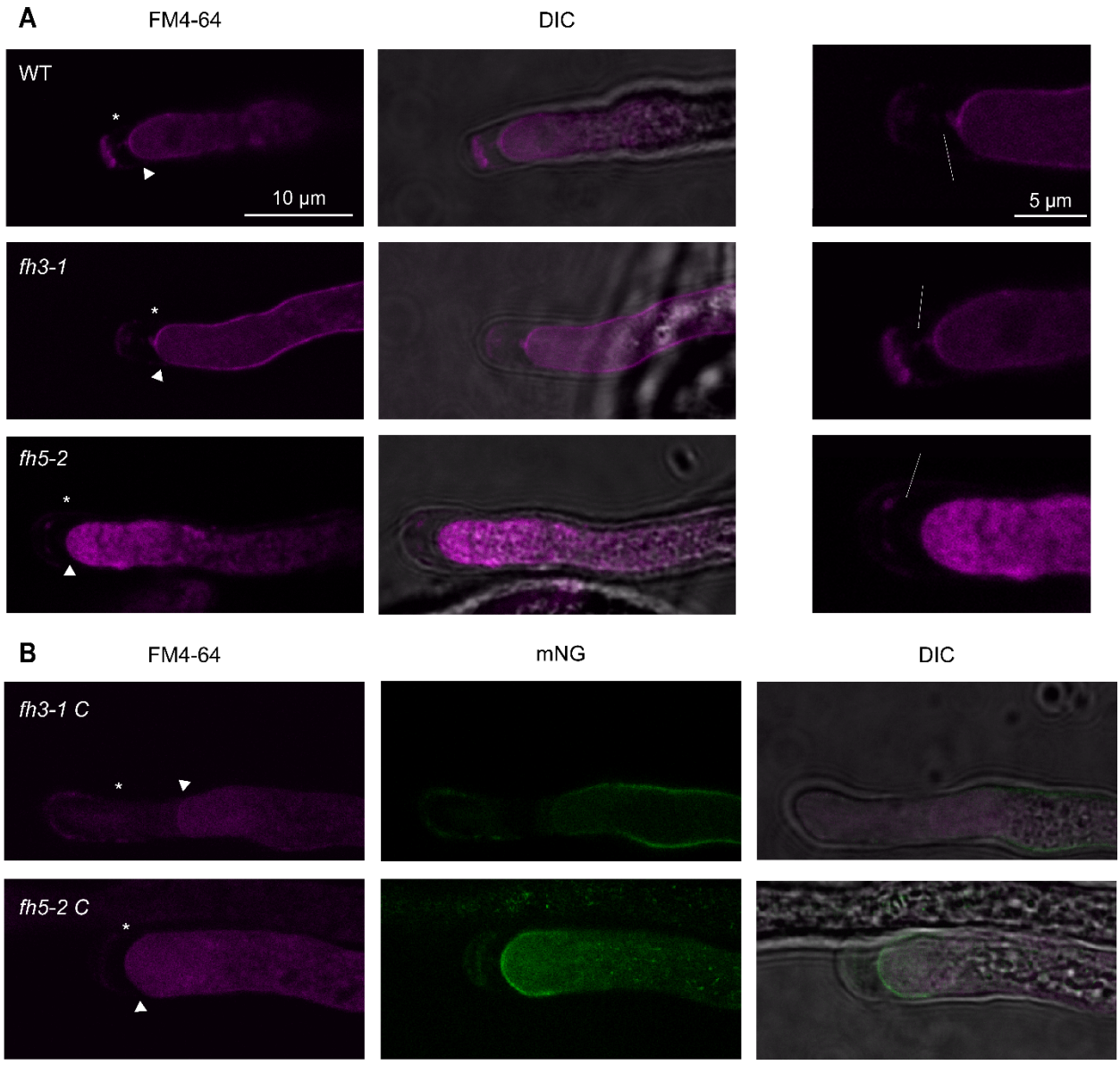

Figure 3-12 AtFH3 and AtFH5 co-localize with Hechtian strands upon plasmolysis.

Wild type, *fh3-1* or *fh5-2* **(A)** pollen tubes, as well as lines complemented with the full length mNG translational fusions (*fh3-1 C* and *fh3-2 C*, **B**) were grown *in vitro* and then placed in hyperosmotic germination medium (25% sucrose) to induce plasmolysis and stained with FM4-64. '*' indicate the apoplastic space, white arrowhead indicates the retracted plasma membrane, arrows right panels in A, indicate membrane extensions (Hechtian strands).

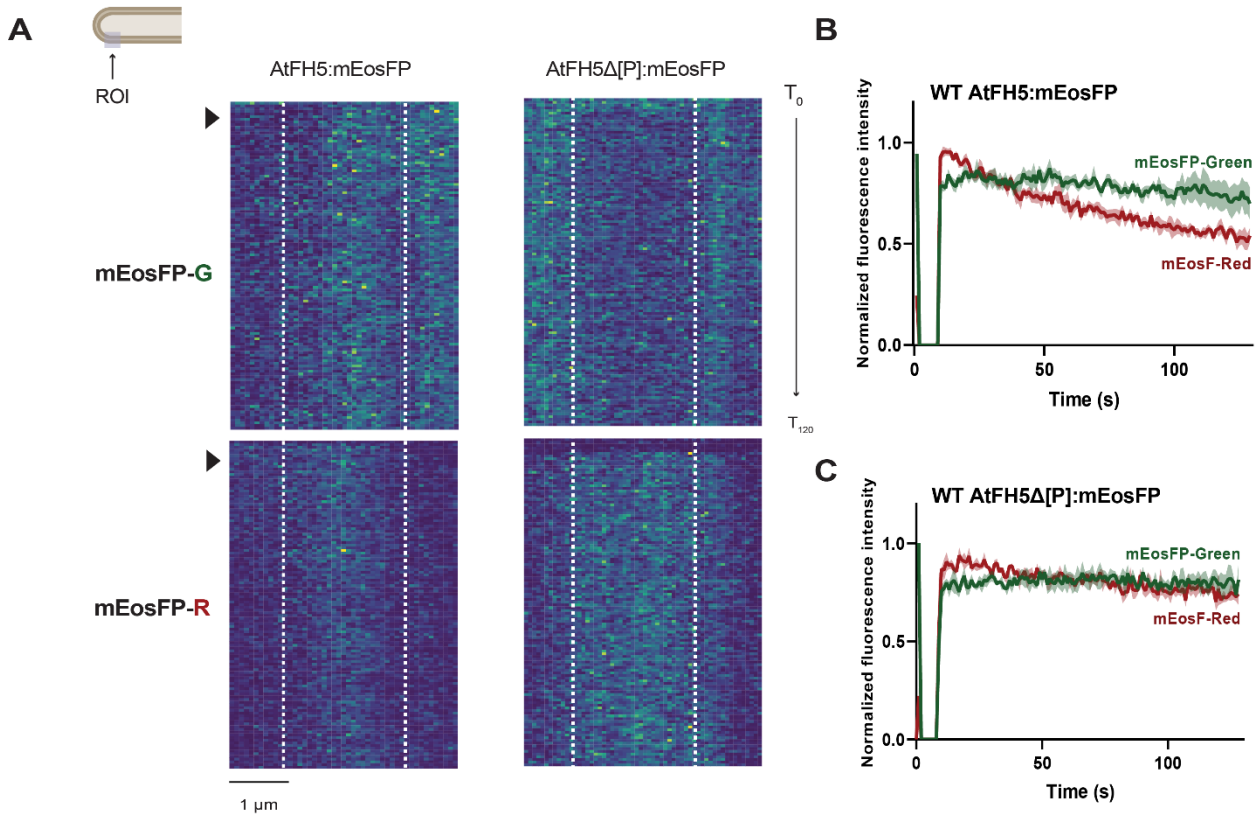

Figure 3-13 AtFH5:mEosFP-G exhibits a high degree of plasma membrane lateral mobility.

A) Lateral diffusion dynamics of AtFH5:mEosFP (left) or AtFH5Δ[P]:mEosFP (right) after photoconversion in the wild-type background. Kymographs represent the normalized fluorescence intensity in the photoconverted region (ROI indicated in pollen tube schematic corresponds to the region delineated with dashed white lines within kymographs) and surrounding area for the green form of mEosFP (mEosFP-G, top panels) or photoconverted red form of mEosFP (mEosFP-R, bottom panels) over time (T). Black arrowhead indicates the time of photoconversion. The color scale indicates the normalized fluorescence intensity from 0 to the highest intensity value possible, 1. **B)** Quantification of AtFH5 mean normalized fluorescence intensity (colored lines) of mEosFP-G or mEosFP-R in the ROI, pre and post photoconversion and standard error (shading), *n*=9. **C)** Quantification of AtFH5Δ[P]:mEosFP-G or AtFH5Δ[P]:mEosFP-R pre and post-photoconversion, *n*=8.

Table 3-1 Primers used in this study.

Target	Purpose	Sequence 5' to 3'
AtFH3 CDS	Cloning	GGGGACAACTTTGTATACAAAAGTTGATGGGGAGATTGAGATTAGC
		GGGGACCACTTTGTACAAGAAAGCTGGGTACGAAGGTGAACTATCCTCTTC
AtFH3ΔECD	Overlap PCR/Cloning	TGTTTCCGAGCTTATCATCGCGGTTGCTTC
		CGATGATAAGCTCGGAAACACAAACGAAAAC
AtFH3Δ[P]	Overlap PCR/Cloning	CAACGGGAGAAGAAGGATGATATC
		ACCGAAAGCTAAATTTGGAGCA
AtFH5 CDS	Cloning	GGGGACAACTTTGTATACAAAAGTTGATGGTTGGAATGATTCGAGGAG
		GGGGACCACTTTGTACAAGAAAGCTGGGTATTAGTCTGAATCTGAACTAGACTGATC
AtFH5ΔECD	Overlap PCR/Cloning	TTTGGAAGAGATCATCATTGCTGTTGTTG
		CAATGATGATCTCTTCCAAAGTTATTACCAATAAC
AtFH5Δ[P]	Overlap PCR/Cloning	GCGAAAAAAAAAAGAGGATCATGA
		GGAAGAGCCGGGTTTAGTAGC
AtFH5Δ{SPPP}	Overlap PCR/Cloning	GCTAAGAAAAACGCTTCTAAAAATTCAACT
		TTTTGGTCGAGTAGGTGGGC
AtFH1ecd	Cloning	GGGGACAAGTTTGTACAAAAAAGCAGGCTATGCTCTTCTTCTTATTCTTCTTC
		GGGGACCACTTTGTACAAGAAAGCTGGGTAGAGTAAAGCGATAAGTAGAGCG
AtFH3ecd	Cloning	GGGGACAAGTTTGTACAAAAAAGCAGGCTATGGGGAGATTGAGATTAGC
		GGGGACCACTTTGTACAAGAAAGCTGGGTAGCAACACAAGAACATCAATGC
AtFH5ecd	Cloning	GGGGACAAGTTTGTACAAAAAAGCAGGCTATGGTTGGAATGATTCGAGG
		GGGGACCACTTTGTACAAGAAAGCTGGGTATAAGAAGAATAATGCAGCCAA
fh3-1 (SALK_150350)	Genotyping	AAGAAGCTCTCGGAACTCTCG
		TCTTCACATCTCGCAAAATCC
fh5-2 (SALK_044464)	Genotyping	AGCGTTTTTCTTAGCAGGAGG
		TGGTTGATTCTGTTTTCTGGG
hpat1 (SALK_120066)	Genotyping	GTGATTATGATATGAAGGTAAGC
		AAATCTAGTGGAGACCAGAC
hpat2 (SM_3_38225)	Genotyping	ATTTCCAATCCCCATATTTGG
		CATTGTCACCAATGTCACCTG
hpat3 (SALK_04668)	Genotyping	AAGATACTGCAGTAAGGTCC
		GACAAGAAGGGAAGTAAAGG
SALK LB1.3	Genotyping	ATTTTGCCGATTTCGGAAC
SPM32 LB	Genotyping	TACGAATAAGAGCGTCCATTTTAGAGTGA

Table 3-2 Likelihood-ratio test (model fit parameters) and modeling output.

Model (lme4 syntax)	**χ^2**	**p-value**
y = MFI ~ group*distance + (1|cell)	16748	<0.001
Random Effects	**Variance**	**SD**
Residual	621.73	24.93
Random effects (cell)	1229.04	35.06
Number of cells	99	
Number of observations	20,988	
Marginal R^2 / Conditional R^2	0.313 / 0.769	

MFI = mean fluorescence intensity
Distance = distance in μm from the tip
Group = combination of genotype-construct (WT AtFH5:mNG, WT AtFH5Δ[P]:mNG, WT AtFH5Δ{SPPP}:mNG and *hpat1,2,3* AtFH5:mNG, *hpat1,2,3* AtFH5Δ[P]:mNG, *hpat1,2,3* AtFH5Δ{SPPP}:mNG).

3.11. References

Baluška, F., Hlavacka, A., Šamaj, J., Palme, K., Robinson, D. G., Matoh, T., McCurdy, D. W., Menzel, D., & Volkmann, D. (2002). F-Actin-Dependent Endocytosis of Cell Wall Pectins in Meristematic Root Cells. Insights from Brefeldin A-Induced Compartments. *Plant Physiology*, *130*(1), 422–431. https://doi.org/10.1104/pp.007526

Baluška, F., Šamaj, J., Wojtaszek, P., Volkmann, D., & Menzel, D. (2003). Cytoskeleton-Plasma Membrane-Cell Wall Continuum in Plants. Emerging Links Revisited. *Plant Physiology*, *133*(2), 482–491. https://doi.org/10.1104/pp.103.027250

Banno, H., & Chua, N.-H. (2000). Characterization of the Arabidopsis Formin-Like Protein AFH1 and Its Interacting Protein. *Plant and Cell Physiology*, *41*(5), 617–626. https://doi.org/10.1093/pcp/41.5.617

Bascom, C. S., Hepler, P. K., & Bezanilla, M. (2018). Interplay between Ions, the Cytoskeleton, and Cell Wall Properties during Tip Growth1[OPEN]. *Plant Physiology*, *176*(1), 28–40. https://doi.org/10.1104/pp.17.01466

Bates, D., Mächler, M., Bolker, B., & Walker, S. (2015). Fitting Linear Mixed-Effects Models Using lme4. *Journal of Statistical Software*, *67*, 1–48. https://doi.org/10.18637/jss.v067.i01

Beuder, S., Dorchak, A., Bhide, A., Moeller, S. R., Petersen, B. L., & MacAlister, C. A. (2020). Exocyst mutants suppress pollen tube growth and cell wall structural defects of hydroxyproline O-arabinosyltransferase mutants. *The Plant Journal*, *103*(4), 1399–1419. https://doi.org/10.1111/tpj.14808

Blanchoin, L., & Staiger, C. J. (2010). Plant formins: Diverse isoforms and unique molecular mechanism. *Biochimica et Biophysica Acta (BBA) - Molecular Cell Research*, *1803*(2), 201–206. https://doi.org/10.1016/j.bbamcr.2008.09.015

Borassi, C., Sede, A. R., Mecchia, M. A., Salgado Salter, J. D., Marzol, E., Muschietti, J. P., & Estevez, J. M. (2016). An update on cell surface proteins containing extensin-motifs. *Journal of Experimental Botany*, *67*(2), 477–487. https://doi.org/10.1093/jxb/erv455

Cannon, M. C., Terneus, K., Hall, Q., Tan, L., Wang, Y., Wegenhart, B. L., Chen, L., Lamport, D. T. A., Chen, Y., & Kieliszewski, M. J. (2008). Self-assembly of the plant cell wall requires an extensin scaffold. *Proceedings of the National Academy of Sciences*, *105*(6), 2226–2231. https://doi.org/10.1073/pnas.0711980105

Chebli, Y., Bidhendi, A. J., Kapoor, K., & Geitmann, A. (2021). Cytoskeletal regulation of primary plant cell wall assembly. *Current Biology*, *31*(10), R681–R695. https://doi.org/10.1016/j.cub.2021.03.092

Chebli, Y., Kaneda, M., Zerzour, R., & Geitmann, A. (2012). The Cell Wall of the Arabidopsis Pollen Tube—Spatial Distribution, Recycling, and Network Formation of Polysaccharides1[C][W][OA]. *Plant Physiology*, *160*(4), 1940–1955. https://doi.org/10.1104/pp.112.199729

Cheung, A. Y., Niroomand, S., Zou, Y., & Wu, H.-M. (2010). A transmembrane formin nucleates subapical actin assembly and controls tip-focused growth in pollen tubes. *Proceedings of the National Academy of Sciences*, *107*(37), 16390–16395. https://doi.org/10.1073/pnas.1008527107

Cheung, A. Y., & Wu, H.-M. (2007). Structural and functional compartmentalization in pollen tubes. *Journal of Experimental Botany*, *58*(1), 75–82. https://doi.org/10.1093/jxb/erl122

Clough, S. J., & Bent, A. F. (1998). Floral dip: A simplified method for Agrobacterium - mediated transformation of Arabidopsis thaliana. *The Plant Journal*, *16*(6), 735–743. https://doi.org/10.1046/j.1365-313x.1998.00343.x
Curtis, M. D., & Grossniklaus, U. (2003). A Gateway Cloning Vector Set for High-Throughput Functional Analysis of Genes in Planta. *Plant Physiology*, *133*(2), 462–469. https://doi.org/10.1104/pp.103.027979
Diao, M., Ren, S., Wang, Q., Qian, L., Shen, J., Liu, Y., & Huang, S. (2018). Arabidopsis formin 2 regulates cell-to-cell trafficking by capping and stabilizing actin filaments at plasmodesmata. *ELife*, *7*, e36316. https://doi.org/10.7554/eLife.36316
Dresselhaus, T., & Franklin-Tong, N. (2013). Male–Female Crosstalk during Pollen Germination, Tube Growth and Guidance, and Double Fertilization. *Molecular Plant*, *6*(4), 1018–1036. https://doi.org/10.1093/mp/sst061
Estévez, J. M., Kieliszewski, M. J., Khitrov, N., & Somerville, C. (2006). Characterization of Synthetic Hydroxyproline-Rich Proteoglycans with Arabinogalactan Protein and Extensin Motifs in Arabidopsis. *Plant Physiology*, *142*(2), 458–470. https://doi.org/10.1104/pp.106.084244
Gisbergen, P. A. C. van, & Bezanilla, M. (2013). Plant formins: Membrane anchors for actin polymerization. *Trends in Cell Biology*, *23*(5), 227–233. https://doi.org/10.1016/j.tcb.2012.12.001
Grebnev, G., Ntefidou, M., & Kost, B. (2017). Secretion and Endocytosis in Pollen Tubes: Models of Tip Growth in the Spot Light. *Frontiers in Plant Science*, *8*. https://doi.org/10.3389/fpls.2017.00154
Hafidh, S., & Honys, D. (2021). Reproduction Multitasking: The Male Gametophyte. *Annual Review of Plant Biology*, *72*(1), null. https://doi.org/10.1146/annurev-arplant-080620-021907
Hsiao, A.-S., Wang, K., & Ho, T.-H. D. (2020). An Intrinsically Disordered Protein Interacts with the Cytoskeleton for Adaptive Root Growth under Stress1 [OPEN]. *Plant Physiology*, *183*(2), 570–587. https://doi.org/10.1104/pp.19.01372
Ingouff, M., Gerald, J. N. F., Guérin, C., Robert, H., Sørensen, M. B., Damme, D. V., Geelen, D., Blanchoin, L., & Berger, F. (2005). Plant formin AtFH5 is an evolutionarily conserved actin nucleator involved in cytokinesis. *Nature Cell Biology*, *7*(4), 374–380. https://doi.org/10.1038/ncb1238
Jaillais, Y., & Ott, T. (2020). The Nanoscale Organization of the Plasma Membrane and Its Importance in Signaling: A Proteolipid Perspective1 [OPEN]. *Plant Physiology*, *182*(4), 1682–1696. https://doi.org/10.1104/pp.19.01349
Johnson, K. L., Cassin, A. M., Lonsdale, A., Bacic, A., Doblin, M. S., & Schultz, C. J. (2017). Pipeline to Identify Hydroxyproline-Rich Glycoproteins. *Plant Physiology*, *174*(2), 886–903. https://doi.org/10.1104/pp.17.00294
Kieliszewski, M. J., & Lamport, D. T. A. (1994). Extensin: Repetitive motifs, functional sites, post-translational codes, and phylogeny. *The Plant Journal*, *5*(2), 157–172. https://doi.org/10.1046/j.1365-313X.1994.05020157.x
Kitazawa, K., Tryfona, T., Yoshimi, Y., Hayashi, Y., Kawauchi, S., Antonov, L., Tanaka, H., Takahashi, T., Kaneko, S., Dupree, P., Tsumuraya, Y., & Kotake, T. (2013). β-Galactosyl Yariv Reagent Binds to the β-1,3-Galactan of Arabinogalactan Proteins. *Plant Physiology*, *161*(3), 1117–1126. https://doi.org/10.1104/pp.112.211722
Knox, J. P., Linstead, P. J., Cooper, J. P. C., & Roberts, K. (1991). Developmentally regulated epitopes of cell surface arabinogalactan proteins and their relation to root tissue pattern

formation. *The Plant Journal: For Cell and Molecular Biology*, *1*(3), 317–326. https://doi.org/10.1046/j.1365-313X.1991.t01-9-00999.x
Lamport, D. T. A., Kieliszewski, M. J., Chen, Y., & Cannon, M. C. (2011). Role of the Extensin Superfamily in Primary Cell Wall Architecture1. *Plant Physiology*, *156*(1), 11–19. https://doi.org/10.1104/pp.110.169011
Lamport, D. T. A., Tan, L., Held, M. A., & Kieliszewski, M. J. (2018a). Pollen tube growth and guidance: Occam's razor sharpened on a molecular arabinogalactan glycoprotein Rosetta Stone. *New Phytologist*, *217*(2), 491–500. https://doi.org/10.1111/nph.14845
Lamport, D. T. A., Tan, L., Held, M. A., & Kieliszewski, M. J. (2018b). Pollen tube growth and guidance: Occam's razor sharpened on a molecular arabinogalactan glycoprotein Rosetta Stone. *The New Phytologist*, *217*(2), 491–500. https://doi.org/10.1111/nph.14845
Lan, Y., Liu, X., Fu, Y., & Huang, S. (2018). Arabidopsis class I formins control membrane-originated actin polymerization at pollen tube tips. *PLOS Genetics*, *14*(11), e1007789. https://doi.org/10.1371/journal.pgen.1007789
Lara-Mondragón, C. M., & MacAlister, C. A. (2020). Chapter 12—Partial purification and immunodetection of cell surface glycoproteins from plants. In C. T. Anderson, E. S. Haswell, & R. Dixit (Eds.), *Methods in Cell Biology* (Vol. 160, pp. 215–234). Academic Press. https://doi.org/10.1016/bs.mcb.2020.05.003
Li, G., Yang, X., Zhang, X., Song, Y., Liang, W., & Zhang, D. (2018). *Rice Morphology Determinant-Mediated Actin Filament Organization Contributes to Pollen Tube Growth | Plant Physiology*. http://www.plantphysiol.org/content/177/1/255
Liang, P., Schmitz, C., Lace, B., Ditengou, F. A., Su, C., Schulze, E., Knerr, J., Grosse, R., Keller, J., Libourel, C., Delaux, P.-M., & Ott, T. (2021). Formin-mediated bridging of cell wall, plasma membrane, and cytoskeleton in symbiotic infections of Medicago truncatula. *Current Biology*, *31*(12), 2712-2719.e5. https://doi.org/10.1016/j.cub.2021.04.002
Liu, C., Zhang, Y., & Ren, H. (2018). Actin Polymerization Mediated by AtFH5 Directs the Polarity Establishment and Vesicle Trafficking for Pollen Germination in Arabidopsis. *Molecular Plant*, *11*(11), 1389–1399. https://doi.org/10.1016/j.molp.2018.09.004
Liu, C., Zhang, Y., & Ren, H. (2021). Profilin promotes formin-mediated actin filament assembly and vesicle transport during polarity formation in pollen. *The Plant Cell*, *33*(4), 1252–1267. https://doi.org/10.1093/plcell/koab027
Liu, X., Wolfe, R., Welch, L. R., Domozych, D. S., Popper, Z. A., & Showalter, A. M. (2016). Bioinformatic Identification and Analysis of Extensins in the Plant Kingdom. *PLOS ONE*, *11*(2), e0150177. https://doi.org/10.1371/journal.pone.0150177
Lopez-Hernandez, F., Tryfona, T., Rizza, A., Yu, X. L., Harris, M. O. B., Webb, A. A. R., Kotake, T., & Dupree, P. (2020). Calcium Binding by Arabinogalactan Polysaccharides Is Important for Normal Plant Development. *The Plant Cell*, *32*(10), 3346–3369. https://doi.org/10.1105/tpc.20.00027
MacAlister, C. A., Ortiz-Ramírez, C., Becker, J. D., Feijó, J. A., & Lippman, Z. B. (2016). Hydroxyproline O-arabinosyltransferase mutants oppositely alter tip growth in Arabidopsis thaliana and Physcomitrella patens. *The Plant Journal*, *85*(2), 193–208. https://doi.org/10.1111/tpj.13079
Martinière, A., Gayral, P., Hawes, C., & Runions, J. (2011). Building bridges: Formin1 of Arabidopsis forms a connection between the cell wall and the actin cytoskeleton. *The Plant Journal*, *66*(2), 354–365. https://doi.org/10.1111/j.1365-313X.2011.04497.x

Martinière, A., Lavagi, I., Nageswaran, G., Rolfe, D. J., Maneta-Peyret, L., Luu, D.-T., Botchway, S. W., Webb, S. E. D., Mongrand, S., Maurel, C., Martin-Fernandez, M. L., Kleine-Vehn, J., Friml, J., Moreau, P., & Runions, J. (2012). Cell wall constrains lateral diffusion of plant plasma-membrane proteins. *Proceedings of the National Academy of Sciences*, *109*(31), 12805–12810. https://doi.org/10.1073/pnas.1202040109
Mathur, J., Radhamony, R., Sinclair, A. M., Donoso, A., Dunn, N., Roach, E., Radford, D., S. Mohammad Mohaghegh, P., Logan, D. C., Kokolic, K., & Mathur, N. (2010). MEosFP-Based Green-to-Red Photoconvertible Subcellular Probes for Plants. *Plant Physiology*, *154*(4), 1573–1587. https://doi.org/10.1104/pp.110.165431
Nelson, B. K., Cai, X., & Nebenführ, A. (2007). A multicolored set of in vivo organelle markers for co-localization studies in Arabidopsis and other plants. *The Plant Journal*, *51*(6), 1126–1136. https://doi.org/10.1111/j.1365-313X.2007.03212.x
Ogawa-Ohnishi, M., Matsushita, W., & Matsubayashi, Y. (2013). Identification of three hydroxyproline O-arabinosyltransferases in Arabidopsis thaliana. *Nature Chemical Biology*, *9*(11), 726–730. https://doi.org/10.1038/nchembio.1351
Parton, R. M., Fischer-Parton, S., Trewavas, A. J., & Watahiki, M. K. (2003). Pollen tubes exhibit regular periodic membrane trafficking events in the absence of apical extension. *Journal of Cell Science*, *116*(13), 2707–2719. https://doi.org/10.1242/jcs.00468
Paul Knox, J., Peart, J., & Neill, S. J. (1995). Identification of novel cell surface epitopes using a leaf epidermal-strip assay system. *Planta*, *196*(2), 266–270. https://doi.org/10.1007/BF00201383
Petersen, B. L., MacAlister, C. A., & Ulvskov, P. (2021). Plant Protein O-Arabinosylation. *Frontiers in Plant Science*, *12*, 645219. https://doi.org/10.3389/fpls.2021.645219
Pont-Lezica, R. F., McNALLY, J. G., & Pickard, B. G. (1993). Wall-to-membrane linkers in onion epidermis: Some hypotheses. *Plant, Cell & Environment*, *16*(2), 111–123. https://doi.org/10.1111/j.1365-3040.1993.tb00853.x
Přerovská, T., Pavlů, A., Hancharyk, D., Rodionova, A., Vavříková, A., & Spiwok, V. (2021). Structural Basis of the Function of Yariv Reagent—An Important Tool to Study Arabinogalactan Proteins. *Frontiers in Molecular Biosciences*, *8*. https://www.frontiersin.org/article/10.3389/fmolb.2021.682858
Qu, X., Jiang, Y., Chang, M., Liu, X., Zhang, R., & Huang, S. (2015). Organization and regulation of the actin cytoskeleton in the pollen tube. *Frontiers in Plant Science*, *5*. https://doi.org/10.3389/fpls.2014.00786
Qu, X., Wang, Q., Wang, H., & Huang, S. (2020). Visualization of Actin Organization and Quantification in Fixed Arabidopsis Pollen Grains and Tubes. *Bio-Protocol*, *10*(1), e3509–e3509.
Röckel, N., Wolf, S., Kost, B., Rausch, T., & Greiner, S. (2008). Elaborate spatial patterning of cell-wall PME and PMEI at the pollen tube tip involves PMEI endocytosis, and reflects the distribution of esterified and de-esterified pectins. *The Plant Journal*, *53*(1), 133–143. https://doi.org/10.1111/j.1365-313X.2007.03325.x
Rodriguez-Enriquez, M. J., Mehdi, S., Dickinson, H. G., & Grant-Downton, R. T. (2013). A novel method for efficient in vitro germination and tube growth of Arabidopsis thaliana pollen. *New Phytologist*, *197*(2), 668–679. https://doi.org/10.1111/nph.12037
Romero, S., Le Clainche, C., Didry, D., Egile, C., Pantaloni, D., & Carlier, M.-F. (2004). Formin Is a Processive Motor that Requires Profilin to Accelerate Actin Assembly and Associated ATP Hydrolysis. *Cell*, *119*(3), 419–429. https://doi.org/10.1016/j.cell.2004.09.039

Sardar, H. S., Yang, J., & Showalter, A. M. (2006). Molecular Interactions of Arabinogalactan Proteins with Cortical Microtubules and F-Actin in Bright Yellow-2 Tobacco Cultured Cells. *Plant Physiology*, *142*(4), 1469–1479. https://doi.org/10.1104/pp.106.088716
Sede, A. R., Borassi, C., Wengier, D. L., Mecchia, M. A., Estevez, J. M., & Muschietti, J. P. (2018). Arabidopsis pollen extensins LRX are required for cell wall integrity during pollen tube growth. *FEBS Letters*, *592*(2), 233–243. https://doi.org/10.1002/1873-3468.12947
Shimada, T. L., Shimada, T., & Hara-Nishimura, I. (2010). A rapid and non-destructive screenable marker, FAST, for identifying transformed seeds of Arabidopsis thaliana. *The Plant Journal*, *61*(3), 519–528. https://doi.org/10.1111/j.1365-313X.2009.04060.x
Showalter, A. M., & Basu, D. (2016). Extensin and Arabinogalactan-Protein Biosynthesis: Glycosyltransferases, Research Challenges, and Biosensors. *Frontiers in Plant Science*, *7*, 814. https://doi.org/10.3389/fpls.2016.00814
Shpak, E., Barbar, E., Leykam, J. F., & Kieliszewski, M. J. (2001). Contiguous Hydroxyproline Residues Direct Hydroxyproline Arabinosylation in Nicotiana tabacum *. *Journal of Biological Chemistry*, *276*(14), 11272–11278. https://doi.org/10.1074/jbc.M011323200
Silva, J., Ferraz, R., Dupree, P., Showalter, A. M., & Coimbra, S. (2020). Three Decades of Advances in Arabinogalactan-Protein Biosynthesis. *Frontiers in Plant Science*, *11*. https://doi.org/10.3389/fpls.2020.610377
Sun, X., Jones, W. T., & Rikkerink, E. H. A. (2012). GRAS proteins: The versatile roles of intrinsically disordered proteins in plant signalling. *Biochemical Journal*, *442*(1), 1–12. https://doi.org/10.1042/BJ20111766
Tan, L., Eberhard, S., Pattathil, S., Warder, C., Glushka, J., Yuan, C., Hao, Z., Zhu, X., Avci, U., Miller, J. S., Baldwin, D., Pham, C., Orlando, R., Darvill, A., Hahn, M. G., Kieliszewski, M. J., & Mohnen, D. (2013). An Arabidopsis Cell Wall Proteoglycan Consists of Pectin and Arabinoxylan Covalently Linked to an Arabinogalactan Protein. *The Plant Cell*, *25*(1), 270–287. https://doi.org/10.1105/tpc.112.107334
Tan, L., Leykam, J. F., & Kieliszewski, M. J. (2003). Glycosylation Motifs That Direct Arabinogalactan Addition to Arabinogalactan-Proteins. *Plant Physiology*, *132*(3), 1362–1369. https://doi.org/10.1104/pp.103.021766
Thomas, C. (2012). Bundling actin filaments from membranes: Some novel players. *Frontiers in Plant Science*, *3*. https://doi.org/10.3389/fpls.2012.00188
Twell, D., Yamaguchi, J., & McCormick, S. (1990). Pollen-specific gene expression in transgenic plants: Coordinate regulation of two different tomato gene promoters during microsporogenesis. *Development (Cambridge, England)*, *109*(3), 705–713.
Uversky, V. N. (2019). Intrinsically Disordered Proteins and Their "Mysterious" (Meta)Physics. *Frontiers in Physics*, *7*, 10. https://doi.org/10.3389/fphy.2019.00010
Wang, J., Xue, X., & Ren, H. (2012). New insights into the role of plant formins: Regulating the organization of the actin and microtubule cytoskeleton. *Protoplasma*, *249*(2), 101–107. https://doi.org/10.1007/s00709-011-0368-0
Wang, Q., Kong, L., Hao, H., Wang, X., Lin, J., Šamaj, J., & Baluška, F. (2005). Effects of Brefeldin A on Pollen Germination and Tube Growth. Antagonistic Effects on Endocytosis and Secretion. *Plant Physiology*, *139*(4), 1692–1703. https://doi.org/10.1104/pp.105.069765
Wozny, M., Schattat, M. H., Mathur, N., Barton, K., & Mathur, J. (2012). Color Recovery after Photoconversion of H2B::mEosFP Allows Detection of Increased Nuclear DNA Content in Developing Plant Cells. *Plant Physiology*, *158*(1), 95–106. https://doi.org/10.1104/pp.111.187062

Wright, P. E., & Dyson, H. J. (2015). Intrinsically Disordered Proteins in Cellular Signaling and Regulation. *Nature Reviews. Molecular Cell Biology*, *16*(1), 18–29. https://doi.org/10.1038/nrm3920
Xue, X.-H., Guo, C.-Q., Du, F., Lu, Q.-L., Zhang, C.-M., & Ren, H.-Y. (2011). AtFH8 Is Involved in Root Development under Effect of Low-Dose Latrunculin B in Dividing Cells. *Molecular Plant*, *4*(2), 264–278. https://doi.org/10.1093/mp/ssq085
Yates, E. A., & Knox, J. P. (1994). Investigations into the occurrence of plant cell surface epitopes in exudate gums. *Carbohydrate Polymers*, *24*(4), 281–286. https://doi.org/10.1016/0144-8617(94)90072-8
Ye, J., Zheng, Y., Yan, A., Chen, N., Wang, Z., Huang, S., & Yang, Z. (2009). Arabidopsis Formin3 Directs the Formation of Actin Cables and Polarized Growth in Pollen Tubes. *The Plant Cell*, *21*(12), 3868–3884. https://doi.org/10.1105/tpc.109.068700
Zhang, X., Ma, H., Qi, H., & Zhao, J. (2014). Roles of hydroxyproline-rich glycoproteins in the pollen tube and style cell growth of tobacco (Nicotiana tabacum L.). *Journal of Plant Physiology*, *171*(12), 1036–1045. https://doi.org/10.1016/j.jplph.2014.02.010
Zheng, C.-Y., Petralia, R. S., Wang, Y.-X., & Kachar, B. (2011). Fluorescence Recovery After Photobleaching (FRAP) of Fluorescence Tagged Proteins in Dendritic Spines of Cultured Hippocampal Neurons. *JoVE (Journal of Visualized Experiments)*, *50*, e2568. https://doi.org/10.3791/2568

Chapter 4. Arabinogalactan Glycoprotein Dynamics During The Progamic Phase In The Tomato Pistil [3]

Cecilia M. Lara-Mondragón and Cora A. MacAlister*

University of Michigan, Department of Molecular, Cellular and Developmental Biology

*Corresponding author, macalist@umich.edu

4.1. Key message

Pistil AGPs display dynamic localization patterns in response to fertilization in tomato. *SlyFLA9* (*Solyc07g065540.1*) is a chimeric Fasciclin-like AGP with enriched expression in the ovary, suggesting a potential function during pollen–pistil interaction.

4.2. Abstract

During fertilization, the male gametes are delivered by pollen tubes to receptive ovules, deeply embedded in the sporophytic tissues of the pistil. Arabinogalactan glycoproteins (AGPs) are a diverse family of highly glycosylated, secreted proteins which have been widely implicated in plant reproduction, particularly within the pistil. Though tomato (*Solanum lycopersicum*) is an important crop requiring successful fertilization for production, the molecular basis of this event remains understudied. Here we explore the spatiotemporal localization of AGPs in the mature tomato pistil before and after fertilization. Using histological techniques to detect AGP sugar

[3] Published chapter: Lara-Mondragón, C. M., & MacAlister, C. A. (2021). Arabinogalactan glycoprotein dynamics during the progamic phase in the tomato pistil. *Plant Reproduction*. DOI: 10.1007/s00497-021-00408-1

moieties, we found that accumulation of AGPs correlated with the maturation of the stigma and we identified an AGP subpopulation restricted to the micropyle that was no longer visible upon fertilization. To identify candidate pistil AGP genes, we used an RNA-sequencing approach to catalog gene expression in functionally distinct subsections of the mature tomato pistil (the stigma, apical and basal style and ovary) as well as pollen and pollen tubes. Of 161 predicted AGP and AGP-like proteins encoded in the tomato genome, we identified four genes with specifically enriched expression in reproductive tissues. We further validated expression of two of these, a Fasciclin-like AGP (*SlyFLA9*, *Solyc07g065540.1*) and a novel hybrid AGP (*SlyHAE*, *Solyc09g075580.1*). Using in situ hybridization, we also found *SlyFLA9* was expressed in the integuments of the ovule and the pericarp. Additionally, differential expression analyses of the pistil transcriptome revealed previously unreported genes with enriched expression in each subsection of the mature pistil, setting the foundation for future functional studies.

4.3. Introduction

Angiosperms constitute the vast majority of our economically important crops and the production of many of their seeds and fruits depends on sexual reproduction. Fertilization involves the delivery of the male gametes to receptive ovules, deeply embedded in the sporophytic tissues of the pistil. During this process, pollen tubes, carriers of the sperm cells, penetrate and elongate through the pistil tissues, establishing a number of interactions with distinct cell types along their journey (Palanivelu & Tsukamoto, 2012). To date, a number of ions and molecules including water, lipids, hormones, peptides and glycoproteins, derived from the pistil and controlling pollen germination and growth have been identified in different species (Cheung et al. 1995; Coimbra et al. 2007; Lush et al. 2000; Okuda et al. 2009; Pereira et al. 2016; Vogler et al. 2014; Wolters-Arts et al. 1998; Zheng et al. 2019).

Pollen behavior is modulated by the sporophytic tissues of the pistil, the stigma and style (pre-ovular guidance) and once the pollen tubes reach the ovary, they are further guided by signaling cues secreted by the female gametophyte or embryo sac (ovular guidance) (Higashiyama and Takeuchi 2015). In the stigma and style, pre-ovular guidance is known to play an important role in maintaining interspecific barriers and, when the pollination is compatible, the stigma and style support pollen adhesion, hydration and germination, pollen tube elongation and directional growth, in addition to rendering pollen tubes competent to recognize ovular signals (Dresselhaus and Franklin-Tong 2013; Kandasamy et al. 1994; Smith et al. 2013; Takeuchi and Higashiyama 2011).

Reports across species have revealed that a family of highly glycosylated proteins, known as Arabinogalactan proteins (AGPs), play an important role during reproduction both in pre-ovular and ovular guidance. In the stigma, secretion of AGPs has been correlated to pistil maturity (apple—Losada and Herrero 2012; magnolia—Losada et al. 2014; Trithuria—Costa et al. 2013; Quercus—Lopes et al. 2016) while in the style, members of this family such as the class III Pistil Extensin-like protein (PELPIII) and Transmitting Tract Specific (TTS) in tobacco promote pollen tube growth (Cheung et al. 1995; de Graaf et al. 2003,). In *Torenia fournieri*, an ovule derived arabinogalactan sugar (AMOR), likely derived from AGPs, is necessary to induce pollen tube competency to respond to ovule cues (Mizukami et al. 2016). In the ovary of *Arabidopsis*, a group of chimeric AGPs known as Early Nodulation-like proteins (ENODLs 11-15) are highly expressed in the embryo sac and the loss of function disrupts signaling necessary for bursting of the pollen tube upon penetration (Hou et al. 2016). Furthermore, an ovule expressed classical

AGP, AGP4/JAGGER is involved in promoting degeneration of the synergid cell post-fertilization and thus, blocking further pollen tube attraction (Pereira et al. 2016).

The structures and molecules involved in sexual reproduction tend to evolve rapidly (Edlund et al. 2004). This is likely true for the AGP family, as evidenced by the versatility of their functions in pollen guidance and the existence of lineage-specific members (e.g. PELPIII stylar proteins in *Nicotiana spp*.; Noyszewski et al. 2017). Therefore, in order to deepen our understanding of the extent of evolutionary conservation and/or emergence of novel AGP functions during sexual reproduction, it is necessary to broaden the spectrum of species studied. The study of species with relevance for agriculture, which, in many cases, remains understudied, is of particular importance due to increasing food demand and the yield sensitivity of crops to increasing global temperatures (Challinor et al. 2014). Tomato is an economically important crop and an emerging model system with structural features that other plant models lack (e.g. compound leaves, fleshy fruits, sympodial growth) (Kimura and Sinha 2008). The tomato genome is publicly available (Sato et al. 2012) and the use of high throughput technologies to study its development, in addition to conventional cellular and genetics techniques, have shown to be extremely useful for identification of new molecular elements involved in floral meristem induction and fruit development/ripening (MacAlister et al. 2012; Pattison et al. 2015; Zhang et al. 2016). Regarding its reproductive biology, most efforts have been directed toward the study of fruit development and ripening, leaving a considerable gap of knowledge in our understanding of fertilization.

To date, despite the evidence pointing to a role for the AGP family in fertilization, their function in tomato reproductive biology prior to fruit development remains elusive. In this study, we

explore the role of the AGP family during pollen–pistil interaction. First, using a series of probes for in situ AGP glycan detection, we characterize the spatiotemporal distribution of AGPs in pistils pre- and post-fertilization. Second, through transcriptome analyses, we evaluate the expression of predicted members of the AGP family in RNA-seq libraries derived from mature tomato pistils. Our search revealed a previously unidentified candidate of the AGP family with potential functions in pollen ovular guidance, setting the basis for future functional studies.

4.4. Materials and methods

4.4.1. Plant growth conditions

Tomato plants cv. Micro-Tom were maintained in a growth chamber under standard conditions (16 h light/18 h dark) until flowering. To avoid self-pollination in mature pistil samples, pre-anthesis flowers (7 mm length) were emasculated and allowed to further mature for 24 h. For pollen samples, the anthers of open flowers were dissected and placed in a microfuge tube with sterile dH_2O, and vortexed vigorously to release mature pollen, anther debris was removed with forceps, spun down and water removed.

4.4.2. In situ β-Yariv staining

To evaluate accumulation of AGPs in the stigmas of tomato pistils through development, two sets of five flowers in five different developmental stages (defined by flower bud length) were collected and sepals, petal and anthers removed under a dissecting microscope (Olympus, SZ61). The individual pistils were placed in a 0.2 ml tube upside down and the stigmas immersed in a solution containing 1 mg/ml of β-Yariv or α-Yariv and incubated for 5 h at room temperature. The stigmas were then washed with 1 × PBS and observed under the dissecting microscope to document accumulation of AGPs visualized as red-brown precipitates. For pistil cryosections,

mature pistils were embedded in OCT medium (Tissue-Tek; Sakura Finetek USA) and flash frozen. Samples were sectioned 10 μm thick using a cryostat (Leica 3040S Cryostat) at −20 °C. Sectioned samples were stained with 1 mg/ml of β-Yariv or α-Yariv for 5 h and washed with 1 × PBS. The samples were imaged using light microscopy (Leica, model DM5500B; camera Leica, model DFC365FX).

4.4.3. Pistil aniline blue staining

Unpollinated pistils and manually pollinated pistils collected after 24 h (five pistils per stage) were harvested and vacuum infiltrated with fixative (Acetic acid: EtOH, 1:3) for 24 h followed by 5 M NaOH overnight. The following day, the samples were washed for 10 min with dH_2O five times. Finally, the samples were incubated overnight with 0.001 mg/ml Aniline Blue Fluorochrome (Biosupplies Australia, 100-1) dissolved in 0.1 M K2HPO4 pH 10, mounted on an imaging chamber with Vectashield (Vector Laboratories, H-1400) and observed under an epifluorescence microscope (Leica, DM5500B) using the DAPI filter (355/455 nm) equipped with a Leica camera (DFC365FX).

4.4.4. AGP immunostaining

For immunolocalization of AGPs in semi-thin sections, we followed the protocol described by Costa et al. 2017. Briefly, unpollinated pistils and pistils 24 h after manual pollination (eight pistils per stage) were vacuum infiltrated with fixative (2% (w/v) Formaldehyde, 2.5% (w/v) Glutaraldehyde, 0.025 M PIPES buffer (pH 7.2) and 0.001% (v/v) Tween 20) for 2 h; the fixative was replaced with fresh solution and incubated overnight at 4 °C. The samples were washed with 0.25 M PIPES buffer pH 7.2 and dehydrated in ethanol series (25%, 35%, 50%, 70%, 80%, 90% and 3 × 100%). After dehydration, sample embedding was performed by incubating the samples

for 24 h in increasing concentrations of LR white (EMS, #14381) according to the manufacturer's recommendations. Following microtome sectioning to 200 nm, sections were incubated with blocking solution (filtered 5% non-fat skim milk in 1 × PBS) for 10 min, washed with 1 × PBS for 10 min and incubated with the primary antibody (JIM8, JIM13 or MAC207 1:5 hybridoma supernatant in blocking buffer) for 2 h at room temperature followed by an overnight incubation at 4 °C. Sections were then washed with 1 × PBS for 10 min and incubated with the secondary antibody (anti-rat-FITC, Sigma, F6258; 1:100 in blocking buffer) in the dark. The samples were then washed with 1 × PBS, followed by a dH20 wash. Calcofluor white was used as a counter stain. Slides were mounted with Vectashield (Vector Laboratories, H-1400) and observed under an epifluorescence microscope (Leica, DM5500B) equipped with a Leica camera (DFC365FX). Calcofluor white staining was visualized using the DAPI filter (355/455 nm) while FITC was observed using the 470/525 nm filter. False colored images were obtained with the Leica Application Suite (LASX) software.

For whole mount immunostaining of ovules, we followed the protocol described by Pasternak et al. (2015). Ovaries dissected from unpollinated pistils and pistils 24 h after manual pollination were fixed in vacuum with 2% formaldehyde in 1 × Microtubule Stabilizing Buffer (MTSB; 50 mM PIPES, 5 mM MgSO4, 5 mM EGTA pH 6.9) supplemented with 0.1% Triton x-100 pH 7, followed by a dH20 wash. Samples were cleared by incubation with methanol at 60 °C for 1 h. The concentration of methanol was gradually decreased by adding water to the samples every 5 min until the concentration of methanol was 20%, followed by a dH_20 wash. The samples were after incubated for 30 min at 37 °C with 0.2% driselase and 0.15% macerozyme in 2 mM MES pH 5 to partially digest the cell walls of the samples and facilitate antibody binding. After cell

wall digest, the samples were permeabilized with 3% IGEPAL and 10% DMSO in 1 × MTSB. The samples were later incubated for 20 min with blocking buffer (2% BSA in 1 × MSTB), followed by incubation with the primary antibody, MAC207 (1:5 in blocking buffer) for 2 h at 37 °C. The samples were later washed three times with 1 × MTSB and incubated with anti-rat-FITC (1:100 in blocking buffer) for 2 h at 37 °C. The samples were washed again three times with 1 × MTSB, co-stained with Calcofluor white and finally mounted in an imaging chamber for confocal microscopy. Imaging was performed using a Leica Sp5 laser-scanning confocal microscope with ×63 magnification. For FITC, the 488 nm excitation laser was used with a RSP500 dichroic beam splitter and PMT detectors were set to capture light at a wavelength range of 495 to 554 nm. For Calcofluor white, we used the 405 nm laser with the Substrat dichroic beam splitter, and PMT detectors were set at 414–474 nm wavelength. Z-slices were automatically optimized, and maximum intensity projections were generated using the LASX software.

4.4.5. mRNA sequencing

Mature pistils were fixed in ice cold acetone using a vacuum chamber followed by subdivision into four sections: stigma (n = 35), apical style (1–1.6 mm below the distal end, n = 35), basal style (3–3.5 mm from base, n = 35) and ovary (n = 35). For pollen samples, dry pollen was collected from mature open flowers and immediately frozen with liquid nitrogen or incubated in liquid germination medium (PGM, recipe based on Covey et al. (2010), 24% w/v PEG 4000, 0.01% Boric acid, 2% Sucrose, 0.02% HEPES buffer, 0.003% Ca(NO3)·4H2O, 0.02% MgSO4·7H2O and 0.01% KNO3) for ~10 h, when the pollen tubes reached the tri-cellular stage (corroborated by DAPI staining in a small subsample). After incubation, the pollen tubes were spun down at 500× g for 1 min, the PGM removed and the tubes immediately frozen with liquid

nitrogen for RNA extraction. We performed a power analysis to determine the required number of biological replicates and sequencing depth to identify differentially expressed genes with at least a twofold difference and a p-value <0.01 (Busby et al. 2013) and data from tomato meristems (MacAlister et al. 2012) and pilot data from mature pollen grains. Four biological replicates of each sample were ground to a fine powder using a Tissue Lyser II (Qiagen, Cat. No. 85300). Total RNA was extracted using the RNeasy Plant kit (Qiagen, Cat. No. 74904) and treated in column with DNAse (Qiagen, Cat. No. 79254) according manufacturer's instructions. After total RNA isolation, the integrity of the samples was analyzed using a NanoDrop (Thermo Scientific) and TapeStation (Agilent). All samples except one stigma replicate passed quality control with A260/280 between 1.8–2.1, A260/230 > 1.5 and RIN value ≥7.6, and were used for library preparation.

Stranded, poly-A enriched mRNA libraries were prepared by the University of Michigan Sequencing Core using the TruSeq mRNA stranded library prep kit (Illumina, Cat. No. 20020594). The samples were multiplexed and 50 bp, single-end sequencing was performed in the Illumina HiSeq4000 platform. We performed quality control of the de-multiplexed reads using FastQC (Wingett and Andrews 2018). The reads were filtered based on quality and trimmed (Trimmomatic, Bolger et al. 2014) of any adapter contamination. Transcript abundance was quantified using kallisto (Bray et al. 2016) pseudoalignment, using the transcriptome of the tomato cv. Heinz 1706, ITAG 3.2 version to build the index (Sol Genomics Network; Sato et al. 2012; Table 4-1).

4.4.6. Data mining and exploratory analyses

To complement our data, we compiled publicly available datasets from different sources including Ezura et al. (2017). The samples correspond to a variety of vegetative tissues collected from tomato cv. Micro-Tom plants, including cotyledon, young, mature and old leaves, 7 days old and mature root and stems. Additionally, datasets corresponding to dissected anthers in three different stages, sepal, petals, and green and red fruits. Additionally, we included in our analysis datasets of mature leaf (2 biological replicates), root (2 replicates) and flower bud (2 replicates) from the cv. Heinz; deposited in the SolGenomics Network (SGN) website (Sato et al. 2012). The raw reads from the aforementioned samples were downloaded from the NCBI database and processed as above. The data was filtered based on their TPM values with genes with TPM higher or equal to 0.1 considered as expressed. After filtering, the data was transformed by the Variance Stabilizing Transformation method (VST) using the *vst* function of the *DEseq2* package (Love et al. 2014). The Principal Component Analysis (PCA) was carried out in R studio using the *plotPCA* function of *DEseq2*. To determine transcriptome complexity (Carninci et al. 2000), the average expression of each gene across biological replicates from the same tissue was calculated. The contribution of each gene to the overall transcriptional load of each tissue (Total Transcriptional Output, TTO) was calculated by sorting the data from highest to lowest expression value and dividing each value by the sum of all average expression values. The cumulative distribution of the transcriptional contribution of each gene and standard deviation was plotted.

4.4.7. Tissue exclusivity and preferential expression

Genes with preferential expression across reproductive tissues were determined using *DEseq2* (Love et al. 2014) by performing pair-wise comparisons of the normalized data between each tissue versus the rest of the tissues. For the differential expression analysis, we used the datasets

from SGN with their respective biological replicates (leaf, root and flower bud). From the datasets of the study of Ezura et al. (2017), we only included the datasets from other floral whorls but pistil (sepal, petal and anther). Genes with False Discovery Rate (FDR) q-value <0.05 and Log Fold Change (LFC) >2 were considered as preferentially expressed. Next, we looked for overlap of the resulting list of genes among tissues and retained the unique elements to each tissue/structure for further analyses. To predict the subcellular localization of the enriched genes, we used *DeepLoc-01* (Almagro Armenteros et al. 2017) and the amino acid sequences of the enriched genes.

4.4.8. AGP expression, quantitative RT-PCR and in situ hybridization

ITAG identifiers of predicted AGP members (161 genes), including canonical AGPs, chimeric and hybrid AGPs were compiled from previously published reports (Ma et al. 2017; Johnson et al. 2017; Showalter et al. 2010). A matrix of the log2 of the mean TPM values per gene was plotted as a heatmap using the *pheatmap* R package. Genes were clustered based on their expression patterns through calculation of Euclidean distances. Out of the initial list, 60 AGP genes were represented in our transcriptomes and the published vegetative transcriptomes. We then selected genes with a high expression in pistil tissues compared to the rest of the tissues for independent validation by quantitative RT-PCR (qRT-PCR). Total RNA was isolated as above from mature leaves, sepals, petals, flower buds (2 mm length), anthers, pollen, ovaries, basal and apical style and stigmas. DNA-free total RNA (200 ng) was used for cDNA synthesis using the SuperScript® III First-Strand Synthesis System (Invitrogen, 18080051) following manufacturer's instructions. Serial tenfold dilutions of pooled cDNA from the different tissues were used to determine primer efficiency curves. Quantitative PCR was performed using the Applied Biosystems® SYBR® Green PCR Master Mix in a StepOnePlus™ Real-Time PCR

System according to the manufacturer's manual. Three independent biological replicates were analyzed per sample per gene using the primers in Table 4-2. Actin and ubiquitin were used as reference genes and the obtained data was normalized using the Livak calculation method (Livak and Schmittgen 2001). For *in situ* hybridization of mature pistil sections, we followed the protocol published by Javelle et al. (2011) using sense or antisense DIG-labeled RNA probe generated from the full *SlyFLA9* cDNA sequence amplified with the primers in Table 4-2.

4.4.9. Sequence homology search and phylogenetic analysis

The Basic Local Alignment Search Tool (BLAST) available in the SolGenomics Network (SGN; https://solgenomics.net/tools/blast/) website or The Arabidopsis Information Resource (TAIR) was used to identify homologous sequences (Table 4-3). Multiple sequence alignment was performed using *Clustal Omega*. The phylogeny of Arabidopsis and tomato GALT/HPGTs was generated with *Phylip* using the neighbor joining method with 200 bootstrap replicates; the consensus tree was calculated by the extended majority rule.

4.5. Results

4.5.1. Arabinogalactan glycoproteins accumulate in mature tomato pistils

Secretion of AGPs to the stigmatic surface correlates with pistil receptivity in several species with wet stigmas (Gell et al. 1986; Losada and Herrero 2012; Losada et al. 2014; Losada and Herrero 2017; Lord and Heslop-Harrison 1984). We asked whether this observation also holds true in tomato pistils, another species that possess a 'wet' stigma upon maturation (Heslop-Harrison and Shivanna 1977). The stigmas of pistils from five different developmental stages (defined by the size of the flower bud) up to anthesis were submerged briefly in a solution containing the AGP-specific synthetic dye, β-Yariv (Yariv et al. 1962). As a negative control, we

used the non AGP-reactive isoform α-Yariv in pistils of the same developmental stages. As shown in Figure 4-1A, a progressive accumulation of the β-Yariv-AGP complex precipitates in the stigma as the pistil reaches maturity, while the negative control does not display any visible staining. Our observations support the hypothesis that pistil receptivity correlates with secretion of AGPs in the stigma of the tomato pistil. We then asked whether AGPs reactive to the β-Yariv reagent are also present in the style and ovary. The transmitting tract of the style is a specialized secretory tissue rich in carbohydrates, flavanols, glycoproteins and lipids (Lennon et al. 1998), while the ovary contains the radially arranged ovules which are attached to the placenta (Figures 4-1B, 4-2). Frozen sections of mature pistils were stained with β-Yariv and α-Yariv and observed under the microscope. Compared to the negative control, clear β-Yariv staining was observed in the transmitting tract of the pistil and ovules, indicating that AGPs are produced by different cell types along the pistil (Fig. 4-1B).

To expand our observations with the β-Yariv reagent, we generated semi-thin sections of tomato pistils and probed them with anti-AGP glycan antibodies: JIM8 (unknown epitope structure), JIM13 and MAC207 (described epitope for both antibodies: β-GlcA1 → 3-α-GalA1 → 2-Rha) (Knox et al. 1991; Pennell et al. 1991; Yates et al. 1996). Even though all of these antibodies bind to AGP glycan moieties, they display differential binding and developmental patterning (Knox 1995). Several studies have also shown AGP localization to be responsive to various physiological and developmental events such as biotic and abiotic stress (Wu et al. 2017), and during male and female gametophytic development (Acosta-García and Vielle-Calzada 2004; Coimbra et al. 2007). Particularly in tomato, reports of AGP redistribution during fruit ripening and softening (Leszczuk et al. 2020) and during fruit development under abiotic stress (Fragkostefanakis et al. 2012; Mareri et al. 2016), support the hypothesis of dynamic

spatiotemporal regulation in response to stimulus in tomato. We, therefore, focused on detecting AGP localization changes during pollen–pistil interaction by collecting pistils before and after fertilization. To determine an appropriate post-fertilization time point, we used aniline blue staining to visualize the position of pollen tubes within the pistil tissues. We found that at 24 h post pollination, pollen tubes had entered the ovary and successfully reached several ovules (Figure 4-6). In contrast to our observations with β-Yariv staining, unpollinated pistils displayed weak labeling with all three antibodies (Supplementary material Figure 4-2), suggesting that these structures produce AGPs which are not recognized by, or with weak affinity to the tested antibodies, though it is also possible that the antibody epitopes may be present, but masked in these samples (Rydahl et al. 2018). Papillae in the stigma and cells along the transmitting tract are highly secretory and the complexity of their extracellular matrices might limit the accessibility of the antibodies to their epitopes. Weak immunolabeling with the antibodies in the stigma cells and style was also observed in samples at several stages during pollen–pistil interaction while strong labeling was observed in pollen grains attached to the papillae cells (Figure 4-7C, MAC207 antibody). In ovary sections, on the other hand, unpollinated pistils displayed a punctate, intracellular labeling in the ovules when stained with JIM8 and JIM13 (Figure 4-2A, B). In tomato pistils, due to the size of their ovules, obtaining sections of the ovary that preserve the embryo sac intact is challenging. We were able, however, to observe strong signal in a restricted area toward the micropylar pole of the ovule when staining with MAC207 (Figure 4-2C); potentially labeling the synergid cells (Figure 4-3C). After pollination, all three antibodies strongly labeled the cell walls of the inner cell layer of the integuments, surrounding the embryo sac (Figure 2D-F).

To have a better visualization of the ovule surface and expand our characterization of the ovular AGP patterning, we performed whole mount immunolocalization with MAC207. Whole mount immunostaining was performed in ovules from the same time points (unpollinated and 24 hap) as above. Our results show that, in ovules from unpollinated pistils, a subset of MAC207-reactive AGPs were restricted to the micropyle (Figure 4-3A). Interestingly, the signal visible in the micropyle of unpollinated ovules was no longer visible at 24 h after pollination (Figure 4-3B). AGP labeling by the MAC207 antibody was also present in the pollen tube (Figure 4-3B).

4.5.2. Identification of genes with enriched expression in tomato reproductive tissues

In tomato, a number of studies have focused on identifying sets of genes with potential function during fruit development (Pattison et al. 2015; Ezura et al. 2017; Zhang et al. 2016); however, a significant gap of knowledge still exists in earlier stages of sexual reproduction, particularly in understanding the molecular basis of pistil receptivity. The pistil is a complex collection of tissues that can be subdivided in three functionally distinct parts: the stigma, the style and the ovary (Figure 4-1). Therefore, we next focused on determining the transcriptional profiles of these regions to identify differences in gene expression that might contribute to their function. Gradients of gene expression throughout the pistil have been previously documented. For example, the transcript of *STIGMA-SPECIFIC PROTEIN1* (*STIG1*), a small Cys-rich protein that promotes pollen tube growth, is expressed only in the stigma and upper style (Huang et al. 2014). A similar expression pattern was reported for the transcript of *MON9612* (Pitto et al. 2001). Based on this information and the visible morphological differences between the apical and basal portion of the style (particularly the presence trichomes in the basal portion), we decided to explore possible differences in gene expression between these subsections. Mature pistils were dissected as shown in Figure 4-4A. To precisely identify female-specific or female-enriched

genes, we included datasets representing male reproductive samples. We generated libraries from mature pollen grains in the bicellular stage (vegetative and generative cells present) and pollen tubes in the tricellular stage (vegetative and sperm cells present, after germination *in vitro* and incubation for 10 h). To accurately account for biological variability in our study when determining preferential gene expression, we generated four biological replicates per sample, with the exception of the stigma samples where three samples passed the RNA quality requirements (A260/280 between 1.8 and 2.1, A260/230 > 1.5 and RIN value ≥7.6). We additionally included single-replicate transcriptomes from a range of Micro-Tom vegetative tissues and floral whorls published by Ezura et al. 2017, as well as transcriptomes from leaf, root and flower bud from the cultivar Heinz, deposited in the SolGenomics Network website (2 biological replicates each, Sato et al. 2012). Raw read quality was analyzed, overall the quality of our libraries was high (Phred score > 30). Sequencing adapter contamination was removed from the libraries if necessary. Transcript abundance was expressed in Transcripts per Million (TPM) and a gene was considered as expressed when TPM ≥ 0.1. After filtering based on this criterion, the pistil subsection samples retained ~70% of genes while pollen and pollen tube samples retained only 35–37% of genes. The latter observation is consistent with previous reports of a drastic reduction of the number of expressed genes in mature pollen in other species (*Arabidopsis*, rice; Honys and Twell 2004; Wei et al. 2010).

The complexity of a transcriptome is determined by the number of genes contributing to the total bulk of transcription or total transcriptional output (TTO) (Carninci et al. 2000; Melé et al. 2015). In tissues with a low transcriptome complexity, few genes will account for the majority of the transcriptional output. We determined the fraction of the TTO for each gene in our datasets

and found that pollen and pollen tubes have lower complexity transcriptomes relative to the pistil subsections with 51 and 44 genes accounting for ~50% of the TTO, respectively (Figure 4-4B). In both cases, the functions of many of the highest expressed genes are related to cell wall metabolism (Table 4-4 and 4-5). Among the pistil samples, stigma had the lowest complexity with 473 genes accounting for half of the TTO. In this case, functions associated with the top expressed genes are lipid metabolism, defense and signal responses (Table 4-6). In the apical subsection of the style, 479 genes account for ~50% of the TTO; the basal portion of the style 526 genes and the same number of genes account for half of the bulk of transcription in the ovary (Figure 4-4B). In the style and ovary subsections of the pistil the highest expressed gene belongs to the Defensin-like protein family (Table 4-7 to 4-9).

We then conducted a Principal Component Analysis (PCA) to visualize the variability among samples from different tissues (Figure 4-4C). In our analysis, Principal Component 1 (PC1) and PC2 together explained 98% of the variation of gene expression among datasets, with 96% of variation explained by the first component (PC1). As expected from samples generated from the same tissue, our replicate samples displayed high similarity with respect to the two principal components. On the other hand, separation of the datasets along PC1 shows that the major differences in transcriptional makeup exist between male/female reproductive tissues. Pistil subsections are clustered together and in close distance with other floral whorls (sepal and petal) excluding anther, with the latter being closer to the cluster formed by the male gametophyte. In addition, distribution along PC2 shows a distinction between reproductive and vegetative tissues as previously reported (Ezura et al. 2017) (Figure 4-4C).

Once we validated the quality of our transcriptomes, we identified genes with enriched expression in the pistil subsections and pollen and pollen tubes. Previous efforts have been done to identify ovary specific genes in tomato (Ezura et al. 2017; Pattison et al. 2015); however, to our knowledge, our study is the first effort to characterize the transcriptional profiles of subsections of the mature pistil. We performed a Differential Expression Analysis (DEA) by comparing each sample to the rest of the tissues, including libraries from other floral whorls (anther, sepal, petal) and vegetative tissues (leaf, root and flower bud). After DEA, we filtered the data and retained only genes with Log Fold Change (LFC) ≥ 2 and Q-value ≤ 0.05. We then looked for overlapping genes between the obtained lists to narrow down the number of genes with preferential expression per tissue/structure. After the second filtering, pollen grains had the greatest number of preferentially expressed genes (1229, Table 4-10), followed by pollen tubes (1126, Table 4-11). Within subsections of the pistil, the ovary displayed the highest number of differentially expressed genes (448, 4-15), followed by the stigma (411, Table 4-12), the apical portion of the style (57, Table 4-13) and lastly, the basal portion of the style (29, Table 4-14) (Figure 4-4D).

In order to gain more insight on the functions of the genes identified in this study, we predicted the subcellular localization of the proteins they encode. Using a prediction tool based on machine learning (DeepLoc-01, Almagro Almenteros et al. 2017), we determined that in all tissues, the highest percent of genes were predicted to be nuclear or cytoplasmic (ranging from 16 to 26% for cytoplasmic and 17–30% for nuclear proteins, Figure 4-8). Consistent with the highly secretory nature of the transmitting tract of Solanaceae species (Lush et al. 2000), the third most abundant localization in the apical (17%) and basal style (33%) is extracellular (Figure 4-4E).

Interestingly, in pollen and pollen tubes the third most abundantly predicted compartment is mitochondria. Although a direct relationship cannot be established solely on transcriptomic data, our findings are consistent with reports of a higher content of mitochondria in pollen relative to vegetative tissues in some species (Lee and Warmke 1979) that presumably supports, at least in part, the highly energy-demanding process of pollen tube elongation (Selinski and Scheibe 2014).

4.5.3. Characterization of expression profiles of the AGP family in tomato reproductive structures

In tomato, only a handful of AGPs had been characterized. To date, *LeAGP1*, a ubiquitously expressed classical AGP, is the biochemically and genetically best studied AGP (Showalter et al. 2000; Gao and Showalter 2000; Sun et al. 2004). In addition, the study of Fragkostefanakis et al. (2012), identified 34 putative genes encoding AGPs, and further characterized the expression dynamics of *SlAGP2* (*Solyc04g074730.1*) and *SlAGP4* (*Solyc04g074730.1*) during fruit ripening and in response to wounding and hypoxia. Our immunological studies suggest an important role for AGPs in tomato reproduction, prior to fruit development (Figures 4-2, 4-3). Therefore, we were interested in investigating the expression of genes encoding AGPs in our datasets.

The AGP family is a highly diverse, multigenic group. They are highly glycosylated (up to 90% of their total weight corresponds to carbohydrates) and possess a high content of (hydroxy)proline (Hyp), alanine, serine and threonine in their sequences. AGP glycosylation occurs on hydroxyproline residues within clustered dipeptide motifs Ala-Hyp, Ser-Hyp, Val-Hyp, Gly-Hyp and Thr-Hyp (Ellis et al. 2010). Depending on the structure of their protein backbones, AGPs can be further divided into subgroups: classical AGPs, small AG-peptides,

lysine-rich AGPs, hybrid AGPs (with glycosylation motifs belonging to different classes of Hydroxyproline-Rich Glycoproteins—HRGPs) and chimeric AGPs (with functionally and phylogenetically unrelated domains). Due to their biased amino acid composition and repetitive nature, several bioinformatics pipelines to predict the number of genes encoding AGPs have been developed (Schultz et al., 2002; Ma et al. 2017; Johnson et al. 2017; Showalter et al. 2010). In general, the available tools make use of different features in order to categorize a gene as member of the AGP family; for example, the percent of Pro, Ala, Ser and Thr present in the protein backbone, presence of a GPI anchor and signal peptide, sequence homology to known AGP genes, the presence of known chimeric domains in the sequence (e.g. Fasciclin-like domains, phytocyanin-like domains, xylogen-like domains, non-specific lipid transfer protein-like domains, early nodulin-like domains, etc.) or the presence and type of other glycosylation motifs for hybrid AGPs. As a consequence, the estimated number of sequences encoding for AGPs for a species varies depending on the prediction pipeline used. Thus, we compiled the ITAG identifiers of predicted sequences encoding for AGPs from three previously published reports (Ma et al. 2017; Johnson et al. 2017; Showalter et al. 2010). We then searched expression profiles among tomato tissues, with special interest in those displaying higher expression levels in our reproductive datasets (pistil subsections, pollen grains and tubes).

Out of the 161 presumed AGP genes in the tomato genome, 60 had detectable expression in our datasets and the vegetative datasets analyzed (Supplementary material Fig. 4). Among the genes represented in our analysis, the majority are classified as classical AGPs (16/60), followed by chimeric AGPs with Fasciclin-like domains (FLAs, 11/60). As anticipated, AGPs were expressed in a broad spectrum of tissues, both vegetative (especially root) and reproductive. Using

hierarchical clustering of the AGP gene expression across tissues, we identified a cluster with enriched expression in reproductive tissues (Figure 4-5A Figure 4-9, Supplementary material Figure 4-5). This cluster included three genes with high expression in the pistil: a hybrid AGP-Extensin (*Solyc09g075580.1*, recently annotated as a short Extensin, *SlEXT14* by Ding et al. 2020), a Lysine-rich AGP (Lys-AGP, *Solyc07g052680.1*, annotated by Leszczuk et al. 2020 as *AGP19*) and a chimeric AGP with two Fasciclin-like domains (*Solyc07g065540.1*, annotated as *SlyFLA9* by Fragkostefanakis et al. 2012). The pistil expressed AGPs are represented in the Tomato Expression Atlas (TEA) in samples taken from dissected ovaries and in some cases through fruit development, although the expression levels reported are relatively low (Figure 4-11A). In this cluster we also observed a classical AGP, *Solyc05g049890.1*, expressed in male reproductive structures (pollen grains and tubes). This AGP was represented in the Plant eFP data, as expressed in unopened flowers, possibly due to the lack of more refined datasets for floral parts other than ovaries (Figure 4-11B). Since the data we analyzed was derived from both the Micro-Tom and Heinz 1706 cultivars, we compared the coding sequences of the reproductive AGPs in these two backgrounds and found that the predicted coding sequences were identical except for *Solyc09g075580.1* which possessed two amino acid substitutions (F15V, L66S) and an indel mutation resulting in an additional proline residue within an extensin $S(P)_{3–5}$ motif in the Micro-Tom sequence (Supplementary material Figure 4-7). As a complement to the identification of AGPs, we also searched for tomato genes encoding hydroxyproline galactosyltransferases (hyp-GALT and HPGT) proteins. These enzymes are required for the initiation of AGP glycosylation and their presence in the tomato genome is predicted by the detection of AGP glycans (Basu et al. 2013; Ogawa-Ohnishi and Matsubayashi 2015). We identified six tomato homologues of the Arabidopsis GALT and HPGT sequences and found

they were broadly expressed in the pistil and vegetative tissue with relatively weaker expression in the pollen samples (Supplementary material Figure 4-8).

From the pistil expressed AGPs, we selected those genes with the highest expression values (mean TPM) for further validation with an independent approach. The expression patterns of *Solyc09g075580.1* (hereafter *SlyHAE*) and *SlyFLA9* were confirmed by quantitative RT-PCR. *SlyHAE* displayed a higher level of expression in the basal portion of the style (Figure 4-5C). The protein sequence encoded by *SlyHAE* has relatively high content of Pro (28%), six predicted AGP glycomodules and two glycosylation motifs found in a different class of HRGPs, Extensins (Figure 4-5B). AGP-EXT hybrids like the class III Pistil Extensin-like Protein (PELPIII) have been reported in other members of the Solanaceae family like tobacco (Eberle et al. 2013; de Graaf et al. 2003); however, *SlyHAE* shares poor sequence similarity to this gene family (<12% sequence similarity to *N. tobaccum* PELPIII). Likewise, alignment of *SlyHAE* to other AGPs in tobacco known to be involved in reproduction (TTS, 120 KDa) displayed poor sequence similarity (Table 4-16). Two genes encoded in the genomes of *Nicotiana benthamiana* (*Niben101Scf01623g08001.1*) and *Solanum melongena* (*SMEL_009g330490.1.01*) displayed high sequence similarity to *SlyHAE* (61.48% and 85.61%, respectively) (Figure 4-11). No known functions for these genes in tobacco or eggplant have been reported. Outside of the Solanaceae family, no homologs of *SlyHAE* were identified. *SlyFLA9*, displayed a high level of expression in the ovary (Figure 4-5C). *SlyFLA9* is a chimeric AGP with two predicted Fasciclin domains (FAS), a C-terminus GPI anchor and 20 putative AGP glycomodules (Figure 4-5B). The FAS domains are conserved in Eukarya and are predicted to participate in cell–cell adhesion by an unknown mechanism (Seifert 2018). Sequence alignment of *SlyFLA9* produces significant hits to *FLA1* in *Arabidopsis thaliana*, which also possesses 2 FAS domains (72.9% similarity). The loss

of function of *FLA1* in *Arabidopsis* displayed shoot regeneration defects and, based on its expression pattern, is presumed to participate during embryogenesis and seed development (Johnson et al. 2011).

Based on the high expression level of *SlyFLA9* observed in the ovary (Figure 4-5B), we hypothesized it may contribute to the AGP glycan signals we observed in this organ (Figures 4-1B, 4-2, 4-3). To evaluate the spatial distribution of *SlyFLA9* transcripts, we generated DIG-labeled RNA probes for in situ detection in ovaries dissected from mature, unpollinated pistils. We observed high accumulation of the *SlyFLA9* transcript in the pericarp of the ovary and the outer integuments of individual ovules (Figure 4-5D). Based on the protein structure of *SlyFLA9* and its expression pattern, our results suggest a role during ovary maturation and ovule receptivity.

4.6. Discussion

The interaction between pollen and pistil is an ephemeral event during a plant's life cycle, yet the proper establishment of their molecular dialogue is crucial for successful fertilization. The AGP family has been implicated in virtually all steps of pollen–pistil interaction, paving the pathway along the sporophytic tissues of the pistil toward a receptive ovule (Dresselhaus and Franklin-Tong 2013; Su and Higashiyama 2018). Here, we report the distribution of AG glycans throughout pistil development and following fertilization (Figures 4-1, 4-2 and 4-3). Our results show that AGPs progressively accumulate in the stigmatic surface of the pistil, consistent with reports in other species with wet stigmas (Losada and Herrero 2012; Costa et al. 2013; Gell et al. 1986) and suggesting that AGPs present in stigmatic exudates play a role for the earlier stages of pollen–pistil interaction.

After pollen tubes penetrate the stigmatic cells, they elongate through the intercellular spaces of the transmitting tract in species with solid styles (Gotelli et al. 2017). Once in the style, directional pollen tube growth is thought to be regulated by chemical cues (Cheung et al. 1995) in combination with mechanical forces (Reimann et al. 2020). AGPs in the transmitting tract of solanaceous species have been implicated in stylar guidance: in tobacco, TTS, a member of the AGP family, displays a basipetal glycosylation gradient along the style of tobacco pistils, where it acts as a pollen tube attractant and as a source of nutrients upon glycan hydrolysis (Wu et al. 1995). Interestingly, genetic studies in the same species demonstrated that, in contrast to species with dry stigmas where incompatible pollination blockage occurs in the papillae (Fujii et al. 2019), the transmitting tract in the style acts as pre-zygotic barrier for interspecific pollination (Goldman et al. 1994). Several studies have highlighted the importance of the hybrid Extensin-AGP, PELPIII, during interspecies incompatibility in tobacco. PELPIII accumulates in the transmitting tract of the style and, after pollination, is translocated to the cell wall of the growing pollen tubes (de Graaf et al. 2003), inhibiting interspecific pollen tube growth (Alves et al. 2019). Our histological studies showed that β-Yariv reactive AGPs accumulate in the transmitting tract of the style of mature pistils (Figure 4-1B), potentially implicating AGPs in stylar guidance.

Due to the thickness and size of the pistil of solanaceous species, little information is available regarding the passage of pollen tubes from the transmitting tract to the ovary and how exactly pollen tubes respond to ovular cues once inside. In a study performed by Lush et al. (2000) in *Nicotiana alata* ovaries, which enclose ~400 ovules, pollen tubes expressing a GUS reporter appear to fertilize ovules in a random fashion. In addition, they reported pollen tube

‘meandering’ within the ovary, where pollen tubes exited the placental surface, bypassing ovules and growing through their external surface in a disorganized manner. We also observed this behavior in tomato ovaries 24 h after pollination when we removed the pericarp to expose the ovules and growing pollen tubes (Figure 4-6). Despite this seemingly random pollen tube behavior, they are capable of finding receptive ovules and fertilizing them, suggesting that a guidance mechanism indeed exists in this species. The micropyle, formed by the integuments that surround the embryo sac, is the pollen tube’s entry point to the ovule. The study of mutants with anomalous integuments revealed partial defects in pollen tube ovule targeting, suggesting a role for the micropyle in guidance (Lora et al. 2019). Although how the micropyle participates in pollen guidance is still unknown, the accumulation of AGPs in this region (Figure 4-3; Coimbra et al. 2007; Hou et al. 2016; Losada and Herrero 2019) suggest potential functions in this process. Additional evidence of AGP involvement in ovular pollen guidance comes from the discovery of AMOR, an arabinogalactan derived sugar produced by the sporophytic tissue of the ovule that renders pollen tubes responsive to synergid signaling peptides (Mizukami et al. 2016). Whether a pollen receptor that binds to AMOR exists, remains to be determined. It has been suggested that given the importance of Ca^{2+} dynamics for pollen tube growth and the ability of AGPs to bind Ca^{2+} in a pH-dependent manner, AGPs might influence cell growth by acting as a periplasmic Ca^{2+} reservoir (Lamport and Várnai 2013) or in the case of AMOR, a diffusible Ca^{2+} carrier (Lamport et al. 2018).

AGPs had been implicated in additional developmental processes, here we also report a reorganization of the AGP epitopes in the ovules after fertilization (Figures 4-2, 4-3), implicating AGPs in latter steps of embryo and/or fruit development. The latter has been reported for fruit ripening and softening (Leszczuk et al. 2019).

Immunological studies have proven useful to determining spatial regulation of AGPs in a number of species; however, for the most part, the identity of their protein backbones remains to be characterized. Several efforts combining amino acid bias quantification, prediction of signal peptides and homology searches have predicted members of the AGP family in different species (Ma et al. 2017; Johnson et al. 2017; Showalter et al. 2010). We compiled the tomato AGP sequences from these datasets; these included sequences corresponding to classical AGPs, hybrid and chimeric AGPs and small peptides (Figure 4-5 and Figure 4-9). To evaluate their expression profiles across reproductive tissues, we first generated a set of RNA-seq libraries derived from subsections of the mature pistil and pollen grains and tubes (Figure 4-4). From the original gene list of 161, we detected expression of 60 genes. Consistent with comprehensive studies in other species like Arabidopsis (Pereira et al. 2014), the AGP family displays different levels of expression across plant organs. Classical AGPs and FLAs were the most abundantly expressed subclasses of AGPs in tomato tissues (Figure 4-9). We identified and validated expression of two AGPs: a hybrid AGP-Extensin, *SlyHAE* (*Solyc09g075580.1*) with no homologs outside the Solanaceae family and with high expression in the style (Figure 4-5) and a Fasciclin-like AGP, *SlyFLA9* (*Solyc07g065540.1*) with high expression levels in the ovary, particularly in the outer cell layer of the integuments and the pericarp (Figure 4-5C,D). Fasciclin-like AGPs have been implicated in the development of pollen in *Arabidopsis* (Li et al. 2010) and fiber development in cotton (Huang et al. 2013). The exact mechanism of action of FLAs is poorly understood. It has been hypothesized that due to the presence of the Fas1 domain in their protein backbones, plant FLAs might function like those reported in metazoans. *Drosophila* Fas1 proteins function as cell–cell adhesion molecules during neuronal development (Zhong and Shanley 1995). The structure of the Fas1 domain has been crystallized; however, the mechanism of action remains to

be elucidated (Twarda-Clapa et al. 2018). The majority of FLAs have predicted GPI-anchors and it has been hypothesized that they can act as diffusible signaling molecules upon phospholipase mediated cleavage (Schultz et al. 1998). Cell–cell adhesion mediated translocation has been proposed as a mode of pollen tube guidance inside the ovary (Lush et al. 2000). The expression pattern of *SlyFLA9* makes it an interesting candidate for future genetic studies to evaluate its role during pollen–pistil interaction.

Although efforts to identify pistil-expressed genes have been published elsewhere (Ezura et al. 2017), our experimental design allowed us to identify the transcriptional profiles corresponding to stigma, apical and basal style and ovary. After differential expression analyses, careful inspection of the identified genes highlighted the potential for widespread usage of our datasets as tools for further characterization of genes upregulated in each pistil subsection. For example, in the stigma libraries, we found significant enrichment of genes related to lipid metabolism (Tables 4-2 and 4-3). Chemical composition studies of stigma exudate in other members of the Solanaceae family, like tobacco and petunia, revealed that it is lipid-rich. These lipids play an important role in pollen hydration, germination and directing pollen growth toward the aqueous phase underneath the hydrophobic exudate (Lush et al. 2000; Konar and Linskens 1966; Wolters-Arts et al. 1998). Several WSD1-like O-acyltransferases genes (*Solyc03g083385.1, Solyc03g083380.3, Solyc01g095930.3* and *Solyc10g009430.3*) had enriched expression in the stigma (LFC > 3). *WSD1* genes in *Arabidopsis* are involved in cuticle biosynthesis (Li et al. 2008). The presence of a cuticle layer in species with wet stigma has been documented either as a continuous layer (in *Vitis vinifera*, Ciampolini et al. 1996) or as a discontinuous layer, ruptured by the secretion of exudates (in *Petunia hybrida*, Konar and Linskens 1966).

In both portions of the style, genes with predicted extracellular localization were the third most enriched category (Figure 4-4D). Consistent with the literature, our apical style library detected enriched expression of genes annotated as STIG1 proteins (*Solyc03g120960.1* and *Solyc03g120955.1*) and the *MON9612* transcript (*Solyc02g093580.3*; Huang et al. 2014; Pitto et al. 2001). In this subsection, we also identified several enriched genes with predicted activities related to carbohydrate metabolism and cell wall polymer remodeling such as cell wall invertases (*Solyc01g088590.4*, *Solyc03g121680.2*), glycosyltransferases (*Solyc08g077080.1*, *Solyc05g012670.1*), pectinesterase (*Solyc01g099960.3*), polygalacturonase (*Solyc12g019180.2*) and α/ β-hydrolases (*Solyc08g083190.3*). Both, carbohydrate metabolism and pectin remodeling have recently been implicated in pollen–pistil interaction. In tomato pistils, cell wall invertases (CWIN) and hexose transporters are upregulated in response to pollination, in the style briefly after pollination to presumably support pollen tube growth, and in the ovary two days after pollination, potentially induced after fertilization (Shen et al. 2019). Pistil expressed polygalacturonases (PGs) are pectin hydrolytic enzymes that have been recently implicated in interspecific incompatibility in tobacco, where in vitro and semi-in vivo assays showed that PG activity inhibits pollen tube growth (Liao et al. 2020).

In our study we identified several genes encoding peroxidases, with expression in the stigma (*Solyc10g075120.2*), four genes in the basal style (*Solyc10g047110.2*, *Solyc05g052280.3*, *Solyc03g025380.3*, *Solyc05g046020.3*) and four genes in the ovary (*Solyc10g078890.2*, *Solyc09g072700.3*, *Solyc01g104860.3*, *Solyc02g084790.3*). Peroxidase activity is commonly used as a test for stigmatic receptivity (Dafni and Maués 1998). Peroxidase activity and accumulation of Reactive Oxygen Species (ROS, specifically H_2O_2) has been described in the stigmas of several species (McInnis et al. 2006). In tobacco, peroxidase activity measured along

the pistil is distributed as a gradient, with the highest activity in the stigma, decreasing activity in the style and a slight increase of activity in the ovary with distinct peroxidase isozymes in each subsection (Bredemeijer 1984). ROS signaling has been linked to pollen germination and hydration in the stigma, to pollen tube elongation in the transmitting tract and to ovular guidance in the ovary (Zhang et al. 2020).

Small secreted Cysteine-rich proteins (CRPs) play an important role during ovular guidance. CRPs are subclassified into three groups: Defense-like proteins (DEFL), Early Culture Abundant 1 proteins (ECA1) and nonspecific Lipid Transfer proteins (Sprunck et al. 2014). *DEFL* genes encode small peptides, some of which have species-specific pollen attractant functions (LURE peptides; Takeuchi and Higashiyama 2012; Higashiyama and Yang 2017). In *Arabidopsis* a member of the *ECA1* subgroup*, Egg Cell 1* (*EC1*) accumulates in the egg cell and promotes sperm cell fusion during fertilization (Sprunck et al. 2012). In our analysis, we identified several CRPs highly expressed in the ovary: four predicted *ECA1* genes (*Solyc05g010190.1*, *Solyc06g048400.1*, *Solyc11g008725.1* and *Solyc07g006210.1*, LFC > 4.7, the first gene was also identified by the study of Ezura et al. 2017) and three predicted *DEFL* genes (*Solyc09g074440.3*, *Solyc06g075200.1* and *Solyc07g017570.2*; LFC > 3.3).

Our study identified, in addition to pistil expressed AGPs, a number of genes with potential functions in the establishment of a receptive pistil in tomato. The predicted functions of the identified genes cover a broad spectrum: from cell wall modifying enzymes to small secreted signaling peptides. Functional characterization of these genes will allow us to further understand the basis of pistil receptivity and by performing comparative studies, understand how these genes involved in sexual reproduction evolved.

4.7. Author contribution statement

CMLM designed and performed experiments, analyzed data and wrote the manuscript. CAM conceived the study, designed experiments and edited the manuscript.

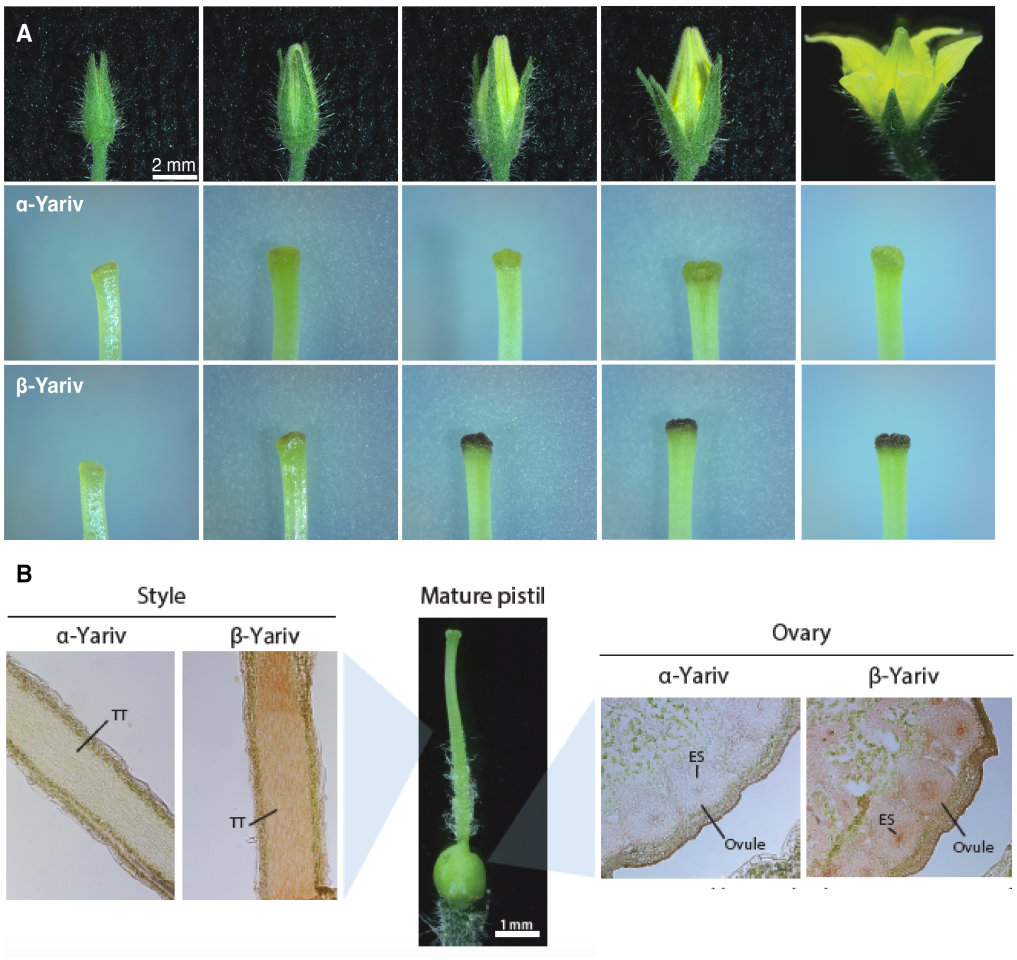

Figure 4-1 Arabinogalactan glycoproteins accumulate in the mature tomato pistil.

A) Pistil in different developmental stages (top) were dissected and stained with α (middle) or β-Yariv (bottom). AGPs react with the β-Yariv reagent, visible by the accumulation of a brown–red precipitate. α-Yariv stained samples serve as negative control, as α-Yariv does not react with AGPs. **B)** In cryosections of mature pistils, β-Yariv reactive AGPs accumulated in the transmitting tract in the style (longitudinal section) and in the ovary (cross section), visible staining is present in the embryo sac and placenta.

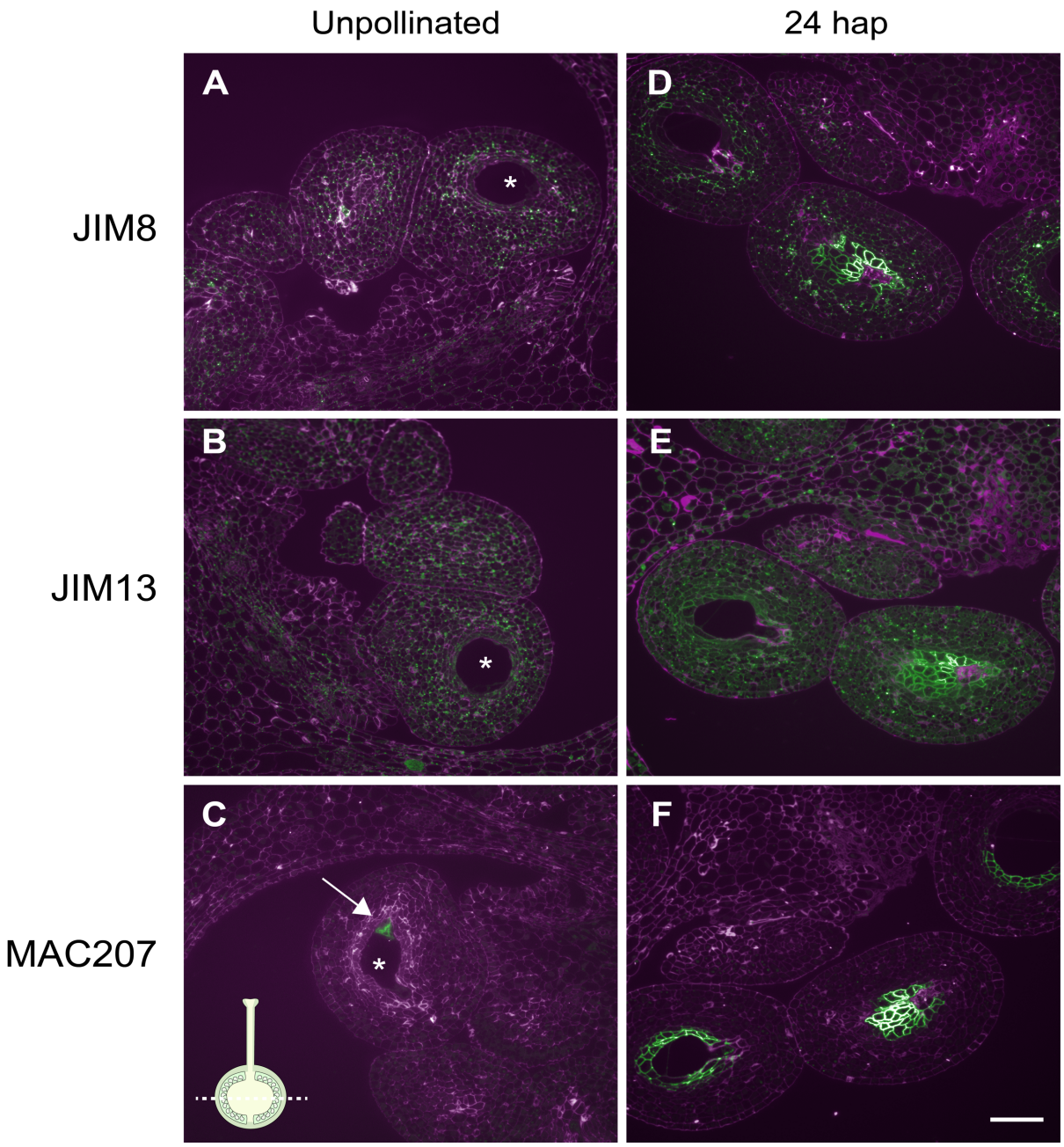

Figure 4-2 Arabinogalactan glycoproteins in the ovule display a distinctive pattern pre- and post-fertilization.

Representative micrographs of semi-thin sections labeled with anti-AGP glycan antibodies (green) and Calcofluor white as a counterstain for the cell wall (magenta). Pictures **A to C** correspond to samples sectioned from unpollinated pistils, from **D** to **F**, samples sectioned from manually pollinated pistils, collected 24 h after pollination. The arrow indicates the signal detected when labeling with MAC207; Stars mark the embryo sac. Scale bar 50 µm. Pistil schematic on C represents section orientation. Note that the embryo sac is difficult to capture in sectioned material due to its large size.

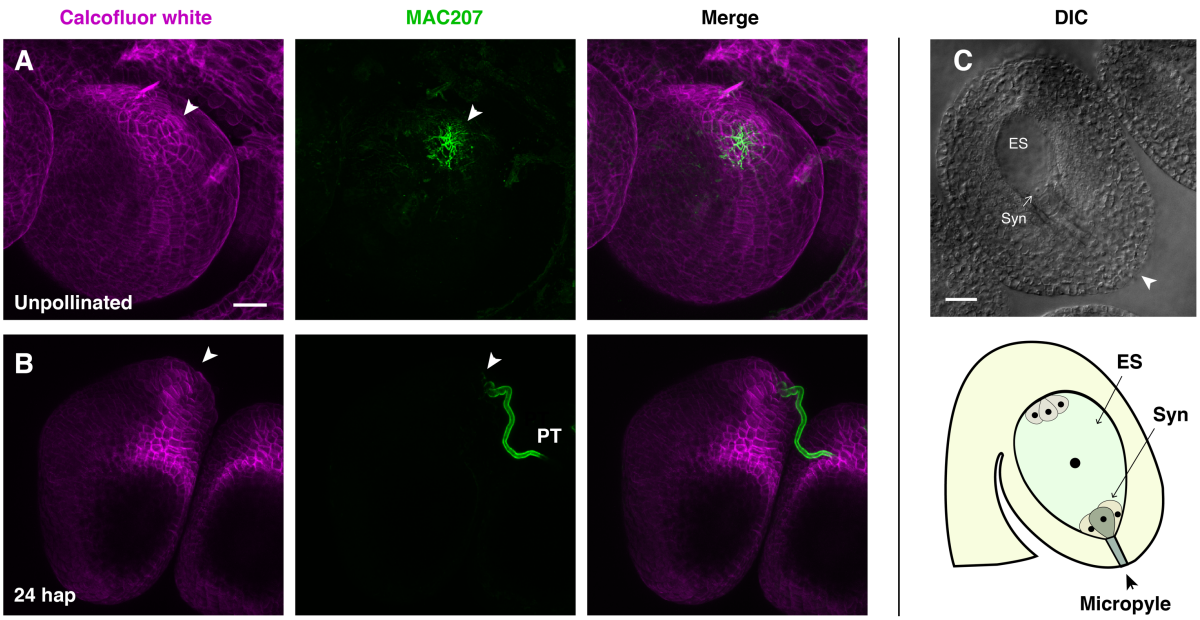

Figure 4-3 Arabinogalactan glycoproteins in the micropyle surface is not detectable post-fertilization.

Confocal laser microscopy of whole mount immunofluorescence of ovules from unpollinated pistils **(A)** or 24 h after pollination (**B**, 24 hap). MAC207 reactive AGPs accumulated in the micropyle (arrowhead) in ovules from unpollinated pistils. After a pollen tube (PT) had fertilized the ovule, the diffuse micropylar AGP signal was no longer detectable. MAC207 also bound to AGPs present in the pollen tube. Magenta channel corresponds to Calcofluor white, staining the cell wall for contrast. **C)** DIC micrograph of cleared ovules to better appreciate the ovule anatomy; bottom, schematic of the tomato ovule. ES embryo sac, Syn synergids.

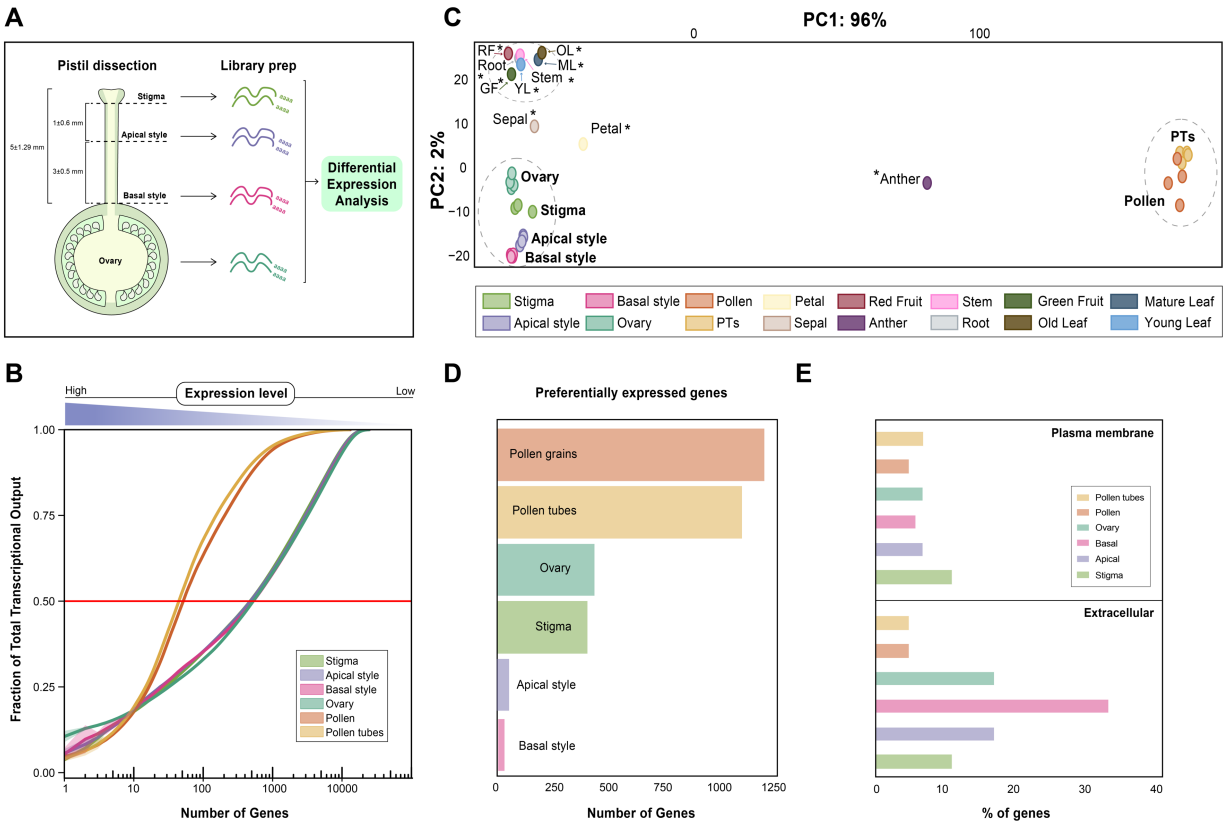

Figure 4-4 Exploratory analysis of transcriptomes from reproductive tissue of tomato.

A) Pipeline for library generation showing subsections of the tomato pistil used to generate libraries. Pistils of pre-anthesis flowers were emasculated, covered and allowed to mature for 24 h before dissection into the four subsections comprising the stigma, the apical style, the basal style and the ovary. **B)** Transcriptome complexity of tomato reproductive tissues. Cumulative distribution of the mean fraction of total transcription per tissue, contributed by genes sorted from highest expressed to lowest expressed (X axis, log10 scale). Per tissue, the lines represent the mean expression values across biological replicates, divided by the sum of all mean expression values from the tissue (Fraction of Total Transcriptional Output, Y axis). The shaded area surrounding each line represents the dispersion of the data, calculated by dividing the standard deviation by the cumulative sum of all mean expression values. The red line indicates half of the Total Transcriptional Output to facilitate comparison. **C)** Principal Component Analysis (PCA) of generated datasets (bold letters) and published transcriptomes form vegetative tissues and other floral parts (stars). Major clusters in gray dashed circles. Published transcriptomes taken from (Ezura et al. 2017). RF Red Fruit, GF Green Fruit, YL Young Leaf, ML Mature Leaf, OL Old Leaf, PTs Pollen tubes in the tri-cellular stage. **D)** Preferentially expressed genes identified by differential gene expression analysis. Each sample was compared to the rest of the tissues and non-overlapping genes were considered as preferentially expressed. **E)** Percentage of preferentially expressed genes per sample with predicted plasma membrane or extracellular (secreted) localization.

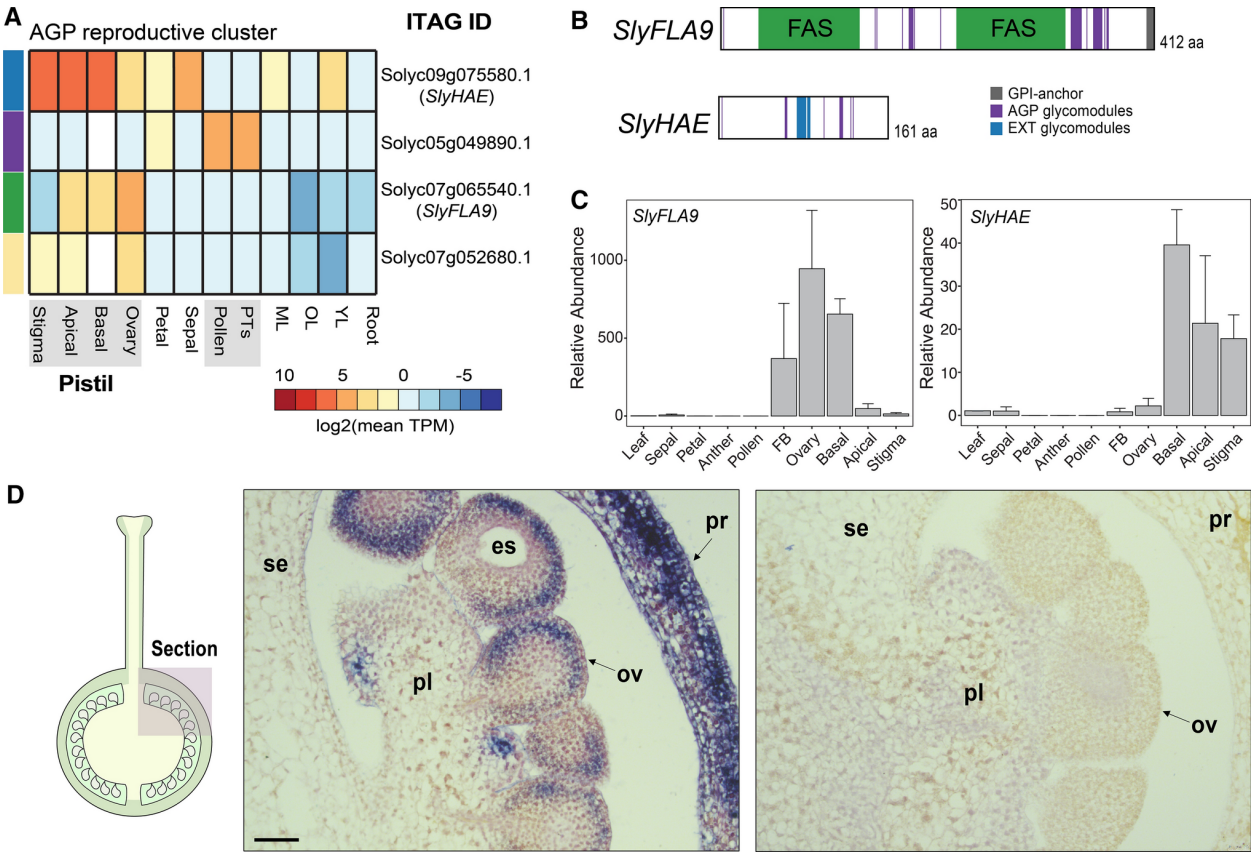

Figure 4-5 Expression profiles of pistil AGPs in tomato.

A) Expression profiles of pistil AGPs represented in our datasets. The heatmap corresponds to a subcluster taken from Supplementary material Fig. 4, where AGP genes had higher expression in reproductive tissues compared to the rest of the tissues. Color code on the left represents distinct classes of AGPs. Blue: AGP-Extensin hybrid; purple: classical AGP; green: Fasciclin-like AGP; yellow: Lysine-rich AGP. **B)** Protein architecture of Fasciclin-like AGP (*SlyFLA9, Solyc07g065540.1*) and hybrid AGP-Extensin (*SlyHAE, Solyc09g075580.1*). **C)** Quantitative RT-PCR of *SlyFLA9* and *SlyHAE* across tomato tissues. Expression values were normalized using SlyACT (Solyc00g017210.1) and SlyUBI (*Solyc01g056940.2*) as references. FB: 2 mm flower buds. **D)** *In situ* detection of the **SlyFLA9** transcript in a sagittal section of the ovary, dissected from an unpollinated pistil. Left: schematic of the pistil sections shown for reference, middle: antisense probe, right: sense probe; es: embryo sac, se: septum, pl: placenta, ov: ovule, pr: pericarp. Scale bar 50 µm.

4.8. Supplemental material

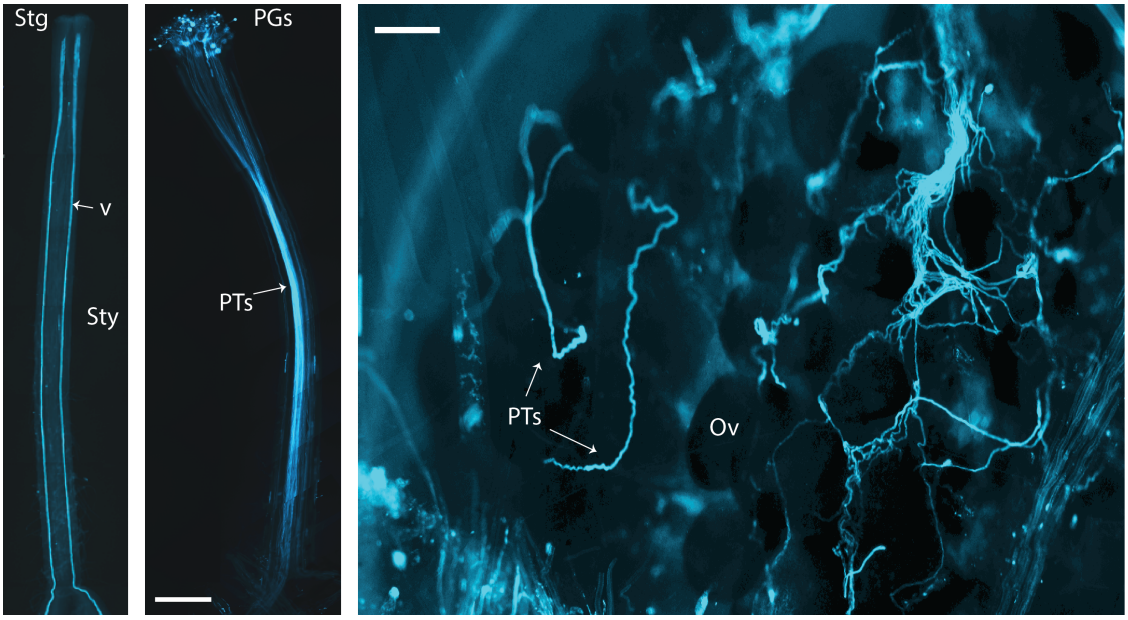

Figure 4-6 Visualization of pollen-pistil interaction in vivo.

Pollen tubes reach ovules and fertilize them after 24 hours post manual pollination. Unpollinated pistils (left) or 24 hours after pollination (middle) were harvested, fixed and stained with aniline blue fluorochrome to visualize pollen tubes growing through pistil tissues. In unpollinated pistils, vascular bundles were visible post-staining. Intact pollen tubes targeting ovules were visualized by dissecting the pericarp of 24 hap pistils (right). Stg: stigma, Sty: style, v: vasculature, PGs: pollen grains, PTs: pollen tubes, Ov: ovule. Scale bar in middle and right panel corresponds to 500 µm.

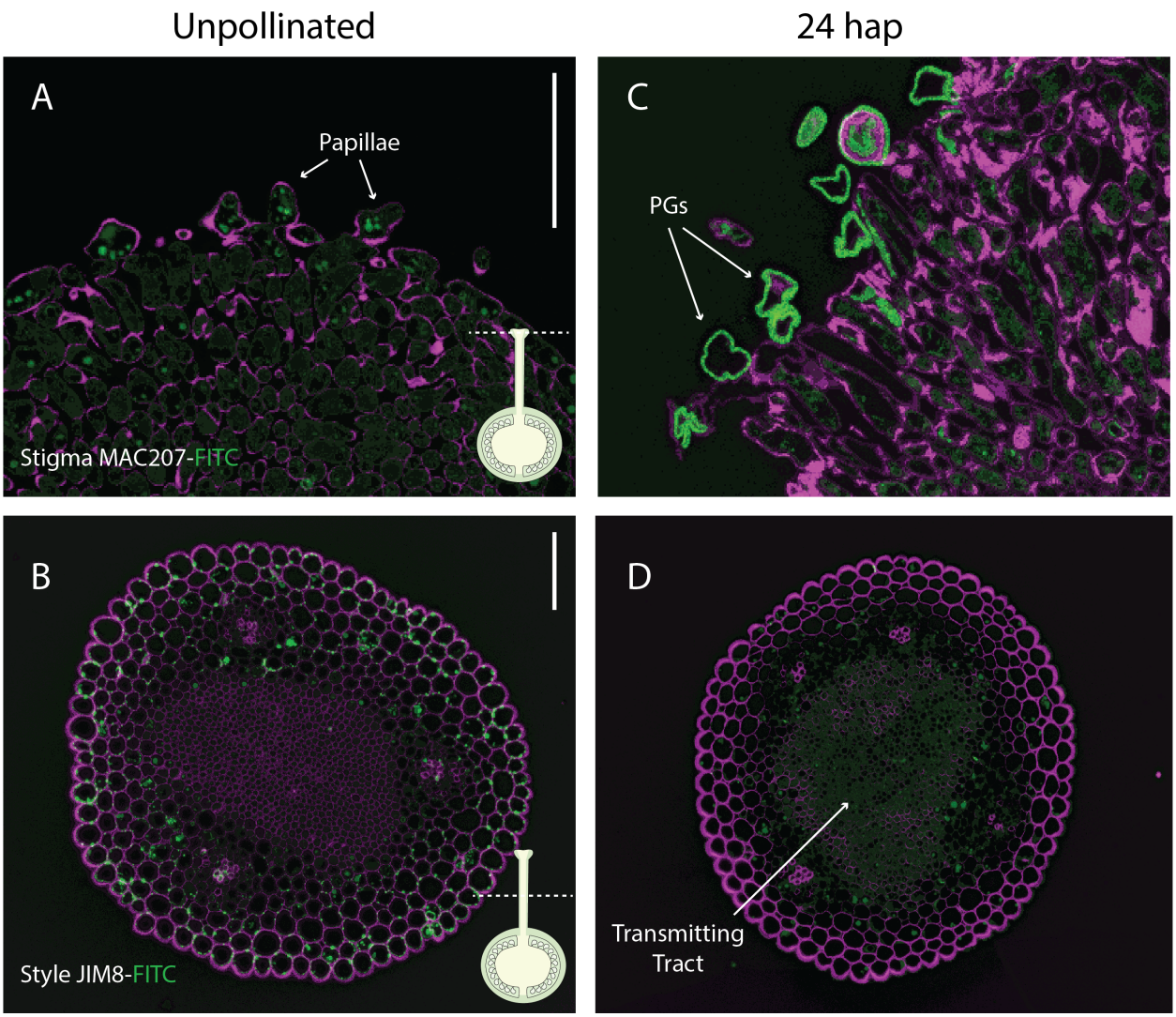

Figure 4-7 AGP immunostaining in the stigma and style of tomato pistils.

Representative images of immunolocalization of AGPs in the stigma and style. In the style, punctate signal in the papillae was observed in unpollinated pistils when staining with MAC207 (**A**). Punctate signal in the papillae was not observed post pollination, whereas strong signal was detected in pollen grains adhered to them (**C**). In the style, punctate signal in the cells surrounding the secretory cells of the transmitting tract were observed when staining with JIM8 in unpollinated pistils (**B**). After pollination, only weak signal was detected (**D**). Both scale bars correspond to 50 μm.

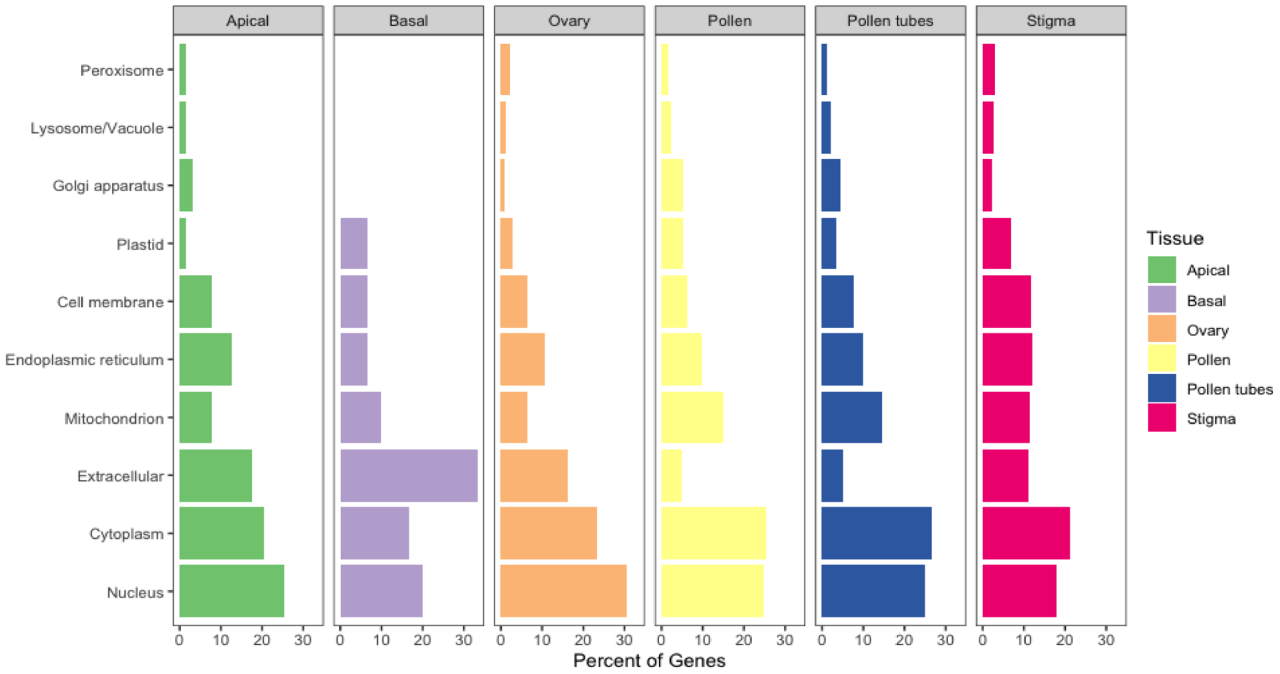

Figure 4-8 Predicted subcellular localization of differentially expressed genes.

Predicted subcellular localization of preferentially expressed genes from pistil subsection and pollen grains/tubes. Subcellular localization was predicted using DeepLoc-01 (Almagro Armenteros et al., 2017).

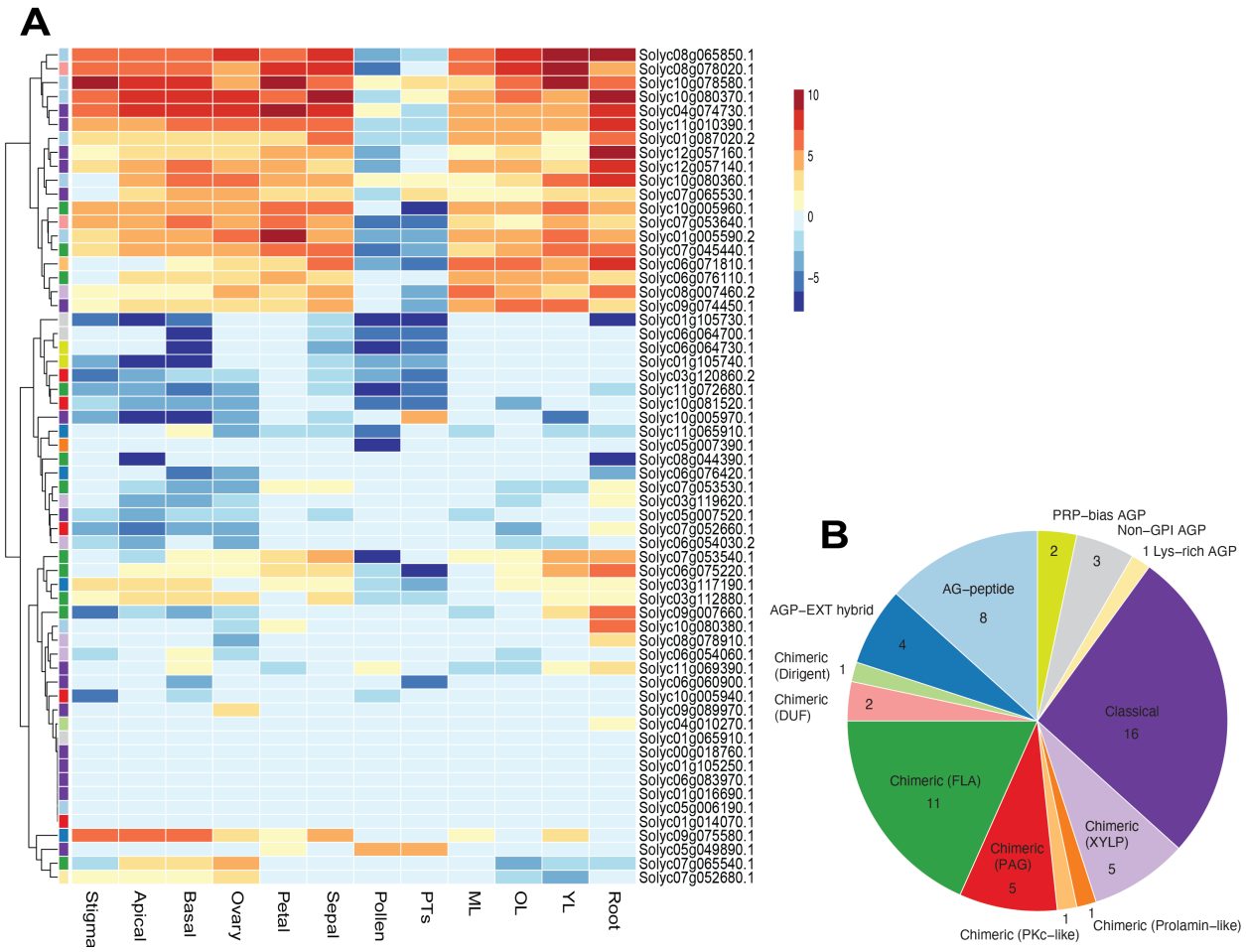

Figure 4-9 Expression patterns for the AGP family in tomato.

A) Hierarchical clustering of AGPs gene expression across tomato tissues. Colors next to the dendrogram, represent the classification color coded as in **B**. The heatmap represents the expression patterns observed for the 60 putative AGP genes across tomato tissues. The color scale in the heatmap represents the log2 mean TPM value per gene. **B)** Classification of the AGP genes in **A**. The majority of genes identified belong to the classical AGP group, followed by Fasciclin-like AGPs (FLA). PAG: phytocyanin-like AGPs; DUF: Domain of Unknown Function AGPs; XYLP: Xylogen-like Protein AGPs; PKc: Protein Kinase-like AGPs; PRP-bias: Proline-rich protein bias AGP; AGP-EXT: AGP Extensin hybrid.

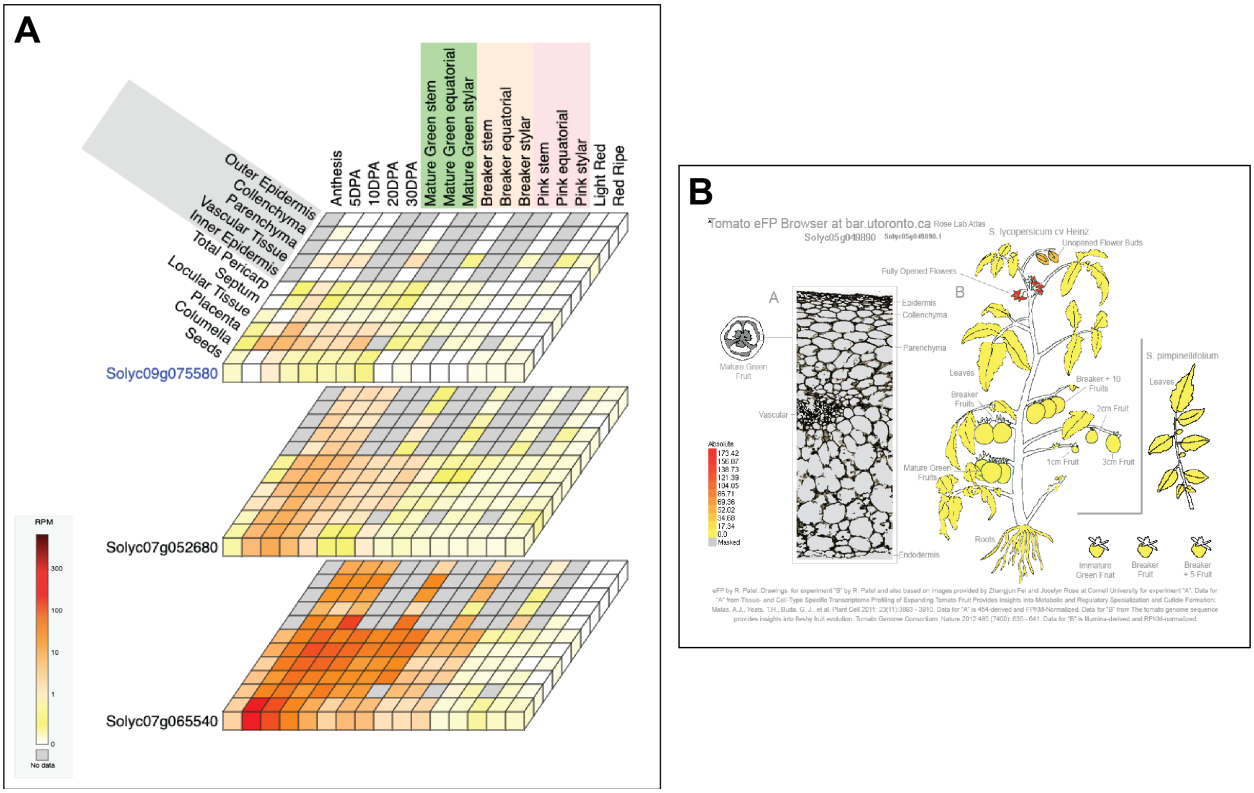

Figure 4-10 Tomato Expression Atlas data for selected pistil AGPs.

A) Expression of pistil AGPs (from Transcriptome Expression Atlas -- TEA from SolGenomics Network) and **B)** Pollen and pollen tube expressed AGP (from Tomato eFP browser).

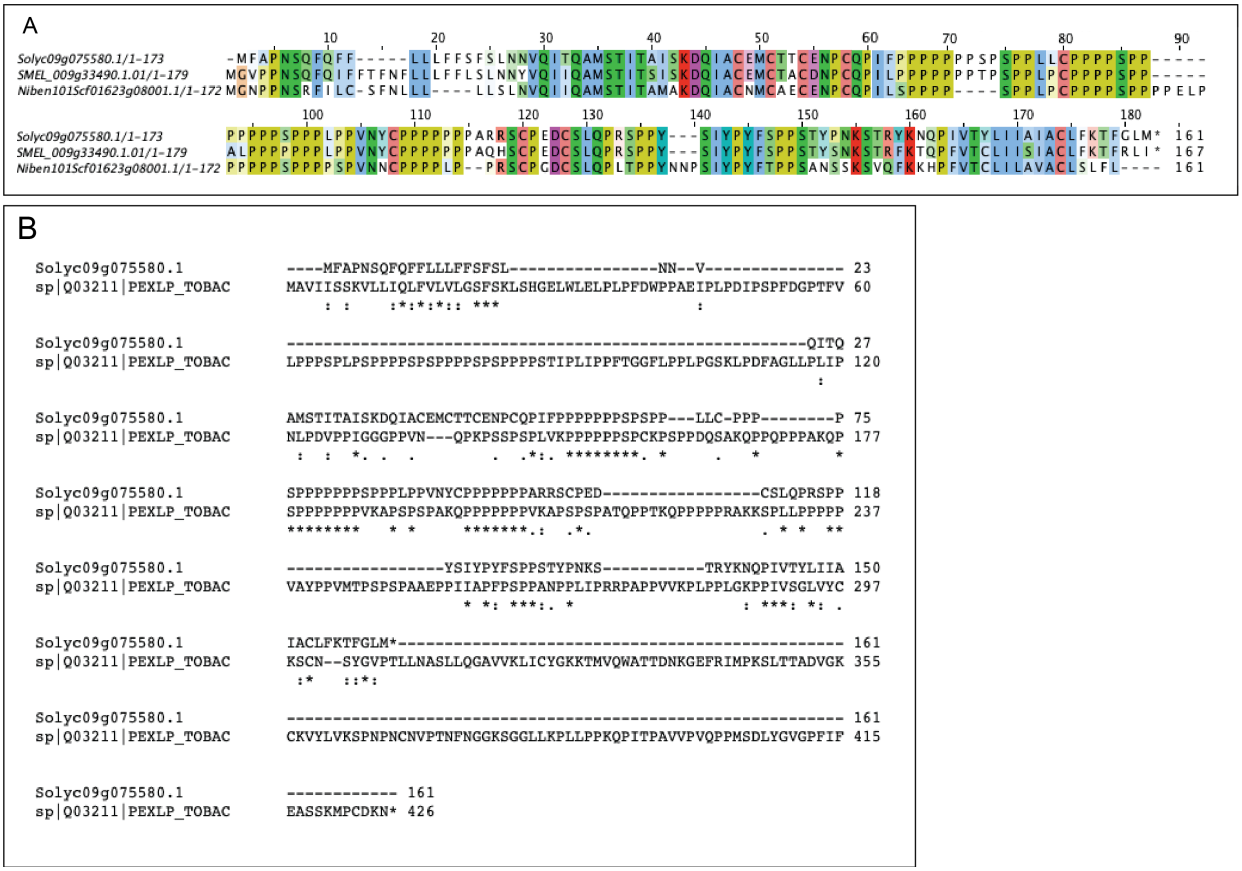

Figure 4-11 Homology search for pistil expressed non-canonical AGPs.

A) Alignment of the *SlyHAE* (*Solyc09g07558.1*) with homologs in eggplant (*SMEL_009g33490.1.01*) and *N. benthamiana* (*Niben101Scf01623g08001.1*). B) Protein sequence alignment between *SlyHAE* and tobacco *PELPIII* (*PEXLP_TOBAC*).

Table 4-1 Pseudo-alignment statistics.

Sample	# reads	# Pseudo-aligned reads	% pseudo-aligned reads
apical_1	32,884,106	22,994,282	69.9
apical_2	29,682,498	22,923,207	77.22
apical_3	22,519,096	17,017,414	75.56
apical_4	25,743,088	19,027,696	73.91
basal_1	27,612,882	21,509,045	77.89
basal_2	27,047,979	20,071,754	74.2
basal_3	24,681,564	12,159,377	49.26
basal_4	24,033,195	17,563,449	71.16
ovary_1	29,110,703	22,325,085	76.69
ovary_2	27,502,126	20,848,950	75.8
ovary_3	25,295,456	19,671,598	73.66
ovary_4	23,737,646	17,968,404	75.69
stigma_1	21,107,590	15,873,222	75.2
stigma_2	26,225,895	17,486,480	66.67
stigma_3	24,965,625	19,835,266	79.45
pg_1	53,936,437	45,867,618	85.04
pg_2	39,755,060	33,803,233	85.02
pg_3	38,385,925	32,187,003	83.85
pg_4	54,654,196	46,298,918	84.71
pt_1	54,846,570	39,905,815	72.75
pt_2	53,976,377	44,089,080	81.68
pt_3	46,542,833	35,269,319	75.77
pt_4	50,916,399	41,888,218	82.26

pg = pollen grains; pt = pollen tubes.

We used kallisto version 0.43.0, index version 10 (Bray et al., 2016). The program was set for single end reads and 100 bootstrap replicates. The transcriptome available from SGN (Sato et al., 2012) version ITAG 3.2 was used to build the index. Read length = 50 bp.

Table 4-2 Primers used in this study.

quantitative RT-PCR primers	
Solyc09g075580.1 (*SlyHAE*)	GCTTGTGAAATGTGCACCAC
	AAGGTGGTGAACGAGGTTGT
Solyc07g065540.1 (SlyFLA9)	GTTTCAAGCTACCGGCTCAG
	ATTCATTTGGCTTGGTCCTG
SlyACT (Solyc00g017210.1)	CTTTAATGAGCTTCGTGTGG
	TCGTTGCCAATTGTGATTGG
SlyUBI (Solyc01g056940.2)	CGTGGTGGTGCTAAGAAGAG
	ACGAAGCCTCTGAACCTTTC
***In situ* probe primers**	
SlyFLA9 cDNA	ATGCAGCTTCCGTCGTC
	TAAACTGAAAACGGCGGCAA
CDs cloning	
SlyHae	ATGTTTGCTCCAAATTCTCAATTCC
	CTACATTAGCCCAAAAGTTTTAAAAAGAC

Table 4-3 Tomato AGP reproductive cluster and GT homologs

Tomato Reproductive AGP cluster					
ITAG ID	**AGP Classification**	**Best hit BLAST (TAIR)**	**% identity**	**Score (bits)**	**E-value**
Solyc09g075580.1	Hybrid AGP-EXT	No hits found	N/A	N/A	N/A
Solyc05g049890.1	Classical AGP	AT4G11050.3	36	34.7	0.007
Solyc07g065540.1	Fasciclin-like AGP	FLA1 (AT5G55730.2, AT5G55730.1)	72.9	375	6.00E-128
Solyc07g052680.1	Lys-rich AGP	AT3G22070.1	63	26.9	7.3
Tomato GALT and HPGT homologs					
ITAG ID	**ITAG 3.2 annotation**	**BLAST query**	**% identity**	**Score (bits)**	**E-value**
Solyc02g070400.3	Hexosyltransferase	GALT2 (AT4G21060.1)	64	901	0
Solyc05g053280.3	Galactosyltransferase family protein	GALT3 (AT3G06440.1)	50	637	0
Solyc05g006680.3	Galactosyltransferase family protein	GALT4 (AT1G27120.1)	64	880	0
Solyc06g071160.3	Galactosyltransferase family protein	GALT5 (AT1G74800.1)	63	890	0
Solyc03g113520.3	Galactosyltransferase family protein	GALT5 (AT1G74800.1)	63	871	0
Solyc08g029170.3	Hexosyltransferase	HPGT2 (AT4G32120.1)	72	492	5.00E-176

Table 4-4 Pollen Grain Top 10 Expressed Genes

ITAG ID	mean TPM	SD	Fraction of TTO	Description
Solyc12g062920.2	46780.27521	0.001996165	0.046793473	LOW QUALITY:Lipid binding protein (AHRD V3.3 --* B6UEB0_MAIZE)
Solyc10g007270.3	17040.01393	0.000887017	0.017044821	Pollen Ole e 1 allergen/extensin (AHRD V3.3 *** A0A103XBC9_CYNCS)
Solyc12g014240.2	16449.2385	0.00106729	0.016453879	Pollen Ole e 1 allergen/extensin (AHRD V3.3 *** A0A103XBC9_CYNCS)
Solyc00g030510.3	15547.21169	0.00059679	0.015551598	Pectin lyase-like superfamily protein (AHRD V3.3 *** AT3G07820.1)
Solyc01g056310.3	15206.79556	0.000747696	0.015211086	anther-specific LAT51
Solyc09g007780.1	14428.22976	0.003134844	0.0144323	LOW QUALITY:alpha/beta-Hydrolases superfamily protein (AHRD V3.3 --* AT5G22460.3)
Solyc12g005320.2	13714.63254	0.000449442	0.013718502	Pectinacetylesterase family protein (AHRD V3.3 *** AT4G19410.1)
Solyc01g005510.3	13204.29013	0.000861066	0.013208015	L-ascorbate oxidase homolog (AHRD V3.3 *** ASOL_TOBAC)
Solyc01g011050.3	12439.90308	0.001076713	0.012443413	leucine rich repeat protein

Full list of genes is available as supplemental material in Lara-Mondragón & MacAlister (2021) *Plant Reproduction*, DOI: https://doi.org/10.1007/s00497-021-00408-1

Table 4-5 Pollen Tube Top 10 Expressed Genes

ITAG ID	mean TPM	SD	Fraction of TTO	Description
Solyc12g062920.2	40519.85104	0.007667801	0.040530649	LOW QUALITY:Lipid binding protein (AHRD V3.3 --* B6UEB0_MAIZE)
Solyc07g039290.1	22698.05195	0.013108283	0.022704101	LOW QUALITY:Senescence-associated protein (AHRD V3.3 *-* A0A072TTZ6_MEDTR)
Solyc06g024370.1	19035.53855	0.013573978	0.019040611	LOW QUALITY:calcium-dependent protein kinase 30 (AHRD V3.3 --* AT1G74740.1)
Solyc10g007270.3	18156.92186	0.00603027	0.01816176	Pollen Ole e 1 allergen/extensin (AHRD V3.3 *** A0A103XBC9_CYNCS)
Solyc12g005320.2	16342.14895	0.002375595	0.016346504	Pectinacetylesterase family protein (AHRD V3.3 *** AT4G19410.1)
Solyc12g014240.2	16293.49158	0.004997505	0.016297834	Pollen Ole e 1 allergen/extensin (AHRD V3.3 *** A0A103XBC9_CYNCS)
Solyc01g056310.3	14706.22003	0.003308213	0.014710139	anther-specific LAT51
Solyc01g011050.3	14539.92159	0.001273093	0.014543796	leucine rich repeat protein
Solyc00g030510.3	14239.62509	0.001266723	0.01424342	Pectin lyase-like superfamily protein (AHRD V3.3 *** AT3G07820.1)

Full list of genes is available as supplemental material in Lara-Mondragón & MacAlister (2021) *Plant Reproduction*, DOI: https://doi.org/10.1007/s00497-021-00408-1

Table 4-6 Stigma Top 10 Expressed Genes

ITAG ID	mean TPM	SD	Fraction of TTO	Description
Solyc10g075110.	37520.35457	0.005195952	0.037524348	Non-specific lipid-transfer protein (AHRD V3.3 *** M1AVB9_SOLTU)
Solyc10g075130.	33599.37329	0.006148249	0.033602949	Non-specific lipid-transfer protein (AHRD V3.3 *** K4D1W2_SOLLC)
Solyc07g039290.	28549.34211	0.019815751	0.02855238	LOW QUALITY:Senescence-associated protein (AHRD V3.3 *-* A0A072TTZ6_MEDTR)
Solyc03g120960.	22116.5258	0.004943091	0.02211888	Protein STIG1 (AHRD V3.3 *** STIG1_SOLLC)
Solyc07g006380.	17448.96336	0.003690135	0.01745082	Defensin-like protein (AHRD V3.3 *** DEF_TOBAC)
Solyc04g071610.	8906.54154	0.00247246	0.008907489	Abscicic acid stress ripening 1
Solyc06g024370.	8717.219888	0.006726481	0.008718148	LOW QUALITY:calcium-dependent protein kinase 30 (AHRD V3.3 --* AT1G74740.1)
Solyc09g010800.	8131.859228	0.000237052	0.008132725	metallothionein II-like protein
Solyc01g058500.	6623.378814	0.00455545	0.006624084	LOW QUALITY:TBP-associated factor 2 (AHRD V3.3 --* AT1G73960.2)

Full list of genes is available as supplemental material in Lara-Mondragón & MacAlister (2021) *Plant Reproduction*, DOI: https://doi.org/10.1007/s00497-021-00408-1

Table 4-Apical style Top 10 Expressed Genes

ITAG ID	mean TPM	SD	Fraction of TTO	Description
Solyc07g006380.3	56414.10206	0.012202328	0.056420415	Defensin-like protein (AHRD V3.3 *** DEF_TOBAC)
Solyc07g039290.1	26121.3748	0.015247336	0.026124298	LOW QUALITY:Senescence-associated protein (AHRD V3.3 *-* A0A072TTZ6_MEDTR)
Solyc10g075130.2	19039.7054	0.002896086	0.019041836	Non-specific lipid-transfer protein (AHRD V3.3 *** K4D1W2_SOLLC)
Solyc02g078100.3	19006.65299	0.001393283	0.01900878	Pollen Ole e 1 allergen/extensin (AHRD V3.3 *-* A0A124SHL8_CYNCS)
Solyc02g061770.3	12906.29503	0.002953166	0.012907739	chitinase 2
Solyc09g010800.4	11477.17928	0.001847312	0.011478464	metallothionein II-like protein
Solyc11g022590.1	10604.59471	0.001957518	0.010605781	trypsin inhibitor-like protein precursor
Solyc02g078050.3	10287.02341	0.002713728	0.010288174	120 kDa pistil extensin-like protein (AHRD V3.3 *-* Q49I27_9SOLA)
Solyc04g071610.3	9788.285843	0.002884938	0.009789381	Abscicic acid stress ripening 1

Full list of genes is available as supplemental material in Lara-Mondragón & MacAlister (2021) *Plant Reproduction*, DOI: https://doi.org/10.1007/s00497-021-00408-1

Table 4-7 Basal style Top 10 Expressed Genes

ITAG ID	mean TPM	SD	Fraction of TTO	Description
Solyc07g006380.3	53771.815	0.018202081	0.053777583	Defensin-like protein (AHRD V3.3 *** DEF_TOBAC)
Solyc07g039290.1	43558.36233	0.040997986	0.043563035	LOW QUALITY:Senescence-associated protein (AHRD V3.3 *-* A0A072TTZ6_MEDTR)
Solyc02g078100.3	15408.53362	0.005644796	0.015410186	Pollen Ole e 1 allergen/extensin (AHRD V3.3 *-* A0A124SHL8_CYNCS)
Solyc06g024370.1	14952.64181	0.016045824	0.014954246	LOW QUALITY:calcium-dependent protein kinase 30 (AHRD V3.3 --* AT1G74740.1)
Solyc01g058500.3	11083.27538	0.01105464	0.011084464	LOW QUALITY:TBP-associated factor 2 (AHRD V3.3 --* AT1G73960.2)
Solyc06g024210.2	9837.573899	0.009559759	0.009838629	LOW QUALITY:Senescence-associated protein (AHRD V3.3 *-* A0A072THV8_MEDTR)
Solyc09g010800.4	9080.694121	0.001326466	0.009081668	metallothionein II-like protein
Solyc00g068970.2	8514.171989	0.008644354	0.008515085	Senescence-associated protein (AHRD V3.3 *-* A0A072THH1_MEDTR)
Solyc02g061770.3	8437.984699	0.00398533	0.00843889	chitinase 2

Full list of genes is available as supplemental material in Lara-Mondragón & MacAlister (2021) *Plant Reproduction*, DOI: https://doi.org/10.1007/s00497-021-00408-1

Table 4-8 Ovary Top 10 Expressed Genes

ITAG ID	mean TPM	SD	Fraction of TTO	Description
Solyc07g006380	105345.3191	0.016213278	0.105357267	Defensin-like protein (AHRD V3.3 *** DEF_TOBAC)
Solyc07g039290	23390.20901	0.0046239	0.023392862	LOW QUALITY:Senescence-associated protein (AHRD V3.3 *-* A0A072TTZ6_MEDTR)
Solyc03g098790	9089.547864	0.003458409	0.009090579	Cathepsin D Inhibitor
Solyc06g024370	7754.475094	0.001290117	0.007755355	LOW QUALITY:calcium-dependent protein kinase 30 (AHRD V3.3 --* AT1G74740.1)
Solyc09g089505	7274.546011	0.002593083	0.007275371	Proteinase inhibitor I (AHRD V3.3 *** K7WNW8_SOLTU)
Solyc03g007780	6643.80136	0.001212095	0.006644555	LOW QUALITY:Ovule Secreted Protein
Solyc09g084480	6255.160605	0.00173237	0.00625587	Type I serine protease inhibitor (AHRD V3.3 *** E0WCF2_SOLTU)
Solyc01g058500	5917.694918	0.000853155	0.005918366	LOW QUALITY:TBP-associated factor 2 (AHRD V3.3 --* AT1G73960.2)
Solyc06g024210	5427.626301	0.000923255	0.005428242	LOW QUALITY:Senescence-associated protein (AHRD V3.3 *-* A0A072THV8_MEDTR)

Full list of genes is available as supplemental material in Lara-Mondragón & MacAlister (2021) *Plant Reproduction*, DOI: https://doi.org/10.1007/s00497-021-00408-1

Table 4-9 Pollen Grain Top 10 Upregulated Genes

ITAG ID	LFC	Q-value	Description
Solyc04g057895.1	9.0446418	0.0001127	phytochrome A (AHRD V3.3 --* AT1G09570.3)
Solyc05g016037.1	8.5153537	9.66E-07	AT hook motif-containing protein, putative (AHRD V3.3 *-* Q2R0W4_ORYSJ)
Solyc07g008500.1	7.5113209	0.0003094	Histone-lysine N-methyltransferase (AHRD V3.3 *-* A0A0K9P7Y1_ZOSMR)
Solyc04g077410.3	7.0844946	6.37E-07	1-aminocyclopropane-1-carboxylate synthase 5
Solyc04g050400.1	6.9730918	0.0228577	60S ribosomal protein L12 (AHRD V3.3 *** Q6RJY1_CAPAN)
Solyc01g060340.1	6.8940245	0.0134546	LOW QUALITY:Endoglucanase (AHRD V3.3 *-* A0A061GAK3_THECC)
Solyc04g040050.1	6.8187085	0.0053778	UDP-3-O-acyl N-acetylglycosamine deacetylase family protein (AHRD V3.3 --* AT1G25210.2)
Solyc06g063060.3	6.6900323	2.80E-05	Auxin-repressed protein-like protein (AHRD V3.3 *** Q84KS0_TOBAC)
Solyc12g006580.2	6.6100719	0.0282972	cytochrome P450, family 705, subfamily A, polypeptide 30 (AHRD

Full list of genes is available as supplemental material in Lara-Mondragón & MacAlister (2021) *Plant Reproduction*, DOI: https://doi.org/10.1007/s00497-021-00408-1

Table 4-10 Pollen Tube Top 10 Upregulated Genes

ITAG ID	LFC	Q-value	Description
Solyc06g062560.2	12.66064	3.31E-16	phosphatase 14B
Solyc08g078200.2	11.971691	2.18E-11	Plasma membrane ATPase (AHRD V3.3 *** M1DGA0_SOLTU)
Solyc12g011210.1	11.908809	6.09E-12	LOW QUALITY:partner of SLD five 1 (AHRD V3.3 --*
Solyc05g013430.1	11.836995	3.55E-08	LOW QUALITY:myb-like transcription factor family protein (AHRD V3.3 *-*
Solyc06g075860.2	11.586342	7.33E-08	LOW QUALITY:Protein yippee-like (AHRD V3.3 *-* M1DX18_SOLTU)
Solyc07g041650.2	11.363845	1.08E-11	Pectin lyase-like superfamily protein (AHRD V3.3 *** AT1G17150.1)
Solyc05g024210.1	11.233753	1.82E-07	LOW QUALITY:Ribonuclease 3 family protein (AHRD V3.3 *** B9GTV4_POPTR)
Solyc04g049860.1	11.115272	7.37E-07	LOW QUALITY:Rho guanine nucleotide exchange factor (AHRD V3.3 *-*
Solyc03g117630.1	10.655692	4.44E-10	heat shock protein 70 (AHRD V3.3 *** AT3G12580.1)

Full list of genes is available as supplemental material in Lara-Mondragón & MacAlister (2021) *Plant Reproduction*, DOI: https://doi.org/10.1007/s00497-021-00408-1

Table 4-11 Stigma Top 10 Upregulated Genes

ITAG ID	LFC	Q-value	Description
Solyc04g015630.2	8.9114419	1.91E-05	NBS-LRR disease resistance protein (AHRD V3.3 *** C6FF78_SOYBN)
Solyc03g083385.1	6.6210315	0.0005788	O-acyltransferase (WSD1-like) family protein (AHRD V3.3 *-* AT5G53390.1)
Solyc03g083380.3	6.4522621	0.0017841	O-acyltransferase (WSD1-like) family protein (AHRD V3.3 *-* AT5G53390.1)
Solyc10g079320.2	6.0184547	6.35E-09	Glycosyltransferase (AHRD V3.3 *** K4D2H3_SOLLC)
Solyc06g048670.3	5.9458292	0.0023924	GDSL esterase/lipase (AHRD V3.3 *** A0A0B2SN40_GLYSO)
Solyc07g053070.2	5.9020096	0.0022714	Purple acid phosphatase (AHRD V3.3 *** K4CFK5_SOLLC)
Solyc02g072280.1	5.8135747	2.45E-05	Subtilisin-like protease (AHRD V3.3 *** A0A151SNY0_CAJCA)
Solyc04g005360.1	5.7200757	0.0019876	Cytochrome P450 family protein (AHRD V3.3 *** A0A072UZE3_MEDTR)
Solyc01g008650.3	5.6708747	0.0015408	Cytochrome P450 (AHRD V3.3 *** Q9AVQ2_SOLTU)

Full list of genes is available as supplemental material in Lara-Mondragón & MacAlister (2021) *Plant Reproduction*, DOI: https://doi.org/10.1007/s00497-021-00408-1

Table 4-12 Apical style Top 10 Upregulated Genes

ITAG ID	LFC	Q-value	Description
Solyc01g009270.1	5.2927315	0.0003698	FAF-like protein (DUF3049) (AHRD V3.3 *-* AT5G22090.2)
Solyc09g090490.2	5.1832015	0.0013816	Amine oxidase (AHRD V3.3 *** K4CW75_SOLLC)
Solyc06g054280.1	4.8904062	2.06E-09	LOW QUALITY:E3 UFM1-protein ligase 1 homolog (AHRD V3.3 --*
Solyc02g093580.3	4.302349	0.0014339	Tomato 9612 mRNA
Solyc08g077080.1	4.2695407	1.92E-05	Glycosyltransferase (AHRD V3.3 *** E5L3R9_SOLLC)
Solyc08g083190.3	4.0653892	0.0004523	Alpha/beta-Hydrolases superfamily protein (AHRD V3.3 *** A0A061G3V4_THECC)
Solyc07g008107.1	3.5817966	0.0102235	Blue copper protein (AHRD V3.3 *-* A0A151SLU0_CAJCA)
Solyc03g121680.2	3.423801	0.0397659	Cell wall invertase (AHRD V3.3 *** K4HUT0_MALDO)
Solyc10g055560.2	3.3154545	0.0030693	SBP (S-ribonuclease binding protein) family protein (AHRD V3.3 ***

Full list of genes is available as supplemental material in Lara-Mondragón & MacAlister (2021) *Plant Reproduction*, DOI: https://doi.org/10.1007/s00497-021-00408-1

Table 4-13 Basal style Top 10 Upregulated Genes

ITAG ID	LFC	Q-value	Description
Solyc06g054670.2	4.7936722	4.54E-05	Acyl-[acyl-carrier-protein] desaturase (AHRD V3.3 *** A0A118HPD5_CYNCS)
Solyc06g065550.2	4.1966411	0.000444	Cysteine/Histidine-rich C1 domain family protein (AHRD V3.3 --* AT5G40590.1)
Solyc11g072790.2	4.1952324	0.0002422	WUSCHEL-like homeobox protein (AHRD V3.3 *-* F6MIV6_ORYSJ)
Solyc07g018250.1	3.6969172	0.0101866	LOW QUALITY:GNS1/SUR4 membrane protein family (AHRD V3.3 *** AT3G06470.1)
Solyc01g010910.2	3.6142717	0.0001717	MYB-related transcription factor (AHRD V3.3 *** A0A059PRK4_SALMI)
Solyc10g047110.2	3.6021143	0.0153399	Peroxidase (AHRD V3.3 *** K4CZX5_SOLLC)
Solyc05g052280.3	3.4888655	0.0149575	Peroxidase (AHRD V3.3 *** K4C1Q9_SOLLC)
Solyc08g007930.2	3.326999	0.0292339	SUN-like protein 20
Solyc03g025380.3	3.2636608	0.0252513	Peroxidase (AHRD V3.3 *** K4BF11_SOLLC)

Full list of genes is available as supplemental material in Lara-Mondragón & MacAlister (2021) *Plant Reproduction*, DOI: https://doi.org/10.1007/s00497-021-00408-1

Table 4-14 Ovary Top 10 Upregulated Genes

ITAG ID	LFC	Q-value	Description
Solyc05g010190.1	8.294319	3.78E-24	LOW QUALITY:ECA1 gametogenesis related family protein (AHRD V3.3 ***
Solyc02g069330.1	8.1089871	8.12E-47	LOW QUALITY:Invertase inhibitor (AHRD V3.3 *** A0A0B5KSF6_MANES)
Solyc08g067640.1	7.2425989	1.03E-09	LOW QUALITY:Zinc finger C-x8-C-x5-C-x3-H type family protein (AHRD V3
Solyc08g074920.1	7.154664	2.32E-23	Eukaryotic aspartyl protease family protein (AHRD V3.3 *** AT5G33340.1)
Solyc04g074320.2	7.0350495	1.17E-15	Protein TRANSPARENT TESTA 1-like protein (AHRD V3.3 *** A0A0B0MYQ3_GOSAR)
Solyc09g011290.1	6.9154996	1.92E-08	LOW QUALITY:cell wall / vacuolar inhibitor of fructosidase 2
Solyc01g067420.3	6.9052731	3.78E-08	Pectinesterase (AHRD V3.3 *** K4AWZ1_SOLLC)
Solyc03g034330.1	6.3704204	1.01E-35	Lipid transfer protein (AHRD V3.3 *** S4TID2_GOSHI)
Solyc06g048400.1	6.3391667	1.97E-06	ECA1 gametogenesis family protein (DUF784) (AHRD V3.3 -** AT5G34905.1)

Full list of genes is available as supplemental material in Lara-Mondragón & MacAlister (2021) *Plant Reproduction*, DOI: https://doi.org/10.1007/s00497-021-00408-1

Table 4-15 Tomato Reproductive AGP cluster (Alignment with known reproductive AGPs)

ITAG ID	AGP Classification	Query sequence	% identity	% similarity	% Gaps	Score
Solyc09g075580.1	Hybrid AGP-EXT	Tobacco TTS (AST51876.1)	15	19.5	58	105
		Tobacco PELPIII (PEXLP_TOBAC)	12.5	15.3	71.3	159
		Tobacco 120 KDa protein (O49986_NICAL)	10.6	13	75.2	145.5
Solyc05g049890.1	Classical AGP	Tobacco TTS (AST51876.1)	12.1	14.8	64.8	64
		Tobacco PELPIII (PEXLP_TOBAC)	6.5	9	83.3	64
		Tobacco 120 KDa protein (O49986_NICAL)	7.3	9.7	80.6	68
Solyc07g065540.1	Fasciclin-like AGP	Tobacco TTS (AST51876.1)	6.6	8.8	80.6	47
		Tobacco PELPIII (PEXLP_TOBAC)	9.7	14	69.5	56
		Tobacco 120 KDa protein (O49986_NICAL)	3.4	5.3	9.1	50
Solyc07g052680.1	Lys-rich AGP	Tobacco TTS (AST51876.1)	13.4	20.5	63.8	120
		Tobacco PELPIII (PEXLP_TOBAC)	11.7	16.6	70.1	149
		Tobacco 120 KDa protein (O49986_NICAL)	11.5	16.2	69	158

4.9. References

Acosta-García, G., & Vielle-Calzada, J.-P. (2004). A classical arabinogalactan protein is essential for the initiation of female gametogenesis in Arabidopsis. *The Plant Cell*, *16*(10), 2614–2628. https://doi.org/10.1105/tpc.104.024588

Almagro Armenteros, J. J., Sønderby, C. K., Sønderby, S. K., Nielsen, H., & Winther, O. (2017). DeepLoc: Prediction of protein subcellular localization using deep learning. *Bioinformatics*, *33*(21), 3387–3395. https://doi.org/10.1093/bioinformatics/btx431

Alves, C. M. L., Noyszewski, A. K., & Smith, A. G. (2019). Structure and function of class III pistil-specific extensin-like protein in interspecific reproductive barriers. *BMC Plant Biology*, *19*(1), 118. https://doi.org/10.1186/s12870-019-1728-8

Bolger, A. M., Lohse, M., & Usadel, B. (2014). Trimmomatic: A flexible trimmer for Illumina sequence data. *Bioinformatics*, *30*(15), 2114–2120. https://doi.org/10.1093/bioinformatics/btu170

Bray, N. L., Pimentel, H., Melsted, P., & Pachter, L. (2016). Near-optimal probabilistic RNA-seq quantification. *Nature Biotechnology*, *34*(5), 525–527. https://doi.org/10.1038/nbt.3519

Bredemeijer, G. M. M. (1984). The role of peroxidases in pistil-pollen interactions. *Theoretical and Applied Genetics*, *68*(3), 193–206. https://doi.org/10.1007/BF00266889

Busby, M. A., Stewart, C., Miller, C. A., Grzeda, K. R., & Marth, G. T. (2013). Scotty: A web tool for designing RNA-Seq experiments to measure differential gene expression. *Bioinformatics*, *29*(5), 656–657. https://doi.org/10.1093/bioinformatics/btt015

Carninci, P., Shibata, Y., Hayatsu, N., Sugahara, Y., Shibata, K., Itoh, M., Konno, H., Okazaki, Y., Muramatsu, M., & Hayashizaki, Y. (2000). Normalization and Subtraction of Cap-Trapper-Selected cDNAs to Prepare Full-Length cDNA Libraries for Rapid Discovery of New Genes. *Genome Research*, *10*(10), 1617–1630. https://doi.org/10.1101/gr.145100

Challinor, A. J., Watson, J., Lobell, D. B., Howden, S. M., Smith, D. R., & Chhetri, N. (2014). A meta-analysis of crop yield under climate change and adaptation. *Nature Climate Change*, *4*(4), 287–291. https://doi.org/10.1038/nclimate2153

Cheung, A. Y., Boavida, L. C., Aggarwal, M., Wu, H.-M., & Feijó, J. A. (2010). The pollen tube journey in the pistil and imaging the in vivo process by two-photon microscopy. *Journal of Experimental Botany*, *61*(7), 1907–1915. https://doi.org/10.1093/jxb/erq062

Cheung, A. Y., Wang, H., & Wu, H. (1995). A floral transmitting tissue-specific glycoprotein attracts pollen tubes and stimulates their growth. *Cell*, *82*(3), 383–393. https://doi.org/10.1016/0092-8674(95)90427-1

CIAMPOLINI, F., FALERI, C., DI PIETRO, D., & CRESTI, M. (1996). Structural and Cytochemical Characteristics of the Stigma and Style in Vitis vinifera L. var. Sangiovese (Vitaceae). *Annals of Botany*, *78*(6), 759–764.

Coimbra, S., Almeida, J., Junqueira, V., Costa, M. L., & Pereira, L. G. (2007). Arabinogalactan proteins as molecular markers in Arabidopsis thaliana sexual reproduction. *Journal of Experimental Botany*, *58*(15–16), 4027–4035. https://doi.org/10.1093/jxb/erm259

Costa, M., Pereira, A. M., Rudall, P. J., & Coimbra, S. (2013). Immunolocalization of arabinogalactan proteins (AGPs) in reproductive structures of an early-divergent angiosperm, Trithuria (Hydatellaceae). *Annals of Botany*, *111*(2), 183–190. https://doi.org/10.1093/aob/mcs256

Covey, P. A., Subbaiah, C. C., Parsons, R. L., Pearce, G., Lay, F. T., Anderson, M. A., Ryan, C. A., & Bedinger, P. A. (2010). A Pollen-Specific RALF from Tomato That Regulates Pollen Tube Elongation. *Plant Physiology*, *153*(2), 703–715. https://doi.org/10.1104/pp.110.155457
da Costa, M. L., Lopes, A. L., Amorim, M. I., & Coimbra, S. (2017). Immunolocalization of AGPs and Pectins in Quercus suber Gametophytic Structures. In A. Schmidt (Ed.), *Plant Germline Development: Methods and Protocols* (pp. 117–137). Springer. https://doi.org/10.1007/978-1-4939-7286-9_11
Dafni, A., & Maués, M. M. (1998). A rapid and simple procedure to determine stigma receptivity. *Sexual Plant Reproduction*, *11*(3), 177–180. https://doi.org/10.1007/s004970050138
de Graaf, B. H. J., Knuiman, B. A., Derksen, J., & Mariani, C. (2003). Characterization and localization of the transmitting tissue-specific PELPIII proteins of Nicotiana tabacum. *Journal of Experimental Botany*, *54*(380), 55–63. https://doi.org/10.1093/jxb/erg002
Ding, Q., Yang, X., Pi, Y., Li, Z., Xue, J., Chen, H., Li, Y., & Wu, H. (2020). Genome-wide identification and expression analysis of extensin genes in tomato. *Genomics*, *112*(6), 4348–4360. https://doi.org/10.1016/j.ygeno.2020.07.029
Dresselhaus, T., & Franklin-Tong, N. (2013). Male–Female Crosstalk during Pollen Germination, Tube Growth and Guidance, and Double Fertilization. *Molecular Plant*, *6*(4), 1018–1036. https://doi.org/10.1093/mp/sst061
Eberle, C. A., Anderson, N. O., Clasen, B. M., Hegeman, A. D., & Smith, A. G. (2013). PELPIII: The class III pistil-specific extensin-like Nicotiana tabacum proteins are essential for interspecific incompatibility. *The Plant Journal*, *74*(5), 805–814. https://doi.org/10.1111/tpj.12163
Edlund, A. F., Swanson, R., & Preuss, D. (2004). Pollen and Stigma Structure and Function: The Role of Diversity in Pollination. *The Plant Cell*, *16*(suppl 1), S84–S97. https://doi.org/10.1105/tpc.015800
Ellis, M., Egelund, J., Schultz, C. J., & Bacic, A. (2010). Arabinogalactan-Proteins: Key Regulators at the Cell Surface? *Plant Physiology*, *153*(2), 403–419. https://doi.org/10.1104/pp.110.156000
Ezura, K., Ji-Seong, K., Mori, K., Suzuki, Y., Kuhara, S., Ariizumi, T., & Ezura, H. (2017). Genome-wide identification of pistil-specific genes expressed during fruit set initiation in tomato (Solanum lycopersicum). *PLOS ONE*, *12*(7), e0180003. https://doi.org/10.1371/journal.pone.0180003
Fragkostefanakis, S., Dandachi, F., & Kalaitzis, P. (2012). Expression of arabinogalactan proteins during tomato fruit ripening and in response to mechanical wounding, hypoxia and anoxia. *Plant Physiology and Biochemistry: PPB*, *52*, 112–118. https://doi.org/10.1016/j.plaphy.2011.12.001
Fujii, S., Tsuchimatsu, T., Kimura, Y., Ishida, S., Tangpranomkorn, S., Shimosato-Asano, H., Iwano, M., Furukawa, S., Itoyama, W., Wada, Y., Shimizu, K. K., & Takayama, S. (2019). A stigmatic gene confers interspecies incompatibility in the Brassicaceae. *Nature Plants*, *5*(7), 731–741. https://doi.org/10.1038/s41477-019-0444-6
Gao, M., & Showalter, A. M. (2000). Immunolocalization of LeAGP-1, a modular arabinogalactan-protein, reveals its developmentally regulated expression in tomato. *Planta*, *210*(6), 865–874. https://doi.org/10.1007/s004250050691
Gell, A. C., Bacic, A., & Clarke, A. E. (1986). Arabinogalactan-Proteins of the Female Sexual Tissue of Nicotiana alata: I. Changes during Flower Development and Pollination. *Plant Physiology*, *82*(4), 885–889. https://doi.org/10.1104/pp.82.4.885

Goldman, M. h., Goldberg, R. b., & Mariani, C. (1994). Female sterile tobacco plants are produced by stigma-specific cell ablation. *The EMBO Journal*, *13*(13), 2976–2984. https://doi.org/10.1002/j.1460-2075.1994.tb06596.x
Gotelli, M. M., Lattar, E. C., Zini, L. M., & Galati, B. G. (2017). Style morphology and pollen tube pathway. *Plant Reproduction*, *30*(4), 155–170. https://doi.org/10.1007/s00497-017-0312-3
Heslop-Harrison, Y., & Shivanna, K. R. (1977). The Receptive Surface of the Angiosperm Stigma. *Annals of Botany*, *41*(6), 1233–1258. https://doi.org/10.1093/oxfordjournals.aob.a085414
Higashiyama, T., & Takeuchi, H. (2015). The Mechanism and Key Molecules Involved in Pollen Tube Guidance. *Annual Review of Plant Biology*, *66*(1), 393–413. https://doi.org/10.1146/annurev-arplant-043014-115635
Higashiyama, T., & Yang, W. (2017). Gametophytic Pollen Tube Guidance: Attractant Peptides, Gametic Controls, and Receptors1[OPEN]. *Plant Physiology*, *173*(1), 112–121. https://doi.org/10.1104/pp.16.01571
Honys, D., & Twell, D. (2004). Transcriptome analysis of haploid male gametophyte development in Arabidopsis. *Genome Biology*, *5*(11), R85. https://doi.org/10.1186/gb-2004-5-11-r85
Hou, Y., Guo, X., Cyprys, P., Zhang, Y., Bleckmann, A., Cai, L., Huang, Q., Luo, Y., Gu, H., Dresselhaus, T., Dong, J., & Qu, L.-J. (2016). Maternal ENODLs Are Required for Pollen Tube Reception in Arabidopsis. *Current Biology*, *26*(17), 2343–2350. https://doi.org/10.1016/j.cub.2016.06.053
Huang, G.-Q., Gong, S.-Y., Xu, W.-L., Li, W., Li, P., Zhang, C.-J., Li, D.-D., Zheng, Y., Li, F.-G., & Li, X.-B. (2013). A Fasciclin-Like Arabinogalactan Protein, GhFLA1, Is Involved in Fiber Initiation and Elongation of Cotton. *Plant Physiology*, *161*(3), 1278–1290. https://doi.org/10.1104/pp.112.203760
Huang, W.-J., Liu, H.-K., McCormick, S., & Tang, W.-H. (2014). Tomato Pistil Factor STIG1 Promotes in Vivo Pollen Tube Growth by Binding to Phosphatidylinositol 3-Phosphate and the Extracellular Domain of the Pollen Receptor Kinase LePRK2. *The Plant Cell*, *26*(6), 2505–2523. https://doi.org/10.1105/tpc.114.123281
Javelle, M., Marco, C. F., & Timmermans, M. (2011). In Situ Hybridization for the Precise Localization of Transcripts in Plants. *JoVE (Journal of Visualized Experiments)*, *57*, e3328. https://doi.org/10.3791/3328
Johnson, K. L., Cassin, A. M., Lonsdale, A., Bacic, A., Doblin, M. S., & Schultz, C. J. (2017). Pipeline to Identify Hydroxyproline-Rich Glycoproteins. *Plant Physiology*, *174*(2), 886–903. https://doi.org/10.1104/pp.17.00294
Johnson, K. L., Kibble, N. A. J., Bacic, A., & Schultz, C. J. (2011). A Fasciclin-Like Arabinogalactan-Protein (FLA) Mutant of Arabidopsis thaliana, fla1, Shows Defects in Shoot Regeneration. *PLoS ONE*, *6*(9). https://doi.org/10.1371/journal.pone.0025154
Johnson, M. A., & Preuss, D. (2002). Plotting a Course: Multiple Signals Guide Pollen Tubes to Their Targets. *Developmental Cell*, *2*(3), 273–281. https://doi.org/10.1016/S1534-5807(02)00130-2
Kandasamy, M. K., Nasrallah, J. B., & Nasrallah, M. E. (1994). Pollen-pistil interactions and developmental regulation of pollen tube growth in Arabidopsis. *Development*, *120*(12), 3405–3418.
Kimura, S., & Sinha, N. (2008). Tomato (Solanum lycopersicum): A Model Fruit-Bearing Crop. *Cold Spring Harbor Protocols*, *2008*(11), pdb.emo105. https://doi.org/10.1101/pdb.emo105

Knox, J. P. (1995). Developmentally regulated proteoglycans and glycoproteins of the plant cell surface. *The FASEB Journal*, *9*(11), 1004–1012. https://doi.org/10.1096/fasebj.9.11.7544308
Knox, J. P., Linstead, P. J., Cooper, J. P., C., & Roberts, K. (1991). Developmentally regulated epitopes of cell surface arabinogalactan proteins and their relation to root tissue pattern formation. *The Plant Journal*, *1*(3), 317–326. https://doi.org/10.1046/j.1365-313X.1991.t01-9-00999.x
Konar, R. N., & Linskens, H. F. (1966). THE MORPHOLOGY AND ANATOMY OF THE STIGMA OF PETUNIA HYBRIDA. *Planta*, *71*(4), 356–371.
Labarca, C., & Loewus, F. (1972). The Nutritional Role of Pistil Exudate in Pollen Tube Wall Formation in Lilium longiflorum: I. Utilization of Injected Stigmatic Exudate. *Plant Physiology*, *50*(1), 7–14. https://doi.org/10.1104/pp.50.1.7
Lamport, D. T. A., & Várnai, P. (2013). Periplasmic arabinogalactan glycoproteins act as a calcium capacitor that regulates plant growth and development. *New Phytologist*, *197*(1), 58–64. https://doi.org/10.1111/nph.12005
Lee, S.-L. J., & Warmke, H. E. (1979). Organelle Size and Number in Fertile and T-Cytoplasmic Male-Sterile Corn. *American Journal of Botany*, *66*(2), 141–148. https://doi.org/10.1002/j.1537-2197.1979.tb06206.x
Lennon, K. A., Roy, S., Hepler, P. K., & Lord, E. M. (1998). The structure of the transmitting tissue of Arabidopsis thaliana (L.) and the path of pollen tube growth. *Sexual Plant Reproduction*, *11*(1), 49–59. https://doi.org/10.1007/s004970050120
Leszczuk, A., Chylińska, M., & Zdunek, A. (2019). Enzymes and vitamin C as factors influencing the presence of arabinogalactan proteins (AGPs) in Solanum lycopersicum fruit. *Plant Physiology and Biochemistry*, *139*, 681–690. https://doi.org/10.1016/j.plaphy.2019.04.035
Leszczuk, A., Kalaitzis, P., Blazakis, K. N., & Zdunek, A. (2020). The role of arabinogalactan proteins (AGPs) in fruit ripening—A review. *Horticulture Research*, *7*(1), 1–12. https://doi.org/10.1038/s41438-020-00397-8
Li, F., Wu, X., Lam, P., Bird, D., Zheng, H., Samuels, L., Jetter, R., & Kunst, L. (2008). Identification of the Wax Ester Synthase/Acyl-Coenzyme A:Diacylglycerol Acyltransferase WSD1 Required for Stem Wax Ester Biosynthesis in Arabidopsis. *Plant Physiology*, *148*(1), 97–107. https://doi.org/10.1104/pp.108.123471
Li, J., Yu, M., Geng, L.-L., & Zhao, J. (2010). The fasciclin-like arabinogalactan protein gene, FLA3, is involved in microspore development of Arabidopsis. *The Plant Journal*, *64*(3), 482–497. https://doi.org/10.1111/j.1365-313X.2010.04344.x
Liao, J., Chen, Z., Wei, X., Tao, K., Zhang, J., Qin, X., Pan, Z., Ma, W., Pan, L., Yang, S., Wang, M., Ou, X., & Chen, S. (2020). Identification of pollen and pistil polygalacturonases in Nicotiana tabacum and their function in interspecific stigma compatibility. *Plant Reproduction*, *33*(3), 173–190. https://doi.org/10.1007/s00497-020-00393-x
Livak, K. J., & Schmittgen, T. D. (2001). Analysis of Relative Gene Expression Data Using Real-Time Quantitative PCR and the 2−ΔΔCT Method. *Methods*, *25*(4), 402–408. https://doi.org/10.1006/meth.2001.1262
Lopes, A. L., Costa, M. L., Sobral, R., Costa, M. M., Amorim, M. I., & Coimbra, S. (2016). Arabinogalactan proteins and pectin distribution during female gametogenesis in Quercus suber L. *Annals of Botany*, *117*(6), 949–961. https://doi.org/10.1093/aob/mcw019
Lora, J., Laux, T., & Hormaza, J. I. (2019). The role of the integuments in pollen tube guidance in flowering plants. *New Phytologist*, *221*(2), 1074–1089. https://doi.org/10.1111/nph.15420

LORD, E. M., & HESLOP-HARRISON, Y. (1984). Pollen-Stigma Interaction in the Leguminosae: Stigma Organization and the Breeding System in Vicia faba L. *Annals of Botany*, *54*(6), 827–836.
Losada, J. M., & Herrero, M. (2012). Arabinogalactan-protein secretion is associated with the acquisition of stigmatic receptivity in the apple flower. *Annals of Botany*, *110*(3), 573–584. https://doi.org/10.1093/aob/mcs116
Losada, J. M., & Herrero, M. (2017). Pollen tube access to the ovule is mediated by glycoprotein secretion on the obturator of apple (Malus × domestica, Borkh). *Annals of Botany*, *119*(6), 989–1000. https://doi.org/10.1093/aob/mcw276
Losada, J. M., & Herrero, M. (2019). Arabinogalactan proteins mediate intercellular crosstalk in the ovule of apple flowers. *Plant Reproduction*, *32*(3), 291–305. https://doi.org/10.1007/s00497-019-00370-z
Losada, J. M., Herrero, M., Hormaza, J. I., & Friedman, W. E. (2014). Arabinogalactan proteins mark stigmatic receptivity in the protogynous flowers of Magnolia virginiana (Magnoliaceae). *American Journal of Botany*, *101*(11), 1963–1975. https://doi.org/10.3732/ajb.1400280
Love, M. I., Huber, W., & Anders, S. (2014). Moderated estimation of fold change and dispersion for RNA-seq data with DESeq2. *Genome Biology*, *15*(12), 550. https://doi.org/10.1186/s13059-014-0550-8
Lush, W. M., Spurck, T., & Joosten, R. (2000). Pollen Tube Guidance by the Pistil of a Solanaceous Plant. *Annals of Botany*, *85*(suppl_1), 39–47. https://doi.org/10.1006/anbo.1999.1059
Ma, Y., Yan, C., Li, H., Wu, W., Liu, Y., Wang, Y., Chen, Q., & Ma, H. (2017). Bioinformatics Prediction and Evolution Analysis of Arabinogalactan Proteins in the Plant Kingdom. *Frontiers in Plant Science*, *8*. https://doi.org/10.3389/fpls.2017.00066
MacAlister, C. A., Park, S. J., Jiang, K., Marcel, F., Bendahmane, A., Izkovich, Y., Eshed, Y., & Lippman, Z. B. (2012). Synchronization of the flowering transition by the tomato TERMINATING FLOWER gene. *Nature Genetics*, *44*(12), 1393–1398. https://doi.org/10.1038/ng.2465
Mareri, L., Faleri, C., Romi, M., Mariani, C., Cresti, M., & Cai, G. (2016). Heat stress affects the distribution of JIM8-labelled arabinogalactan proteins in pistils of Solanum lycopersicum cv Micro-Tom. *Acta Physiologiae Plantarum*, *38*(7), 184. https://doi.org/10.1007/s11738-016-2203-x
Mazzucato, A., Olimpieri, I., Ciampolini, F., Cresti, M., & Soressi, G. P. (2003). A defective pollen-pistil interaction contributes to hamper seed set in the parthenocarpic fruit tomato mutant. *Sexual Plant Reproduction*, *16*(4), 157–164. https://doi.org/10.1007/s00497-003-0188-2
McInnis, S. M., Desikan, R., Hancock, J. T., & Hiscock, S. J. (2006). Production of reactive oxygen species and reactive nitrogen species by angiosperm stigmas and pollen: Potential signalling crosstalk? *New Phytologist*, *172*(2), 221–228. https://doi.org/10.1111/j.1469-8137.2006.01875.x
Melé, M., Ferreira, P. G., Reverter, F., DeLuca, D. S., Monlong, J., Sammeth, M., Young, T. R., Goldmann, J. M., Pervouchine, D. D., Sullivan, T. J., Johnson, R., Segrè, A. V., Djebali, S., Niarchou, A., Consortium, T. Gte., Wright, F. A., Lappalainen, T., Calvo, M., Getz, G., … Guigó, R. (2015). The human transcriptome across tissues and individuals. *Science*, *348*(6235), 660–665. https://doi.org/10.1126/science.aaa0355
Mizukami, A. G., Inatsugi, R., Jiao, J., Kotake, T., Kuwata, K., Ootani, K., Okuda, S., Sankaranarayanan, S., Sato, Y., Maruyama, D., Iwai, H., Garénaux, E., Sato, C., Kitajima, K.,

Tsumuraya, Y., Mori, H., Yamaguchi, J., Itami, K., Sasaki, N., & Higashiyama, T. (2016). The AMOR Arabinogalactan Sugar Chain Induces Pollen-Tube Competency to Respond to Ovular Guidance. *Current Biology*, *26*(8), 1091–1097. https://doi.org/10.1016/j.cub.2016.02.040
Mizuta, Y., & Higashiyama, T. (2018). Chemical signaling for pollen tube guidance at a glance. *Journal of Cell Science*, *131*(2). https://doi.org/10.1242/jcs.208447
Noyszewski, A. K., Liu, Y.-C., Tamura, K., & Smith, A. G. (2017). Polymorphism and structure of style–specific arabinogalactan proteins as determinants of pollen tube growth in Nicotiana. *BMC Evolutionary Biology*, *17*(1), 186. https://doi.org/10.1186/s12862-017-1011-2
Okuda, S., Tsutsui, H., Shiina, K., Sprunck, S., Takeuchi, H., Yui, R., Kasahara, R. D., Hamamura, Y., Mizukami, A., Susaki, D., Kawano, N., Sakakibara, T., Namiki, S., Itoh, K., Otsuka, K., Matsuzaki, M., Nozaki, H., Kuroiwa, T., Nakano, A., … Higashiyama, T. (2009). Defensin-like polypeptide LUREs are pollen tube attractants secreted from synergid cells. *Nature*, *458*(7236), 357–361. https://doi.org/10.1038/nature07882
Palanivelu, R., & Tsukamoto, T. (2012). Pathfinding in angiosperm reproduction: Pollen tube guidance by pistils ensures successful double fertilization. *Wiley Interdisciplinary Reviews. Developmental Biology*, *1*(1), 96–113. https://doi.org/10.1002/wdev.6
Pasternak, T., Tietz, O., Rapp, K., Begheldo, M., Nitschke, R., Ruperti, B., & Palme, K. (2015). Protocol: An improved and universal procedure for whole-mount immunolocalization in plants. *Plant Methods*, *11*(1), 50. https://doi.org/10.1186/s13007-015-0094-2
Pattison, R. J., Csukasi, F., Zheng, Y., Fei, Z., Knaap, E. van der, & Catalá, C. (2015). Comprehensive Tissue-Specific Transcriptome Analysis Reveals Distinct Regulatory Programs during Early Tomato Fruit Development. *Plant Physiology*, *168*(4), 1684–1701. https://doi.org/10.1104/pp.15.00287
Pennell, R. I., Janniche, L., Kjellbom, P., Scofield, G. N., Peart, J. M., & Roberts, K. (1991). Developmental Regulation of a Plasma Membrane Arabinogalactan Protein Epitope in Oilseed Rape Flowers. *The Plant Cell*, *3*(12), 1317–1326. https://doi.org/10.1105/tpc.3.12.1317
Pereira, A. M., Lopes, A. L., & Coimbra, S. (2016). Arabinogalactan Proteins as Interactors along the Crosstalk between the Pollen Tube and the Female Tissues. *Frontiers in Plant Science*, *7*. https://doi.org/10.3389/fpls.2016.01895
Pereira, A. M., Masiero, S., Nobre, M. S., Costa, M. L., Solís, M.-T., Testillano, P. S., Sprunck, S., & Coimbra, S. (2014). Differential expression patterns of arabinogalactan proteins in Arabidopsis thaliana reproductive tissues. *Journal of Experimental Botany*, *65*(18), 5459–5471. https://doi.org/10.1093/jxb/eru300
Pitto, L., Giorgetti, L., Turrini, A., Evangelista, M., Luccarini, G., Colella, C., Collina, F., Caltavuturo, L., & Nuti Ronchi, V. (2001). Floral genes expressed in tomato hypocotyl explants in liquid culture. *Protoplasma*, *218*(3), 168–179. https://doi.org/10.1007/BF01306606
Reimann, R., Kah, D., Mark, C., Dettmer, J., Reimann, T. M., Gerum, R. C., Geitmann, A., Fabry, B., Dietrich, P., & Kost, B. (2020). Durotropic Growth of Pollen Tubes. *Plant Physiology*, *183*(2), 558–569. https://doi.org/10.1104/pp.19.01505
Rydahl, M. G., Hansen, A. R., Kračun, S. K., & Mravec, J. (2018). Report on the Current Inventory of the Toolbox for Plant Cell Wall Analysis: Proteinaceous and Small Molecular Probes. *Frontiers in Plant Science*, *9*. https://doi.org/10.3389/fpls.2018.00581
Sato, S., Tabata, S., Hirakawa, H., Asamizu, E., Shirasawa, K., Isobe, S., Kaneko, T., Nakamura, Y., Shibata, D., Aoki, K., Egholm, M., Knight, J., Bogden, R., Li, C., Shuang, Y., Xu, X., Pan, S., Cheng, S., Liu, X., … Universitat Pompeu Fabra. (2012). The tomato genome sequence

provides insights into fleshy fruit evolution. *Nature*, *485*(7400), 635–641. https://doi.org/10.1038/nature11119
Schultz, C., Gilson, P., Oxley, D., Youl, J., & Bacic, A. (1998). GPI-anchors on arabinogalactan-proteins: Implications for signalling in plants. *Trends in Plant Science*, *3*(11), 426–431. https://doi.org/10.1016/S1360-1385(98)01328-4
Schultz, C. J., Rumsewicz, M. P., Johnson, K. L., Jones, B. J., Gaspar, Y. M., & Bacic, A. (2002). Using Genomic Resources to Guide Research Directions. The Arabinogalactan Protein Gene Family as a Test Case. *Plant Physiology*, *129*(4), 1448–1463. https://doi.org/10.1104/pp.003459
Seifert, G. J. (2018). Fascinating Fasciclins: A Surprisingly Widespread Family of Proteins that Mediate Interactions between the Cell Exterior and the Cell Surface. *International Journal of Molecular Sciences*, *19*(6). https://doi.org/10.3390/ijms19061628
Selinski, J., & Scheibe, R. (2014). Pollen tube growth: Where does the energy come from? *Plant Signaling & Behavior*, *9*(12), e977200. https://doi.org/10.4161/15592324.2014.977200
Shen, S., Ma, S., Liu, Y., Liao, S., Li, J., Wu, L., Kartika, D., Mock, H.-P., & Ruan, Y.-L. (2019). Cell Wall Invertase and Sugar Transporters Are Differentially Activated in Tomato Styles and Ovaries During Pollination and Fertilization. *Frontiers in Plant Science*, *10*. https://doi.org/10.3389/fpls.2019.00506
Showalter, A. M., Gao, M., Kieliszewski, M. J., & Lamport, D. T. A. (2000). Characterization and Localization of a Novel Tomato Arabinogalactan-Protein (LeAGP-1) and the Involvement of Arabinogalactan-Proteins in Programmed Cell Death. In E. A. Nothnagel, A. Bacic, & A. E. Clarke (Eds.), *Cell and Developmental Biology of Arabinogalactan-Proteins* (pp. 61–70). Springer US. https://doi.org/10.1007/978-1-4615-4207-0_6
Showalter, A. M., Keppler, B., Lichtenberg, J., Gu, D., & Welch, L. R. (2010). A bioinformatics approach to the identification, classification, and analysis of hydroxyproline-rich glycoproteins. *Plant Physiology*, *153*(2), 485–513. https://doi.org/10.1104/pp.110.156554
Smith, A. G., Eberle, C. A., Moss, N. G., Anderson, N. O., Clasen, B. M., & Hegeman, A. D. (2013). The transmitting tissue of Nicotiana tabacum is not essential to pollen tube growth, and its ablation can reverse prezygotic interspecific barriers. *Plant Reproduction*, *26*(4), 339–350. https://doi.org/10.1007/s00497-013-0233-8
Sprunck, S., Hackenberg, T., Englhart, M., & Vogler, F. (2014). Same same but different: Sperm-activating EC1 and ECA1 gametogenesis-related family proteins. *Biochemical Society Transactions*, *42*(2), 401–407. https://doi.org/10.1042/BST20140039
Sprunck, S., Rademacher, S., Vogler, F., Gheyselinck, J., Grossniklaus, U., & Dresselhaus, T. (2012). Egg Cell–Secreted EC1 Triggers Sperm Cell Activation During Double Fertilization. *Science*, *338*(6110), 1093–1097. https://doi.org/10.1126/science.1223944
Su, S., & Higashiyama, T. (2018). Arabinogalactan proteins and their sugar chains: Functions in plant reproduction, research methods, and biosynthesis. *Plant Reproduction*, *31*(1), 67–75. https://doi.org/10.1007/s00497-018-0329-2
Sun, W., Kieliszewski, M. J., & Showalter, A. M. (2004). Overexpression of tomato LeAGP-1 arabinogalactan-protein promotes lateral branching and hampers reproductive development. *The Plant Journal*, *40*(6), 870–881. https://doi.org/10.1111/j.1365-313X.2004.02274.x
Takeuchi, H., & Higashiyama, T. (2011). Attraction of tip-growing pollen tubes by the female gametophyte. *Current Opinion in Plant Biology*, *14*(5), 614–621. https://doi.org/10.1016/j.pbi.2011.07.010

Takeuchi, H., & Higashiyama, T. (2012). A Species-Specific Cluster of Defensin-Like Genes Encodes Diffusible Pollen Tube Attractants in Arabidopsis. *PLoS Biology*, *10*(12). https://doi.org/10.1371/journal.pbio.1001449
Tian, T., Liu, Y., Yan, H., You, Q., Yi, X., Du, Z., Xu, W., & Su, Z. (2017). agriGO v2.0: A GO analysis toolkit for the agricultural community, 2017 update. *Nucleic Acids Research*, *45*(W1), W122–W129. https://doi.org/10.1093/nar/gkx382
Twarda-Clapa, A., Labuzek, B., Krzemien, D., Musielak, B., Grudnik, P., Dubin, G., & Holak, T. A. (2018). Crystal structure of the FAS1 domain of the hyaluronic acid receptor stabilin-2. *Acta Crystallographica Section D: Structural Biology*, *74*(7), 695–701. https://doi.org/10.1107/S2059798318007271
Vogler, F., Schmalzl, C., Englhart, M., Bircheneder, M., & Sprunck, S. (2014). Brassinosteroids promote Arabidopsis pollen germination and growth. *Plant Reproduction*, *27*(3), 153–167. https://doi.org/10.1007/s00497-014-0247-x
Wei, L. Q., Xu, W. Y., Deng, Z. Y., Su, Z., Xue, Y., & Wang, T. (2010). Genome-scale analysis and comparison of gene expression profiles in developing and germinated pollen in Oryza sativa. *BMC Genomics*, *11*(1), 338. https://doi.org/10.1186/1471-2164-11-338
Wingett, S. W., & Andrews, S. (2018). FastQ Screen: A tool for multi-genome mapping and quality control. *F1000Research*, *7*, 1338. https://doi.org/10.12688/f1000research.15931.2
Wolters-Arts, M., Lush, W. M., & Mariani, C. (1998). Lipids are required for directional pollen-tube growth. *Nature*, *392*(6678), 818–821. https://doi.org/10.1038/33929
Wu, H.-M., Wang, H., & Cheung, A. Y. (1995). A pollen tube growth stimulatory glycoprotein is deglycosylated by pollen tubes and displays a glycosylation gradient in the flower. *Cell*, *82*(3), 395–403. https://doi.org/10.1016/0092-8674(95)90428-X
Wu, Y., Fan, W., Li, X., Chen, H., Takáč, T., Šamajová, O., Fabrice, M. R., Xie, L., Ma, J., Šamaj, J., & Xu, C. (2017). Expression and distribution of extensins and AGPs in susceptible and resistant banana cultivars in response to wounding and Fusarium oxysporum. *Scientific Reports*, *7*(1), 42400. https://doi.org/10.1038/srep42400
Yariv, J., Rapport, M., & Graf, L. (1962). The interaction of glycosides and saccharides with antibody to the corresponding phenylazo glycosides. *Biochemical Journal*, *85*(2), 383–388. https://doi.org/10.1042/bj0850383
Yates, E. A., Valdor, J.-F., Haslam, S. M., Morris, H. R., Dell, A., Mackie, W., & Knox, J. P. (1996). Characterization of carbohydrate structural features recognized by anti-arabinogalactan-protein monoclonal antibodies. *Glycobiology*, *6*(2), 131–139. https://doi.org/10.1093/glycob/6.2.131
Zhang, M. J., Zhang, X. S., & Gao, X.-Q. (2020). ROS in the Male–Female Interactions During Pollination: Function and Regulation. *Frontiers in Plant Science*, *11*. https://doi.org/10.3389/fpls.2020.00177
Zheng, R. H., Su, S. D., Xiao, H., & Tian, H. Q. (2019). Calcium: A Critical Factor in Pollen Germination and Tube Elongation. *International Journal of Molecular Sciences*, *20*(2). https://doi.org/10.3390/ijms20020420
Zhong, Y., & Shanley, J. (1995). Altered nerve terminal arborization and synaptic transmission in Drosophila mutants of cell adhesion molecule fasciclin I. *The Journal of Neuroscience: The Official Journal of the Society for Neuroscience*, *15*(10), 6679–6687.

Chapter 5. Conclusions And Future Directions

The HRGP family comprises a complex, heterogeneous group of cell surface glycoproteins. As plants adapted to the terrestrial environment, novel functions for members of the family, especially chimeric and hybrid HRGPs, emerged. Understanding the function of HRGPs requires knowledge of their post-translational modifications. In the second chapter of this work, we developed a protocol that was not only useful to detect for the first time the presence of *O*-glycans in chimeric HRGPs (Chapter 3) but may also serve as a tool for biochemical studies of other cell surface or cell wall-associated proteins in plants.

Within the plant kingdom, angiosperms are considered as the most abundant and diverse clade. The unique mechanism of sexual reproduction in this clade is thought to have played an important role for their current dominance of the terrestrial environment. Angiosperm sexual reproduction involves active cell-cell communication between the male and female organs, as well as extremely rapid cell expansion to deliver the male gametes. Considering the great expansion on the number of genes encoding for HRGPs in the angiosperm clade compared to non-vascular plants, the emergence of novel functions involved in a crucial process such as sexual reproduction is a likely event. In this work, we sought to unravel novel functions for non-canonical members of the family during sexual reproduction. In Chapter 3 we focused on two members of the class I formin family, AtFH3 and AtFH5, and their roles during polarized growth in *Arabidopsis thaliana*'s pollen tubes. Our study suggested that the extracellular domains (ECD)

of these proteins, which contain distinct HRGP-like motifs, is necessary for their proper function. Since class I formins lack the autoinhibitory motifs present in yeast and metazoan formin homologs, it is possible that additional mechanisms regulate their intracellular functions. Interestingly, our study sheds light on a possible mechanism to constrain pollen-expressed formins to specific plasma membrane domains mediated by their ECDs, consequently, influencing their intracellular actin nucleating activities. HRGP-like motifs are found in the ECDs across the class I formin clade. Our study also indicated that, following the predictions of the hydroxyproline contiguity hypothesis, the ECDs of AtFH3 and AtFH5 bear distinct *O*-glycans; indicating that *O*-glycosylation might a occur in a similar fashion across this family. Although our study constitutes a step forward to understand how class I formins mediate coordination between the cell wall, plasma membrane and the actin cytoskeleton to allow cell growth, multiple questions remain to be explored. The identification of potential extracellular interactors, either (glyco)proteins or wall polysaccharides as well as cytoplasmic interactors, would contribute to further dissect protein function. The protocol developed in Chapter 2, combined with other analytical methods (e.g., mass spectrometry) could be a useful starting point to address this question.

In Chapter 4, we investigated potential functions of members in the HRGP family in the female floral organ, the pistil. In tomato, little is known about the molecular mechanisms that mediate pistil receptivity, pollen recognition and control of pollen tube behavior. Our study suggests that the acquisition of receptivity correlated with a progressive accumulation of AGP glycans as the pistil reached maturity. Furthermore, we identified a small subpopulation of AG glycans that accumulate in the surface of the micropyle in unfertilized ovules and dissipates post pollen tube

penetration. Using transcriptomic analysis, we identified two noncanonical members of the HRGP family, *SlyHAE* and *SlyFLA9*, with high expression levels in the style and ovary, respectively. Such expression patterns suggest potential functions in pollen tube recognition (interspecies compatibility, similar to PELPIII in tobacco) for *SlyHAE* and pollen tube guidance for *SlyFLA9*. The datasets generated in our study also identified sets of genes with enriched expression in the functionally distinct subsections of the pistil (stigma, style and ovary), setting the basis for further dissection of the molecular basis of tomato pistil receptivity. To date, CRSIPR/Cas9 has been successfully used in tomato to disrupt gene function. Similarly, this technique allows simultaneous disruption of multiple targets, which could potentially overcome the problem of functional redundancy, a phenomenon often observed in the HRGP family. Thus, evaluation of the effects of CRISPR-Cas9 mediated disruption of *SlyFLA9* and *SlyHAE* expression will be the focus for future studies.

Lastly, due to the inherently challenging features of wall biomolecules, the question of our how HRGPs co-exist with other proteins and/or polysaccharides *in muro* remains essentially unexplored. Rapid advances of techniques in the structural biology field, such as electron cryotomography (cryo-ET) or single particle analyses (SPA), are allowing visualization of subcellular structures *in situ* with unprecedented detail. While the broader application of cryo-ET and SPA currently faces certain technical limitations, the prospects of their use to address questions regarding the cell wall and its nanoscale organization are an exciting possibility for the near future.